CHARACTERISATION OF NOVEL MATRIX-BINDING INTERACTIONS FOR LATENT TRANSFORMING GROWTH FACTOR-β-BINDING PROTEIN-2 (LTBP-2), WITH EMPHASIS ON HEPARIN AND HEPARAN SULPHATE PROTEOGLYCANS

Mahroo Parsi

Discipline of Pathology
School of Medical Sciences, The University of Adelaide, Australia

A thesis submitted for the degree of Doctor of Philosophy (PhD) in July, 2010 with permission from the Faculty of Health Sciences, the University of Adelaide

DECLARATION

This work contains no material which has been accepted for the award of any other degree or diploma in any university or other tertiary institution and, to the best of my knowledge and belief, contains no material previously published or written by another person, except where due reference has been made in the text.

I give consent to this copy of my thesis, when deposited in the University Library, being made available for loan and photocopying, subject to the provisions of the Copyright Act 1968.

I also give permission for the digital version of my thesis to be made available on the web, via the University's digital research repository, the Library catalogue, the Australasian Digital Theses Program (ADTP) and also through web search engines, unless permission has been granted by the University to restrict access for a period of time.

Mahroo Parsi **July 2010**

SUPERVISORS: **Dr. Mark A. Gibson**
Dr. Christopher Bagley
Dr. Eric Hanssen

ACKNOWLEDGEMENTS

Early in this project, it became very clear to me that I could not have completed this journey alone. Although the list of people I wish to thank extends beyond the limits of this format, I would like to thank the following persons for their dedication, advice and support.

My Primary supervisor, Dr. Mark Gibson, you have been a significant presence in my life. My achievements over the last five years have been all because of your many helpful suggestions, important advice and constant encouragement. There are no words to express my gratitude, except to say I am forever grateful for your wisdom, knowledge and also believing in me. I hope to make you proud one day.

I also wish to express my appreciation to Dr. Chris Bagley for always being available and supplying me with resources to carryout some of the proteomic techniques. Also further thanks for the many valuable suggestions and constructive advice.

Special thanks to Dr. Julian Adams for reading my thesis over and over again and the many valuable suggestions that indeed help improve the quality of this thesis. Also for all the random conversations during the short period of time we worked together.

My keen appreciation goes to the staff of the Discipline of pathology and Adelaide Microscopy at University of Adelaide for their valuable assistance and technical support.

To my family, mom, dad and Golroo and also dearest friends, all I can say is it would take another thesis to express my deep love for you. Your patience, love and encouragement have upheld me, particularly in those many months in which I spent all my time with my computer than with you. I will make it up to each and everyone of you.

TABLE OF CONTENTS

ABBREVIATIONS ..... **viii**

LIST OF FIGURES ..... **x**

LIST OF TABLES ..... **xii**

SUMMARY ..... **xiii**

CHAPTER 1

INTRODUCTION **1**

1.1 Extracellular Matrix **1**

1.1.1 Collagens 1

1.1.2 Elastin and Elastic fibres 2

1.1.3 Proteoglycans 5

1.1.3.1 Perlecan 7

1.1.3.2 Syndecans 9

1.1.4 Glycoproteins 111

1.2 Microfibrillar structures of the matrix **12**

1.2.1 Collagen VI microfibrils 12

1.2.1.1CollagenVI 12

1.2.1.1.1 Structure 12

1.2.1.1.2 Function and distribution of Collagen VI 14

1.2.1.1.3 Interaction of collagen VI with other matrix components 16

1.2.1.1.4 Heritable disorders of collagen VI 17

1.2.1.2 Transforming growth factor-β-inducible gene-h3 (βig-h3) 18

1.2.1.2.1 Structure of βig-h3 19

1.2.1.2.2 Possible function of βig-h3 and its interaction with other matrix proteins 19

1.2.1.2.3 Expression and tissue distribution of βig-h3 21

1.2.1.2.4 Diseases associated with βig-h3 21

1.2.2 Fibrillin-microfibrils 22

1.2.2.1 Fibrillins 23

1.2.2.1.1 Structure of fibrillins 23

1.2.2.1 2 Tissue distribution of Fibrillins 24

1.2.2.1.3 Functions of fibrillins 25

1.2.2.1.4 Interaction of fibrillins with other matrix components 26

1.2.2.1.5 Congenital disorders related to fibrillins 29

1.2.2.2 Latent transforming growth factor-β binding proteins 30

1.2.2.2.1 Structure and function of LTBPs 31

1.2.2.2.2 Tissue distribution of LTBP-2 34

1.2.2.2.3 Possible function of LTBP-2 35

1.2.2.2.4 Diseases associated with the LTBP-2 36

Aims of the present study **37**

CHAPTER 2

MATERIALS AND METHODS **39**

2.1 General molecular biology protocols **39**

2.1.1 Polymerase Chain Reaction (PCR) 39

2.1.2 DNA Purification by Agarose Gel Electrophoresis 39
2.1.3 “A”-tailing and Ligation 40
2.1.4 Transformation of Competent Cells 40
2.1.5 Restriction digests 41
2.1.6 DNA Sequence Analysis 41
2.1.7 Dephosphorylation 42
2.2 Production of human LTBP-2 fragments 42
2.2.1 LTBP-2C(H) 42
2.2.2 LTBP-2NT(H) 43
2.3 Expression of recombinant LTBP-2C(H) 44
2.4 Purification of recombinant full length LTBL-2, βig-h3 and LTBP-2C(H) fragment 45
2.5 Freezing and Thawing of recombinant protein expressing cells. 47
2.6 SDS-PAGE coomassie blue staining and western immunoblotting 47
2.7 Silver staining 49
2.8 Determining the molecular weight of unknown proteins 49
2.9 Mass spectrometric analysis 50
2.10 Synthesis and Fractionation of Covalently bound conjugates of heparin and albumin 51
2.11 Uronic acid assay 52
2.12 Determination of protein concentration using Bradford assay 52
2.13 Solid phase binding assay 53
2.13.1 Detecting interaction between two proteins 53
2.13.2 Saturation binding curve 53
2.13.3 Inhibition of binding 54
2.13.4 Determination of dissociation constants 54
2.13.5 Statistical analysis 55
2.13.6 Digestion of glycosaminoglycans (GAGs) 55
2.14 Tissue sectioning and immunofluorescence 55
2.15 Coupling of rβig-h3 and rLTBP-2 to Cyanogen Bromide (CNBr)-activated Sepharose 4B 56
2.16 Using nickel chelate chromatography for identification of binding partners of rβig-h3 56
2.17 Two-Dimension Gel Electrophoresis (2-DGE) 57
2.18 Difference Gel Electrophoresis (DIGE) using CyDye DIGE Fluor Dyes 57

CHAPTER 3

BINDING INTERACTION OF HUMAN LTBP-2 WITH HEPARIN/HEPARAN SULPHATE PROTEOGLYCANS 58

3.1 Expression and purification of human recombinant LTBP-2 59
3.2 Synthesis and purification of Heparin-Albumin Conjugate 61
3.3 The analysis of LTBP-2 interaction with heparin. 61
3.3.1 Solid phase immuno-assays 61
3.3.2 LTBP-2 interacts with heparin-albumin conjugate (HAC) 65
3.3.3 The interaction of LTBP-2 with heparin is not a non-specific interaction with polyanionic GAG 68
3.3.4 LTBP-2 interaction with heparin depends on calcium or other divalent cations 68
3.3.5 Kinetic analysis of the interaction between LTBP-2 and heparin 70

CHAPTER 4

THE CENTRAL REGION OF LTBP-2 CONTAINS A BINDING SITE FOR HEPARIN 72

4.1 Expression, purification and characterisation of the central region of LTBP-2 (LTBP-2C(H)) 72
4.1.1 Expression and purification of LTBP-2C(H) 72
4.1.2 Analysis and authentication of rLTBP-2C(H) 73
4.1.3 Peptide mass finger-printing of rLTBP-2C(H) 74
4.2 The central region of LTBP-2 contains a binding site for heparin 75
4.2.1 Defining the affinity between central region of LTBP-2 and heparin 76

CHAPTER 5

LTBP-2 INTERACTIONS WITH PERLECAN AND SYNDECANS. 79

5.1 LTBP-2 interacts with Perlecan 79
5.2 The interaction of LTBP-2 with perlecan is via the heparan sulphate side chains ... 81
5.3 The interaction of LTBP-2 with perlecan is cation dependent 83
5.4 LTBP-2 interacts with syndecan-4 but not syndecan-2 83

CHAPTER 6

IMMUNOHISTOCHEMICAL ANALYSIS OF HUMAN FOETAL AORTA INDICATES LTBP-2 HAS AREAS OF COLOCALISATION WITH PERLECAN 86

6.1 Localisation of LTBP-2 on microfibrils and perlecan on basement membrane in human foetal aorta 86
6.1.1 LTBP-2 localises on fibrillin-1-microfibrils in the human foetal aorta 86
6.1.2 Perlecan is predominantly associated with smooth muscle BM in foetal aorta 89
6.1.3 Colocalisation of fibrillin-1 with perlecan 90
6.1.4 Colocalisation of LTBP-2 and perlecan in the foetal aorta 92

CHAPTER 7

IDENTIFICATION OF MATRIX MOLECULAR BINDING PARTNERS OF βig-h3 AND LTBP-2 USING AFFINITY BINDING AND PROTEOMICS TECHNIQUES 94

7.1 Expression and purification of recombinant βig-h3 95
7.2 Preparation of the affinity column; coupling of rβig-h3 and rLTBP-2 to CNBr-activated sepharose-4B 96
7.3 Selection of tissue extracts for identification of binding partners for rβig-h3 and rLTBP-2 97
7.4 The use of BNLPMs-1M NaCl for identification of novel binding partners 99
7.4.1 Selecting a suitable binding buffer 99
7.4.2 Incubation of BNLPM with a sepharose column for detection of non-specific interactions 100
7.5 Identification of potential binding partners for rβig-h3 from the BNLPM-1M NaCl 102
7.5.1 Analysis of the binding proteins using Coomassie Blue staining 102
7.5.2 Detection of βig-h3 in proteins eluted from rβig-h3-sepharose 103
7.5.3 Detection of the potential binding proteins for rβig-h3 using silver staining 105

7.5.4 Isolation of potential binding partners of βig-h3 using immobilised-Metal Affinity chromatography 107
7.6 Identification of binding partners for rLTBP-2 from BNLPM using silver staining 111
7.7 Isolation of binding partners for rLTBP-2 from a basement membrane-rich mixture 112
7.8 Affinity chromatography improvements for isolation of binding ligands for βig-h3 and LTBP-2 from BNLPM....113
7.8.1 Dilution of BNLPM....113
7.8.2 Reducing the size of the 'bait' protein columns 114
7.9 Separation of proteins eluted from rβig-h3- and rLTBP-2- sepharose by 2-D Gel Electrophoresis (2-DGE) 116
7.9.1 Silver staining detection of proteins separated by 2-DGE....116
7.9.2 Improving the resolution of 2-DGE....118
7.9.3 Detection of proteins separated by 2-DGE using 2-D-DIGE technology 122
7.9.3.1 Labelling of the proteins with CyDye DIGE Fluor minimal dye 122
7.9.3.2 Labelling of the proteins with CyDye DIGE Fluor saturation dyes 126

CHAPTER 8

DISCUSSION AND FUTURE DIRECTIONS....128

8.1 Discussion 130
8.2 Future Directions 137
8.2.1 Experiments for the comprehensive understanding of LTBP-2 interactions with HSPG 137
8.2.2 Possible alternatives for the identification of binding partners for βig-h3 and LTBP-2....138

APPENDIX A....140

APPENDIX B....141

APPENDIX C....144

REFERENCES....146

PRESENTATIONS AND PUBLICATION ARISING

Conference presentations and published abstracts

2007- Pan Pacific Connective Tissue Societies Symposium with Matrix Biology Society of Australia and New Zealand (MBSANZ) annual scientific meeting (Cairns, Australia)
Mahroo Parsi, John Whitelock and Mark A. Gibson
Interaction of Latent Transforming Growth factor –beta- Binding Protein-2 (LTBP-2) with heparin and heparan sulphate proteoglycan, Perlecan

2007- Gordon Research Conference for Elastin and Elastic Fibres (Massachusetts, USA)
Mahroo Parsi and Mark A. Gibson
Latent Transforming Growth factor-beta-Binding Protein-2 (LTBP-2) Interaction with heparin and heparan sulfate proteoglycans

2006- National Health and Medical Research Council, (Melbourne, Australia)
Mahroo Parsi and Mark A. Gibson
Identifying matrix binding partners of LTBP-2 and beta-igh3 using Fluorescence 2D Difference Gel electrophoresis (DIGE) method

2006- National Health and Medical Research Council, (Melbourne, Australia)
Mahroo Parsi and Mark A. Gibson
Interaction of Latent Transforming Growth factor –beta- Binding Protein-2 (LTBP-2) with heparin and heparan sulphate proteoglycans

2005- Matrix Biology Society of Australia and New Zealand (MBSANZ) annual scientific meeting, (Victor Harbor, Australia)
Mahroo Parsi, Eric Hanssen and Mark A. Gibson
Identification of Matrix Binding Proteins for Transforming Growth factor-beta-Inducible Gene-h3 (beta-igh3)

PUBLICATION

Mahroo Parsi, **Julian Adams and Mark A. Gibson**
LTBP-2 has multiple heparin/heparan sulphate binding sites. Matrix Biol 2010 Apr 9[Epub ahead of print].

AWARDS ARISING FROM PhD CANDIDATURE

2007-	**Postgraduate travelling fellowship** (The University of Adelaide)
2006 -	**Research abroad scholarship** (The University of Adelaide)
2005-2007-	**Australian Postgraduate Award**, University of Adelaide Scholarship

ABBREVIATIONS

Δ	heat deactivated
2-DGE-	Two-Dimension Gel Electrophoresis
2D DIGE-	2D difference Gel Electrophoresis
8-cys-	8-cysteine
A_{260}-	absorbance at 260 nm
A_{450}-	absorbance at 450 nm
A_{520}-	absorbance at 520 nm
A_{595}-	absorbance at 595 nm
βig-h3-	transforming growth factor-β-inducible gene-h3
BM-	basement membrane
BMP-	bone morphogenetic protein
BNLPMs-6M GuHCl-	Bovine nuchal ligament protein mixtures extracted with 6M GuHCl
BNLPMs-1M NaCl-	Bovine nuchal ligament protein mixtures extracted with 1M NaCl
BNLPs-	Bovine nuchal ligament proteins
bp-	base pairs
BSA-	bovine serum albumin
c-	complementary
C-6-S-	chondroitin-6-sulphate
cbEGF-	calcium binding epidermal growth factor
CCA-	congenital contractural arachnodactyly
CNBr-	cyanogen bromide
CoIP-	co-immunoprecipitation
Col-	column
CS-	chondroitin sulphate
ddH_2O-	double distilled water
DEAE-	Diethylaminoethyl
DIGE-	Difference Gel Electrophoresis
DMEM-	Dulbecco's Modification of Eagles Medium
E-	embryonic day
EBP-	elastin binding protein
ECM-	extracellular matrix
EDTA-	ethylene diamine tetraacetic acid
EGTA-	ethylene glycol tetraacetic acid
ELISA-	enzyme-linked immuno-sorbent assay
FCS-	foetal calf serum
g-	gravity
GAG-	glycosaminoglycan
GuHCl-	Guanidine hydrochloride
HAC-	heparin-albumin conjugates
HEK-	human embryo kidney
his_{6}-	6-histidine
HS-	heparan sulphate
HSPGs-	heparan sulphate proteoglycans
IgG-	Immunoglobulin G
K_d-	dissociation constant
kDa-	kiloDalton
LDL-	low-density lipoprotein
LTBP-	latent transforming growth factor-β binding protein
LTBP-2C(H)-	LTBP-2 C-terminal

LTBP-2NT(H)-	LTBP-2 N-terminal
µA-	microampere
µl-	microliter
M-	molar
MAGP-	microfibrillar-associated glycoprotein
MALDI-TOF-MS-	Matrix-assisted laser-desorption/ionisation time-of-flight mass spectrometry
min-	minutes
mM-	millimolar
NEAA-	non-essential amino acids
ng-	nanogram
Ni-	nickel
PCR-	polymerase chain reactions
PG-	proteoglycan
PVDF-	polyvinylidene difluoride
r-	recombinant
R_f -	relative mobility
RGD-	Arg-Gly-Asp
RT-	room temperature
SDS-PAGE-	sodium sulphate polyacrylamide gel electrophoresis
TBS	tris buffered saline
TGF-β-	transforming growth factor-β
UCMD-	Ullrich Congenital Muscular Dystrophy
V-	volts
v or vol-	volume
w-	weight

LIST OF FIGURES

Figure 1.1 Structure of glycosaminoglycans (GAGs) and proteoglycans (PGs) 5

Figure 1.2 Schematic molecular structure of human perlecan 8

Figure 1.3 Cell surface HSPGs syndecans 10

Figure 1.4 Domain organisation and assembly of the alpha chains from collagen VI 13

Figure 1.5 Model for supramolecular assembly in the ECM of connective tissue 16

Figure 1.6 Schematic diagram of the domain structure of βig-h3 molecule 19

Figure 1.7 Schematic representation of the three fibrillins 24

Figure 1.8 The schematic illustration of the binding sites of various ECM components on fibrillin-1. 27

Figure 1.9 Schematic representation of human LTBPs 1-4 31

Figure 3.1 Schematic representation of rLTBP-2 and rLTBP-2 fragments 59

Figure 3.2 Optimisation of expression and purification of rLTBP-2 62

Figure 3.3 Fractionation of un-conjugated albumin and heparin-albumin conjugate (HAC) on DEAE sepharose Cl4B 62

Figure 3.4 Optimisation of the conditions for solid phase assays 64

Figure 3.5 Reducing non-specific interaction of LTBP-2 with the addition of carrier protein in solution 64

Figure 3.6 Saturation binding curve of the interaction of LTBP-2 and heparin 66

Figure 3.7 Inhibition binding curve of LTBP-2 interaction with heparin 67

Figure 3.8 Interaction of LTBP-2 with heparin is specific and is not a non-specific charge-related interaction 69

Figure 3.9 The interaction of LTBP-2 with heparin is cation dependent 69

Figure 3.10 Kinetic analysis of the interaction between LTBP-2 and heparin using solid phase binding assay 71

Figure 4.1 PCR amplification of a cDNA encoding rLTBP-2C(H) and analysis of purified recombinant protein 74

Figure 4.2 Heparin binds specifically to rLTBP-2C(H) 77

Figure 4.3 Kinetic analysis of the interaction between central fragment of LTBP-2 and heparin using solid phase binding assay 78

Figure 5.1 LTBP-2 interacts specifically with perlecan 80

Figure 5.2 Perlecan interacts with LTBP-2 via its HS-side chains 82

Figure 5.3 Preparation of the perlecan core protein 82

Figure 5.4 The interaction of perlecan with LTBP-2 is cation dependent 85

Figure 5.5 LTBP-2 interacts with syndecan-4 but not with syndecan-2 85

Figure 6.1 The distribution of LTBP-2, fibrillin-1, perlecan and laminin in the foetal aorta 88

Figure 6.2 Fibrillin-1 and perlecan have potential areas of colocalisation within the medial layer of human foetal aorta 91

Figure 6.3 Regions of partial colocalisation of LTBP-2 and perlecan within the medial layer of foetal aorta 93

Figure 7.1 Purification of rβig-h3 aorta 98

Figure 7.2 Determination of the extent of coupling of rβig-h3 or rLTBP-2 to CNBr-activated sepharose 98

Figure 7.3 Solubility of BNLPM-1M NaCl following different treatments 101

Figure 7.4 BNLPs interacting with sepharose- CL-4B 101

Figure 7.5 BNLPs interacting with rβig-h3-sepharose 103

Figure 7.6 Identification of rβig-h3 in the eluted protein fractions 104

Figure 7.7 Detection of BNLPs binding to rβig-h3-sepharsose using silver staining 107

Figure 7.8 Affinity chromatography on columns of rβig-h3 bound to Ni-sepharose 110

Figure 7.9 Identification of matrix proteins potentially interacting with LTBP-2 112

Figure 7.10 Effect of decreased concentration of BNLPM on isolating binding ligands for rβig-h3 and rLTBP-2 115

Figure 7.11 Effect of reducing the size of the sepharose affinity columns on non-specific background binding 115

Figure 7.12 2-DGE analysis of BNLPs bound to rβig-h3 and rLTBP-2 117

Figure 7.13 The effect of a prolonged conditioning step or different solubilisation solution on isoelectric focusing of proteins 120

Figure 7.14 Comparison of the bound proteins to rβig-h3 and rLTBP-2 using 2-D-DIGE technology 124

Figure 7.15 Repeat of CyDye DIGE fluor minimal labelling of bound proteins to rβig-h3 and rLTBP-2 125

LIST OF TABLES

Table 1.1 Key differences between heparan sulphate and heparin 7

Table 1.2 Tissue distribution of type VI collagen using immunofluorescence. 15

SUMMARY

Elastic fibres are important components of the extracellular matrices, being composed of an elastin core and fibrillin-microfibrils around the periphery. Elastic fibre formation is a complex developmentally regulated process whereby fibrillin-microfibrils act as templates for the deposition of elastin. Additional matrix macromolecules, including fibulin-4, fibulin-5 and as yet unidentified heparan sulphate proteoglycans (HSPGs), have also been identified as playing important roles in this process.

Fibrillins-1, -2, -3 and latent transforming growth factor-β binding protein (LTBP)-1, -2, -3, -4, associated components of fibrillin-microfibrils, make up a superfamily of extracellular matrix proteins. Fibrillins and LTBPs share a high degree of structural similarity since they both have rod-like structures of tandem EGF-like 6-cysteine repeats interspersed with unique 8-cysteine motifs. LTBP-1, -3 and -4 covalently bind TGF-β and target and store the latent growth factor in the matrix. Unlike the other LTBPs, LTBP-2 does not bind latent TGF-β and its function is poorly understood. LTBP-2 has been shown to bind fibulin-5, an elastin-binding protein and through this interaction it may target tropoelastin-fibulin-5 complexes on to fibrillin-1-microfibrils during elastic fibre assembly. In order to understand more about the role of LTBP-2 in the assembly of elastic fibres and to identify other novel functions, this study involved screening for potential molecular interactions of LTBP-2 with other matrix components, particularly heparin/HSPGs. In elastic tissues HSPGs are found on cell surfaces as syndecans and glypicans and in basement membranes as perlecan.

Full length human recombinant LTBP-2 (rLTBP-2) was expressed in 293 EBNA cells using a modified pCEP-4 vector and purified by nickel affinity chromatography. Upon validation of the purified protein using western blots, solid phase binding assays were used to screen for interaction between rLTBP-2 and heparin. Heparin serves as a useful model for heparan sulphate; due to the lack of adherence of heparin to microtitre plates heparin-BSA conjugate was synthesised and purified for the binding assays. Recombinant LTBP-2 was found to interact with heparin-BSA conjugates using an established solid phase binding assay. The binding was blocked by the addition of heparin (but not chondroitin sulphate) to the liquid phase, confirming the specificity of the interaction. Furthermore, the binding was blocked by the addition of 5mM EDTA and 5mM EGTA, showing that the interaction was cation (calcium) dependent. An apparent K_d of 14.5±3.7nM was calculated from non-linear regression analysis of the LTBP-2-heparin binding curve, indicating a strong affinity. To identify the location of the heparin binding site(s) on LTBP-2, expression constructs were produced encoding three fragments of LTBP-2, i.e. rLTBP-2NT(H), rLTBP-2C(H) and rLTBP-2CT(H), corresponding to the N-terminal, central and C-terminal regions of the

molecule. Good yields of rLTBP-2C(H) were obtained using the pCEP4-293-EBNA system, and rLTBP-2CT(H) was previously expressed and purified by members of the Gibson laboratory. However, difficulties were encountered with the rLTBP-2NT(H) expression construct and no LTBP-2NT(H) was available during the candidature. The central fragment LTBP-2C(H), (but not the C-terminal fragment LTBP-2CT(H)), was found to bind heparin. However, the apparent K_d of 52.2±6.9nM was significantly higher than that for full length LTBP-2, indicating that LTBP-2C(H) had relatively lower heparin-binding affinity. This result suggested that an additional heparin binding site(s) is present in the N-terminal region of the molecule.

It was considered that the true tissue ligand(s) for LTBP-2 would be a HSPG rather than heparin. Therefore, LTBP-2 was screened for interaction with HSPGs, recombinant syndecans-2 and -4, and endothelial cell-derived perlecan. Interestingly, LTBP-2 bound strongly to r-syndecan-4 but not r-syndecan-2 even though both molecules were produced in the same mammalian cell system and had been screened for binding to HS-binding growth factor, fibroblast growth factor-2. This finding indicates that LTBP-2 does not interact with all HS and must recognise specific microstructures within the heparan sulphate chains. It appears that syndecan-4 is now a strong candidate as mediator of LTBP-2-cell signalling. LTBP-2 was also found to specifically interact with perlecan in a cation-dependent, heparin-inhibitable manner. Confocal immunohistochemical studies using foetal human aorta showed that LTBP-2 and perlecan generally had distinct distribution patterns within the medial layer, located on fibrillin-microfibrils and basement membranes respectively. However, there were small but widespread regions of LTBP-2-perlecan colocalisation which showed a similar pattern to the fibrillin-1-perlecan colocalisation. Thus it would appear that LTBP-2 is present at microfibril-basement membrane interfaces and may be involved in stabilising the interaction between these two structural elements of the matrix. This concept needs to be confirmed at the ultrastructural level. The interaction of LTBP-2 with perlecan during embryonic development is also worthy of investigation.

In parallel studies, a proteomic approach was used to identify other matrix binding proteins for LTBP-2. This was carried out in parallel with another matrix protein of poorly defined function, transforming growth factor-beta-inducible gene-h3 (βig-h3). Recombinant LTBP-2 and βig-h3 coupled to sepharose were used as bait proteins to screen complex mixtures of matrix proteins from the elastic tissue nuchal ligament and basement membrane preparation Matrigel. Initial studies showed that non-specific background binding to these proteins was a major problem. In efforts to overcome this difficulty, binding conditions were varied with limited success. A two-dimensional gel approach was used to fractionate and compare proteins binding to LTBP-2 with those binding to βig-h3. The differentially-

displayed protein spots were to be identified by mass spectrometry. However, complications in comparing the patterns on two separate gels made identification of candidate spots challenging. Finally, CyDye DIGE fluor dyes were used to fractionate proteins binding to LTBP-2 and βig-h3 on the same gel, but unfortunately this work could not be completed in the time frame of the candidature.

CHAPTER 1
INTRODUCTION

1.1 Extracellular Matrix

The extracellular matrix (ECM) is a complex structural entity that surrounds and supports cells that are found within tissues. This ECM is composed of collagens (Wess, 2005), elastin (Mithieux and Weiss, 2005), proteoglycans (PGs) (Hocking *et al.*, 1998) and glycoproteins (Mark, 2002) that include fibrillins, fibronectin, laminins, as well as thrombospondin, tenascin and vitronectin. These components are organised into a meshwork that provides mechanical strength and elasticity to mammalian tissues and also creates a structural framework for cell adhesion and migration. In addition, there are also specialised extracellular matrices that can create barriers for cell penetration and also filtration of macromolecules (Hocking *et al.*, 1998). The ECM is not an inert structure; it is an environment in which there is extensive interplay between the resident cells, structural proteins, growth factors and cytokines and numerous cell surface receptors. It has been shown that there is signalling of one form or another that operates in a bi-directional manner in the ECM and examples of this occur in both normal and disease processes (Hocking *et al.*, 1998).

1.1.1 Collagens

Collagens are major components of the ECM, and the most abundant proteins found in the body. There are at least 26 different types of collagens described in vertebrates thus far that have distinct properties in the matrix. Structurally, collagens are triple helical structures formed by three extended protein chains that wrap around one another. The sequence of these protein chains consists predominately of repeats of G-X-Y (Ottani *et al.*, 2002), where the first position of the repeat is glycine, and the second and third positions of the repeat can be any residues but are frequently proline and hydroxyproline (Kielty, 2002).

Fibrous collagens are synthesised as precursor proteins called procollagens. The procollagen begins to assemble in the endoplasmic reticulum and golgi complexes of fibroblasts cells and some epithelial cells, where they undergo numerous modifications. For example, the specific proline residues in the procollagen molecule are hydroxylated by prolyl-4-hydroxylase and prolyl-3-hydroxylase, and the specific lysine residues are hydroxylated by lysyl hydroxylase. Glycosylation of the hydroxylysine residues within the triple helix also occurs by two enzymes in the rough endoplasmic reticulum (Kielty, 2002).

Following the completion of this process, the procollagens are secreted into the extracellular space where they undergo further modification before the collagen molecules polymerise to form collagen fibrils (Kielty, 2002).

Collagens are major components of skin, ligament, bone, cartilage, tendon, lung and teeth. The most distinctive characteristic feature of collagen is the formation of rigid structures to withstand mechanical force. In the matrix, the distribution and the orientation of collagen reflects the function of the tissue in which it is found. For example, collagen transmits tension in the tendon by running parallel to the axis, lends structural support in skin by forming interlaced and branched structures, while in bone it mineralises to provide tensile strength and in the arteries it limits the expansion of the walls. Alterations in the stability of the triple helical structure of collagens resulting from missense mutations can lead to a range of heritable connective tissue disorders. For example, osteogenesis imperfecta results from mutations in type I collagen, Ehlers-Danlos syndrome type IV from mutations in type III collagen, Alport syndrome from mutations in type IV collagen, and Dystrophic epidermolysis bullosa from mutations in type VII collagen (Masse *et al.*, 2005). However, instability of the collagen structures is not the only way that collagens contribute to the pathogenesis of connective tissue disorders. There is evidence that mRNA levels of collagen I and collagen II are increased during progression of osteoarthritis, suggesting the involvement of both collagens in the development of osteoarthritis (Miosge *et al.*, 2004). In addition, structural remodelling of the left atrial tissue due to increased concentration of collagen I and III has been shown to be responsible in part for the pathogenesis of human arterial fibrillation (Boldt *et al.*, 2004).

1.1.2 Elastin and Elastic fibres

In tissues such as large arteries and lung parenchyma where both strength and extensibility are necessary for proper functioning, collagen fibres are accompanied by elastic fibres in the ECM. This allows the tissue to stretch and recoil without damage (Mecham, 1994). The elastic fibres are composed of two distinct parts, one being an abundant amorphous core component, elastin, which is surrounded by a sheet of fibrillin-rich microfibrils (Cleary, 1996; Kielty *et al.*, 2002; Robb *et al.*, 1999). Elastin in turn is synthesised as a soluble precursor tropoelastin. The tropoelastin molecule is composed of two main domain types; hydrophilic and hydrophobic domains (Miao *et al.*, 2005; Mithieux and Weiss, 2005). The hydrophobic domains are rich in the non-polar residues glycine, valine and proline, which typically occur in repeating motifs. There have been suggestions that these domains are responsible for the self-assembly properties of elastin and for its elastomeric properties (Miao *et al.*, 2003; Miao *et al.*, 2005). Alternating with these domains are

hydrophilic regions which are rich in alanine and contain lysine residues which are destined to be involved in formation of covalent cross-links. Cross-linking is initiated by the extracellular enzymes lysyl oxidase which catalyses the oxidative deamination of lysyl ε-amino groups. This allows the modified groups in the tropoelastin molecule to participate in covalent linkages that form the functional polymer. The cross-linking of tropoelastin is essential for stability and insolubility of the protein.

Tropoelastin is initially secreted primarily from vascular smooth muscle cells and fibroblasts and it has been proposed that tropoelastin is chaperoned to the cell surface by elastin binding protein (Hinek *et al.,* 2004). Secreted tropoelastin monomers then self-aggregate via coacervation, a process that aligns and concentrates the protein into quantised spheres prior to cross-linking (Clarke *et al.,* 2006; Vrhovski *et al.,* 1997). Coacervation is an important prerequisite for cross-linking (Narayanan *et al.,* 1978). The coacervate package remains attached to the cell surface possibly by binding to integrins, glycosaminoglycans (GAG) on cell surfaces, and non-integrin proteins (Broekelmann *et al.,* 2005), which are then released on to the preformed fibrillin-microfibrils. Finally, lysyl oxidase promotes covalent cross-links of tropoelastin molecules to form mature elastic fibres.

Elastogenesis in tissues involves a far more complex biochemical mechanism. This process involves the association of multiple extracellular proteins including fibulin-5, for directing elastin onto the microfibrils (Hirai *et al.,* 2007; Nakamura *et al.,* 2002; Yanagisawa *et al.,* 2002; Zheng *et al.,* 2007) and fibulin-4 which is important for the cross-linking of elastin by lysyl oxidase (McLaughlin *et al.,* 2006). Recent studies have demonstrated that fibulin-4 interaction with lysyl oxidase enhances formation of a ternary complex with tropoelastin (Choudhury *et al.,* 2009). The ability of microfibrillar-associated glycoprotein (MAGP)-1 to interact with tropoelastin (Brown-Augsburger *et al.,* 1994; Jensen *et al.,* 2001) and fibrillin-1 (Brown-Augsburger *et al.,* 1994; Trask *et al.,* 2000a), suggests that MAGP-1 may serve as a bridging molecule between the two elastic fibre components during the assembly of elastic fibres. However, the involvement of MAGP-1 is not crucial for elastic fibre assembly as elastic fibre assembly is normal in mice lacking MAGP-1 (Wagenseil and Mecham, 2007).

Several models have been proposed for the assembly of elastic fibres. One such model involves the self-aggregated tropoelastin on the cell surface interacting with fibulin-4 to aid in the cross-linking of these aggregates by lysyl oxidase (McLaughlin *et al.,* 2006). The aggregates stay attached to the surface of cells long enough for newly secreted tropoelastin to be added to the aggregates. The larger aggregates collected by cells are then transferred onto pre-existing fibrillin-microfibrils. The deposition of elastin aggregates on microfibrils is facilitated by fibulin-5, which is present on the microfibrils. The elastin aggregates on the

microfibrils come together to form larger structures and are further cross-linked by lysyl oxidase to form mature elastic fibre (Choudhury *et al.,* 2009; Hirai *et al.,* 2007; Wagenseil and Mecham, 2007).

It has long been assumed that microfibrils provide a scaffold for elastin assembly before it is displaced to the periphery of the growing fibre (Cleary and Gibson, 1983; Mecham, 1994; Midwood and Schwarzbauer, 2002). Microfibrils are complex structures composed primarily of fibrillins, described in more detail in section 1.2.2.1.

Mutations within the elastin gene cause several elastinopathies in humans. An example is the autosomal dominant cutis laxa (OMIM# 123700), characterised by lax skin due to markedly reduced elastin content of the dermis (Milewicz *et al.,* 2000). The majority of elastin mutations associated with this disease are single nucleotide deletions near the 3'end of the gene (Urban *et al.,* 2005; Zhang *et al.,* 1999). These mutations result in a missense sequence that leads to alterations at the C-terminus of the tropoelastin molecule and thus interferes with deposition of normal elastin in dominant negative fashion (Milewicz *et al.,* 2000). In contrast to the dominant negative mutation typical of cutis laxa, supravalvular aortic stenosis (OMIM# 185500) results from a loss of function mutation that produces haploinsufficiency of the *ELN* gene. Supravalvular aortic stenosis is characterised by narrowing of the ascending aorta and other blood vessels (Dridi *et al.,* 2005). Supravalvular aortic stenosis occurs sporadically or as a familial condition with autosomal dominant traits (Curran *et al.,* 1993; Eisenberg *et al.,* 1964; Ewart *et al.,* 1993; Olson *et al.,* 1993). There have been more than 50 different mutations identified which lead to supravalvular aortic stenosis (Ewart et al., 1994; Ewart et al., 1993; Li et al., 1997; Metcalfe et al., 2000; Urban et al., 2000; Urban et al., 2001). It has been reported that abnormal deposition of elastin in arterial walls of patients with supravalvular aortic stenosis leads to increased proliferation of arterial smooth muscle cells which results in the formation of hyperplastic intimal lesions. This is in accordance with studies of mice hemizygous for the elastin gene, which showed 50% thinner elastic lamellae, with additional lamellar units in the aortae of hemizygous mice compared to wildtype mice (Li *et al.,* 1998b). These findings indicate that reduced levels of elastin mRNA result in the formation of abnormal elastic fibres which in turn lead to an increase in the number of individual lamellae deposited in the aortae during development (Li *et al.,* 1998b). These hemizygous mice also display altered aging processes in the aorta, signalling that the early elastin arrangement determines the way the vessel evolves (Pezet *et al.,* 2008).

Elastin null mice generated by Li *et al.,* (1998a) have highlighted the importance of elastin in development and provided a possible mechanism by which absent or damaged elastin may contribute to the pathogenesis of not only the inheritable disorders, but the more

common disorders such as atherosclerosis. Elastin deficient mice have been shown to be viable, but die within the first week after birth, due to subendothelial accumulation of proliferating smooth muscle cells that eventually obliterate the vascular lumen (Li *et al.*, 1998a). Similar reduction in luminal diameter in the systemic and pulmonary arteries of elastin null mice has also been detected. The results of the null mice studies therefore suggested that cell proliferation is promoted by the absence of elastin, raising the possibility that disruption of elastin by endothelial injury, thrombosis, or inflammation may contribute to obstructive arterial pathology by altering the proliferation rate of vascular cells at the site of injury (Dietz and Mecham, 2000).

In addition to hereditary defects of elastin, uncontrolled protease activity causing destruction of elastin has been implicated in the manifestation of several disease states including emphysema, rheumatoid arthritis, cystic fibrosis, and aortic rupture (Hu *et al.*, 2006).

1.1.3 Proteoglycans

Proteoglycans (PGs) are synthesised by most cells and are abundant components of the ECM, basement membrane (BM) and cell surfaces (Gallagher, 1989; Perrimon and Bernfield, 2001; Staprans *et al.*, 1986). They are primarily composed of a protein core to which GAGs chains are covalently attached (**figure 1.1**). GAG chains are negatively charged, long, unbranched polysaccharides containing repeating disaccharide units of either of two modified sugars, N-acetylgalactosamine (GalNAc) or N-acetylglucosamine (GlcNAc), and an uronic acid, glucuronate or iduronate (**figure 1.1**). The specific GAGs of physiological significance are hyaluronic acid, dermatan sulphate, chondroitin sulphate (CS), heparin, heparan sulphate (HS) and keratan sulphate. HS, CS and

Figure 1.1. Structure of glycosaminoglycans (GAGs) and proteoglycans (PGs). Heparan sulphate (HS), chondroitin sulphate (CS) and dermatan sulphate GAG side chains are linked to a protein core via a serine residue. Hyaluronic acid is not covalently linked to a PG, but synthesised directly into the extracellular space. HS, CS and DS are assembled via a serine residue to a PG backbone. Diagram taken from Taylor and Gallo (2006).

dermatan sulphate are assembled via a serine residue to the protein cores, defining them as PGs. Due to the differences in the basic carbohydrate backbone of the GAG chain, the length of the chains and the subsequent modifications in sulphation pattern, deacetylation and epimerisation of the chains, great diversity in GAG chains can be achieved. These modifications are also the factors that provide for the specific activities of the PG molecules (Taylor and Gallo, 2006). In particular in HS, CS and dermatan sulphate sulphation plays an important role in the GAG chain activity. The exception is hyaluronic acid, which is not sulphated and is not attached to a core protein. GAGs play important roles in biological processes such as in cell signalling and development (Hacker *et al.*, 2005; Lin, 2004), angiogenesis (Iozzo and San Antonio, 2001), axonal growth (Chung *et al.*, 2000), tumour progression (Breborowicz *et al.*, 1996; Breborowicz *et al.*, 1998), metastasis (Breborowicz *et al.*, 1998; Teder *et al.*, 2002) and anti-coagulation (Haslinger *et al.*, 2001; McKee *et al.*, 1996). Heparin and heparan sulphate proteoglycans (HSPGs) have recently been shown to be critical for fibrillin-microfibril assembly (Ritty *et al.*, 2003a; Tiedemann *et al.*, 2001). However, their precise roles are as yet not clear. HS is composed of a repeated disaccharide structure (-4-glucuronic acid-β1-4-N-acetylglucosamine-α1-)*n*, which is modified in varying degrees by N-deacetylation and N-sulphation of the glucosamine, epimerisation of the D-glucuronic acid to L-iduronic acid, and also by additional O-sulphation on both sugars (Sasisekharan *et al.*, 2006). Structurally, what makes heparin distinct from HS is that heparin is more heavily modified (**table 1.1**), although HS can contain heparin-like regions (Taylor and Gallo, 2006). Heparin is less abundant *in vivo*, and is synthesised by, and stored primarily in, mast cells (Forsberg *et al.*, 1999; Humphries *et al.*, 1999; Rose and Page, 2004). HS, on the other hand, is more ubiquitously found on cell surfaces and in the ECM as part of a PG.

There are essentially three broad classes of HSPGs: (1) those that are secreted by cells and located in the ECM, e.g. perlecan, agrin, collagen type XVIII, (2) those associated with the cell membrane, such as glypicans, a family of six HSPGs, which are linked to the cell surface via glycosylphosphatidyl inositol anchors and (3) the transmembrane HSPGs, e.g. the syndecan family, consisting of four members (Beauvais and Rapraeger, 2004). A component of this project is to further define the role of HS-side chains of HSPGs in the assembly of elastic fibres, as well as to verify potential roles independent of elastic fibres for the candidate HSPGs in elastic tissues. Two of the HSPGs, and possible candidates, are discussed in more detail in section 1.1.3.1 and 1.1.3.2.

Table 1.1. Key differences between heparan sulphate and heparin. Table taken and modified from Gandhi and Ricardo, (2008).

1.1.3.1 Perlecan

Perlecan is one of the major components of BM together with collagen IV, laminin and nidogen (Timpl and Brown, 1996). BMs are thin amorphous sheets of specialised ECM that form a close association with adjacent cells and can affect their survival, migration, proliferation and differentiation. They compartmentalise tissues, providing a barrier that allows the filtration of macromolecules while preserving tissue architecture (Miner *et al.*, 2004; Yurchenco *et al.*, 2004). BMs are the first ECM made during embryogenesis, first occurring at embryonic day (E)-3.

The complete sequence of perlecan was determined from a human colon cDNA library (Cohen *et al.*, 1993; Dodge *et al.*, 1991) and is encoded by the HSPG2 gene (Arikawa-Hirasawa *et al.*, 2002; Cohen *et al.*, 1993). Perlecan is a large HSPG (**figure 1.2**) with a mature core protein of approximately 467 kDa. When including the numerous post translational modifications, such as six potential GAG side chains of approximately 30 kDa each, and large number of potential glycosylations (Iozzo *et al.*, 1994), the complete PG could reach the size of 850 kDa (Murdoch *et al.*, 1994). The perlecan core protein contains five distinct domains (**figure 1.2**): domain I, a globular amino terminal domain containing three HS attachment sites; domain II, with four copies of sequences similar to the low-density lipoprotein (LDL) receptor ligand binding repeats; a central domain III, resembling the short arm of laminin chains with three globules and four regions of cysteine rich repeats; domain IV containing immunoglobulin (Ig) repeats; and domain V, a large globular carboxyl-terminal domain resembling a part of the G domain of the laminin A chain where an additional GAG attachment site is present (Kallunki and Tryggvason, 1992).

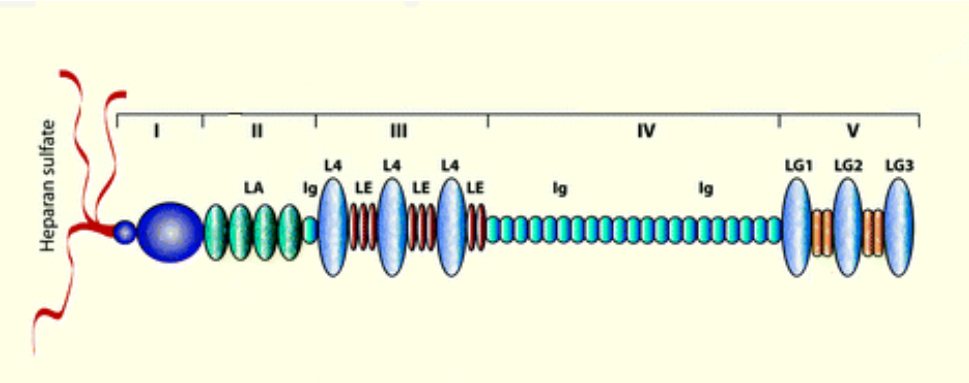

Figure 1.2. Schematic molecular structure of human perlecan. Illustrating the various domains (Roman numerals) and the abbreviations for each module (top). **LA,** LDL receptor type A. **L4,** Laminin type IV domain. **LE,** Laminin EGF-like. **Ig,** Immunoglobulin superfamily. **LG,** Laminin type-G domain. The figure was taken from Whitelock *et al.,* (2008) and modified.

Perlecan protein binds to a number of ECM proteins including fibronectin (Hopf *et al.,* 1999; Hopf *et al.,* 2001), laminin (Friedrich *et al.,* 1999), collagen type IV (Battaglia *et al.,* 1992; Hopf *et al.,* 1999), and fibulin-2 (Heremans *et al.,* 1990; Hopf *et al.,* 1999). Perlecan also binds to cell surface receptors such as α-dystroglycan (Peng *et al.,* 1999) and integrins α2β1, β1 and β3 (Bix *et al.,* 2004; Hayashi *et al.,* 1992). Furthermore, perlecan binds to various growth factors such as platelet derived growth factors (Gohring *et al.,* 1998), fibroblast growth factor -7, and -2 (Govindraj *et al.,* 2006; Mongiat *et al.,* 2000; Smith *et al.,* 2007). Some of these interactions are heparin/HS dependent, some are heparin influenced, and still others are with the core protein that occur independently of heparin/HS. Perlecan's ability to interact with such a wide spectrum of matrix proteins suggests that perlecan is involved in matrix organisation and stabilisation, cell-matrix interaction, and in modulating growth factor signalling for cell growth and differentiation (Farach-Carson and Carson, 2007; Iozzo, 2005; Iozzo *et al.,* 1994; Melrose *et al.,* 2008; Timpl and Brown, 1996). Furthermore, perlecan has been shown to promote mitogenesis and angiogenesis through its interaction with fibroblast growth factor-2 (Aviezer *et al.,* 1994; Iozzo and San Antonio, 2001), and to play key roles in the development of blood vessels and cartilage (Arikawa-Hirasawa *et al.,* 1999; Costell *et al.,* 1999).

Tiedemann *et al.,* (2005) demonstrated the interaction of perlecan with fibrillin-1 microfibrils *in vitro,* as well as the colocalisation of the two proteins close to BM zones in human skin, blood vessels and eyes. The functional relevance of this interaction was also studied through analysis of microfibrils in perlecan knockout mice (Tiedemann *et al.,* 2005). The significant reduction of fibrillin-1-microfibrils at the dermal-epidermal junction

suggested the involvement of perlecan in microfibril assembly (Tiedemann *et al.*, 2005). The combined results of Tiedemann *et al.*, (2005), was used as one of the reasons for selecting perlecan as a potential candidate HSPG for investigation in this project.

Beside tissue development, perlecan plays an important role in embryogenesis. Early studies have shown perlecan expression in pre-implanted embryos prior to the formation of a BM (Dziadek *et al.*, 1985). Perlecan has not only been detected in the blastocyst interior, but perlecan epitopes have been detected on the outer surface of the trophectoderm cells at the time of implantation. The obtained expression pattern of perlecan in developing embryos suggested the potential participation of this HSPGs in blastocyst attachment (Carson *et al.*, 1998; Carson *et al.*, 1993; Smith *et al.*, 1997). These findings supported previous reports of initial embryo attachment to the uterine epithelial surface being via a HS-dependent interaction with its various binding ligands such as laminin and fibronectin (Farach *et al.*, 1987). Aside from the embryo, expression of perlecan has also been detected in uterine tissues of mice during pregnancy (San Martin *et al.*, 2004), thus preparing the uterine microenvironment for embryo attachment (San Martin *et al.*, 2004).

Costell *et al.*, (1999) have demonstrated that almost half of mice lacking the perlecan gene die as embryos around E-11.5 due to either cardiac system failure caused by intrapericardial haemorrhage, or failure of the neural system to develop. Studies of perlecan knockout mice hence highlighted the importance of perlecan in the development of the embryo itself.

1.1.3.2 Syndecans

Syndecans are cell surface HSPGs composed of an extracellular ectodomain specific for each syndecan, a conserved transmembrane domain and a short cytoplasmic domain (Beauvais and Rapraeger, 2004; Couchman, 2003) (**figure 1.3**). The divergent ectodomains share conserved attachment sites for GAGs, predominantly HS (Couchman, 2003). Syndecans interact with matrix proteins (David, 1993), growth factors including vascular endothelial growth factor and basic fibroblast growth factors (Chen *et al.*, 2004; Chernousov and Carey, 1993; Rapraeger, 2000), and possibly growth factor receptors (Mundhenke *et al.*, 2002) via the HS-side chains. The ectodomains can be shed from cells by proteolytic cleavage (Fears *et al.*, 2006; Fitzgerald *et al.*, 2000). Once released from the cell surface, ectodomains can sequester soluble factors and compete for cell surface binding (Bellin *et al.*, 2002; Kato *et al.*, 1998). The cytoplasmic domain contains a region unique to each syndecan (Couchman, 2003). In syndecan-1 the region regulates cell spreading, and actin and fascin bundling (Chakravarti *et al.*, 2005). In syndecan-2, this region has been implicated in matrix assembly in fibroblasts (Klass *et al.*, 2000), and left-right asymmetry in Xenopus (Kramer *et*

al., 2002; Kramer and Yost, 2002). The function of this region in syndecan-3 has not been described, while in syndecan-4 this unique region has been implicated in signal transduction and activation of protein kinase Cα (Horowitz *et al.,* 2002; Lim *et al.,* 2003).

Syndecan-1 is primarily expressed in epithelial (Hinkes *et al.,* 1993) and plasma cells (Seftalioglu and Karakus, 2003), and can also contain CS-GAGs in addition to HS-GAGs (Rapraeger *et al.,* 1985). Syndecan-2 is highly expressed in fibroblasts and endothelial cells (Couchman, 2003; Fears *et al.,* 2006) and is involved in cell adhesion, proliferation, angiogenesis and matrix assembly (Fears *et al.,* 2006; Han *et al.,* 2004; Klass *et al.,* 2000). In addition a role for syndecan-2 has been shown in cell motility (Fears *et al.,* 2006). Syndecan-2 is also expressed in rat hippocampal neurons and interacts with the receptor tyrosine kinase, EphB2, to mediate dendritic spine formation in mice (Ethell *et al.,* 2001). Syndecan-3 is the least investigated syndecan, and similar to syndecan-1 it can contain CS-GAG chains in addition to HS-GAGs (Tkachenko *et al.,* 2005). It has been suggested that syndecan-3 is involved in mediating the formation of neuronal connections during development (Goutebroze *et al.,* 2003), and acts as a receptor for the axonal growth factor, pleiotrophin (Raulo *et al.,* 1994). Syndecan-4 is involved in focal adhesions; *in vitro* binding studies demonstrated that syndecan-4 interacts with cytoskeletal protein, α-actinin (Alexopoulou *et al.,* 2007; Greene *et al.,* 2003). Over-expression of syndecan-4 in the presence of phosphatidylinositol 4, 5 bisphosphate can activate protein kinase Cα and downstream signalling that promotes the formation of focal adhesions and cytoskeletal stress fibres (Oh *et al.,* 1997).

NOTE:
This figure is included on page 10 of the print copy of the thesis held in the University of Adelaide Library.

Figure 1.3. Cell surface HSPGs syndecans. Potential and identified GAG attachment sites are indicated by red lines. The homologous transmembrane domain (dark blue) and intracellular domain (stipple) with conserved tyrosines (dots), as well as the Threonine, Serine, and Proline rich domain of syndecan-3 (crosshatch) are indicated. The image is a modified version of Lopes *et al.,* (2006)**.**

1.1.4 Glycoproteins

Glycoproteins in the ECM generally have structural and adhesive properties. Numerous extracellular glycoproteins have been isolated and characterised as cellular effectors in the matrix which have specific adhesive affinities on one hand for the cell surface and on the other hand for other molecules of the matrix (Mark, 2002). A number of glycoproteins in the matrix are large molecules which are able to mediate cellular activities, both directly through interaction with cell surface receptors such as integrins, and indirectly by structuring a defined 3-dimentional ECM which is required by most cells to express their tissue specific features. Some of these glycoproteins with adhesive properties are fibronectins, laminins, tenascins, vitronectin, thrombospondin, and fibrillins (Mark, 2002).

Fibronectin occurs as a soluble dimer with molecular weight of 540 kDa in plasma or as a fibrillar form in tissue extracellular matrices. Fibronectin has a wide range of biological activities which have been identified through *in vitro* and *in vivo* studies (George *et al.,* 1993; Giancotti and Ruoslahti, 1999; Pearlstein *et al.,* 1980). The importance of fibronectin has been demonstrated by the embryonic lethal effect of the fibronectin knockout in mice. Mice lacking fibronectin die near E-8.5 due to severe defects in embryonic development (George *et al.,* 1993). Morphologically, the foetuses of fibronectin null mice display abnormalities in the heart and vasculature, and have a deformed neural tube. They also lack somites and notochords (Mark, 2002). In humans, mutations in the fibronectin gene have been linked to glomerulopathy with fibronectin deposits (Castelletti *et al.,* 2008). Glomerulopathy with fibronectin deposits is a hereditary kidney disease (OMIM# 601894) which is characterised by proteinuria, microscopic hematuria, and hypertension, that results in end-stage renal failure between second to sixth decade of life (Castelletti *et al.,* 2008).

Structurally, fibronectin is a dimer of two similar polypeptide chains, with each chain being 60-70nm long, 2-3nm thick and having a molecular weight of 220-250 kDa. The two chains are held together by two disulphide bonds near the C-terminal region (Schwarzbauer, 1991; Sottile and Mosher, 1993). There are at least 20 different fibronectin chains that arise from alternative RNA splicing of the primary transcript from the single fibronectin gene (Gutman and Kornblihtt, 1987; Kornblihtt *et al.,* 1984; Schwarzbauer *et al.,* 1987; Schwarzbauer *et al.,* 1983).

Fibrillins are another family of glycoproteins found in the matrix which form polymers that are the backbone structure of microfibrils. Fibrillin-microfibrils support the mature functional integrity of a particular organ by providing organs with a tissue specific architectural framework. Fibrillin-microfibrils also play a role in targeting growth factors to the right location in the ECM of organs (Charbonneau *et al.,* 2004; Sengle *et al.,* 2008). The importance of fibrillins *in vivo* has been highlighted by the development of inheritable

connective tissue disorders as a result of mutations in the fibrillin genes (Kielty *et al.,* 2002; Ramirez and Dietz, 2007). Fibrillins will be discussed in more detail in section 1.2.2.

1.2 Microfibrillar structures of the matrix

Fibrillins and collagen VI are two matrix proteins present in a wide range of tissues that form distinct microfibrils (Cleary and Gibson, 1983; Finnis and Gibson, 1997). These microfibril-forming proteins have been well documented and have been shown to be structurally unrelated. In early studies the structure of these microfibrils and their composition was extensively studied using immuno-electron microscopy techniques and molecular approaches such as tissue extraction and cell culture (Engvall *et al.,* 1986; Furthmayr *et al.,* 1983; Kielty and Shuttleworth, 1995; Prosser *et al.,* 1984). The structure and composition of these microfibrils are described in further detail in section 1.2.1 and 1.2.2.

1.2.1 Collagen VI microfibrils

Type VI collagen microfibrils are 3-5nm in diameter and are present as an extensive network in virtually all types of connective tissues where they are found in loose association with collagen fibres, BMs and cells (Timpl, 1994). Various molecules that specifically associate with type VI collagen include integrins (Pfaff *et al.,* 1993), transforming growth factor-β-inducible gene-h3 (βig-h3) (Gibson *et al.,* 1997; Hanssen *et al.,* 2003) and matrix PGs including biglycan (Wiberg *et al.,* 2002) and decorin (Nareyeck *et al.,* 2004). Biglycan and decorin interact with matrilins in both native and reconstituted microfillar assemblies. Complexes between matrilin-1 and biglycan/decorin are found bound to native collagen VI microfibrils, mediating binding of type VI collagen to major constituents of ECM (Wiberg *et al.,* 2003). Collagen VI microfibrils are involved in ECM signalling and cell-matrix stability, which makes them important components of the matrix (Alexopoulos *et al.,* 2005; Guilak *et al.,* 2006; Poole, 1997).

1.2.1.1CollagenVI

1.2.1.1.1 Structure

Collagen VI monomers have relatively short triple-helical regions that are 60nm long separated by globular domains of 40nm long (Furthmayr *et al.,* 1983; Kuo *et al.,* 1989; Spissinger and Engel, 1995). The collagen VI monomers are comprised of three different polypeptide chains α1 (VI), α2 (VI), and α3 (VI), which have a triple helix flanked with the N-and C-terminal globular domains at each end (**figure 1.4**). Furthermore, the collagen VI polypeptide chains α1 (VI) and α2 (VI) have a molecular mass of 140,000 kDa, and α3 (VI)

has a molecular mass of 260,000-280,000 kDa (Colombatti *et al.,* 1987; Kielty and Shuttleworth, 1997). The stabilisation of these monomers is made possible by both intrachain and interchain disulphide bonds present within the monomers (Odermatt *et al.,* 1983).

Type VI collagen dimers are formed by lateral aggregation of two antiparallel monomers with their helical rods overlapped by about 75nm (**figure 1.4b**). Tetramers, the basic unit of type VI collagen filaments, are formed by the aggregation of two dimers in a parallel fashion, with their ends in register (**figure 1.4b**) (Kuo *et al.,* 1989). Their assembly into tetramers occurs intracellularly, before being secreted into the ECM. The evidence for this was first provided by biosynthetic studies on type VI collagen in fibroblast cultures (Engvall *et al.,* 1986). It is possible that the initial associations for the formation of tetramers are guided by the specific interaction of the inner carboxyl globular domain with a binding site within the triple helix, or perhaps specific interactions between the helical domains. Intramolecular disulphide bonds are responsible for further stabilising the dimers and tetramers of type VI collagen (Engel *et al.,* 1985; Odermatt *et al.,* 1983).

Figure 1.4. Domain organisation and assembly of the alpha chains from collagen VI. **a,** A diagram showing the organisation of domains in α1, α2, and α3 chains of collagen VI. The blue and red rectangle represents the N- and C-terminal domains structurally. The collagenous region is shown in black as a molecular structure. **b,** Diagram showing the assembly of collagen VI microfibrils from three α chains. The formation of monomers, dimers and tetramers occurs intracellularly while the microfibril assembly occurs in the extracellular space. This diagram is taken from Baldock *et al.,* (2003).

Microfibril assembly occurs by end to end overlapping of the outer amino-terminal domains of the tetramers at, or close to, the cell surface (**figure 1.4**), through non-covalent interactions (Bruns *et al.,* 1986; Furthmayr *et al.,* 1983). Several studies have supported these non-covalent interactions of tetramers by showing the ready dissociation of collagen VI microfibrils into tetrameric subunits by treatment with a chaotropic agent (Kuo *et al.,* 1989) or low pH (Spissinger and Engel, 1995). Adjacent microfibrils have been shown in some

tissues, such as the human placenta at term and the rat lung (Reale *et al.,* 2001), to associate laterally to form extensive networks that interact with collagen fibrils, other matrix molecules, and cells (Bruns *et al.,* 1986; Hanssen *et al.,* 2003; Kielty *et al.,* 1998; Reale *et al.,* 2001).

1.2.1.1.2 Function and distribution of Collagen VI

The microfibrillar type VI collagen is one of the major collagenous components of neonatal and foetal skin, where it was first identified beneath the dermal-epidermal junction, the subcutis, and to lesser extent in the dermis, at 6-weeks estimated gestational age (Smith, 1994). As the gestation stages progress, collagen VI was observed to have overlapping distribution with other dermal collagens such as collagen type I, III and V in the dermal and subcutaneous connective tissue of developing skin (Smith, 1994). In the same study by Smith (1994), cell culture experiments showed the deposition of collagen type VI in the matrix precedes the matrix deposition of type I and II collagen. Thus one of the functions proposed for collagen VI from the study was that collagen VI networks provide the framework for assembly of collagen I and III in the matrix.

Collagen VI microfibrils are also found in various other tissues (**table 1.2**). They are a significant component of the hyaline articular cartilage matrix (Ayad *et al.,* 1984; Eyre *et al.,* 1987; Hagiwara *et al.,* 1993; Keene *et al.,* 1988; Poole *et al.,* 1988; Wu *et al.,* 1987) and are localised within the pericellular microenvironment around chondrocytes in adult canine articular cartilage. The results thus suggested that collagen VI coordinates cell-matrix and matrix-matrix interactions and maintains the pericellular microenvironment surrounding articular cartilage chondrocytes (Chang *et al.,* 1997). Type VI collagen is also present in the sub-endothelium, the media and adventitia of the arteries, and in different areas of venous walls where it has been shown to associate with laminins.

In the cornea, collagen VI is the second major collagen present, making up approximately 17% of the total collagen, after collagen I which makes up more than 80% of the collagen in this tissue (Michelacci, 2003; Zimmermann *et al.,* 1986). Indirect immunofluorescence analysis has demonstrated that distribution of collagen VI occurs throughout the corneal stroma and in the Bowman's layer, but not in the epithelium and endothelium cell layers or in the BM (Zimmermann *et al.,* 1986). Therefore, collagen VI appears to be playing an important role in the architecture of the corneal tissue (Michelacci, 2003).

Disruption of the *Col6α1* gene in mice results in significant musculoskeletal changes such as muscle weakness and wasting and contractures of multiple joints (Bertini *et al.,* 2002**)**. Mice lacking collagen VI show signs of accelerated development of hip osteoarthritis, delayed secondary ossification process and reduced bone mineral density (Alexopoulos *et al.,*

2009). Furthermore, the stiffness of the articular cartilage pericellular microenvironment is significantly reduced in collagen VI knockout mice (Alexopoulos *et al.,* 2009). Therefore collagen VI plays a vital role in the mechanical environment of chondrocytes and in modulating chondrocytes and mesenchymal cell differentiation and proliferation activities (Alexopoulos *et al.,* 2009). The skeletal muscles of both homozygous and heterozygous mutant mice showed histological signs of myopathy (Bonaldo *et al.,* 1998). In particular, the myopathy of collagen VI knockout mice had features in common with the human autosomal dominant inherited muscular dystrophy, Bethlem myopathy. Therefore, the *Col6α1* mutant mice was considered as an animal model of Bethlem myopathy (Bonaldo *et al.,* 1998).

Table 1.2. Tissue distribution of type VI collagen using immunofluorescence. Table taken from Keene *et al.,* (1988).

NOTE:
This table is included on page 15 of the print copy of the thesis held in the University of Adelaide Library.

In humans, Hambach *et al.,* (1998) observed an increased amount of type VI collagen in the middle and deep layers of cartilage with moderate osteoarthritis. Horikawa *et al.,* (2004), also reported an increase in the volume of the pericellular microenvironment in which collagen VI is very specifically localised, as well as an increase in the pericellular microenvironment to chondrocyte ratio as cartilage degeneration progressed. From this evidence it was concluded that type VI collagen may be playing an essential role in protecting the chondrocytes from mechanical stress, which occurs in association with the progress of osteoarthritis, by enlarging the volume of the pericellular microenvironment.

1.2.1.1.3 Interaction of collagen VI with other matrix components

Collagen VI has been shown to interact via its triple helical domain with the BM perlecan (Kielty *et al.,* 1991; McDevitt *et al.,* 1991), and with collagen XIV isolated from human placenta (McDevitt *et al.,* 1991). In addition, collagen VI has recently been shown to covalently interact with βig-h3 (Hanssen *et al.,* 2003).

Collagen VI has also been shown to have a high-affinity, specific interaction with decorin (Bidanset *et al.,* 1992). Furthermore, this interaction has been demonstrated to be inhibited by PGs with related leucine-rich repeat modules such as biglycan and fibromodulin, suggesting that a common structural motif is recognised by collagen VI (Bidanset *et al.,* 1992). Wiberg *et al.,* (2001) have further characterised the interaction of both decorin and biglycan as being within a domain localised close to the N-terminal part of the triple helical region of collagen VI. Moreover, a role for these small leucine-rich repeat PGs in the modification of collagen VI supramolecular structure and function has been suggested (Wiberg *et al.,* 2001). An important role of biglycan and decorin is to serve as an adaptor protein connecting collagen VI to the major constituents of the ECM cartilage, collagen II and aggrecan, as well as to a number of procollagen molecules (Wiberg

NOTE:
This figure is included on page 16 of the print copy of the thesis held in the University of Adelaide Library.

Figure 1.5. Model for supramolecular assembly in the ECM of connective tissue. Collagen VI filaments interact with collagen II or aggrecan networks via a complex formed by the small proteoglycans biglycan and decorin with matrillin-1. MATN-1, matrilin-1; BGN, biglycan; DCN, decorin. Diagram modified from Wiberg *et al.,* (2003).

et al., 2003) (**figure 1.5**). These may represent immobilised nucleation centres for collagen II fibril assembly. Thus collagen VI microfibrils act as a scaffold for the formation of the fibrillar collagen network, as well as presenting fibrillogenesis modulators, including decorin and biglycan, in proximity to the growing fibrils (Wiberg *et al.,* 2003).

Ultrastructurally, collagen VI microfibrils are often in close proximity to thicker fibrillin-microfibrils in a wide range of tissues (Wu *et al.,* 1996), suggestive of molecular interaction between the two structures (Finnis and Gibson, 1997). *In vitro* binding studies of MAGP-1 and -2 with native and pepsin-treated collagen VI revealed that MAGP-1, but not MAGP-2, interacts with a site close to the triple helix region of the α3 (VI) chain specifically. This result provided biochemical evidence that fibrillin-microfibrils may indirectly link elastic fibres to collagen fibres via interaction of MAGP-1 with type VI collagen (Finnis and Gibson, 1997).

Collagen VI binds cell surface receptors such as integrin, α1β1 (Loeser, 1997), and α2β1 (Pfaff *et al.,* 1993). Integrins are αβ heterodimeric transmembrane receptors that mediate cell adhesion to the ECM, usually through a Arg-Gly-Asp (RGD) motif, and have widespread essential functions in development, tissue organisation, and the immune system (Roberts and Critchley, 2009). In addition, NG2, a PG widely expressed on numerous cell surfaces, has been shown through solid phase binding assays to interact with type VI collagen (Burg *et al.,* 1996). Kuo *et al.,* (1997) also demonstrated the interaction of intact native collagen type VI with type IV collagen, a major component of BMs, which is of significance as it provides a plausible explanation (section 1.2.1.1.4) for the Bethlem myopathy phenotype, a genetic disease caused by mutation in type VI collagen (Kuo *et al.,* 1997). In addition, an interaction of intact type VI collagen with hyaluronan has been identified though Enzyme-linked Immuno-Sorbent Assay (McDevitt *et al.,* 1991), and a recombinant N-terminal region of human collagen VI has been shown to interact with both heparin and hyaluronic acid (Specks *et al.,* 1992).

1.2.1.1.4 Heritable disorders of collagen VI

Three COL6A genes encode 3 subunits of collagen VI, α-1, α-2 and α-3, respectively. The COL6A1 and COL6A2 genes form a cluster on chromosome 21q22.3, whereas the COL6A3 gene is situated on chromosome 2q37. Deficiency of collagen VI in humans caused by mutations of COL6A genes leads to two main congenital muscular dystrophies; Bethlem myopathy (OMIM# 158810) and Ullrich Congenital Muscular Dystrophy (UCMD) (OMIM # 254090) (Lampe and Bushby, 2005).

Bethlem myopathy is an autosomal dominant form of slowly-progressive muscular dystrophy, and mutations can affect any of the subunits (Mercuri *et al.,* 2005). Mutations in

any of the subunits may interrupt the assembly of collagen VI, and subsequently its anchorage to other ECM, resulting in Bethlem myopathy. The majority of these mutations result in amino-acid substitution, notably glycine, in the triple helix region (Jobsis *et al.,* 1996; Sasaki *et al.,* 2000; Scacheri *et al.,* 2002). This disorder shows mild clinical features with proximal muscle weakness and early contractures predominantly in the fingers. The onset is usually in early childhood or sometimes at birth and occasionally patients become wheelchair-bound after 25 to 40 years of age (Jobsis *et al.,* 1999).

A complete loss or reduction of collagen VI due to mutations in any one of the three collagen VI genes has been associated with UCMD (Brockington *et al.,* 2004; Camacho and Vajda, 2001; Ishikawa *et al.,* 2004). UCMD is a more severe congenital muscular dystrophy, characterised by early onset with patients usually presenting with UCMD at birth or within the first six months of life. UCMD is characterised by generalised and rapid progression of muscle wasting and weakness, proximal joint contractures and distal joint hyperflexibility. UCMD patients usually have an early death due to respiratory failure caused by the rapid progression of the clinical symptoms (Camacho Vanegas *et al.,* 2001; Demir *et al.,* 2002). Other features such as foot deformities, rigidity of the spine, high arched palate, and tendency to have early respiratory failure have also been reported. Immunohistochemical studies have demonstrated a decrease or absence of collage VI in skeletal muscle (Higuchi *et al.,* 2001; Ishikawa *et al.,* 2004), foetal muscles and chorionic villus samples (Brockington *et al.,* 2004) and skin biopsies of patients with Ullrich disease (Higuchi *et al.,* 2001). In addition, through electron microscopy Ishikawa *et al.,* (2004) showed that the absence of collagen VI results in the loss of anchoring between the basal lamina and the interstitium of skeletal muscles in these patients.

1.2.1.2 Transforming growth factor-β-inducible gene-h3 (βig-h3)

Transforming growth factor-β-inducible gene-h3 (βig-h3) is expressed as a 68 kDa protein in humans and is associated with collagen VI. Initially, βig-h3 was identified as two polypeptides in reductive saline extracts of bovine nuchal ligament and named microfibrillar protein (MP78/70) (Gibson *et al.,* 1989). At the time, βig-h3 was assumed to be associated with fibrillin-microfibrils. However, subsequent immuno-electron microscopy studies in a range of tissues showed βig-h3 to be associated with collagen VI microfibrils rather than fibrillin-microfibrils (Gibson *et al.,* 1997).

In humans, Skonier *et al.,* (1992) identified βig-h3 by differential screening of a cDNA library made from A549 human lung adenocarcinoma cells after stimulation with transforming growth factor-β (TGF-β)-1, so as to identify biological markers of TGF-β activity. Amino acid sequencing of this gene showed that βig-h3 is 93% identical to RGD-

CAP, which was isolated from a fibre-rich fraction of pig cartilage (Hashimoto *et al.,* 1997), thus suggesting that RGD-CAP/βig-h3 are orthologs. Furthermore, βigh3 has also been found to have similarities with the rat osteoblast-specific factor-2 (Takeshita *et al.,* 1993), and *Drosophila* fasciclin-1 (Zinn *et al.,* 1988). The high degree of homology between these species therefore suggests the importance of conserved sequences for the function of βig-h3.

1.2.1.2.1 Structure of βig-h3

The predicted 683-amino acid sequence of secreted βig-h3 contains the following important features: 1) a signal peptide sequence at the amino-terminus (residues 1-23), therefore indicating the protein is secreted; 2) an RGD sequence in the carboxyl-terminal domain that can bind integrins (Hynes, 1992) and 3) four repeat domains of 140 residues each that are homologous to the *Drosophila* fasciclin-I, an intercellular adhesion molecule (**figure 1.6**) (Zinn *et al.,* 1988). All the repeats of βig-h3 contain two short regions, H1 and H2 which are highly conserved across species. The H1 and H2 regions are composed of hydrophobic amino acids forming a β-sheet-like structure (Hashimoto *et al.,* 1997), and they may interact with other macromolecules. Evidence suggests that the βig-h3 molecule appears to undergo posttranslational modifications at the carboxyl terminus, to yield a 68-70 kDa isoform (Skonier *et al.,* 1994; Anserson *et al.,* 2004).

NOTE:
This figure is included on page 19 of the print copy of the thesis held in the University of Adelaide Library.

Figure 1.6. Schematic diagram of the domain structure of βig-h3 molecule. The signal peptide (S), the cysteine-rich region (C), the four repeated fasciclin like-domains (I-IV), and the RGD sequence. The photograph is modified from Hanssen *et al.,* (2003).

1.2.1.2.2 Possible function of βig-h3 and its interaction with other matrix proteins

A possible physiological function for βig-h3 is to serve as a bifunctional linker protein, interconnecting different matrix components with each other and resident cells (Billings *et al.,* 2000; Billings *et al.,* 2002; Gibson *et al.,* 1997). It has been shown through quantitative binding assays using purified recombinant (r) full length βig-h3 (rβig-h3) and human bladder fibroblast cells that βig-h3 functions as an adhesion molecule (Billings *et al.,* 2002). The presence of actin stress fibres within the seeded cells further suggests that βig-h3 supports attachment and spreading of cells (Billings *et al.,* 2002). Stress fibre formation as a result of actin polymerisation is one response of cells following adhesion to the ECM. βig-h3

mediates the adhesion of several other cell types (Kim *et al.,* 2002) including dermal fibroblast cells (LeBaron *et al.,* 1995), corneal epithelial cells (Kim *et al.,* 2000), bronchial smooth muscle cells (Billings *et al.,* 2000) and human astrocyte cells (Kim *et al.,* 2002). The mechanisms through which βig-h3 mediates cell adhesion and spreading have also been investigated. Blocking experiments using various antibodies to integrin subunits have suggested the involvement of α6β4 integrin in βig-h3 mediated adhesion of astrocyte cells (Kim *et al.,* 2002). Also a report by Ohno *et al* (1997), suggested that βig-h3 enhanced the spreading of fibroblasts via integrin α1β1 and that its RGD motif was not necessary for mediating cell spreading. Similar conclusions on the role of βig-h3 in mediating cell adhesions were reached from other studies. For example, Kim *et al.,* (2000) demonstrated that two conserved amino acids, aspartic acid and isolucine, near H2 in the second and fourth repeated domains of βig-h3, were necessary for mediating human corneal epithelial cell adhesion by binding to α3β1. Kim *et al.,* (2002) demonstrated βig-h3 motifs containing tyrosine and histidine and many leucine/isoleucine amino acid residues flanking the tyrosine and histidine are part of the αvβ5 integrin binding motif in βig-h3, promoting human lung fibroblast cell adhesion. Other studies have shown that βig-h3 can interconnect with other matrix proteins. For example, solid phase binding studies showed the stable binding of βig-h3 to collagen I and fibronectin, which are abundant glycoproteins of the ECM (Billings *et al.,* 2000; Billings *et al.,* 2002). Overall, these results verify the proposition that βig-h3 is capable of interacting with a range of matrix proteins and integrins.

βig-h3 is a collagen VI-associated protein, as βig-h3 has been demonstrated to co-purify with collagen VI microfibrils extracted from foetal nuchal ligament, even under denaturing conditions. The analysis of the molecular composition of the microfibrils by SDS-PAGE and immunoblotting showed that βig-h3 was covalently bound to collagen VI by intermolecular reducible cross-links (Hanssen *et al.,* 2003). Furthermore, ultrastructural analysis of the purified collagen VI microfibrils revealed that βig-h3 was predominantly associated with at least some of the microfibrils from nuchal ligament, and immunogold labelling localised the covalent binding site of βig-h3 to the N-terminal region of the collagen VI molecule. The demonstrated interaction of collagen VI and βig-h3 *in vivo* suggests that they are likely to be important for the normal development and morphology of a range of tissues including the cornea.

In vitro binding assays using rβig-h3 protein found that it bound native and pepsin-treated collagen VI, and the binding site was identified to be at the N-terminal end of the triple helix (Hanssen *et al.,* 2003). Further analysis showed that the binding characteristics between rβig-h3 and collagen VI were those of a strong but reversible non-covalent interaction. These findings indicated that βig-h3 possesses both covalent and non-covalent

binding activities with collagen VI suggesting that βig-h3 may play an important role in collagen VI biology in developing tissues. These roles of βig-h3 therefore may be in cell-microfibril interactions, and in the organisation and modulation of different collagen VI architectures to suit particular tissue environments (Hanssen *et al.,* 2003). The important physiological functions of βig-h3 are being increasingly realised. In order to further define the role of this protein in living organisms, the interactions of βig-h3 with a wider spectrum of matrix proteins will be investigated as part of my project.

1.2.1.2.3 Expression and tissue distribution of βig-h3

Investigations through northern blot analysis have demonstrated that βig-h3 is widely distributed in various tissues such as the lung, heart, spleen, kidney, liver, adrenal glands and in the growth plate of new born pigs (Hashimoto *et al.,* 1997). Furthermore, βig-h3 expression has been identified in a variety of human and mouse tissues. During mouse development, βig-h3 expression is first detected during E-15.5 and is sustained until E-18.5 with localisation in the corneal epithelium and stroma (Ferguson *et al.,* 2003). The highest expression levels were found in the human corneal epithelium (Escribano *et al.,* 1994), adult human skin (LeBaron *et al.,* 1995) and in uterine tissue of both species. In addition, moderate mRNA levels of βig-h3 were found in the heart, breast, prostate, skeletal muscle, testes, thyroid, kidney, liver and stomach tissues of humans (Skonier *et al.,* 1994). However, the expression of βig-h3 was absent from the brain (Escribano *et al.,* 1994), spleen, and parathyloid tissues of humans (Skonier *et al.,* 1994).

At the protein level, the distribution of βig-h3 was examined in foetal bovine tissues (Gibson *et al.,* 1997). Analysis showed βig-h3 had extensive co-distribution with type VI collagen in developing nuchal ligament, aorta, lung and mature cornea (Gibson *et al.,* 1997). Immunoreactive material was also present in capsule and tubule BMs of developing kidneys, and reticular fibres in foetal spleen. The study thus revealed βig-h3 to be a widely-expressed component of the ECM in a number of organ systems where it associates with other matrix macromolecules. In normal adult skin, βig-h3 is abundant in the epidermis and the dermis, and it has been suggested that this protein may play a role in wound healing (LeBaron *et al.,* 1995). In fact, Cha *et al.,* (2008), demonstrated fibroblasts from chronic wounds show decreased differential expression of βig-h3 using differential display analysis.

1.2.1.2.4 Diseases associated with βig-h3

Mutations in the coding region of the βig-h3 gene is linked to human autosomal dominant corneal dystrophies (Fujiki *et al.,* 1998; Munier *et al.,* 1997). More than 20 mutations in the βig-h3 gene have been identified, and these have been shown to cause

distinct phenotypic characteristics (Klintworth, 2003). The most common mutation identified in βig-h3 (R124C) is on the N-terminal side of its first fasciclin domain (Munier *et al.,* 2002; Nakamura *et al.,* 2002), but others are in the third (P501T) (Ha *et al.,* 2000) and fourth (L518P) fasciclin domains (Hirano *et al.,* 2000; Yamamoto *et al.,* 1998). These mutations are believed to cause the βig-h3 protein to denature, and result in the formation of amyloidogenic intermediates that eventually precipitate in the cornea (Munier *et al.,* 1997). This condition results in a progressive loss of vision, which can ultimately lead to blindness. Similar corneal opacity has been identified in transgenic mice in which human βig-h3 was over expressed (Kim *et al.,* 2007). From these findings it was concluded that βig-h3 needs to be properly expressed for normal development of the anterior segment of the eye (Kim *et al.,* 2007). The anterior segment of the eye in vertebrates is structurally defined by the cornea, iris, ciliary body and the lens (Pei and Rhodin, 1970). Therefore, βig-h3 plays a vital role in the corneolenticular adhesion and the normal development of the cornea during ocular morphogenesis, and specific changes in its primary protein sequence could alter its functional role in the corneal ECM (Billings *et al.,* 2000; Kim *et al.,* 2007).

Furthermore, a complex relationship between βig-h3 and cancer has been established (Sasaki *et al.,* 2002). βig-h3 has been shown to be up-regulated in colorectal carcinoma when compared with the normal colonic mucosa (Kitahara *et al.,* 2001). Also, βig-h3 gene expression has been found to be increased in most of the highly invasive breast cancer cell lines, but not in the weakly invasive cell lines (Zajchowski *et al.,* 2001), and in lung cancer as well (Sasaki *et al.,* 2002).

1.2.2 Fibrillin-microfibrils

Fibrillin-microfibrils are individually 10-12nm in diameter (Rosenbloom *et al.,* 1993) and are found in association with elastin in elastic fibres present in some tissues (Kielty *et al.,* 2005). These tissues include the lungs, skin and large blood vessels as mentioned previously. They also occur as elastin-free bundles in tissues such as kidney, ocular zonule, and spleen (Ashworth *et al.,* 2000; Cleary and Gibson, 1983; Gibson and Cleary, 1987; Henderson *et al.,* 1996; Keene *et al.,* 1991; Kielty *et al.,* 2002). In contrast to type VI collagen microfibrils, fibrillin-microfibrils appear to be complex structures that may contain or be closely associated with a number of glycoproteins in a tissue-specific manner (Kielty, 2006) including MAGPs (Gibson *et al.,* 1996; Gibson *et al.,* 1991; Trask *et al.,* 2000b), latent transforming growth factor-β binding proteins (LTBPs) (Dallas *et al.,* 2000; Dallas *et al.,* 1995; Isogai *et al.,* 2003; Sakai *et al.,* 1986), Emilins (Bressan *et al.,* 1993; Colombatti *et al.,* 2000), fibulins (Reinhardt *et al.,* 1996b; Roark *et al.,* 1995), and PGs (Kielty *et al.,* 1996; Tiedemann *et al.,* 2005; Unsold *et al.,* 2001). However, fibrillin molecules are the primary

components that assemble to form the scaffold of fibrillin microfibrils, and to date three fibrillins, namely fibrillins-1, -2 and -3, have been identified (Charbonneau *et al.,* 2003; Corson *et al.,* 1993; Nagase *et al.,* 2001; Sakai *et al.,* 1986; Zhang *et al.,* 2005).

Microfibril assembly is a multi-step cell-associated process with one of its initial steps involving N- to C-terminal self interactions of fibrillins (Hubmacher *et al.,* 2008; Marson *et al.,* 2005; Reinhardt *et al.,* 1996a). In addition to linear N-to-C terminal interactions, lateral homotypic interactions in various regions of fibrillin-1 may be crucial for the stabilisation of the initial multimers or the lateral associations of individual microfibrils (Marson *et al.,* 2005; Trask *et al.,* 1999).

1.2.2.1 Fibrillins

1.2.2.1.1 Structure of fibrillins

Structurally, fibrillins are large 350 kDa rod-like glycoproteins that are calcium binding. All three fibrillins have very similar complex multidomain molecular structures that are dominated by calcium binding epidermal growth factor (cbEGF)-like domains. As expected these cbEGF-like domains bind calcium and it has been shown through ultrastructural and X-ray diffraction studies that binding of calcium profoundly influences the packing and periodicity of isolated microfibrils and hydrated microfibril arrays (Cardy and Handford, 1998). Calcium binding is also necessary for fibrillin interaction with other proteins and for protection from proteolysis (Downing *et al.,* 1996; Reinhardt *et al.,* 1997a; Reinhardt *et al.,* 1997b). Mutations in the cbEGF-like domains in fibrillin-1 have been claimed to introduce protease-sensitive sites into the molecule, causing significant structural changes (Cardy and Handford, 1998; McGettrick *et al.,* 2000). The EGF-like domains of fibrillins are interspersed by an 8-cysteine (8-cys) domain (Hubmacher *et al.,* 2006) (**figure 1.7**). Furthermore, fibrillins contain two hybrid domains which are composed of 8-cysteine modules and cbEGF-like domains (Ramirez and Sakai). The N- and C-terminal regions are homologous with the respective segments of LTBPs and fibulins (Giltay *et al.,* 1999; Ramirez and Sakai). All three fibrillins also have cleavage sites of furin-type proprotein convertases at their N- and C-termini, and processing at these sites may be important steps in regulating fibrillin assembly (Raghunath *et al.,* 1999; Ritty *et al.,* 1999). It has been widely considered that microfibrils assemble pericellularly, following furin processing, through high affinity N- and C-terminal interactions (Hubmacher *et al.,* 2006; Kielty, 2006).

The major differences between the fibrillins are in the unique hydrophobic region towards the N-terminal that may act as a hinge region, the number of intergrin-binding RGD sequences they contain and in the number of glycosylation sites (Hubmacher *et al.,* 2006; Kielty *et al.,* 2005; Ramirez *et al.,* 2007). The predicted hinge region, which is a 58 amino

acid region, is rich in proline in fibrillin-1, while the corresponding region in fibrillin-2 is rich in glycine. In fibrillin-3 however both glycine and proline are equally present in this region. It has been speculated that the hinge region is the flexible region of the protein which allows bending of the fibrillin molecule (Baldock *et al.,* 2001; Baldock *et al.,* 2006). While fibrillin-1 has only one RGD putative cell recognition site, there are two RGD cell recognition sites in fibrillin-2 and -3. Furthermore, there are 15, 12 and 10 potential *N*-glycosylation sites in fibrillin-1, -2 and -3 respectively (Corson *et al.,* 1993; Corson *et al.,* 2004).

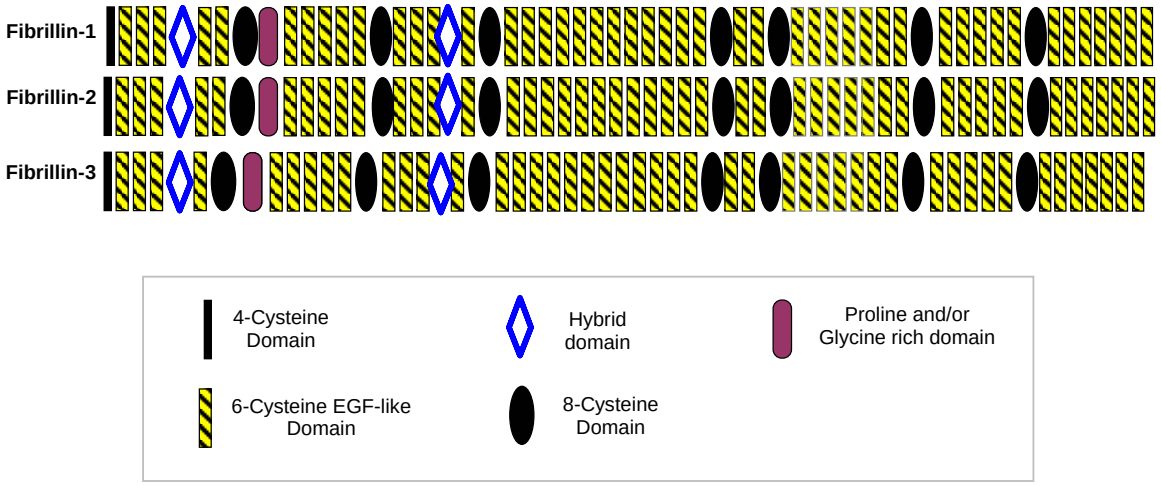

Figure 1.7. Schematic representation of the three fibrillins, showing high homology between them with some distinct differences. Fibrillin-3 lacks one of the EGF-like domains near the N-terminal region. The diagram for fibrillin-1 and -2 is generously given by Dr. Mark Gibson.

1.2.2.1 2 Tissue distribution of Fibrillins

All three fibrillins are expressed during human development, but fibrillin-1 is by far the most abundant isoform in adult tissue (Charbonneau *et al.,* 2003; Corson *et al.,* 2004; Quondamatteo *et al.,* 2002). Moreover, investigators have documented the overlapping but distinct distribution pattern of fibrillins in various tissues. Quondamatteo *et al.,* (2002) showed, using immuno-labelling techniques, that the localisation patterns of fibrillins-1 and -2 were overlapping in embryonic and early foetal human tissues such as in the skin, central nervous system anlagen, ganglia, aorta, lung, and heart. However there were differences in other human tissues such as kidneys, and notochords. Fibrillin-3 has a similar pattern of expression to the other two fibrillins in most human foetal tissues except in the kidney and lung, where it appeared to be absent from glomerular and tubular regions of the kidney and

from the blood vessels of the lungs (Corson *et al.,* 2004). The distribution of fibrillins has also been studied in canine flexor digitorum profundus tendons. Fibrillin-1 is present in the outer-most cell layer of tenocytes, while fibrillin-2 is detected in the pericellular matrix of linearly-arrayed internal tendon cells (Ritty *et al.,* 2002; Ritty *et al.,* 2003b).

The gene expression patterns of fibrillins have also been studied through northern blotting in embryonic and early human foetal tissues. Generally fibrillin-2 is expressed during organ development and it decreases rapidly thereafter (Zhang *et al.,* 1995). In adults fibrillin-2 is found in limited elastic tissues such as cartilage (Zhang *et al.,* 1995). In contrast fibrillin-1 expression increases at a gradual rate during development and fibrillin-1 continues to be expressed throughout postnatal growth and in adults (Kelleher et al., 2004). Studies by Quondamatteo *et al.,* (2002) have demonstrated fibrillin-1 gene expression in human embryos as early as the time of gastrulation and all the way through to postnatal life. Similar to fibrillin-2, fibrillin-3 is mainly expressed in foetal tissues associated with microfibrils close to amorphous elastin (Corson *et al.,* 2004).

1.2.2.1.3 Functions of fibrillins

Mouse models are providing powerful tools for unravelling the biological roles of fibrillins (Dietz and Mecham, 2000). Pereira *et al.,* (1997) created fibrillin-1 gene-targeted mouse models, giving rise to a mutant allele (mgΔ) that resulted in a ten-fold reduction in fibrillin-1 expression. The heterozygous fibrillin-1 mutant mice expressed very low levels of mutant protein and were morphologically and histologically indistinguishable from wild type mice. Homozygous mutant mice which produced only small amounts of mutant fibrillin-1, appeared normal at birth but died of vascular complications prior to weaning (Arteaga-Solis *et al.,* 2001). Some mice showed thinning of the proximal aortic wall, which suggested that they experienced aneurismal dilatation of the aorta as in human marfan syndrome (section 1.2.2.1.5). Substantially reduced extracellular fibrillin-1 staining but normal elastin staining suggested that organised elastic fibres can accumulate in the absence of normal fibrillin-1-rich microfibrils.

Mutant mouse models have been used to demonstrate the role of fibrillins in controlling TGF-β signalling in the ECM. A deficiency of fibrillin-1 gene expression in mice leads to TGF-β-mediated failure of distal alveolar septation (Neptune *et al.,* 2003). The mechanism by which fibrillin-1 targets TGF-β and regulates its activation is through interacting with LTBPs (Dallas *et al.,* 1995; Isogai *et al.,* 2003; Rifkin, 2005). The interaction of TGF-β with LTBPs is discussed in more detail in section 1.2.2.2.

Fibrillin-microfibrils are involved in sequestration of another of the TGF-β-related growth factors, bone morphogenetic proteins (BMPs) (Gregory *et al.,* 2005; Sampath *et al.,*

1990). However, the mechanisms that modulate extracellular control of BMP bioavailability differ from those of TGF-β. Unlike TGF-β, BMPs are directly targeted to microfibrils by non-covalent association between the pro-domain of BMP-7 and the N-terminal of fibrillins (**figure 1.8**) (Sengle *et al.,* 2008). It appears that through the interaction with the pro-domain of BMP-7, fibrillins target and modulate the activity of this growth factor in the matrix (Gregory *et al.,* 2005; Sengle *et al.,* 2008). Mice with fibrillin-2 mutations demonstrate this biological role of fibrillin-microfibrils. Fibrillin-2 knockout mice display auditory defects and limb-patterning defects, which include fusion of third and fourth phalanges that are not observed in fibrillin-1 null mice (Arteaga-Solis *et al.,* 2001; Chaudhry *et al.,* 2001; Penner *et al.,* 2002). Digit formation is the combined result of chondrogenic outgrowth and interdigital cell death. This process is under the control of several signalling molecules, some of which are BMPs (Dahn and Fallon, 2000). Therefore, it has been hypothesised that the defects observed in the outer extremities are due to either aberrant fibrillin-2-rich microfibrils in the cartilaginous limb skeleton, or impaired commitment of mesenchymal cells in the prospective interdigital tissue to undergo apoptosis due to failed activation of BMP-induced cell death (Arteaga-Solis *et al.,* 2001).

Mice lacking both fibrillins (fib-$1^{-/-}$; fib-$2^{-/-}$) die in the middle of gestation (E1-4.5), which is significantly earlier than in both fibrillin-1 (fib-$1^{-/-}$) and fibrillin-2 (fib-$2^{-/-}$) mutant mice (Carta *et al.,* 2006). Histologically, the aortic media of these double mutant mice is poorly developed, due to impaired or delayed elastogenesis (Carta *et al.,* 2006). The heterozygous fib-$1^{-/-}$; fib-$2^{+/-}$ mutant mice survive through neonatal and early postnatal life, while 50% of heterozygous fib-$1^{+/-}$; fib-$2^{-/-}$ mutant mice die as embryos (Carta *et al.,* 2006). The findings from the analysis of the double mutant mouse models indicated that fibrillin-1 compensates for the absence of fibrillin-2 during embryonic development (Carta *et al.,* 2006). Collectively these mouse models demonstrate the importance of fibrillins in organ formation and tissue homeostasis.

1.2.2.1.4 Interaction of fibrillins with other matrix components

One of the first functions suggested for microfibrils in the extracellular space was to provide a molecular scaffold for the deposition and alignment of tropoelastin molecules (Kielty et al., 2005; Kielty et al., 2002; Mecham, 1994). This alignment presumably allows for proper cross-linking and maturation of the elastic fibre as previously mentioned (section 1.1.2). The prevalence of fibrillins within microfibrils made them candidates for the binding and alignment of tropoelastin molecules. Trask *et al.,* (2000b) has showed that recombinant and purified tropoelastin binds to recombinantly expressed N-terminal fragments of fibrillin-1 (**figure 1.8**) and fibrillin-2. Using solid phase binding assays and co-immunoprecipitation

experiments the site of interaction on fibrillin-2 was localised to a region encompassing the glycine-rich region down-stream EGF-like domains and most of the second 8-cys domain. From the results the authors concluded that both fibrillins could be playing a role in the organisation of the elastic matrix. Following from this, Rock *et al.,* (2004), demonstrated with the use of *in vitro* binding assays additional tropoelastin binding sites on fibrillin-1 (**figure 1.8**). It is possible that the ability of tropoelastin to bind to both fibrillins may be an advantage that ensures that elastin can assemble on any microfibrillar bed.

Other matrix components that have been identified as binding ligands for fibrillin-1 include three of the five members of the fibulin family, fibulin-2, -4 and -5 (**figure 1.8**) (Choudhury *et al.,* 2009; El-Hallous *et al.,* 2007; Freeman *et al.,* 2005). All three fibulins have been shown to not just interact with fibrillin-1, but to associate with microfibrils (El-Hallous *et al.,* 2007). Indirect immunofluorescence was used to demonstrate the colocalisation of endogenously-produced fibulin-2 and exogenously-produced fibulin-4 and -5 with immature and mature microfibrils. Thus fibulin-2, -4 and -5 can associate with microfibrils at different stages of maturity (El-Hallous *et al.,* 2007). The interaction of fibrillin-1 with fibulin-2, -4 and -5 has been suggested to be important in the assembly of elastic fibres (El-Hallous *et al.,* 2007; Freeman *et al.,* 2005). Choudhury *et al.,* (2009) further defined the roles of fibulin-4 and -5 in biogenesis of elastic fibres, and respectively suggested an important role in regulating elastin cross-linking and elastin deposition on microfibrils for these two.

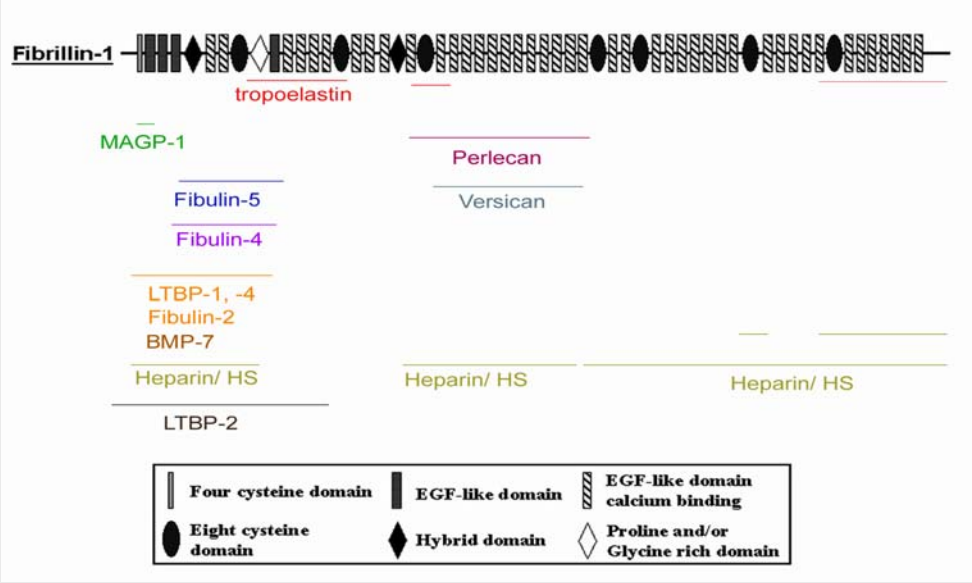

Figure 1.8. The schematic illustration of the binding sites of various ECM components on fibrillin-1.

Fibrillin-microfibril assembly itself is a poorly understood process. Recent cell culture and RNA interference studies have demonstrated the deposition of microfibrillar arrays is dependent on the assembly of fibronectin (Kinsey *et al.,* 2008; Sabatier *et al.,* 2009). The knockdown of fibronectin in human dermal fibroblasts using RNA interference resulted in severe reduction in both fibronectin and fibrillin-microfibril deposition. Furthermore, specific antibodies to integrins α5 and β1 were shown to inhibit fibronectin assembly and, as a consequence, fibrillin-microfibril assembly. Therefore, α5β1 integrin is also critical for the deposition of fibrillin-1 microfibrils (Kinsey *et al.,* 2008).

It is becoming increasingly clear that fibrillin-1 is a major heparin/HS binding molecule (Cain *et al.,* 2005; Ritty *et al.,* 2003a; Tiedemann *et al.,* 2001) (**figure 1.8**). Based on inhibition of fibrillin-1 assembly by heparin/HS, it has been hypothesised that interaction of fibrillin-1 with HSPGs is necessary for mediating fibrillin-1 assembly (Ritty *et al.,* 2003a; Tiedemann *et al.,* 2001). A study by Cain *et al.,* (2005), demonstrated that heparin has no effect on the homotypic fibrillin-1 (N- and C- terminal) interaction using solid phase inhibition assays. However, the same group show that heparin does compete with both MAGP-1 and tropoelastin for binding to fibrillin-1. These findings showed the potential regulatory role of heparin 1) on deposition of elastin on fibrillin-1 microfibrils and 2) on the association of MAGP-1 with the fibrilln-1 microfibrils. Since HS occurs in two main sites *in vivo*, on cell surfaces and in BMs in the matrix, interaction of fibrillin-1 with HS at both sites was considered important (Cain *et al.,* 2005). For instance, HS on cell surfaces may be involved in alignment and multimerisation of fibrillin-1 molecules (Cain *et al.,* 2005). Therefore, HSPGs are major players in elastic fibre organisation.

Recently double immunofluorescence studies demonstrated the colocalisation of fibrillin-1 and perlecan in fibroblast cultures as well as in dermal and ocular tissues (Tiedemann *et al.,* 2005). Furthermore, double immunogold labelling confirmed the colocalisation of perlecan to microfibrils in various tissues at ultrastructural level. A detailed study of the interactive regions by solid phase binding assays revealed that perlecan binds to the central region of fibrillin-1 (**figure 1.8**). This result suggested that the interaction between perlecan and fibrillin-1 is important to anchor the microfibrils to the BM (Tiedemann *et al.,* 2005). Another PG, decorin, has been shown to interact with the N-terminal region of fibrillin-1 near the proline rich region through immunoprecipitation studies (Kielty *et al.,* 1996; Trask *et al.,* 2000a). This interaction is important for fibrillin formation as treating purified microfibrils with chondroitinase ABC disrupts the beaded microfibrillar architecture. The significance of fibrillins interacting with decorin in elastic fibre assembly or function is not yet known. However, decorin has been shown to influence collagen fibril assembly both *in vitro* and *in vivo* (Danielson *et al.,* 1997) by regulating fibre diameter and interfibrillar

spacing. Thus decorin may play a similar role in regulating the assembly of microfibrils. Isogai *et al.,* (2002), also revealed that versican has the ability to bind centrally to the fibrillin-1 molecule. However, its non-periodic association with microfibrils indicates that versican is probably not an integral structural component. Instead because of the ability of versican to bind hyaluronan, it has been suggested that it connects microfibrils to a hyaluronan-rich matrix (Isogai *et al.,* 2002).

Fibrillins can communicate with neighbouring cells through their RGD sequence by interacting with cell surface integrin receptors (Lee *et al.,* 2004). Several studies using rfibrillin-1 fragments demonstrated integrins αvβ3 and α5β1 to be major receptors mediating adhesion to fibrillin-1 peptides (Bax *et al.,* 2003; Pfaff *et al.,* 1996), which in turn influence cell shape, migration and ECM deposition. Fibrillin-1 has further been shown to mediate cell adhesion through αvβ6 (Jovanovic *et al.,* 2007). Integrin αvβ6 is expressed at low levels in adult tissues and is up-regulated in response to injury, inflammation and wound healing, as well as during development (Jovanovic *et al.,* 2007). Therefore, fibrillin-1 acts as a linker molecule between cells and their micro-environment and may play a role in regulating cell behaviour in connective tissue.

1.2.2.1.5 Congenital disorders related to fibrillins

Human disorders caused by mutations in fibrillins include marfan syndrome and congenital contractural arachnodactyly (CCA) (Pyeritz, 2000; Ramos Arroyo *et al.,* 1985). Marfan syndrome (OMIM # 154700) is an autosomal dominant disorder that occurs as a result of mutations in the fibrillin-1 gene located on the long arm of chromosome 15 (Milewicz *et al.,* 2000). The majority of these mutations are missense or nonsense point mutations (Dietz and Pyeritz, 1995; Eldadah *et al.,* 1995; Milewicz *et al.,* 2000; Zhao *et al.,* 2009). However, exon deletions in fibrillin-1 have also been reported in children with severe marfan syndrome (Blyth *et al.,* 2008). Marfan syndrome is characterised by cardiovascular, ocular and skeletal defects (Whiteman and Handford, 2003). The skeletal abnormalities of marfan syndrome are the most striking features. The skeletal complications typical of marfran syndrome patients include arachnodactyly, dolichostenomelia, pectus deformities and kyphoscoliosis. The most life threatening aspect of this disease is the cardiovascular complications (Whiteman and Handford, 2003). The most common cardiovascular abnormalities caused in marfan syndrome patients are mitral valve prolapse and more importantly dilation of the ascending aorta owing to cystic medionecrosis. The major ocular complications seen in marfan syndrome patients are ectopia lentis and myopia. Additional manifestations seen in a number of individuals with marfan syndrome include congenital pulmonary emphysema (Hennekam, 2005).

The underlying pathogenesis of these conditions was originally considered to be due to the loss of fibrillin-1 as a structural component that prevented proper assembly of elastic fibres (Ng *et al.,* 2004). Therefore, marfan syndrome patients were thought to lack functional elastic fibres starting from late foetal development. However, the structural and functional integrity of normal vessel walls is maintained by elastic lamina anchored to the intima and smooth muscle cells through connecting filaments of fibrillin-1. Consequently, the loss of these filaments subsequently initiates vascular smooth muscle cells to over-produce matrix elements and elastin proteases including matrix metalloproteinases -2 and -9, resulting in medial degeneration. Therefore, the marfan vascular phenotype develops gradually throughout life rather than developing from prenatal defect.

As mentioned in section 1.2.2.1.3, fibrillin-microfibrils are involved in sequestration and proper activation of TGF-β. There has been an important discovery that the dysregulated TGF-β signalling is linked to the clinical severity of marfan syndrome (Neptune *et al.,* 2003). Subsequently, the association of fibrillin-1 mutations and dysregulation of TGF-β signalling have been linked to the progression of mitral valve prolapse, muscle hypoplasia and aortic aneurysm (Habashi *et al.,* 2006; Ng *et al.,* 2004).

The fibrillin-2 gene has been mapped to chromosome 5q23-31 through *in situ* hybridisation (Lee *et al.,* 1991; Putnam *et al.,* 1995). Mutations in this gene have been shown to cause CCA (OMIM # 612907) which is an autosomal dominant condition that is clinically related to marfan syndrome (Chaudhry *et al.,* 2001). CCA patients present with similar skeletal features to marfan patients e.g. they have tall, slender bodies with long limbs. CCA is also characterised by a crumpled appearance to the pinna of the external ear. The major difference between the two disorders is that CCA patients do not typically present with the ocular and life threatening cardiovascular complications associated with marfan syndrome (Whiteman and Handford, 2003).

1.2.2.2 Latent transforming growth factor-β binding proteins

LTBPs and fibrillins constitute a family of large extracellular glycoproteins. LTBPs have molecular masses between 120-220 kDa, so they are considerably smaller than fibrillins. LTBPs are mainly composed of repeated structures of EGF-like domains and conserved 8-cys domains. There are four human LTBP genes (Oklu and Hesketh, 2000; Saharinen *et al.,* 1999; Shipley *et al.,* 2000) (**figure 1.9**) that have been isolated and characterised. All LTBPs except LTBP-2 covalently bind latent-TGF-ß intracellularly, and play a central role in modulating tissue levels of this potent cytokine through regulation of its secretion, localisation and activation (Annes *et al.,* 2003; Koli *et al.,* 2001; Mangasser-Stephan and Gressner, 1999).

As mentioned previously, TGF-ßs are multifunctional cytokines that modulate growth, differentiation and apoptosis of mammalian cells (Hyytiainen *et al.*, 2004). TGF-β is secreted primarily as a latent complex consisting of the TGF-β homodimer, the TGF-β pro-peptides latency-associated peptide and the LTBP. The mature TGF-β remains associated with latency-associated peptide by non-covalent interactions that block TGF-β from binding to its receptor. Complex formation between latency-associated peptide and LTBP is mediated by an intramolecular disulfide exchange between the third 8-cys domain of LTBP with a pair of cysteine residues in latency-associated peptide, this complex is called the large latent complex. The release of TGF-β from inhibition by latency-associated peptide can be mediated by several different molecules including proteases, thrombospondin-1, and the integrins αvβ6 and αvβ8 (Annes *et al.*, 2003).

NOTE:
This figure is included on page 31 of the print copy of the thesis held in the University of Adelaide Library.

Figure 1.9. Schematic representation of human LTBPs 1-4. The small (s) isoforms of LTBP-1 and -4 are illustrated. Photograph taken and modified from (Saharinen and Keski-Oja, 2000)**.**

1.2.2.2.1 Structure and function of LTBPs

The overall structure of all known LTBPs is similar and it can be divided into four regions; the N-terminal region, the adjacent hinge domain, a central cluster of EGF-like domains and the C-terminal TGF-β binding region (Olofsson *et al.*, 1995; Saharinen *et al.*,

1996). The N-terminal region of LTBPs does not contain the repetitive structures of EGF-like or 8-cys domains. However there are cysteine residues present in this region that may be involved in disulfide binding of LTBPs with the ECM structures on which they are deposited (Nunes *et al.,* 1997; Saharinen *et al.,* 1999). LTBPs (except LTBP-3) contain a RGD sequence for putative cell adhesion (**figure 1.9**). Moreover, all LTBPs contain numerous glycosylation sites. The hinge domain has the highest degree of sequence diversity. The hinge sequence of LTBP-1 and -2 are sensitive to proteolytic cleavage which, at least for LTBP-1, may be for the release of TGF-B from the matrix (Hyytiainen *et al.,* 1998; Taipale *et al.,* 1995) (**figure 1.9**), while the hinge sequences of LTBP-3 and -4 are not (Penttinen *et al.,* 2002).

In LTBP-1 the N-terminus contains transglutaminase substrate motifs which are required for the proteins' incorporation into the matrix (Nunes *et al.,* 1997). The importance of the N-termini of LTBPs in binding ECM is highlighted by the observation that soluble LTBP-1 from platelets is lacking the N-terminal region, possibly due to proteolytic events in the regulated secretary pathway in the megakaryocytes (Miyazono *et al.,* 1991). In addition, Unsold *et al.,* (2001) demonstrated the association of LTBP-1 with fibroblast ECM through its N-terminal region and suggested the first interactions with the ECM may involve this very region.

The central part of all LTBPs is composed of EGF-like domains (**figure 1.9**), which are suggested to form a rod-like structure found in similar regions of fibrillins (Downing *et al.,* 1996). The EGF-like domains are found in many extracellular proteins, functioning as structural components and also mediating protein-protein interactions. However, how they mediate this interaction is not well understood. This region is resistant to proteolysis (Saharinen *et al.,* 1998; Taipale *et al.,* 1995) and the majority of the EGF-like domains in LTBPs, as in the fibrillins, are of the calcium binding type (Rosenbloom *et al.,* 1993; Sakai *et al.,* 1986; Zhang *et al.,* 1994).

The 8-cys domains are found only in LTBPs and fibrillins, thus characterizing the two glycoprotein groups as one superfamily (Oklu and Hesketh, 2000; Saharinen *et al.,* 1999). All of the cysteine residues in the 8-cys domains are involved in intradomain disulphide bonding. Although the third 8-cys domain in LTBPs binds latent TGF-β as mentioned previously, the binding affinity for the growth factor varies amongst the LTBP family members. LTBP-1 and -3 readily form disulphide bonds with TGF-β propeptide latency-associated peptide (Gleizes *et al.,* 1996; Saharinen *et al.,* 1999; Saharinen *et al.,* 1996), while the 8-cys3 domain in LTBP-4 is less efficient in binding with latency-associated peptide (Saharinen and Keski-Oja, 2000). Nuclear magnetic resonance studies have shown that the initial interaction of LTBPs with latency-associated peptide is facilitated by a region of negative electrostatic surface

potential, created by acidic amino acid residues surrounding the 2-6 cysteine pair disulphide bond, which has been identified in the exchange of disulphide bonds with latency-associated peptide (Lack *et al.,* 2003). The eight cysteine residues in 8-cys3 bind in a 1-3, 2-6, 4-7, 5-8 pattern for stabilisation of the domain's conformation (Lack *et al.,* 2003). In the same study, comparison of 8-cys3 structure in LTBP-1 and-4 revealed a ring of five negatively charged amino acid residues surrounding the 2-6 disulphide bind in LTBP-1, whereas the same site in LTBP-4 is surrounded by only three negatively charged amino acid residues, explaining poorer LTBP- latency-associated peptide complex formation (Lack *et al.,* 2003).

Various isoforms of all LTBPs can be produced by alternative promoters (Moren *et al.,* 1994). It has been shown that in human LTBP-1 and -4, there is more than one alternative N-terminal region (Olofsson *et al.,* 1995; Saharinen *et al.,* 1998). Through northern blots, two mRNA sequences coding for two different N-terminal variants of LTBP-1 were detected (Moren *et al.,* 1994). In LTBP-1, the mRNA sequences coding for a shorter LTBP-1S lack a 346 amino acid extension which was found to be present in the long LTBP-1L isoform (Kanzaki *et al.,* 1990; Noguera *et al.,* 2003; Tsuji *et al.,* 1990). The longer form has been found to interact more efficiently with the ECM (Olofsson *et al.,* 1995), further supporting the importance of the N-termini of the LTBP in the ECM association. Moreover, different distribution patterns have been observed for LTBP-1S and LTBP-1L. High LTBP-1L expression has been detected in the heart, kidney, lung, testes and placenta, while a broader distribution has been observed for LTBP-1S (Noguera *et al.,* 2003). In LTBP-4 at least three different N-terminal regions have been identified at the cDNA level (Saharinen *et al.,* 1998). Since the N-terminal region of LTBPs is thought to be important for interacting with the ECM structures (Dallas *et al.,* 1995), the variation in the N-terminal region of these glycoproteins could result in them having different affinities with various ECM components. There are also reports of alternative splicing of the hinge region of LTBP-1, and -3 (Oklu *et al.,* 1998; Yin *et al.,* 1998), and also in the long stretches of EGF-like repeats in LTBP-1, -3 and -4 (Oklu and Hesketh, 2000).

The full spectrum of the biological roles of LTBPs is still uncertain. Mouse models have aided in understanding the *in vivo* functions of LTBPs. Null (loss of function) or hypomorphic (partially functional) mutations in *Ltbp-1L, Ltbp-3 and Ltbp-4* genes causes abnormalities in the development of the heart, bones and lungs respectively (Dabovic *et al.,* 2002a; Dabovic *et al.,* 2002b; Sterner-Kock *et al.,* 2002; Todorovic *et al.,* 2007). For example, severely reduced expression of LTBP-4 in mice leads to the development of severe pulmonary emphysema, cardiomyopathy and colorectal cancer (Sterner-Kock *et al.,* 2002), associated with fragmented and disintegrated elastic fibres, and with an improper deposition of TGF-β in the matrix (Sterner-Kock *et al.,* 2002). In contrast, mice deficient in LTBP-3

suffer from premature obliteration of synchondroses, osteosclerosis and osteoarthritis (Dabovic et al., 2002a) that is associated with impaired TGF-β signalling on bone physiology. Studies by Todorovic *et al.,* (2007) demonstrated the congenital heart defects present in mice lacking *Ltbp-1L* genes are caused by a decrease in TGF-β activity. Overall, the mouse models described here highlight LTBPs as crucial components of the matrix that regulates TGF-β bioavailability during development. In addition to regulating TGF-β signalling, a second role as a structural component of elastic fibres has been suggested for LTBP-4 (Sterner-Kock *et al.,* 2002).

A study by Dallas *et al.,* (2005) has shown that fibronectin is critical for the incorporation of LTBP-1 and TGF-ß into the ECM of osteoblasts and fibroblasts. Through immunolocalisation studies it was suggested that fibronectin provides an initial scaffold that precedes the deposition of LTBP-1. This initial template has been suggested to be later lost as both fibronectin and LTBP-1 localise in separate fibrillar networks. To further support the hypothesis, Dallas *et al.,* (2005) showed that the absence of fibronectin impaired the incorporation of LTBP-1 and TGF- ß into the ECM. Furthermore, LTBP-1 failed to assemble in embryonic fibroblasts that lacked the gene for fibronectin, and the addition of full length fibronectin rescued the assembly of LTBP-1. Fibronectin is also essential for fibrillin-1 microfibril assembly (Sabatier *et al.,* 2009).

From the members of LTBP family, LTBP-2 is the only member that is not involved in the targeting of TGF-β as well as in regulating its activity. Structurally, LTBP-2 is similar to LTBP-1 except that LTBP-2 has 13 copies of consecutive EGF-like domains in the middle of the molecule compared to LTBP-1 which has 11 copies (Saharinen and Keski-Oja, 2000).

Alternative splicing of the N-terminal region of LTBP-2 mRNA results in different isoforms of LTBP-2 protein. In humans, LTBP-2 occurs as a protein of 240 kDa under reducing conditions which is larger than LTBP-1 (190-200 kDa) (Miyazono *et al.,* 1991; Moren *et al.,* 1994), whereas the size of LTBP-2 protein found in bovine cell cultures and in tissue extracts appeared even larger (260-310 kDa) (Gibson *et al.,* 1995). In addition, similar to LTBP-1, LTBP-2 was found to be released from the matrix by direct processing of the N-terminal region of LTBP-2 with elastase and plasmin (Hyytiainen *et al.,* 1998).

1.2.2.2.2 Tissue distribution of LTBP-2

The mRNA expression levels of LTBP-2 in various tissues have been investigated and compared with the expression of other LTBP family members. It has been established that LTBPs have only partial overlap of expression patterns. *In situ* hybridisation and immunohistochemical studies have shown LTBP-2 expression mainly in the lung, heart, placenta, skeletal muscle, liver and the aorta (Hirani *et al.,* 2007; Moren *et al.,* 1994). LTBP-

1 expression is also detected in the same tissues as LTBP-2, except for the liver, and in additional tissues including the kidney, prostate, testis, aorta and the ovary (Hirani *et al.,* 2007; Olofsson *et al.,* 1995). Meanwhile, LTBP-3 and -4 are predominantly expressed in the aorta, heart, small intestine and ovaries (Giltay *et al.,* 1997; Saharinen *et al.,* 1999). The expression levels of LTBP-3 and -4 are significantly lower in foetal tissues than in adult.

The temporal and spatial pattern of LTBP-2 expression has also been determined in developing mouse and rat in order to gain insight into the likely function of LTBP-2 in development. The expression of LTBP-2 by *in situ* hybridisation was revealed to be largely parallel to tropoelastin expression (Giltay *et al.,* 1997). Both proteins were expressed at embryonic day E-13.5 in the perichondrium surrounding developing vertebrae, at E-15.5 in the snout, lung, and dermis, and at E-17.5 both proteins were primarily detected in the aorta and other large vessels. In the rat tissue, LTBP-2 and tropoelastin were co-expressed in the lung, pericardium, epicardium and heart valves (Shipley *et al.,* 2000). In the young adult mouse, both proteins were expressed in the capsule of the spleen and ubiquitously throughout the mesenchyme of the lung (Shipley *et al.,* 2000). Additionally, there were tissues where LTBP-2 was differentially expressed to tropoelastin. For example, in the testes tropoelastin expression was weak and only observable in cells lining the outside of spermatic ducts (Shipley *et al.,* 2000). In contrast there was intense LTBP-2 expression observed in cells within the lumen of the epididymis (Shipley *et al.,* 2000). More recently, it has been shown using *in situ* hybridisation analysis that LTBP-2 expression is highly restricted in the brain (Dobolyi and Palkovits, 2008).

1.2.2.2.3 Possible function of LTBP-2

Knockout studies in mice revealed LTBP-1, -3 and -4 have specific functions in targeting of TGF-β as well as in the regulation of its activity (Dabovic *et al.,* 2002a; Sterner-Kock *et al.,* 2002; Todorovic *et al.,* 2007). However, the function of LTB-2 is less clear. Knockout mouse studies carried out by Shipley *et al.,* (2000) demonstrated the vital importance of LTBP-2 during development. Distinct from heterozygous mice with a disrupted LTBP-2 gene which were phenotypically normal in all aspects, the complete knockout of the LTBP-2 gene resulted in an embryonic lethal phenotype. More detailed experiments determined that the homozygous mutant affected implantation of the blastocysts, implying that LTBP-2 may play an essential developmental role during implantation (Shipley *et al.,* 2000). Using genome-wide linkage scan, LTBP-2 was identified as a candidate gene for contributing to bone mineral variation in the hip and fracture etiology (Cheung *et al.,* 2008). In a cell culture study by Goessler *et al.,* (2005), the expression of LTBP-2 during chondrogenic differentiation of mesenchymal stem cell and chondrocytes was found to be up-

regulated during dedifferentiation and down-regulation during chondrocyte differentiation. In addition, LTBP-2 expression level in the joint varied between patients and controls with osteoarthritis (Appleton *et al.,* 2007) and in the synovium of patients with systemic lupus erythematosus arthritis (Nzeusseu Toukap *et al.,* 2007). Based on these findings, it has been proposed that LTBP-2 may be involved in osteoblast differentiation and matrix homeostasis (Appleton *et al.,* 2007; Nzeusseu Toukap *et al.,* 2007).

Cell interaction with ECM components is important for events during development as well as later stages of life (Gumbiner, 1996). Cells adhere to the ECM through the interaction of cell surface receptors with integrin receptors, non-integrin receptors and RGD recognition sequences of ECM proteins (Ruoslahti, 1996). Since LTBP-2 contains a RGD sequence *in vitro* binding assays implicated a role for it in the modulation of cell adhesion (Hyytiainen and Keski-Oja, 2003; Vehvilainen *et al.,* 2003). Further experiments demonstrated that melanoma cell adhesion to LTBP-2 could be mediated at least by the α3β1 integrin receptor. Recently *in vitro* binding assays have demonstrated that LTBP-2 competes with LTBP-1 for binding to fibrillin-1 in the developing aorta (Hirani *et al.,* 2007) (**figure 1.8**). This suggests that LTBP-2 may be playing a role in modulating the storage of TGF-β on microfibrils in-directly. Moreover, examination of LTBP-2 and fibrillin expression in cultured cell lines and their distribution in the matrix resulted in the conclusion that fibrillin-1 is necessary for efficient assembly of LTBP-2 (Vehvilainen *et al.,* 2009). Suppression of fibrillin-1 resulted in the inability of LTBP-2 to deposit in the matrix (Vehvilainen *et al.,* 2009). Furthermore, using a cell culture system of human skin fibroblasts, LTBP-2 was demonstrated to regulate assembly of elastic fibres by binding to fibulin-5 promoting its deposition on fibrillin-1 microfibrils, and thus promoting elastogenesis preferably onto fibrillin-1 microfibrils (Hirai *et al.,* 2007). From these findings a potential involvement in elastic fibre assembly can be elucidated for LTBP-2.

1.2.2.2.4 Diseases associated with the LTBP-2

Recently null mutations in LTBP-2 have been reported to be the cause of primary congenital glaucoma in a number of consanguineous families (Ali *et al.,* 2009). Primary congenital glaucoma is a rare cause of glaucoma that is inherited as an autosomal recessive condition in most families. Primary congenital glaucoma usually manifests within the first year of life and it is characterised by high intraocular pressure causing irreversible damage to the optic nerve (Anderson, 1981; Kupfer and Kaiser-Kupfer, 1979). This in turn leads to permanent loss of vision if it is left untreated. Affected patients usually present with tearing, photophobia, corneal clouding and enlargement of the cornea (Ho and Walton, 2004).

Aims of the present study

The components of the matrix have an influencing role in normal development of mammalian organs and homeostasis of mammalian tissues. The matrix components interact with various other structural proteins in the matrix to link the matrix together, as well as with resident cells via cell surface receptors or integrins to control and regulate cascade of events during embryo and organogenesis and later stages of life (Gumbiner, 1996). In addition, components of the matrix have the potential to interact with growth factors to store these cytokines in tissues and subsequently regulate their activation. For proper functioning of the connective tissue appropriate assembly of the matrix is required. Genetic studies have demonstrated the correlation between proper construction of the matrix and its function. For instance, generated LTBP-2 null mutant mice do not survive past E-6.5, prior to implantation.

LTBP-2, a matrix protein well documented to be associated with elastic fibres in humans, mouse and bovine tissues, has been demonstrated to bind to fibrillin-1 and to colocalise with fibrillin-1-microfibrils in human foetal aorta and bovine nuchal ligaments. LTBP-2 interacts with other microfibrillar/elastic fibre-associated proteins such as fibulin-5. Through these interactions it has been proposed that LTBP-2 plays a regulatory role in the deposition of elastin on fibrillin-1 microfibrils. Previously, Hirani *et al.,* (2007) demonstrated the lack of interaction between recombinantly expressed LTBP-2 and fibrillin-2, MAGP-1 and -2, tropoelastin and the small CS/dermatan sulphate-PGs, decorin and biglycan, using solid phase binding assays. With the emerging data on the involvement of HSPGs in elastic fibre biology, as yet studies have not been conducted to analyse the consequence of the interaction between LTBP-2 and HSPGs on assembly of elastic fibres.

This research project focused on the role of LTBP-2 in assembly of elastic fibres. In particular it aimed to establish if LTBP-2 interacts with HSPGs in the matrix or on cell surfaces and to further characterise the interaction if such an interaction was identified. It also aimed to determine if LTBP-2 and its HSPGs binding ligands have similar distributions in elastic tissues, the developing human foetal aorta, which is a major elastic tissue. In conjunction with studying the role of LTBP-2 within elastic fibre biology, through these aims we intend to find out if LTBP-2 has functions independent of elastic fibrillogenesis.

It is also an aim to elucidate clues for novel potential functions for LTBP-2 through isolating binding ligands for this matrix protein using a more systematic approach. Also using the same system, it is aimed to isolate binding partners for βig-h3, a matrix protein which is associated with collagen VI microfibrils, which can be used for comparing and verifying the specificity of the isolated binding partners by the two distinct matrix proteins.

Specific aims

1. To define and characterise molecular interactions of LTBP-2 with heparin/HSPGs, in particular perlecan and syndecans using solid phase binding assays.

2. To determine if LTBP-2 colocalises with these HSPGs within tissues.

3. To identify novel molecular binding partners for LTBP-2 and βig-h3 using affinity binding and proteomics.

CHAPTER 2
MATERIALS AND METHODS

2.1 General molecular biology protocols

The following molecular biology protocols were adopted to facilitate cloning of human LTBP-2 fragments LTBP-2NT(H) and LTBP-2C(H) complementary (c) DNA sequences into mammalian expression vectors.

2.1.1 Polymerase Chain Reaction (PCR)

Polymerase chain reactions (PCR) were carried out using an Eppendorf mastercycler gradient PCR machine (Eppendorf, Hamburg, Germany) as previously described in Kitahama *et al.,* (2000). Each PCR reaction mix contained 100ng of template DNA (BM40:LTBP-2:his_6 in pGEM-T-easy) (Hirani *et al.,* 2007), 10µM of each primer pair (specific for the central or amino-terminal fragments) (**appendix A**), 0.2mM of each dNTP, PCR reaction buffer provided by Stratagene as a 10×stock (**appendix B**), and 2.5U of *Pfu* turbo DNA polymerase (Stratagene, La Jolla, CA). The final reaction volume of 50µl was made up using ddH_2O. PCR cycles were conducted with a heated lid at 100˚C, and denaturation of template and activation of DNA polymerase was set at 94˚C for 3 min. This was followed by 25 cycles with denaturation temperature at 94˚C for 1 min, annealing temperature (at 57˚C for LTBP-2NT(H) and 59˚C for LTBP-2C(H) fragments) for 1 min, extension temperature at 72˚C for 3 min and a final extension step at 72˚C for 10 min. All completed reactions were chilled to 4˚C prior to long term storage at -20˚C.

2.1.2 DNA Purification by Agarose Gel Electrophoresis

The PCR product (approximately 50-200ng of cDNA) was mixed with 6×DNA loading buffer (**appendix B**) to a final concentration of 1× and was loaded into wells of a 0.8% (w/v) agarose gel (Invitrogen, Carlsbad, CA) dissolved in 1×TAE buffer (**appendix B**). Electrophoresis was carried out at 120V for 1 hr in 1×TAE buffer. Resolved DNA bands were stained with Ethidium bromide (2µg/ml) (Boehringer Mannheim GmbH, Mannheim, Germany) and they were visualised by an ultraviolet illuminator, wavelength= 254nm (Chromato-VUE Transilluminator, Model 0-62, Ultraviolet Products INC) and photographed using a Nikon COOLPIX-990 digital camera. Specific DNA bands were excised from the agarose gel using a clean scalpel blade and purified using the ultraclean gelspin filter kit (MoBio, Solana Beach, CA) exactly following the manufacturer's instructions. cDNA yields

were approximately 20-40µg/ml. Concentration of purified cDNA was calculated from A_{260} readings of 1:25 dilution of cDNA in ddH2O in a UV-1601 spectrophotometer (Shimadzu, Kyoto, Japan). The cDNA fragment was then "A"-tailed in preparation for ligation into pGEM-T-easy vector (Promega, Madison, WI).

2.1.3 "A"-tailing and Ligation

"A"-tailing of the LTBP-2NT(H) and LTBP-2C(H) cDNA fragments was carried out by incubating the PCR (section 2.1.3) insets with 5U of platinum *taq* DNA polymerase (Stratagene, La Jolla, CA), 1×platinum *taq* DNA polymerase buffer supplied by Stratagene as a 10×stock, 2.5mM $MgCl_2$ and 0.2mM dATP in a total volume of 10µl. The volume was made up using ddH_2O. Incubation was carried out in the Eppendorf mastercycler gradient PCR machine (Eppendorf, Hamburg, Germany) for 1 hr at 70˚C with the heated lid of 94˚C.

Ligation of the cDNA PCR fragments was conducted using a 5:1 ratio of insert to vector. "A"-tailed PCR fragments of LTBP-2NT(H), 191ng, or LTBP-2C(H), 200ng, were incubated overnight at 4˚C with 50ng of pGEM-T-easy vector (Promega, Madison, WI), 3U of T4 DNA ligase and 1×ligation buffer (supplied by Promega as a 10×solution) in a total volume of 10µl.

Ligated cDNA fragments were purified by ethanol precipitation. Briefly, 0.1 vol of 3M sodium acetate (pH 5.2) and 2.5 vol of ice-cold 100% ethanol were incubated with the ligation reaction respectively for 30 min at -20˚C. Following incubation, the mixture was immediately centrifuged at 4˚C for 25 min at 17,500×g. The DNA pellet was washed with ice-cold 70% (v/v) ethanol and centrifuged at 17,500×g for 10 min before decanting the ethanol and air-drying the pellet. The DNA was resuspended in 10µl of ddH_2O prior to use in transformation of JM109 competent cells (Promega, Madison, WI).

2.1.4 Transformation of Competent Cells

JM109 competent cells (107 colony forming units/µg), totalling of 100µl were incubated on ice for 20 min with 50ng of ligated and purified DNA in a volume of 10µl. Competent cells were heat shocked at exactly 42˚C in a water bath for 45 sec and were immediately returned to ice for a further 2 min. Cells were incubated in 900µl of SOC media (**appendix B**) for 1.5 hrs at 37˚C with agitation and pelleted by centrifugation at 2,000×g for 5 min at RT. The pellet of transformed cells was resuspended in 100µl of SOC media before being spread onto solid agar plates containing luria broth (**appendix B**), 100µg/ml ampicillin, 0.5mM IPTG and 40µg/ml X-Gal. The coated plates were incubated overnight at 37˚C. The X-Gal and IPTG allows for blue/white colony selection. White colonies indicate the transformation of JM109 competent cells with pGEM-T-easy vector containing the required

cDNA insert, while blue colonies indicate cells transformed with re-ligated, empty pGEM-T-easy vector. The presence of a cDNA insert in the vector interrupts the transcription of the Lac-Z gene whose protein product metabolises X-Gal and IPTG into a blue compound. White colonies were selected and were sub-cloned onto solid agar plates containing Luria broth and 100µg/ml ampicillin. The coated plates were incubated in a 37˚C incubator for 16 hrs, prior to propagation of the colonies in Luria broth (**appendix B**) containing 100µg/ml of ampicillin for plasmid DNA purification. The liquid cultures were incubated for 16 hours at 37˚C with agitation. Plasmid DNA was purified from 2ml of Luria broth culture using the high pure plasmid isolation kit (Roche Diagnostics GmbH, Mannheim, Germany), following manufacturer's instructions. The DNA was eluted from the spin column using ddH_2O and DNA yields were calculated at A_{260} using 1:25 dilutions of stock DNA in ddH_2O. DNA yields in the range of 4.3-20µg/ml were generally obtained. The presence of a correct size insert was confirmed by PCR as described in section 2.1.2, using 100ng of the purified DNA as template.

2.1.5 Restriction digests

Restriction digests with *HindIII* restriction enzyme were carried out by incubating 0.136-1µg of DNA with 5U of restriction enzyme *HindIII* (Promega, Madison, WI) in the presence of 1×buffer E (Promega, Madison, WI), and 2µg acetylated BSA in a volume of 20µl made up using ddH_2O. The mixture was incubated for 2 hrs at 37˚C.

Digestion of the pCEP-4:BM40:LTBP-2C(H):his_6 was carried out as follows; 1µg of purified plasmid was incubated at 37˚C for 3 hrs with 5U of restriction enzyme *KpnI* (Promega, Madison, WI), 2µg acetylated BSA and 1×buffer J (Promega, Madison, WI) in a volume 20µl. Digested DNA samples were analysed on a 0.8% agarose gel.

2.1.6 DNA Sequence Analysis

To ensure the integrity of the DNA and to confirm the orientation of cDNA inserts, DNA sequencing was conducted by incubating Big-Dye version 3.0 ready reaction mix (1µl) with 200ng of purified plasmid DNA, 1×Big Dye sequencing buffer (supplied Molecular Pathology sequencing, Institute of Medical and Veterinary Science, Adelaide as 5×stock) and 5pmol sequencing primers (M13F or M13R (**appendix A**), in a reaction volume of 20µl made up with ddH_2O. Sequencing was carried out using the PCR conditions of heating of the samples to 96˚C for 1 min, then 25 cycles of 96˚C for 10 sec, 50˚C for 10 sec, 60˚C for 4 min, followed by a final step of incubating samples at 25˚C for 10 sec before holding the reaction at 4˚C prior to DNA precipitation with isopropanol.

Sequencing reactions were precipitated by adding 80µl of 75% (v/v) isopropanol to the sequencing reaction and vigorously agitating it for a few seconds before incubating at RT for 20 min to precipitate PCR products. Samples were centrifuged for 20 min at 17,500×g and the isopropanol was carefully aspirated. To wash the pellet 250µl of 75% isopropanol was added, agitated briefly and centrifuged for 10 min at 17,500×g. The isopropanol was removed without disturbing the pellet and the pellet was air dried. The samples were then sent to the Molecular Pathology Sequencing Centre, Institute for Medical and Veterinary Science, Adelaide, Australia for automated sequence analysis using the 3700 DNA analyser (Applied Biosystems, Foster City, CA). Further sequencing was undertaken of the full length of LTBP-2C(H) cDNA insert using LTBP-R2 or HLTBP-F3 primers (**appendix A**) to select error-free clones. Cells containing error free clones were grown in luria broth sterile glycerol in a 7:3 ratio and the stocks were stored at -70˚C.

2.1.7 Dephosphorylation

After linearization, the modified pCEP-4 vector (pCEP-4:BM40:his_6) (section 2.1.5), was dephosphorylated using Shrimp alkaline phosphatase (Boehringer Mannheim GmbH, Mannheim, Germany). For the 500ng of vector DNA, 20U of shrimp alkaline phosphatase with 1×dephosphorylation buffer supplied by Boehringer Mannheim GmbH as 10×stock was incubated in a volume of 100µl at 37˚C for 2 hrs. The enzyme was deactivated by incubation at 65˚C for 15 min and the dephosphorylated vector was recovered using ethanol precipitation (section 2.1.3). The recovered vector was resuspended in ddH_2O to give 10ng/µl. DNA T4 ligase was used in conjunction with 4:1 ratio of insert to vector for ligation of LTBP-2C(H) into the dephosphorylated modified pCEP-4 vector.

2.2 Production of human LTBP-2 fragments

2.2.1 LTBP-2C(H)

The central fragment (LTBP-2C(H)) cDNA was obtained by PCR amplification of bases (2758-5142) from full length human LTBP-2 clone (LTBP-2:BM40:his_6:pCEP-4) constructed by Dr. E. Hanssen (see Hirani *et al.*, 2007). Primers LTBP-2 Central Forward and LTBP-2 Central Reverse (**appendix A**) containing *HindIII* restriction site were used under the conditions described in section 2.1.1 to produce a PCR product of 2373 base pairs. The LTBP-2C(H) PCR product was purified from 0.8% (w/v) agarose gel and was “A”-tailed and ligated to pGEM-T-easy vector (section 2.1.2 & 2.1.3). The pGEM-T:LTBP-2C(H) construct was transformed into JM109 competent cells (section 2.1.4) and purified plasmid DNA from selected clones was sequenced to identify error-free clones (section 2.1.6).

The LTBP-2C(H) insert was excised from the pGEM-T-easy vector with *HindIII* restriction enzyme (section 2.1.5) for ligation into the dephosphorylated modified pCEP-4 vector (section 2.1.7). The modified vector contained a BM40 signal peptide at the 5'end and a his_6-tag at the 3' end.

For preparation of the pCEP-4:BM40:his_6 modified vector, the full length LTBP-2 insert was removed from the pCEP-4:LTBP-2 plasmid by *HindIII* restriction enzyme digestion (section 2.1.5). The pCEP-4:BM40:his_6 vector and full length LTBP-2 cDNA insert were separated using agarose gel electrophoresis (section 2.1.2). The pCEP-4:BM40:his_6 vector band (approximately 10356bp) was purified from 0.8% agarose gel, a portion of it being ligated back to itself using T4 DNA ligase (section 2.1.7) and propagated in JM109 cells (section 2.1.4). Glycerol stock of a clone was made for future use of the vector. The remaining portion was dephosphorylated (section 2.1.7) prior to ligation with the *HindIII*-digested LTBP-2C(H) cDNA insert. JM109 cells were transformed with the ligated construct and plasmid DNA from individual colonies was purified (section 2.1.4). The desired pCEP-4:LTBP-2C(H) clones in the correct orientation were identified using *KpnI* (Promega, Madison, WI) enzymatic digestion (section 2.1.5). Digestion of the modified pCEP-4 content in the correct orientation produces two fragments of approximately 728 base pairs and 12013 base pairs.

The recombinant pCEP-4:LTBP-2C(H) expression construct needed to be highly purified, and larger quantities of the plasmid were required for transfection into mammalian cells. Luria broth cultures of the selected clone were prepared (section 2.1.4) and plasmid DNA was purified using the QIAfilter® midi kit (Qiagen GmbH, Hilden, Germany), following the manufacturer's instructions for low-copy number plasmids. Purification of plasmid DNA was carried out from 50ml of Luria broth cultures. A slight modification in the final elution step was made where eluted DNA (8ml) was aliquoted equally between 8 tubes with the manufacturer's recommended amount of isopropanol (2.5ml) equally divided between them. The DNA was precipitated by centrifugation and the pellet in each individual tube was resuspended in ddH_2O and then pooled together. The concentration of the purified plasmid DNA was found to be 0.5-1mg/ml from the absorbance reading (A_{260}) using 1:25 dilution of stock DNA in ddH_2O.

2.2.2 LTBP-2NT(H)

A cDNA encoding the amino-terminal region of human LTBP-2, LTBP-2NT(H), corresponding to bases 2758-5142, was obtained by PCR amplification from a full length human LTBP-2 clone as described above using primers LTBP-2NT(H) Forward and Reverse (**appendix A**) (section 2.1.1). The PCR product of 2272 base pairs was analysed by

electrophoresis on a 0.8% agarose gel, and the LTBP-2NT(H) cDNA was excised from the gel (section 2.1.2) and purified. The purified cDNA fragment was "A"-tailed and ligated into the pGEM-T-easy vector (section 2.1.3) and the pGEM-T-easy:LTBP-2NT(H) construct was transformed into JM109 competent cells (section 2.1.4). Purified plasmid DNA from selected clones was digested with a *HindIII* restriction enzyme to confirm the presence of the *HindIII* restriction sites (section 2.1.5) on the insert, prior to sequencing using pGEM-T-easy primers (pUC/M13 forward & reverse) (**appendix A**). However, only a low number of colonies in transformed JM109 cells were obtained and I was unable to identify any error-free clones. Time constraints prevented the repeat of the procedure.

2.3 Expression of recombinant LTBP-2C(H)

For expression of rLTBP-2C(H), 293 EBNA human embryo kidney (HEK) cells (Invitrogen, Carlsbad, CA) were grown in Dulbecco's Modification of Eagles Medium (DMEM) to confluency at 37˚C and in the presence of 0.5% CO_2. The medium was reconstituted from powder following the manufacturer's instructions (Gibco, Carlsbad, CA) (**appendix B**) and it was supplemented with 1×non-essential amino acids (NEAA) (Thermo electron, Australia), 10% (v/v) heat deactivated (Δ) foetal calf serum (FCS) and 250mg/L geneticin (for selection of EBNA-1 containing cells) (Gibco, Carlsbad, CA). Cells were counted with trypan blue stain, using a 1:1 ratio of trypan blue to cell solution and were plated at 2×10^5 cells/ml. Transfection of the plated cells was carried out with 2μg/ml of plasmid DNA and 4μg/ml of lipofectamine 2000 reagent (Invitrogen, Carlsbad, CA). The DNA was substituted with ddH_2O in one set of control wells, while the second set of control wells lacked both Lipofectamin 2000 and DNA.

24 hrs after transfection the medium was removed from the cells and the cells were gently washed with Dulbecco's PBS (**appendix B**) to remove the entire transfection reagent. Dulbecco's PBS was used to remove cells from the surface of the wells by agitation and these were washed in 5ml of DMEM (no supplement). The cells were pelleted by centrifugation for 5 min at 260×g, gently resuspended in 25ml DMEM/10% (v/v) ΔFCS/ 1×NEAA/ geneticin (250mg/L) and then divided equally into 10 fresh wells. Only two fresh wells were plated for each control.

48 hours after transfection, the medium was changed to a fresh medium (DMEM, 10% (v/v) ΔFCS, 1×NEAA, geneticin (250mg/L), hygromycin (250mg/L)). This medium had the addition of hygromycin (Roche Diagnostics GmbH, Mannheim, Germany) which is the selective antibiotic for the pCEP-4:LTBP-2C(H) plasmid. Selection continued until the control cells in the selection medium had died, which was suggestive that the remaining viable cells in the transfection wells contained the selected recombinant plasmid.

Prior to full scale protein production, individual clones were tested for expression of the recombinant protein using small scale Nickel Chelate chromatography (section 2.4). The colony expressing the highest level of the specific recombinant protein was chosen for propagation. When the hygromycin-selected cells had reached confluency, the cells were washed with Dulbecco's PBS, removed with agitation and pelleted (centrifuged 260×g for 5 min). Cells from each well of 9.6cm^2 were divided in two 80cm^2 propagation flasks with 10ml of culture medium (DMEM, 10% (v/v) ΔFCS, 1×NEAA, geneticin (250mg/L), and hygromycin (250mg/L)) and grown until the cells were confluent. One of the confluent flasks was used for recombinant protein expression described below, while the other was used for continued propagation of transfected cells.

Full Length human LTBP-2 cDNA and βig-h3 cDNA expression constructs were prepared as previously described (Hanssen *et al.*, 2003; Hirani *et al.*, 2007), and the recombinant proteins were expressed and purified as described below.

2.4 Purification of recombinant full length LTBL-2, βig-h3 and LTBP-2C(H) fragment

Standard practice was to use 12×175cm^2 flasks of propagating cells; 11 were placed into a serum-free medium for production of recombinant protein and a flask was passaged into 4 flasks and then 12 flasks for continuation of cell propagation. Confluent cells were washed with 3×Dulbecco's PBS (**appendix B**) prior to incubation with serum-free DMEM supplemented with 1×NEAA, geneticin (250mg/L) and hygromycin (250mg/L) for 3 days prior to harvest.

To maximise the quantity of recombinant protein harvested from the 11 flasks, the cells were re-incubated with DMEM supplemented with heat deactivated new born calf serum (ΔNBCS) (Invitrogen, Carlsbad, CA) (ΔFCS was substituted with ΔNBCS during protein production) overnight followed by a second round of serum free-medium for an additional three days.

The serum-free conditioned medium was centrifuged at 260×g for 5 min to remove the cells and then centrifuged at 50,000×g for 30 min at 4˚C in a Heraeus Biofuge stratos centrifuge (Kendro laboratory products GmbH, Hanau, Germany) to remove any residual cell debris that may have not been previously removed. The medium was then filtered through a 0.45μm bell filter (Pall Corporation, Pensacola, FL) to remove further cell debris. To prepare the medium for Ni-Chelate chromatography, the medium was adjusted to contain a final concentration of 20mM NaH_2PO_4 and 10mM imidazole using 8×phosphate buffer and 2M imidazole (BDH Chemicals, Carle Place, NY) (**appendix B**). The addition of a low concentration of imidazole to the medium prior to incubation with Ni-sepharose resin had

been found to reduce the amount of non-specific binding of proteins without competing with the his_6-tagged protein.

Recombinant proteins were purified using a His-trap sepharose column, following the manufacturer's instructions (Pharmacia Biotech, Uppsala, Sweden). Briefly, for every 100ml of serum-free media, 1ml of Ni-sepharose for rLTBP-2 and rLTBP-2CH and 400µl of Ni-sepharose for rβig-h3 was used. Preparation of the sepharose was carried out as follows: the ethanol storage solution was washed from the beads with 5 column (col) vol of ddH_2O, then 1.5 col vol of $NiSO_4$ (0.1M) (**appendix B**) was added and incubated with the sepharose beads for 5 min. The nickel solution was then drained and the sepharose was washed with 5 col vol of ddH_2O prior to equilibration with 10 col vol of 10mM imidazole buffer (**appendix B**). Successfully charged sepharose beads appeared blue in colour.

The Ni-sepharose beads were incubated with the serum-free medium on a rotator wheel for 3 hrs at RT, or overnight at 4˚C. Beads were collected by centrifuging at 260×g for 2 min and were then transferred to a 2ml Econo column. The media was drained and further unbound proteins were eluted with 5 col vol of 10mM imidazole buffer the first three col vol of washes were combined with the drained medium and were stored at 4˚C for re-application to a fresh Ni-sepharose column to recover further recombinant protein. Three rounds of purification were performed per batch of serum-free medium to recover all of the recombinant protein. Bound recombinant protein was eluted with 10 col vol of 500mM imidazole buffer (**appendix B**) and 10 fractions were collected, each corresponding to one col vol. It is the high concentration of imidazole that displaces the his_6-tag protein from the Ni-sepharose. After collection of recombinant protein from the Ni-sepharose, the column was washed with 10 col vol of 10mM imidazole buffer in preparation for a second round purification of recombinant protein.

When the final round of purification was completed, Ni-ions were stripped from the chelating-sepharose beads using 10 col vol of 0.05M EDTA solution (**appendix B**). Removal of any precipitated proteins in the column was then carried out by incubation of the nickel stripped sepharose with 0.1M NaOH solution (from a 1M NaOH solution, **appendix B**) for at least 2 hrs at RT, followed by extensive washing of the beads with ddH_2O. The Ni-sepharose beads were to be either charged with nickel to use for the next batch or stored in 20% (v/v) ethanol at RT. The purification and authenticity of recombinant proteins was checked by SDS-PAGE and western blot analysis (section 2.6). Concentrations of purified proteins were determined from a SDS-PAGE resolved sample using the public domain NIH Image program version 1.63 (developed at the U.S. National Institutes of Health and available on the Internet at http://rsb.info.nih.gov/nih-image/).

The first two fractions of 500mM imidazole elution for full length rLTBP-2 were generally found to contain the highest concentration of recombinant proteins. These fractions were pooled and dialysed into TBS containing 0.5M NaCl (TBS/0.5M NaCl) (**appendix B**). The addition of salt was to prevent the precipitation of purified recombinant protein from the solution. The removal of 500mM imidazole from purified protein was essential as it was found to interfere with assays where anti-(his_6-tag) antibodies were used for protein detection. Dialysis was carried out in Spectrapor membrane with a pore size of 6-8000Da (Spectrum Laboratories, Inc., Rancho Dominguez, CA), overnight at 4˚C or for 3 hrs at RT with several changes of buffer at least 100 times the volume of the sample. Dialysed protein was aliquoted and stored at -20˚C. For longer storage the aliquots were stored at -80˚C.

A similar eluting pattern was observed for rLTBP-2C(H) where the highest concentration of the recombinant protein was found in the first two collected fractions. However, in contrast to this result, only fraction two of the full length rβig-h3 was found to have a majority of the recombinant protein. Fractions containing recombinant proteins were pooled, dialysed and stored similarly as described for full length rLTBP-2. The exception is the storage of rβig-h3 at 4˚C since freezing of the protein causes precipitation.

2.5 Freezing and Thawing of recombinant protein expressing cells.

Cells at 5×10^6/ml were rinsed with Dulbecco's PBS and were collected in a 10ml tube with 5ml of Dulbecco's PBS with the 10ml made up with DMEM. The cells were pelleted (centrifuged 260×g for 5 min) and once the supernatant was removed the pellet was resuspended in 5ml of freezing solution A (**appendix B**). Freezing solution B (5ml) (**appendix B**) was then added drop wise with shaking prior to preparation of 1ml aliquots in cryovials. The cryovials were stored at -70˚C overnight prior to storage in liquid nitrogen.

The frozen vials (5×10^6/vial) of transfected cells were thawed by placing the vial into a 37˚C water bath until almost thawed, then 10ml of DMEM (no supplements) was added to the cells at RT and it was incubated for 5 min, before centrifuging at 260×g for 5 min. The cells were then resuspended in 1ml of DMEM and transferred into a $80cm^2$ flask with 10mls of culture medium (DMEM, 10% (v/v) ΔFCS, 1×NEAA, geneticin (250mg/L), and hygromycin (250mg/L).

2.6 SDS-PAGE Coomassie Blue staining and western immunoblotting

Purified proteins were analysed using microslab SDS-PAGE, and the discontinuous buffer system of Laemmli (Laemmli, 1970). The separating gel ranged from 6.5-15% (v/v) acrylamide and stacking gel concentration of 3% (v/v) acrylamide (Sigma-Aldrich, St. Louis, MO) (**appendix B**). Protein samples were precipitated with 10 vol of ice-cold 90% (v/v)

acetone at -20˚C for 20 min. This was followed by pelleting of the precipitated protein by centrifugation at 17,500×g for 10 min. The supernatant was removed carefully and discarded and the pellet was washed with 90% (v/v) acetone for 10 min, at 17,500×g. Acetone was carefully removed, the pellet was resuspended in protein sample loading buffer (**appendix B**) containing 2% (v/v) β-mercaptoethanol (Sigma-Aldrich, St Louis, MO) and boiled for 2 min. The samples were loaded into individual wells of a polyacrylamide gel and resolved at 150V in the chamber buffer (**appendix B**) until the dye front was a few millimetres from the bottom of the gel. Broad range molecular weight protein standards (Bio-Rad Laboratories, Hercules, CA) at 0.5µg/protein band were run simultaneously.

For visualisation and quantitation of protein bands, SDS-PAGE gels were stained with fresh Coomassie Blue (**appendix B**) for 15 min with gentle agitation. The gels were destained by rinsing and then incubated in 40% (v/v) methanol/acetic acid solution (**appendix B**) for 5 min. This was followed by incubation of the gel with 7.5% (v/v) methanol/acetic acid solution (**appendix B**) for a minimum of 30 min or until sufficient destaining of the gel was achieved. The gel was washed in ddH_2O prior to drying overnight between cellophane sheets. Protein quantitation was performed on a Macintosh computer using the NIH Image program version 1.63 (developed at the U.S. National Institutes of Health and available on the Internet at http://rsb.info.nih.gov/nih-image/).

For western immunoblotting, SDS-PAGE gels were used as above but the proteins were transferred onto polyvinylidene difluoride (PVDF) membrane as follows. The gel was washed twice in a Tris/Glycine buffer (**appendix B**) for 10-15 min, while the Bio-trace PVDF membrane (0.45µm) (Pall Corporation, Pensacola, FL) was activated by rinsing in 100% (v/v) methanol for 1 min, followed by rinsing in ddH_2O for 5 min and Tris/Glycine buffer for 10 min. The gel was sandwiched between the smooth side of the PVDF membrane and Whatman paper (3mm grade, Whatman International Ltd, Maidstone, England) prior to placing it into the wet transfer apparatus. Protein bands were transferred onto PVDF membrane using 60V in a negative to positive direction for 90 min with gentle stirring of the Tris/Glycine buffer using a magnetic stirrer. After transfer, the lane containing the Bio-Rad standard proteins was cut off and stained with Coomassie Blue. The remainder of the membrane was washed 2×5-10 min in TBS (**appendix B**) and incubated into a blocking solution (**appendix B**) for 1 hr at RT with gentle shaking.

The primary antibody at the designated concentration (**appendix C**) was incubated with the blot for 2.5 hrs at RT or at 4˚C overnight in antibody solution (**appendix B**). The PVDF membrane was washed 2×5 min in Tris/Tween-20/Triton X-100 solution (**appendix B**) followed by 5 min in TBS with gentle agitation. Diluted secondary antibody conjugated with alkaline phosphatase (Bio-Rad Laboratories, Hercules, CA) in the antibody solution was

incubated with the membrane for 1.5 hrs at RT with gentle agitation. The membrane was then washed in Tris/Tween-20/Triton X-100 solution (**appendix B**) for 3×5 min with gentle shaking, rinsed with substrate buffer (**appendix B**) and developed with developing solution (**appendix B**). When sufficient development of the protein bands was achieved, colour development was stopped by rinsing the membrane in ddH_2O prior to air drying of the membrane.

2.7 Silver staining

The silver staining method used at first to detect protein bands separated by SDS-PAGE was adopted from Cheng *et al.,* (1994). Upon separation of protein samples under reduced conditions (section 2.6), the proteins were fixed by incubating the gel with 25% (v/v) isopropanol, 10% (v/v) acidic acid for 30 min, followed by 2× 10min washes with 10% (v/v) isopropanol 5% (v/v) acetic acid. Sensitisation of the gels was carried out by incubating in 5µg/ml (w/v) of dithiothreitol for 15 min, prior to staining with 0.1% (w/v) silver nitrate for 15 min. The gels were then rapidly rinsed in ddH_2O once and then twice with the developing solution (0.5% (v/v) paraformaldehyde, 3% (w/v) sodium carbonate). The gels were exposed to the developing solution until protein bands were developed satisfactorily, when further development was terminated by rinsing the gels in 1% (v/v) acetic acid. The gels were washed in ddH_2O and then dried overnight between cellophane sheets.

The second silver staining protocol used for protein detection was a method obtained from Dr. Wilson, R. of Murdoch Children's Research Institute and Department of Paediatrics, University of Melbourne, Australia, a modified version being described in (Gromova, 2006). Briefly, protein samples were separated under reduced conditions using SDS-PAGE. Each gel was fixed in 50% (v/v) methanol, 12% (v/v) acetic acid, and 0.05% (v/v) formalin with gentle shaking for 30 min. The gel was then washed in 35% (v/v) ethanol for 3×10 min, sensitised with 0.02% (w/v) sodium thiosulphate for 2 min and rinsed quickly in ddH_2O. The gel was stained in ddH_2O containing 0.2% (w/v) $AgNO_3$, 0.076% (v/v) formalin for 20 min and rinsed with ddH_2O. The gel was rinsed quickly and then stained with developer (5% (w/v) $NaCO_3$, 0.05% (v/v) formalin, and 0.008% (w/v) $Na_2S_2O_3$) until the desired level of protein staining was reached. Development was stopped with 50% (v/v) methanol, 12% (v/v) acetic acid solution and the gel was washed in ddH_2O for 5 min before drying overnight between cellophane sheets.

2.8 Determining the molecular weight of unknown proteins

Protein samples of unknown size were electrophoresed under denaturing or non-denaturing conditions along side standard proteins of known size (section 2.6) prior to

Coomassie Blue staining. The unknown molecular weights were determined by preparing a standard curve of relative mobility (R_f) of the standard proteins versus the log of the molecular weight of each standard protein. Briefly, the distance from the top of the resolving gel to the top of each standard protein band in SDS-PAGE was measured in millimetres. The distance from the top of the resolving gel to the top of the dye front was also obtained. The R_f of each protein standard was calculated using the equation R_f= distance of protein migration/ distance of the dye front. The log of the molecular weight was plotted against the R_f value of the standard proteins and the line of best fit was drawn through the data points. The molecular weights of other proteins run on the same gel was determined by measuring the migration distance of the band, calculating the R_f value and then using the standard curve to read the log of the molecular weight from the graph.

2.9 Mass spectrometric analysis

For verification of the rLTBP-2C(H) mass fingerprinting was performed at the Adelaide Proteomics Centre under the supervision and guidance of Dr. C. Bagley. Under reducing conditions the sample was separated by SDS-PAGE (section 2.6) and Coomassie Blue stained. The gel was rinsed with H_2O prior to excision of the band. The band was cut again in two and each half was placed into a 1.5ml eppendorf and each half was cut again into 2 or 3 smaller pieces followed by 2× 500µl washes with 100mM NH_4HCO_3 at RT with shaking. After the removal of the solution, the gel pieces were destained by incubating with 500µl of 100mM NH_4HCO_3 in 50% (v/v) acetonitile for 15 min at RT with agitation. The gel particles were spun down by pulse centrifugation and excess liquid was then removed. The step was repeated until gel pieces were 90% clear. Two rounds of this step were required for sufficient destaining. The gel pieces were then incubated with acetonitrile (200µl) for 15 min at RT until they had shrunk, at which point they became white and stuck together. The gel pieces were collected at the bottom of the tube by centrifugation and the liquid was removed prior to using a vacuum centrifuge for 4 min to dry the gel pieces. To reduce the protein, dried gel pieces were re-swelled with 50µl of 10mM dithiothreitol in 100mM NH_4HCO_3 at 56˚C for 15 min, rinsed with 100mM NH_4HCO_3 and shrunk with 200µl of acetonitrile for 15 min at RT with agitation. After collecting the gel pieces by centrifugation and removal of the supernatant, the gel pieces were incubated with 50µl of 55mM iodoacetamide in 100mM NH_4HCO_3 in the dark for 30 min. The iodoacetamide solution was removed and the gel pieces were rinsed and incubated with 100µl with 5mM NH_4HCO_3 at RT for 10 min. The solution was then removed and the gel pieces were shrunk and dried by vacuum centrifuge as previously described. At this stage one sample was stored and the other sample was digested with trypsin as follows. The gel pieces were rehydrated with 10µl of diluted trypsin (100ng/µl

in 5mM NH_4HCO_3) for 10 min before the addition of 20µl of 5mM NH_4HCO_3 solution (no trypsin) and incubation at 37˚C overnight with shaking. Digested peptides were present in the solution, so the 20µl solution was transferred into a new eppendorf tube. To ensure all of the digested peptides were removed from the gel, the gel was sonicated with 20µl of 1% (v/v) Trifluoroacetic acid for 5 min, 20µl of 0.1% Trifluoroacetic acid (v/v) in 50-60% (v/v) acetonitrile for 15 min and 50µl 100% acetonitrile for 15 min respectively in a water bath. After each incubation the solution was transferred to a new tube before the next solution was added to the gel. Finally the solutions containing the extracted peptide were pooled and dried down to 2-10µl using vacuum centrifugation. Matrix-assisted laser-desorption/ionisation time-of-flight mass spectrometry (MALDI-TOF-MS) analysis was used to authenticate LTBP-2C(H) by comparing the originated molecular weights of the peptide to the published LTBP-2 amino acid sequence and also to the protein sequence databases.

2.10 Synthesis and Fractionation of Covalently bound conjugates of heparin and albumin

For synthesis of heparin-albumin conjugates (HAC) a method modified from Hennink *et al.,* (1983) was used. Briefly, a 1.6:1 ratio of molar concentration of heparin sodium salt from porcine intestinal mucosa (Sigma-Aldrich, St Louis, MO) to albumin (bovine serum albumin (BSA) (Sigma-Aldrich, St Louis, MO)) was resuspended in ddH_2O (for 77mg of heparin 5ml of ddH_2O was used) and the solution was adjusted to pH 5. A white precipitate was formed which contained both heparin and albumin, and the precipitate dissolved within 1 hr. To the solution 8×100µl portions of N-(3-Dimethylaminopropyl)-N'-ethylcarbodiimide hydrochloride (EDC) (Sigma-Aldrich, St Louis, MO) (32.5mg/ml) were added at 30 min intervals with stirring. The solution was maintained at pH 5. Half an hour after the last addition of EDC, the solution was adjusted to pH 7.6 and stirring was continued for 20 hrs at 4˚C. The solution was dialysed for 2×1 hr against 0.025M Tris, pH 7 (in volume of 50ml each time) for subsequent ion chromatography.

Fractionation of unreacted albumin and HAC was achieved by ion exchange chromatography on a column of DEAE-sepharose Cl4B (2.3ml of resin to 5ml of solution), which had been pre-washed with 10 col vol of ddH_2O to remove ethanol and equilibrated with 10 col vol of equilibration buffer (0.3M NaCl/0.025M Tris pH 7). Unreacted albumin was eluted with an equilibration buffer (0.3M NaCl/0.025M Tris pH 7) (15×2ml fractions), then unfractionated purified conjugate (HAC) was eluted with 0.9M NaCl/0.025M Tris-HCl, pH 7 (10×2ml fractions) and stored at -70˚C.

The albumin concentrations of eluted fractions (free or conjugated) were determined from A_{280} readings of 1:4 dilution of eluted fractions (50µl) to 0.3M NaCl/0.025M Tris pH7

(for determining free albumin) or 0.9M NaCl/0.025M tris pH 7 (for detection of conjugated albumin) (150µl) in UV-1601 spectrophotometer (Shimadzu, Kyoto, Japan), using a BSA standard curve (0-200µg) diluted in the same buffer. The amount of albumin present in each fraction was determined by correlating the (A_{280}) with an established BSA standard curve. The majority of albumin (free or conjugated) was present in the first four fractions, and after that no albumin was detected in the fractions. The heparin concentration was determined using an uronic acid assay described in section 2.11.

2.11 Uronic acid assay

Hexosamine and uronic acid are components of the repeating unit of all GAGs with the exception of keratosulphate. To determine the quantity of GAGs in biological substances, uronic acid assay is widely used (Blumenkrantz and Asboe-Hansen 1973). A standard curve was established using a serial dilution of D-glucuronic acid (0-200µg) diluted in 0.9M NaCl/0.025M Tris pH 7. The volume was made up to 200µl using ddH_2O. Individual fractions containing HAC (1/50 and 1/100) in 0.9M NaCl/0.025M Tris pH 7 were also diluted and transferred into pyrex disposable culture tubes (Borosilicate Glass). Sulphuric acid (H_2SO_4)/sodium tetraborate solution (1.2ml) (**appendix B**) was added to the sample tubes, and the samples were vortexed and heated for 5 min at 100˚C, before cooling in an ice water bath. After cooling, 20µl m-hydroxydiphenyl solution was added and the samples were vortexed well before reading at A_{520} within 10 min of preparing the samples.

2.12 Determination of protein concentration using Bradford assay

The Bradford assay (Bradford, 1976) was used to determine the concentration of proteins in tissue extracts and proteins eluted from affinity chromatography columns. This assay uses coomassie brilliant blue G250 which binds protein causing a shift in the absorption maximum from 465nm to 595nm. To prepare the assay solution, Coomassie Brilliant Blue G250 (25mg) was dissolved in a mixture of 12.5ml of 95% ethanol and 25ml of 85% phosphoric acid. The volume was made up to 250ml using ddH_2O and the solution was mixed for at least 40 min on a stirrer. The solution was filtered through Whatman's paper before use to remove any Coomassie Brilliant Blue that had not dissolved. A serial dilution of ovalbumin (0-10µg) was prepared in a total volume of 100µl of appropriate buffer for establishment of a standard curve. To each diluted protein sample or standard 1ml of the Coomassie Blue reagent was added. The samples were then vortexed and left for 2 min to allow the binding of Coomassie Blue to the protein before analysis in a spectrophotometer (UV-1601, Shimadzu, Kyoto, Japan) at 595nm. The A_{595} readings of the samples were used to determine their concentration from the established standard curve.

2.13 Solid phase binding assay

2.13.1 Detecting interaction between two proteins

The wells of Immuno-Maxisorb modules (Nalge-Nunc International, Roskilde, Denmark) were coated with 400ng of test protein diluted in TBS/2mM $CaCl_2$ (unless otherwise stated) and incubated overnight at 4˚C in a humidity chamber. Candidate proteins used for coating of the wells were HAC (see section 2.10), human recombinant syndecan-2 and syndecan-4 (R&D Systems, Minneapolis, MN) or purified perlecan (Whitelock, 2001). Control wells were coated with the molar equivalent of BSA. All experiments were carried out using triplicate wells and each experiments was performed a minimum of three times for consistency. Unbound material was washed with 3×TBS/ 2mM $CaCl_2$, and wells were blocked for 1.5 hrs at RT with 5% (w/v) low fat dried milk (Diploma instant, Rowville, Vic, Australia) in TBS/2mM $CaCl_2$ with gentle agitation. The wells were then rinsed with 3×TBS/2mM $CaCl_2$ prior to incubation with 200ng of second test protein (LTBP-2 and its fragments unless otherwise stated in the figure legends) diluted in TBS/2mM $CaCl_2$. Controls of HAC-coated wells were incubated with the molar equivalent of BSA in solution to assess the level of cross reactivity of the antibodies being used. After the wells were washed with 3×TBS/2mM $CaCl_2$ the wells were incubated with primary antibodies specific to the second test protein (concentrations as stated in **appendix C**) in TBS/2Mm $CaCl_2$/0.05% low fat milk for 2.5 hrs in humidity chamber at 37˚C. Following antibody incubation the wells were then washed with 3×TBS/0.05% (v/v) Tween-20/2mM $CaCl_2$ before they were incubated with the secondary antibody, horseradish peroxidase-conjugated (Bio-Rad Laboratories, Hercules, CA) at required dilution (**appendix C**) in TBS/2mM $CaCl_2$ for 1.5 hrs at 37˚C in the humidity chamber. After final washes with 4×TBS/ 0.05% (v/v) tween-20/2mM $CaCl_2$, interaction was detected using 100µl of 3,3',5,5'-tetramethylbenzidine substrate (Sigma-Aldrich, St. Louis, MO) at RT. Colour was allowed to develop for up to 1 hr at RT with no agitation and colour development was stopped by using 0.5M H_2SO_4 (50µl per well). Absorbance was detected at 450nm, using Titertek Multiskan MC (Flow Laboratories, North Ryde, NSW, Australia).

2.13.2 Saturation binding curve

For saturation curves, maxisorb modules were coated with uniform amounts of the solid phase test protein and blocked as stated previously in section 2.13.1. Control wells were coated with a molar equivalent of BSA. A serial dilution of the liquid phase protein (in TBS/2mM $CaCl_2$) was added to the wells and incubated for 2.5 hrs in a humidity chamber at 37˚C. Reciprocal curves were also produced where serial dilution of a solid phase test protein was incubated with a constant amount of second test protein in a liquid phase (TBS/2mM $CaCl_2$). The control wells contained a serial dilution of molar equivalent of BSA coated on

the wells. After blocking, the appropriate primary antibody was used for the detection of protein-protein interaction using horseradish peroxidase-conjugated secondary antibody and 3,3',5,5'-tetramethylbenzidine substrate revelation as stated previously.

2.13.3 Inhibition of binding

For inhibition of binding experiments, maxisorb modules were coated overnight at 4˚C in a humidity chamber with test proteins (HAC or perlecan) diluted in TBS/2mM $CaCl_2$, and blocked as described previously in section 2.13.1. Control wells were coated with the molar equivalent of BSA. For complete inhibition, full length rLTBP-2 (in TBS/2mM $CaCl_2$/0.05% (w/v) diploma brand low fat dried milk) was pre-treated with 10-fold molar excess of free heparin or chondroitin-6-sulphate (C-6-S) for 15 min at RT with gentle agitation. Positive controls where full length rLTBP-2 in the absence of free heparin or C-6-S was incubated for 15 min at RT were included. The pre-treated rLTBP-2 was added to triplicate wells and incubated for 2.5 hrs at 37˚C. Unbound proteins were washed with 3×TBS/2mM $CaCl_2$ and bound LTBP-2 was detected using anti-(LTBP-2) antibody (LTBP-2C) followed by goat anti-rabbit IgG horseradish peroxidase-conjugate. The interaction was detected with 3,3',5,5'-tetramethylbenzidine substrate as stated above.

For inhibition binding curves, maxisorb plates were coated with HAC or BSA (2pmol/well) and were blocked with milk as described above. Full length rLTBP-2 (1pmol/well) was pre-treated with increasing molar excess of free heparin (0-20pmol) as described previously.

2.13.4 Determination of dissociation constants

Dissociation constants (K_d) for specific interactions were calculated from the ELISA binding curves. Maxisorb modules were coated with a constant amount of HAC (33ng/well) overnight at 4˚C, followed by incubation with an increasing amount of recombinant test protein (full length LTBP-2 or LTBP-2C(H)) for 3 hrs at 37˚C, to establish a saturation curve. A standard curve of recombinant test protein was concurrently constructed where maxisorb wells were coated overnight with an increasing amount of recombinant test protein. Control wells were coated with a molar equivalent of BSA. Anti-LTBP-2 antibody (LTBP-2C) was used for detection of full length LTBP-2, and anti-(tetra-his) antibody was used for detection of LTBP-2C(H). The amount of recombinant test protein bound to heparin in the saturation experiment was calculated from the standard curve. After subtraction of the background binding to the BSA-coated control wells, the amount bound was plotted against the total amount added using data from three repeat experiments. Non-linear regression analysis using

Graphpad Prism version 4.02 software for windows (Graphpad Software, San Diego, CA, www.graphpad.com) was used to determine the dissociation constant.

2.13.5 Statistical analysis

The statistical analysis was calculated by two-tailed unpaired *t* test using Graphpad Prism version 4.02 software. $P < 0.05$ was considered sufficiently significant. The Error bars indicate standard error of the mean.

2.13.6 Digestion of glycosaminoglycans (GAGs)

HS-side chains were removed from perlecan by treatment with heparitinase. Briefly, perlecan (12.5µg) was digested in 100µl of 0.2M Tris/6mM calcium acetate pH 7, containing 1.7U/mg-HS heparitinase (Seikagaku Corp, Tokyo, Japan). Digestion with 0.021U enzyme was carried out for 1hr at 43˚C, then for another 5 hrs following addition of an equal amount of fresh enzyme. The extent of digestion was determined by SDS-PAGE and Coomassie Blue staining (section 2.6).

2.14 Tissue sectioning and immunofluorescence

Frozen sections (5µm thick) were cut using a cryostat 1720 (Leitz, Solms, Germany) from tissue blocks of 20-weeks-old human foetal thoracic aorta and human placenta embedded in optimal cutting temperature compound (Miles Inc., Elkhart, IN). The sections were air-dried for 30 min, fixed in cold 100% acetone for 2 min and rehydrated in PBS (**appendix B**) for 5 min. The rehydrated sections were then incubated with antibodies specific for LTBP-2, perlecan, fibrillin-1, and laminin at the required concentration (**appendix C**) diluted in PBS overnight at 4˚ in humidity chamber. Control sections were incubated with a matched concentration of rabbit IgG for polyclonal antibodies and with mouse IgG for monoclonal antibodies. Sections were gently washed in PBS for 10 min prior to incubation with the appropriate secondary antibody conjugated to flurophore Alexa 488 (Invitrogen, Carlabad, CA) or Cy5 (Jackson Immunoresearch, West Grove, PA) at the required concentration (**appendix C**) for 90 min at RT in the dark. Sections were then washed with PBS for 10 minutes and mounted in anti-fade solution (90% (v/v) glycerol/10% (v/v) PBS and 0.1% p-phenylenediamine (Sigma-Aldrich, St. Louis, MO)) prior to laser confocal microscopy. Labelled sections were examined using a Leica SP5 spectral scanning microscope.

2.15 Coupling of rβig-h3 and rLTBP-2 to Cyanogen Bromide (CNBr)-activated Sepharose 4B

Recombinant protein (rβig-h3 or rLTBP-2) (1.2μM) was dialysed into a coupling buffer (**appendix B**) in preparation for coupling to CNBr-activated sepharose 4B (Amersham Biosciences).

The CNBr-activated sepharose was prepared following the manufacturer's instruction. Briefly, 0.036g of freeze-dried powder was swollen in 500μl of 1mM HCl (to give a total sepharose volume of 126μl), and washed with 1mM HCl in aliquots (500μl/min) for 15 min. Immediately after draining recombinant protein was incubated with the activated-CNBr sepharose overnight at RT on a rotator. Unbound ligand was washed out with 5 col vol of coupling buffer (0.1M $NaHCO_3$, 0.5M NaCl) and analysed by SDS-PAGE (see section 2.6) to determine the percentage of bound ligand. The sepharose was then incubated with a blocking buffer (**appendix B**) for 3 hrs at RT to block the remaining CNBr groups on sepharose and washed extensively with alternating pH buffers 3×(5 col vol of 0.1M acetate, 0.5M NaCl, pH 4, and 5 col vol of 0.1M Tris-HCl, 0.5M NaCl, pH 8), followed by equilibration with 10 col vol of TBS/0.5M NaCl.

A protein mixture extracted from 210-250-day-old foetal nuchal ligament with 1M NaCl was diluted with TBS to give a 1mg/ml of solubilised proteins in TBS/0.5M NaCl. The extracted protein was tested for non-specific binding to sepharose CL4B before it was incubated with the protein coupled-sepharose overnight at RT.

After incubation, the sepharose was drained and washed with the 10×1ml of TBS/0.5M NaCl (if matrigel TBS was used) to remove unbound proteins followed by elution of the bound proteins with 6M urea. The eluted proteins were analysed by SDS-PAGE and either Coomassie Blue stained or silver stained. After eluting the bound protein, the columns were washed with the binding buffer and the columns were stored at 4˚C. Columns of sepharoseCL4B or BSA coupled to CNBr-activate sepharose were used as controls.

2.16 Using nickel chelate chromatography for identification of binding partners of rβig-h3.

Chelating sepharose CL4B (Amersham Pharmacia), 100μl, was primed with nickel prior to incubating the column with rβig-h3 (30μg/600μl) as described in section 2.4. Control columns were incubated with 600μl of 10mM imidazole buffer (**appendix B**) in place of rβig-h3. The flow-through was analysed by SDS-PAGE to confirm that all of the rβig-h3 was bound to the Ni-sepharose. The coupled sepharose and the control-sepharose were then washed with PBS, and incubated for 3 hrs at RT while rotating gently with a protein mixture. This protein mixture was extracted from bovine nuchal ligament with 1M NaCl then dialysed

into PBS, and had prior incubation with Ni-sepharose to remove non-specifically-binding proteins. After the incubation with the protein mixture, the Ni-sepharose was centrifuged at 1000 rounds per minute for 5 min and was washed with 10 col vol of 10mM imidazole buffer. Bound rβig-h3, plus its potential binding partners, was eluted with 10 col vol of 500mM imidazole buffer (**appendix B**) and 500µl fractions were collected. Further bound proteins were then eluted with 10mM imidazole buffer containing 6M urea. Each fraction was analysed by silver staining. The Ni-sepharose was washed with 10 col vol of 10mM imidazole buffer and stored at 4˚C.

2.17 Two-Dimension Gel Electrophoresis (2-DGE)

Using the manufacturer's recommendation (Bio-Rad Laboratories Inc, Hercules, CA), samples (175µg/125µl) in a rehydration buffer (**appendix B**) were applied to a 7cm linear pH 3-10 IPG strip and incubated overnight at RT. The proteins were separated according to their isoelectric charge using a slow ramping preset method, where the voltage is increased quadratically. This mode is used for high resistance samples to minimise high power input initially while achieving high voltage as quickly as possible. Maximum voltage was set at 4,000V, which is the recommended level for 7cm IPG strips. In this mode the voltage is increased quadratically. The conditions were a running temperature of 20˚C, a maximum of 50µA/Gel, a conditioning step of 250V for 15 min and a total focusing time of 60,000 volt-hrs on Protean IEF Cell (Bio-Rad Laboratories Inc, Hercules, CA). After the isoelectric focusing step, the IPG strip was equilibrated with a dithiothreitol equilibration buffer and an iodoacetamide equilibration buffer (**appendix B**) respectively, for 20 min before separation in the second dimension by 15% polyacrylamide gel. The final gel was silver stained (section 2.7). Except for Cydye DIGE Fluor dye labelled samples the gel was scanned with Typhoon Trio+ variable mode imager and analysed using DeCyder 2-D Differential Analysis Software (GE Healthcare, Uppsala, Sweden).

2.18 Difference Gel Electrophoresis (DIGE) using CyDye DIGE Fluor Dyes

Using the manufacture's recommendation (GE Healthcare Fairfield NY), proteins eluates (5µg) from rβig-h3-sepharose and rLTBP-2-sepharose columns were dialysed into the rehydration buffer containing thiourea (**appendix B**), and labelled with fluorescent dye Cye 3 or Cy 5 (40pmol) on ice in the dark for 30 min. The reaction was then stopped by addition of 10mM lysine, samples were pooled, the volume was made up to 125µl with the rehydration buffer containing thiourea and analysed as previously described in section 2.17.

CHAPTER 3
BINDING INTERACTION OF HUMAN LTBP-2 WITH HEPARIN/ HEPARAN SULPHATE PROTEOGLYCANS

LTBP-2 is a member of LTBP/Fibrillin superfamily and it has been found to colocalise with microfibrils and directly interact with fibrillin-1 *in vitro* (Gibson *et al.,* 1995; Hirani *et al.,* 2007). A number of other matrix components have been identified to interact with fibrillin-1-microfibrils, including MAGP-1, -2 (Gibson *et al.,* 1998; Gibson *et al.,* 1996; Henderson *et al.,* 1996), fibulin-2, -4, and -5 (El-Hallous *et al.,* 2007; Freeman *et al.,* 2005; Reinhardt *et al.,* 1996b), LTBP-1, -2 and -4 (Hirani *et al.,* 2007; Isogai *et al.,* 2003), various PGs such as decorin, biglycan (Reinboth *et al.,* 2002; Trask *et al.,* 2000a), perlecan (Tiedemann *et al.,* 2005) and isolated HS-GAG chains (Tiedemann et al., 2005). Not all of these components are associated with microfibrils in all tissues. Associated components vary as they have tissue-specific functions (depending on the functional and mechanical requirements of a given tissue) (Kobayashi *et al.,* 2007; Penttinen *et al.,* 2002; Sterzel *et al.,* 2000). The biological roles of many of the associated proteins are far from clear and continuing study of these associated components is needed to understand how each contributes to the structure and function of fibrillin-microfibrils.

Research into the biological roles of LTBP-2 in relation to microfibrils has shown that LTBP-2 is not an integral component of microfibrils (Kielty *et al.,* 1998). Also, in contrast to other LTBPs, LTBP-2 does not appear to be directly involved in tissue storage of TGF-β on microfibrils as LTBP-2 does not bind covalently to latent TGF-β (Gibson *et al.,* 1995; Saharinen and Keski-Oja, 2000). However, the findings of Hirani *et al.,* (2007) have indicated that LTBP-2 may be a major modulator of the storage of the growth factor on fibrillin-1-microfibrils. This was elucidated from solid phase binding assays showing that LTBP-2 competes with LTBP-1 for binding to fibrillin-1 (Hirani *et al.,* 2007). Therefore, the examination of the interaction of LTBP-2 with other potential binding ligands is required to determine if any additional binding partners of LTBP-2 can be identified to further elucidate its full tissue function. In this regard, associated components of microfibrils are the best candidates for investigation for relevant interactions. LTBP-2 does not interact directly with MAGP, biglycan, decorin, and tropoelastin (Hirani *et al.,* 2007), but its ability to interact with heparin/HS-GAGs has not yet been investigated.

In chapters 3 to 5, the interaction of rLTBP-2 with heparin conjugated to albumin (HAC) was studied using solid phase binding assay. Heparin was used because it is

structurally similar structure to HS and is a suitable substitute for HS-GAG, and is also commercially available in large quantities. To determine the physiological relevance of the interaction between LTBP-2 and heparin, the HSPGs perlecan and syndecans were also tested for interactions with rLTBP-2 and its fragments.

The expression clone for human full length rLTBP-2 has been previously used in our laboratory to produce rLTBP-2 protein. In addition, three recombinant fragments of LTBP-2 were made to cover the entire length of the LTBP-2 molecule, consisting of the amino-terminal fragment (LTBP-2NT(H)), the central fragment (LTBP-2C(H)), and the carboxy-terminal fragment (LTBP-2CT(H)) (**figure 3.1**). The construction of LTBP-2CT(H) has previously been described (Hirani *et al.,* 2007). The construction and expression of rLTBP-2NT(H) and rLTBP-2C(H) will be described in section 4.1. The purified rLTBP-2 fragments were used for mapping of the heparin binding site(s) on LTBP-2.

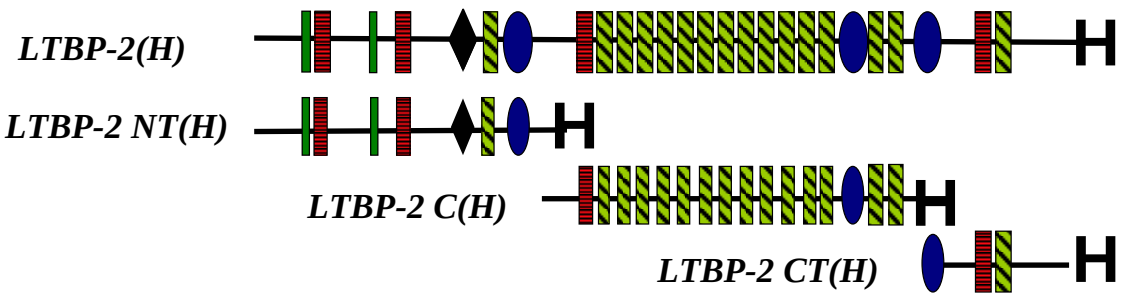

Figure 3.1. Schematic representation of rLTBP-2 and rLTBP-2 fragments. Domain structure of rLTBP-2 constructs. Domain structures: green box, 4-cys domain; red and black striped box, EGF-like domain; green crosshatched box, cbEGF-like domain; black diamond, hybrid domain; blue ovoid, 8-cys domain; H, his_6-tag.

3.1 Expression and purification of human recombinant LTBP-2

Full length human LTBP-2 cDNA had previously been cloned into the episomal expression vector pCEP-4 (Hirani *et al.,* 2007). For production of human rLTBP-2, a number of amino acid changes were introduced compared with the published sequence. The endogenous LTBP-2 signal peptide was substituted by the signal sequence of human BM protein BM40 (Hirani *et al.,* 2007) to allow for enhanced gene expression within the HEK cell line (Nischt *et al.,* 1991). A his_6-tag was also added to the C-terminus to allow for protein purification. The expression LTBP-2 construct was transfected into mammalian 293 EBNA cells and rLTBP-2 protein was purified from the conditioned medium using Ni-sepharose chromatography (section 2.4). Initially rLTBP-2 was purified from cells that had been incubated in three different media to determine which was the most suitable for maximum expression of rLTBP-2. The three tested media were serum-free DMEM, DMEM containing

serum and serum-free Ex-Cell 293 medium which is designed specifically for use with suspension cultures of 293 EBNA cell lines.

Purified samples from different media were analysed by western blotting with anti-(tetra-his) antibody used to detect purified recombinant protein (section 2.6). A single band was detected at 210 kDa in serum-free DMEM and DMEM plus serum, with the intensity of the band in serum-free DMEM appearing to be greater (**figure 3.2A**). In contrast, no antibody staining was detected in the sample purified from serum-free Ex-Cell 293 (**figure 3.2A**). The results indicated that rLTBP-2 was not highly expressed using Ex-Cell 293 medium, while the highest expression of rLTBP-2 was in serum-free DMEM medium. Hence serum-free DMEM was used for larger scale rLTBP-2 production.

Recombinant LTBP-2 was purified from serum-free DMEM migrated on SDS-PAGE as two bands at 226 kDa and 210 kDa under reducing conditions and was free of major contaminants (**figure 3.2B**). The observed molecular weight values of the rLTBP-2 protein corresponded well to the previously-reported size of purified rLTBP-2 which was 210 and 219 kDa under reducing conditions (Hirani *et al.,* 2007), and to the predicted LTBP-2 polypeptide molecular weight of 195 kDa (Gibson *et al.,* 1995; Moren *et al.,* 1994). The discrepancy between the measured molecular mass compared with the theoretical mass calculated from the protein sequence of the mature recombinant protein and/or the multiple bands present is possibly due to varying degrees of post-translational modifications of the protein. LTBP-2 has been shown to contain 10 potential N-glycosylation sites (Hyytiainen *et al.,* 1998). Furthermore, the size of the rLTBP-2 doublet was reduced by 15 kDa in the presence of N-glycosidase with no dramatic changes in the presence of O-glycosidase (Hirani *et al.,* 2007). Western blots showed the purified protein was immunoreactive to anti-(LTBP-2) antibody (LTBP-2C) confirming the identity of the purified protein as LTBP-2 (**figure 3.2B**). Approximately 1.7µg of rLTBP-2 was produced per ml of DMEM medium and a total of 2.1mg of rLTBP-2 was purified.

There were differences with regard to the medium selected for expression and purification of rLTBP-2 between reports of Hirani *et al.,* (2007) and the observed results in the present study. Hirani *et al.,* (2007) previously described the purification of larger quantities of rLTBP-2 free of contaminants from the Ex-Cell 293 medium compared to the observed lower qualities of less pure rLTBP-2 purified from cells grown in serum-free DMEM. The differences between the results of Hirani *et al.,* (2007) and those described here may be due to batch variation in the composition of the Ex-Cell 293 media supplied by the manufacturer.

3.2 Synthesis and purification of heparin-albumin conjugate

Covalent conjugates of BSA and heparin were prepared for use in the coating of individual wells of maxisorb microtitre plates which have a high affinity for proteins with both hydrophilic and hydrophobic domains. The conjugates were obtained by a condensation reaction between albumin and heparin using 1-ethyl-3-(dimethylaminopropyl)-carbodiimide (section 2.10). Unfractionated conjugate was purified by ion-exchange chromatography on diethyl-aminoethyl (DEAE) sepharose CL4B (section 2.10). Briefly, after the mixture was applied to the column, un-conjugated albumin was washed with 0.3M NaCl, and 0.9M NaCl was used to elute the more strongly bound heparin-albumin conjugates (HAC) bound to the sepharose (**figure 3.3**).

The concentration of heparin in HAC was determined by an uronic acid assay using a produced D-glucuronic acid standard curve (section 2.11). The A_{520} readings for the HAC fractions were plotted against the standard curve to determine the amount of heparin present in the conjugates.

The amount of free or conjugated albumin in the collected fractions was determined spectrophotometrically (A_{280}) using a BSA standard curve (see section 2.10). Fraction 12 (**figure 3.3**) contained the highest amount of both heparin and albumin and this was selected for solid phase binding studies. It should be noted that this fraction provided a sufficient amount of HAC for the binding studies, and that purification of HAC that remained in the initial column flow through was not performed. Hence not all of the conjugate was purified from the condensation reaction mixture. The yields of heparin and albumin in the conjugate were 4.8mg and 19mg, giving an average (wt/wt) ratio of 1:4 heparin to albumin in the conjugate. It was estimated that 6% and 7% of heparin and albumin respectively from the original material were conjugated.

3.3 The analysis of LTBP-2 interaction with heparin

3.3.1 Solid phase immuno-assays

For examining the interaction between LTBP-2 and heparin, a solid phase binding method was employed (section 2.13.1). These assays involved coating HAC onto individual wells of maxisorb microtitre plates. The non-specific binding sites were blocked with 3-5% low fat dried milk or BSA solution. The rLTBP-2 was then added in solution (TBS/2mM $CaCl_2$) and incubated with the coated wells. Interaction was detected using rLTBP-2 specific antibody followed by colour detection. Control wells replaced the HAC with the molar equivalent of BSA to determine the level of background binding of LTBP-2 and LTBP-2 fragments to the well. In addition, an initial control where LTBP-2 was replaced with the

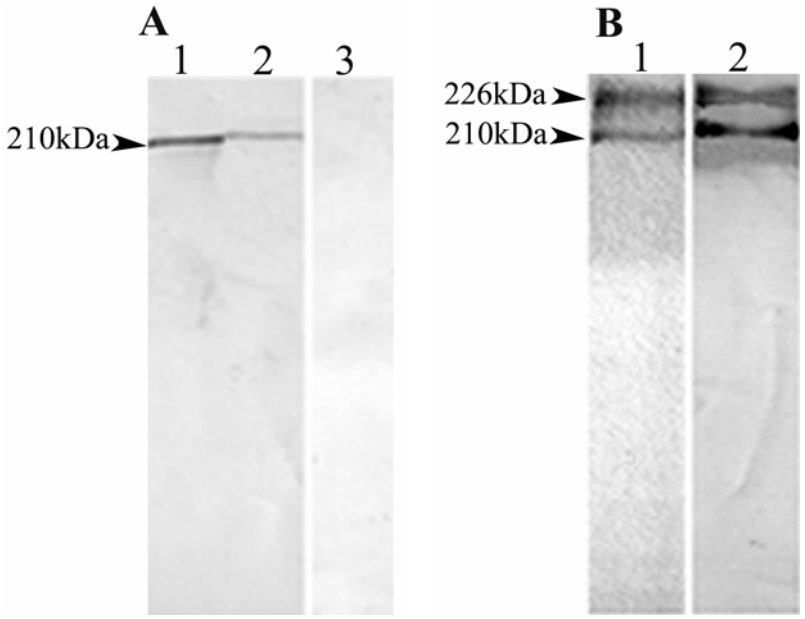

Figure 3.2. Optimisation of expression and purification of rLTBP-2. **A,** Optimisation of rLTBP-2 expression by 293 EBNA cells grown in three different media compared using SDS-PAGE and immunoblotting with anti-(tetra-his) antibody. Serum-free DMEM **(lane 1)**, DMEM plus serum **(lane 2)**, and serum-free Ex-Cell 293 **(lane 3)**. **B,** Serum-free DMEM was selected for the further production of rLTBP-2 and a typical analysis is shown of the purified protein, Coomassie Blue staining **(lane 1)**, immunoblotting with anti-(LTBP-2) antibody (LTBP-2C) **(lane 2)**. Two specific immunoreactive bands at 226kDa and 210 kDa were identified with no contaminants.

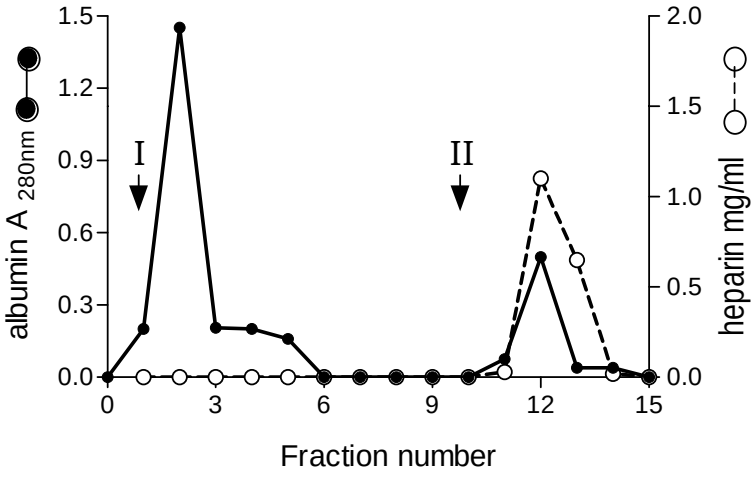

Figure 3.3. Fractionation of un-conjugated albumin and heparin-albumin conjugate (HAC) on DEAE sepharose Cl4B. The arrows indicate **I,** elution of free albumin bound on the column with 0.3M NaCl/0.025M tris pH 7. **II,** elution of heparin-albumin conjugate with 0.9M NaCl/0.025M tris pH 7. The concentration of free or conjugated albumin was determined spectrophotometrically (A_{280}) from a BSA standard curve, while an uronic acid assay (A_{520}) was used to determine the concentration of heparin in HAC using a glucuronic acid standard curv.

molar equivalent of BSA was used for detection of any cross-reaction of the HAC with antibodies specific to rLTBP-2. Equilibrium dissociation constants were calculated from specific binding curves to determine the strength of each association.

Firstly, binding conditions needed to be optimised to prevent non-specific background binding of LTBP-2 to the wells and to maximize detection of authentic LTBP-2-heparin binding. For sensitive detection of authentic binding between LTBP-2 and heparin-coated wells, two antibodies were considered, anti-(tetra-his) antibody and anti-(LTBP-2) antibody (LTBP-2C) (**appendix C**). While comparing the detection capabilities of the two antibodies, a higher specific binding signal was observed for the interaction of LTBP-2 with heparin using anti-(LTBP-2) antibody (LTBP-2C) compared to anti-(tetra-his) antibody (**figure 3.4**). Neither antibody cross-reacted with the HAC-coated on the wells (**figure 3.4**). However, both antibodies detected a high level of non-specific interaction of LTBP-2 with BSA-coated wells, even though the wells were incubated with 3% BSA solution prior to incubation with LTBP-2 (**figure 3.4**). Overall the results of the initial binding assays indicated that the interaction of LTBP-2 and heparin was specific, although a large amount of LTBP-2 was interacting non-specifically with BSA-coated wells resulting in a high background.

To reduce the background signal caused by non-specific interaction of LTBP-2 with BSA-coated wells, 5% low fat dried milk was tested as an alternative blocking solution. This resulted in a slight decrease in the background signal. However, the reduction was not achieved at satisfactorily low levels (data not shown). Therefore, the addition of carrier proteins such as BSA or low fat dried milk in solution was considered. The addition of up to 0.04% BSA to the solution did not reduce the non-specific interaction of LTBP-2 with the wells. However, the addition of 0.05% low fat dried milk to the solution dramatically reduced the non-specific background binding of LTBP-2 (**figure 3.5**). These data suggested that the optimised protocol for conducting solid phase binding assays included blocking of the wells with 5% low fat dried milk solution, dilution of rLTBP-2 in TBS/2mM $CaCl_2$ containing 0.05% low fat dried milk and using anti-(LTBP-2) antibody (LTBP-2C) for detection of heparin/HSPG binding.

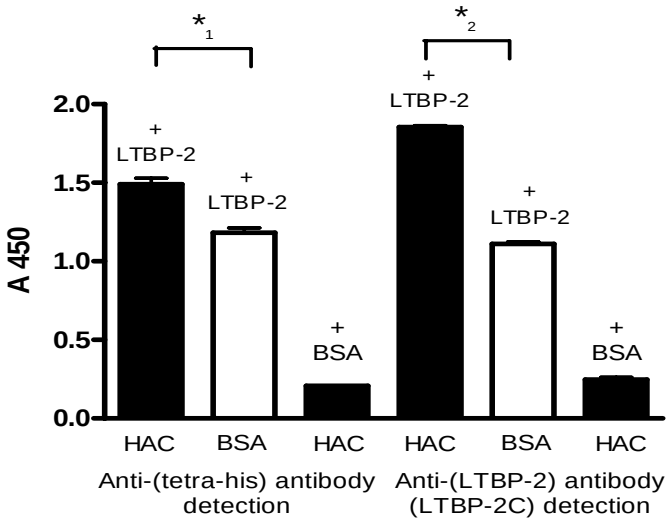

Figure 3.4. Optimisation of the conditions for solid phase assays. Wells coated with molar equivalent of HAC or BSA control were blocked with 3% BSA solution prior to incubation with rLTBP-2 or a molar equivalent of BSA as a control. Two antibodies, anti-(tetra-his) antibody (0.1µg/ml), and anti-(LTBP-2) antibody (LTBP-2C) (0.1µg/ml), were tested for their effectiveness in detecting specific binding. At the concentration of 0.1µg/ml used, anti-(LTBP-2) antibody (LTBP-2C) produced a higher binding signal. Neither of the antibodies cross-reacted with HAC on the wells. * indicates statistical significance of $P \leq 0.05$. $*_1$, P= 0.003 and $*_2$, P= 0.0001.

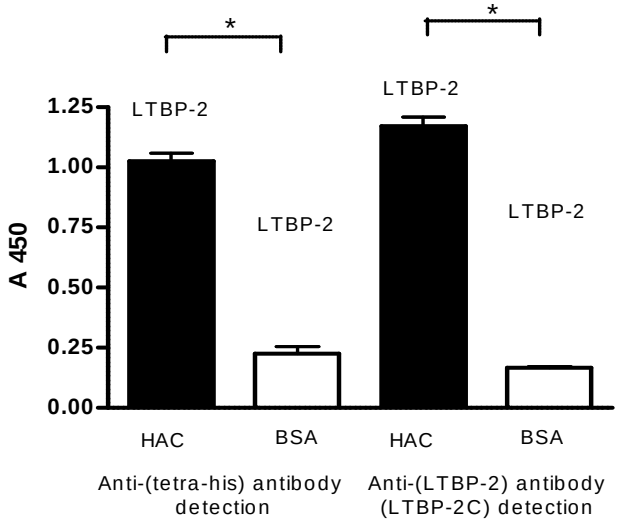

Figure 3.5. Reducing non-specific interaction of LTBP-2 with the addition of carrier protein in solution. Heparin (HAC) (11.1pmol) and molar equivalent of BSA were coated on the wells prior to blocking the excess binding sites with 5% low fat dried milk solution. Recombinant LTBP-2 (10nM) in liquid phase containing 0.05% low fat dried milk was incubated with the wells and binding was detected with either anti-(tetra-his) antibody (0.1µg/ml) or with anti-(LTBP-2) antibody (LTBP-2C) (0.1µg/ml). Non-specific background was reduced significantly with the addition of a carrier protein in solution. * indicates statistical significance of $P \leq 0.05$. * P= 0.001.

3.3.2 LTBP-2 interacts with heparin-albumin conjugate (HAC)

To investigate the interaction of LTBP-2 with heparin, solid phase binding assays were conducted under optimised conditions (section 3.3.1). A negative control of molar equivalent of BSA-coated on the wells was included and experiments were performed in triplicate. Incubation of LTBP-2 in the liquid phase with immobilised heparin (HAC) resulted in a strong binding signal, while in comparison a minimal signal was observed for the interaction of LTBP-2 with BSA-coated control wells, as seen previously in **figure 3.5**. The results indicated that LTBP-2 interacted specifically with heparin and non-specific interactions with BSA or the plastic wells were minimal. To authenticate the novel interaction between LTBP-2 and heparin, binding and inhibition curves were produced (section 2.13.2 & 2.13.3). Increasing molar concentrations of rLTBP-2 in solution were incubated with a constant molar amount of heparin (HAC)- or BSA-coated on the wells. The resulting binding curve showed a dose-dependent increase. The specific binding of LTBP-2 with heparin increased as the concentration of added LTBP-2 increased until saturation was reached (**figure 3.6A**).The non-specific interaction of LTBP-2 protein with the BSA-coated wells was in direct proportion to the increase in LTBP-2 concentration, indicative of non-specific binding. The established curve showed specific binding was proportional to the concentration of rLTBP-2. The reverse of the experiment was also performed to confirm the saturating interaction between LTBP-2 and heparin. Incubating increasing molar amounts of heparin (HAC) coated on the well with constant LTBP-2 concentration resulted in a saturable binding curve (**figure 3.6B**). Furthermore, there was a low background signal detected for the constant concentration of LTBP-2 added in solution (**figure 3.6B**).

The specific interaction of LTBP-2 with heparin was further confirmed by blocking the binding of LTBP-2 with heparin-coated wells with the addition of un-conjugated heparin in solution. An inhibition curve was prepared by incubating an increasing excess molar concentration of free heparin (compared with heparin coated on wells) with LTBP-2 in solution prior to incubation with the heparin-coated wells. This resulted in a decrease in binding which was in a non-linear relationship to the increase in molar amounts of un-conjugated heparin added (**figure 3.7**). The signal dropped to background levels when the un-conjugated heparin in solution was five-fold in excess of the molar amount of heparin (HAC) coated on the wells. Furthermore, background binding to BSA-coated wells was consistently low. The results indicated that the un-conjugated heparin completely blocked the interaction of LTBP-2 with the heparin-coated wells through competition for binding to LTBP-2. Based on the above results, it was deduced that the interaction between LTBP-2 and heparin was specific.

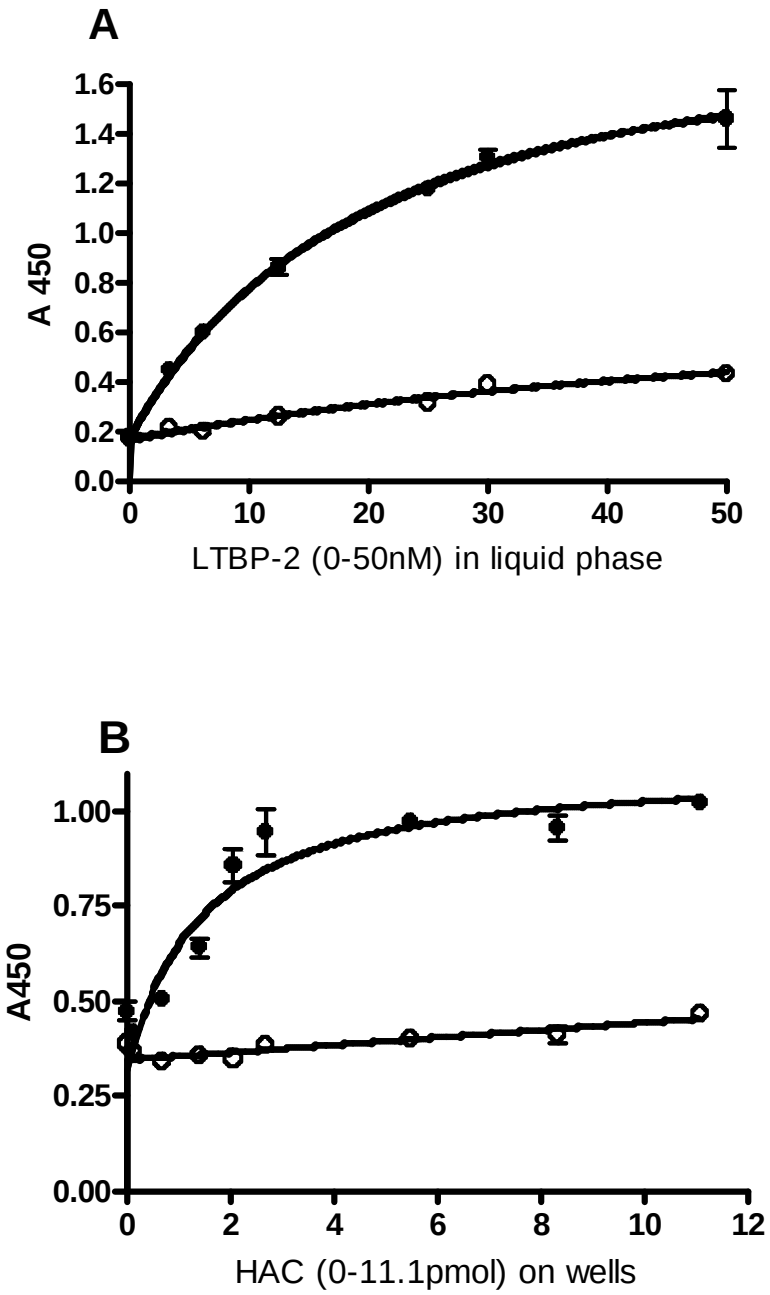

Figure 3.6. Saturation binding curve of the interaction of LTBP-2 and heparin. **A,** Increasing concentration of rLTBP-2 (0-50nM) in solution was incubated with constant molar amount of immobilised heparin (HAC) (2.8pmol), *black circles*, or BSA, *white circles*, at molar equivalent to HAC. Anti-(LTBP-2) antibody (LTBP-2C) (0.1μg/ml) was used for detection of binding. **B,** Constant LTBP-2 (10nM) in solution was incubated with increasing molar amounts of heparin (HAC) (0-11.1pmol), *black circles*, or BSA, *white circles*, at the same molar equivalent, which had been coated on the wells.

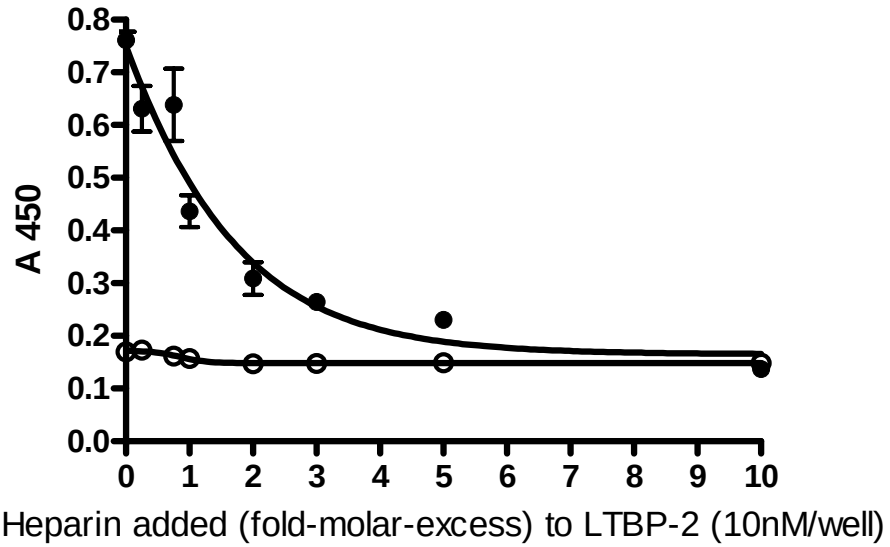

Figure 3.7. Inhibition binding curve of LTBP-2 interaction with heparin. Increase in excess molar concentration of free heparin (0-208nM) was incubated with LTBP-2 (10nM) in solution for 15 minutes prior to incubation with constant heparin (HAC) (2.1pmol), *black circles*, or molar equivalent of BSA, *white circles*. Free heparin in solution blocked the interaction of LTBP-2 with heparin-coated wells.

3.3.3 The interaction of LTBP-2 with heparin is not a non-specific interaction with polyanionic GAGs

Sulphated GAGs which include CS, dermatan sulphate, heparin and HS are repeating disaccharide units composed of uronic acid (GlcA or IdoA) and an amino sugar (galactosamine or glucosamine) (Mulloy *et al.,* 2006). All of these GAG chains are strongly negatively-charged due to their high content of uronic acids and sulphate groups. To confirm that the interaction of LTBP-2 with heparin is not solely a charge-related interaction with all GAGs, the blocking of the binding with an alternative negatively-charged GAG, CS, was conducted. Using the solid phase binding assay, LTBP-2 in solution was incubated with a ten-fold molar excess of C-6-S (compared to heparin coated on the wells), prior to incubation with the heparin-coated wells. A positive control where LTBP-2 was incubated with heparin in the absence of C-6-S was included, in addition to the BSA negative controls. As shown previously (**figure 3.6**), a strong signal was detected for the interaction of LTBP-2 with heparin (HAC) in the absence of C-6-S (**figure 3.8**) and a similarly strong signal was detected for the interaction of LTBP-2 with heparin (HAC) in the presence of C-6-S. Furthermore, there was minimal non-specific binding detected for the interaction between LTBP-2 and BSA-coated wells in the presence or absence of C-6-S. These findings indicate that the interaction of LTBP-2 with heparin is not a non-specific charge-related interaction with GAGs, but is a specific heparin/HSPG interaction.

3.3.4 LTBP-2 interaction with heparin depends on calcium or other divalent cations

LTBP-2 protein is composed mainly of a large number of cbEGF-domains and their conformation is dependent on calcium ions (Gibson *et al.,* 1995). Recently, Hirani *et al.,* (2007) showed the addition of 2mM calcium ions in solution enhanced the interaction of LTBP-2 with fibrillin-1. Thus, the interaction studies described in this chapter between LTBP-2 and heparin had been initially performed in the presence of 2mM calcium ions. To determine if calcium ions actually influence the interaction between LTBP-2 and heparin, immuno-assays were conducted under three different conditions, a) in the absence of added calcium ions or, in the presence of b) 5mM EDTA or c) 5mM EGTA. EDTA and EGTA are chelating agents that sequester divalent metal ions, but EGTA has a much higher specificity for calcium ions. The highest level of binding was detected when the interaction was conducted in the presence of calcium ions (**figure 3.9**). The absence of added 2mM calcium ions was found to give slightly lower interaction levels compared to those with added calcium. However this difference was considered to be insignificant. When the non-specific

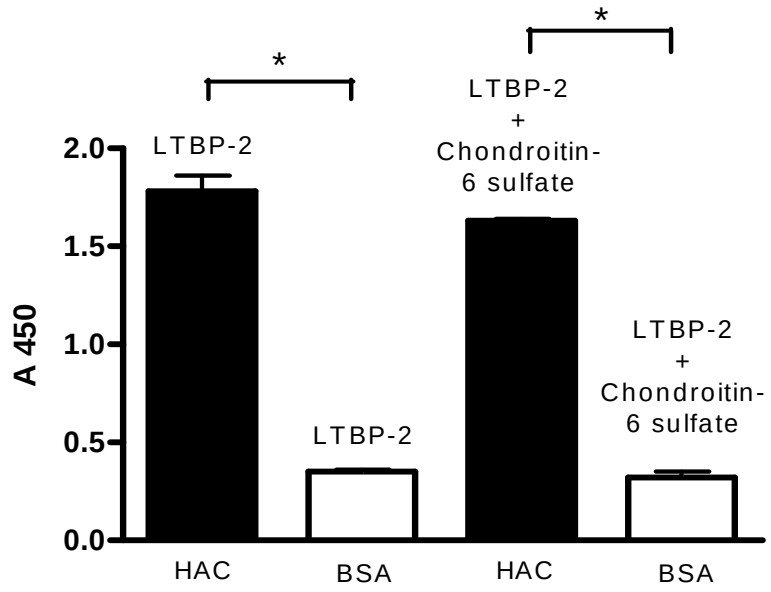

Figure 3.8. Interaction of LTBP-2 with heparin is specific and is not a non-specific charge-related interaction. Incubation of Chondroitin-6-sulfate (208nM) with LTBP-2 (10nM) in solution for 15 minutes prior to incubation with heparin (HAC) (2.1pmol) or molar equivalent of BSA coated on the wells. LTBP-2 does not interact with negatively-charged GAGs. Interaction is specific to heparin. * indicates statistical significance of P≤ 0.05. *, P= 0.001.

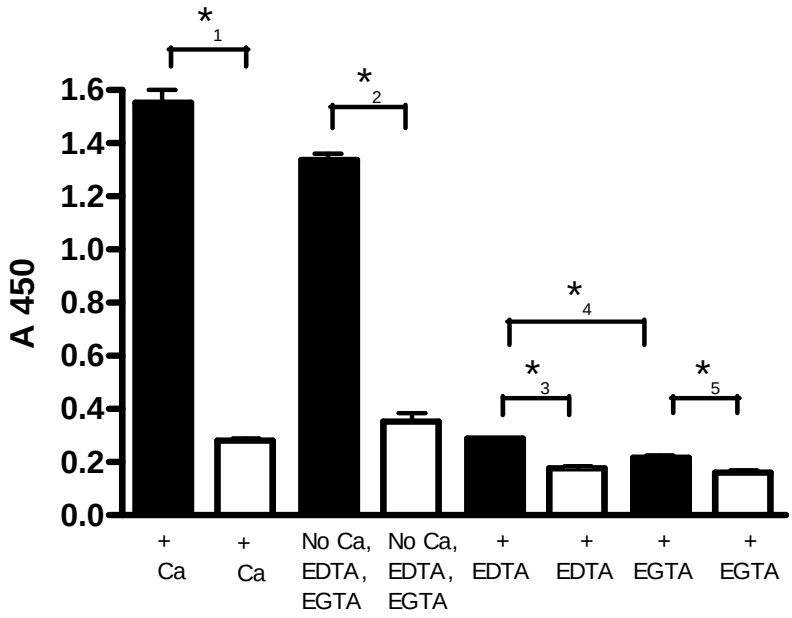

Figure 3.9. The interaction of LTBP-2 with heparin is cation dependent. Recombinant LTBP-2 (10nM) in various solutions; TBS+2mM calcium, TBS only, TBS+5mM EDTA or TBS+5mM EGTA was incubated with immobilized heparin (HAC) (2.8pmol) or molar equivalent of BSA. Antibody specific to LTBP-2 was used to detect specific binding of LTBP-2 with heparin in the various solutions. Presence of EDTA or EGTA blocked the interaction of LTBP-2 with heparin, while the presence of calcium ions enhanced the interaction. * indicates statistical significance of P≤ 0.05. $*_{1,2}$, P= 0.0001. $*_3$, P= 0.002. $*_4$, P= 0.003. $*_5$, P= 0.01.

binding of LTBP-2 to the wells was compared in the presence and absence of calcium ions a decrease was detected in the presence of calcium, but again the difference was insignificant.

In the presence of EDTA or EGTA, there was much lower binding with signals close to background levels (**figure 3.9**), compared with binding detected in the presence of calcium. It was also noted that the presence of these chelating agents also slightly decreased the non-specific background interaction of LTBP-2 with the wells. Overall, the data showed that the presence of a chelating agent such as EDTA or EGTA almost completely abolished the interaction between LTBP-2 and immobilised heparin (HAC). Thus from the results it was concluded that the interaction between LTBP-2 and heparin is dependent on the presence of divalent metal ions. This may be due to either direct or indirect alterations of the conformation of one or more cbEGF-domains of LTBP-2. EGTA inhibited the binding of LTBP-2 with heparin (HAC) more effectively than EDTA. This indicates that the interaction between LTBP-2 and heparin is most likely to be calcium dependent.

3.3.5 Kinetic analysis of the interaction between LTBP-2 and heparin

To analyse the dynamic interaction between LTBP-2 and heparin, the K_d was calculated from saturation binding experiments using non-linear regression analysis for one site binding (GraphPad Prism version 4 for windows, GraphPad Software, San Diego California USA, www.graphpad.com) (section 2.13.4). The K_d is expressed in molar units (M) and corresponds to the concentration of ligand at which the binding site on the target protein is half occupied. More importantly, it is a measure of the affinity (strength) of the interaction. Producing a saturation binding curve for binding of LTBP-2 with heparin involved the incubation of a constant molar amount of heparin (HAC)- or BSA-coated on the wells with increasing molar concentrations of LTBP-2 in solution. **Figure 3.10A** illustrates the binding curve after subtraction of the BSA background. Simultaneously, a standard curve was established by directly coating wells with known molar amounts of LTBP-2 or BSA, as the relative signal of the known quantities was determined with anti-LTBP-2 antibody (LTBP-2C) (**figure 3.10B**). A standard curve was necessary to determine the molar amount of LTBP-2 that bound to the heparin-coated wells. After subtraction of the background, using data from three repeated experiments, the molar amount of LTBP-2 bound was calculated for each HAC amount and plotted against the total molar concentration of LTBP-2 added (**figure 3.10C**). The K_d was calculated as 14.5±3.7nM. Therefore, binding of heparin to LTBP-2 was considered to be of strong affinity.

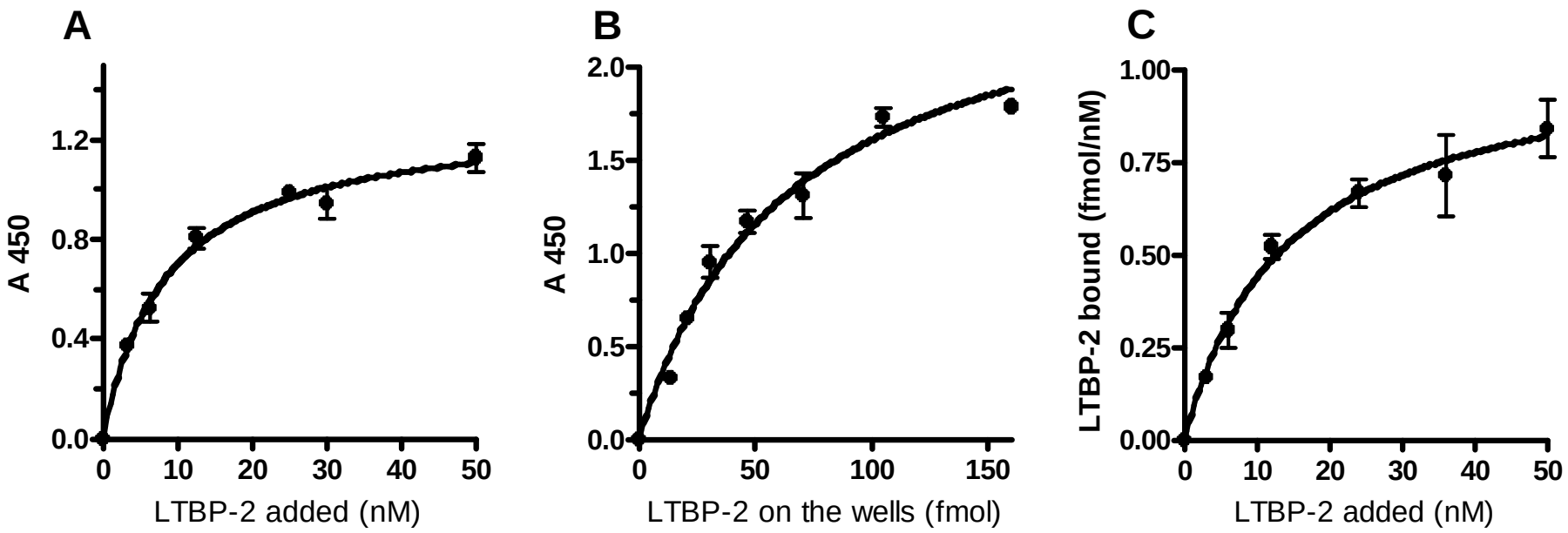

Figure 3.10. Kinetic analysis of the interaction between LTBP-2 and heparin using solid phase binding assay. **A,** Saturation binding curve for LTBP-2 and heparin after subtraction of the background BSA. Increasing molar concentration of LTBP-2 in solution was incubated with constant molar amount of heparin (HAC) (2.1pmol) or molar equivalent of BSA coated on the wells. **B**, Standard ELISA curve for LTBP-2 after subtraction of the background. Increasing molar amount of LTBP-2 (0-160fmol) was coated on the wells overnight and signal levels for each specific quantity was determined using anti-LTBP-2 antibody (LTBP-2C) (0.1µg/ml). **C,** LTBP-2-heparin (HAC) binding curve used to calculate K_d. The total molar concentration of LTBP-2 added in solution in **A** was plotted against the molar amount bound determined in **B**. The K_d.was calculated to be 14.5±3.7nM, suggesting LTBP-2 has a strong affinity for heparin.

CHAPTER 4
THE CENTRAL REGION OF LTBP-2 CONTAINS A BINDING SITE FOR HEPARIN

Results from Chapter 3 indicate that LTBP-2 has a specific and moderately strong interaction with heparin. The interaction was shown to be probably calcium dependent (section 3.3.4), thus heparin may be interacting with LTBP-2 via one of its many cbEGF domains. Narrowing down the heparin binding site(s) on LTBP-2 will aid in further characterisation of this interaction. As more binding partners for LTBP-2 are identified and characterised, we can deduce how these novel ligands may influence each other's interaction with LTBP-2 and modulate the function of LTBP-2.

To define the binding regions for heparin on LTBP-2, production of expression constructs for rLTBP-2 fragments was necessary. Our laboratory had already cloned an expression cDNA encoding the carboxyl-terminus of LTBP-2 (LTBP-2CT(H) (Hirani *et al.*, 2007). This chapter describes the construction of the expression plasmids in order to express the amino-terminal region of LTBP-2 and the central fragment of LTBP-2, for use in the solid phase binding analyses with heparin.

4.1 Expression, purification and characterisation of the central region of LTBP-2 (LTBP-2C(H))

4.1.1 Expression and purification of LTBP-2C(H)

A cDNA encoding the central region of LTBP-2 (bases 2758-5142, and residues 750-1584 of the published LTBP-2 sequence, Genbank accession number NM_000428) was amplified from the full length LTBP-2 cDNA template, using designed primers containing *HindIII* restriction sites at their 5' ends (section 2.2.1). The presence of the *HindIII* sites is important for subsequent subcloning into the modified mammalian expression vector pCEP-4. These primers flank the region of the cDNA encoding the third EGF-like domain to the region just prior to the last 8-cys domain. The amplified PCR product of 2384 bases (**figure 4.1A**) was subcloned into modified pCEP-4 (Hanssen and Gibson unpublished). The LTBP-2C(H) expression construct was transfected into 293 EBNA cells and rLTBP-2C(H) was purified using affinity chromatography from the serum-free conditioned medium (section 2.3 & 2.4). Purification produced yields of approximately 0.7µg/ml of medium. Purified rLTBP-2C(H) was stored in TBS/0.5M NaCl at -20˚C.

4.1.2 Analysis and authentication of rLTBP-2C(H)

Purified rLTBP-2C(H) was resolved free of major contaminants as a single band at 97 kDa under non-reducing conditions and at 130 kDa under reducing conditions (**figure 4.1B**) (section 2.6). This size was larger than the predicted molecular weight of 85 kDa. A discrepancy between the predicted and the apparent molecular weight has been reported for other recombinant LTBP-2 fragments including LTBP-2CT(H), and some of the fibrillin constructs (Hirani *et al.,* 2007). These differences are often the result of post-translational modifications including glycosylation, as LTBP-2 is N-glycosylated (Hirani *et al.,* 2007). Aside from LTBP-2, the predicted size of the mature MAGP-2 polypeptide encoded by the cDNA for both the bovine and human forms of the protein was also smaller than its apparent molecular weight observed on SDS-PAGE (Gibson *et al.,* 1996). This discrepancy was suggested to be due to glycosylation of the protein which has a consensus sequence for *N*-linked carbohydrate attachment (Gibson *et al.,* 1996). Furthermore, it is not uncommon for polypeptides to appear on gels as differently sized from their predicted size. These differences may occur as a result of a particular conformation of the proteins which may affect the mobility of the proteins through the polyacrylamide pores during electrophoresis and thus result in the protein migrating at a different size compared to the predicted size. For instance, the deviation in molecular mass of MAGP-1 on SDS-PAGE compared with its actual molecular mass was suggested to be a function of the primary structure of MAGP-1 (Gibson *et al.,* 1991). Other examples were fibulin-3 and -4, which showed an increase in electrophoretic mobility when the recombinant proteins were examined under reducing conditions, due to the many intracellular disulphide bonds present in both recombinant proteins (Giltay *et al.,* 1999). When the purified recombinant protein was examined for reactivity to anti-(tetra-his) antibody under reducing conditions, a single band at 130 kDa was detected (**figure 4.1C**). No other bands were detected by the antibody suggesting purified LTBP-2C(H) was free of his-rich contaminants. Overall the results confirmed the purification of a recombinant protein from serum-free DMEM with relatively high purity, though the size of the purified protein was substantially different to the predicted size of the expected recombinant protein. Furthermore, the discrepancy observed for size of rLTBP-2C(H) was substantial compared to the differences reported for other recombinant proteins. Therefore it was necessary to authenticate the recombinant protein as LTBP-2C(H).

The simplest method of authentication of the purified protein as LTBP-2C(H) was through western blot analysis using a LTBP-2 antibody. However, the available anti-LTBP-2 antibody (LTBP-2C) produced in the Gibson laboratory (Hirani *et al.,* 2007) was specific to the carboxy-terminal 8-cys domain and thus it was unable to recognise the central fragment

of LTBP-2. To confirm that the recombinant protein was a fragment of LTBP-2, peptide mass finger-printing was considered (section 2.9).

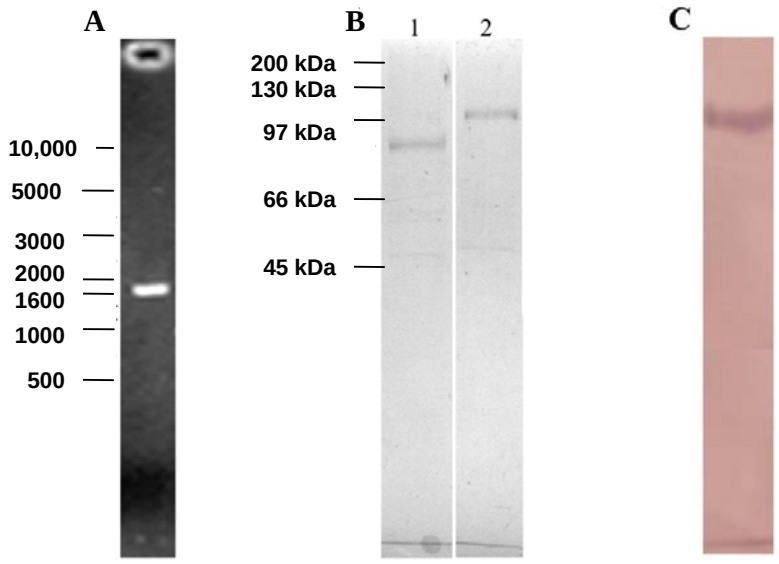

Figure 4.1. PCR amplification of a cDNA encoding rLTBP-2C(H) and analysis of purified recombinant protein. **A,** LTBP-2C(H) PCR product analysed on a 0.8% (w/v) agarose gel and stained with ethidium bromide. A single band of expected product size of 2384 bases was detected. **B,** Purified rLTBP-2C(H) resolved by 12% SDS-PAGE. Coomassie Blue indicated a contaminant-free protein band of 97 kDa when sample is non-reduced **(lane 1)** and 130 kDa when sample is reduced **(lane 2)**. **C,** Anti-(tetra-his) antibody confirmed the purified protein as recombinant protein.

4.1.3 Peptide mass finger-printing of rLTBP-2C(H)

MALDI-TOF-MS was used to perform peptide mass finger-printing for identification of the purified recombinant protein as LTBP-2C(H) (section 2.9). To do this, the LTBP-2C(H) band was excised from SDS-PAGE and digested with trypsin. Trypsin was the favoured protease enzyme for peptide mass finger-printing as it is relatively cheap, highly effective and generates peptides with an average size of about 8-10 amino acid (Thiede *et al.*, 2005). Trypsin also generates peptides with C-terminal basic residues which facilitates ionisation and, if necessary, *de novo* sequencing (Olsen *et al.*, 2004). The experimentally-obtained molecular masses for the peptides were compared with the theoretical peptide masses present in databases using mass search programs (Aebersold and Mann, 2003). Results were statistically analysed to find the best match.

Peptide mass finger-printing was carried out on the putative rLTBP-2C(H) fragment. After acquiring a mass spectrum using the Adelaide Proteomics Centre, the generated data were simplified to lists of monoisotopic masses and analysed by an in-house MASCOT

server, matching against SwissProt and also against the human LTBP-2C(H) protein sequence for protein identification. The MALDI-TOF spectrum of the digested LTBP-2C(H) sequence with matching peptide signals identified the protein as LTBP-2C(H). A search on Expasy proteomics (http://www.expasy.ch/) for glycosylation modifications identified five potential sites of N-linked glycosylation of the LTBP-2C(H) protein. This therefore can explain the discrepancy in the predicted and the apparent size of the recombinant protein. Following the authentication that the recombinant fragment is LTBP-2C(H), binding studies were performed to determine if this region contains heparin binding site(s).

4.2 The central region of LTBP-2 contains a binding site for heparin

In order to narrow down the binding region(s) for heparin on LTBP-2, solid phase binding assays were conducted to screen for interactions between the rLTBP-2 fragments, rLTBP-2C(H) and rLTBP-2CT(H) and heparin. Moreover, in light of the C-terminal region of rLTBP-2 containing the fibrillin-1 binding site (Hirani *et al.*, 2007), it was of interest to see if this region also interacted with heparin. Molar equivalents of each rLTBP-2 fragment in the solution were incubated with HAC-coated wells. A positive control using full length rLTBP-2 was included for comparison. BSA-coated wells were included as negative controls for determining the non-specific protein interaction of each fragment. Using anti-(tetra-his) antibody a strong signal was detected for full length rLTBP-2 and a marginally lower but positive signal was detected for rLTBP-2C(H) (**figure 4.2A**). In comparison to full length rLTBP-2 and its central fragment, rLTBP-2C(H), only a background signal was detected for the C-terminal rLTBP-2CT(H).

To demonstrate the specificity of the LTBP-2C(H) interaction with heparin, a saturation binding curve was established using a range of molar concentrations of rLTBP-2C(H) in solution with the amount of immobilised heparin constant. The binding signal between the two molecules was found to intensify with the increase in molar concentration of rLTBP-2C(H) (**figure 4.2B**). However, saturation was not achieved even with the rLTBP-2C(H) in solution being three times the molar concentration of heparin coated on the well. This was in contrast to the ability of full length rLTBP-2 to saturate the interaction at twice the molar concentration of heparin. The binding curve for rLTBP-2C(H) interaction with heparin supports the hypothesis that LTBP-2 contains more than one heparin binding site. This assumption is possible under the conditions that a) the rLTBP-2C(H) fragment contains only one heparin binding site and b) the second binding site contains equal binding affinity to the binding site identified in rLTBP-2C(H). Briefly, if full length rLTBP-2 contained only one heparin binding site in its central region (see **figure 4.2A**), then the binding curve established for rLTBP-2C(H) should be similar to that of the full length rLTBP-2. With this

not being the case, the alternative explanation was that LTBP-2 contains two heparin binding sites of equal affinity, hence four times the molar concentration of rLTBP-2C(H) would be required for saturation. As a result, the highest molar concentration of rLTBP-2C(H) used was insufficient for saturating heparin binding.

Since the binding curve appeared sigmoidal in shape, an alternative explanation for the curve was that the heparin binding site in rLTBP-2C(H) was of low affinity. Weak interactions take longer to reach equilibrium and are easier to disrupt. Thus it was possible that at low concentrations equilibrium had not been reached and/or that rigorous washing had disrupted much of the bound ligand. To confirm the possibility of additional heparin binding sites on LTBP-2, as well as the strength of the interaction, the K_d of rLTBP-2C(H) for heparin needed to be determined and this is further discussed in the following section.

4.2.1 Defining the affinity between central region of LTBP-2 and heparin

The K_d for rLTBP-2C(H) and heparin was calculated to determine the strength of binding relative to full length rLTBP-2 (section 2.13.4). A saturation curve for rLTBP-2C(H) interacting with heparin (HAC) was established by incubating increasing molar concentrations of rLTBP-2C(H) in solution with a constant molar amount of heparin coated on the wells (**figure 4.3A**). The saturation binding curve had an obvious sigmoidal appearance, once again implying binding is especially weak at low concentrations of rLTBP-2C(H). Concurrently a standard curve to calculate the molar amount of rLTBP-2C(H) bound was established by coating increasing molar amounts of rLTBP-2C(H) directly on the wells and detecting the signal with anti-(tetra-his) antibody (**figure 4.3B**). The molar amount of bound rLTBP-2C(H) was plotted against the total molar concentration added (**figure 4.3C**) and the value of K_d was estimated using non-linear regression analysis for one site binding (GraphPad Prism). The K_d was calculated to be 52.2±6.9nM. This result confirmed that the binding site in rLTBP-2C(H) fragment has a strong affinity for heparin.

Comparison of the binding affinity of rLTBP-2C(H) to heparin with full length rLTBP-2, revealed that the interaction of heparin with rLTBP-2C(H) is not as strong as with the full length rLTBP-2, therefore suggesting that there may be additional heparin binding site(s) in the N-terminal region of LTBP-2.

Construction of the rLTBP-2NT(H) expression plasmid was commenced concurrently with that of rLTBP-2C(H) (section 2.2.2). However, I was unable to express rLTBP-2NT(H) during candidature in 293 EBNA cells due to time constraints. Continuation of this work in our laboratory by others showed an additional binding site in the amino-terminus of LTBP-2 (Parsi *et al.*, 2010).

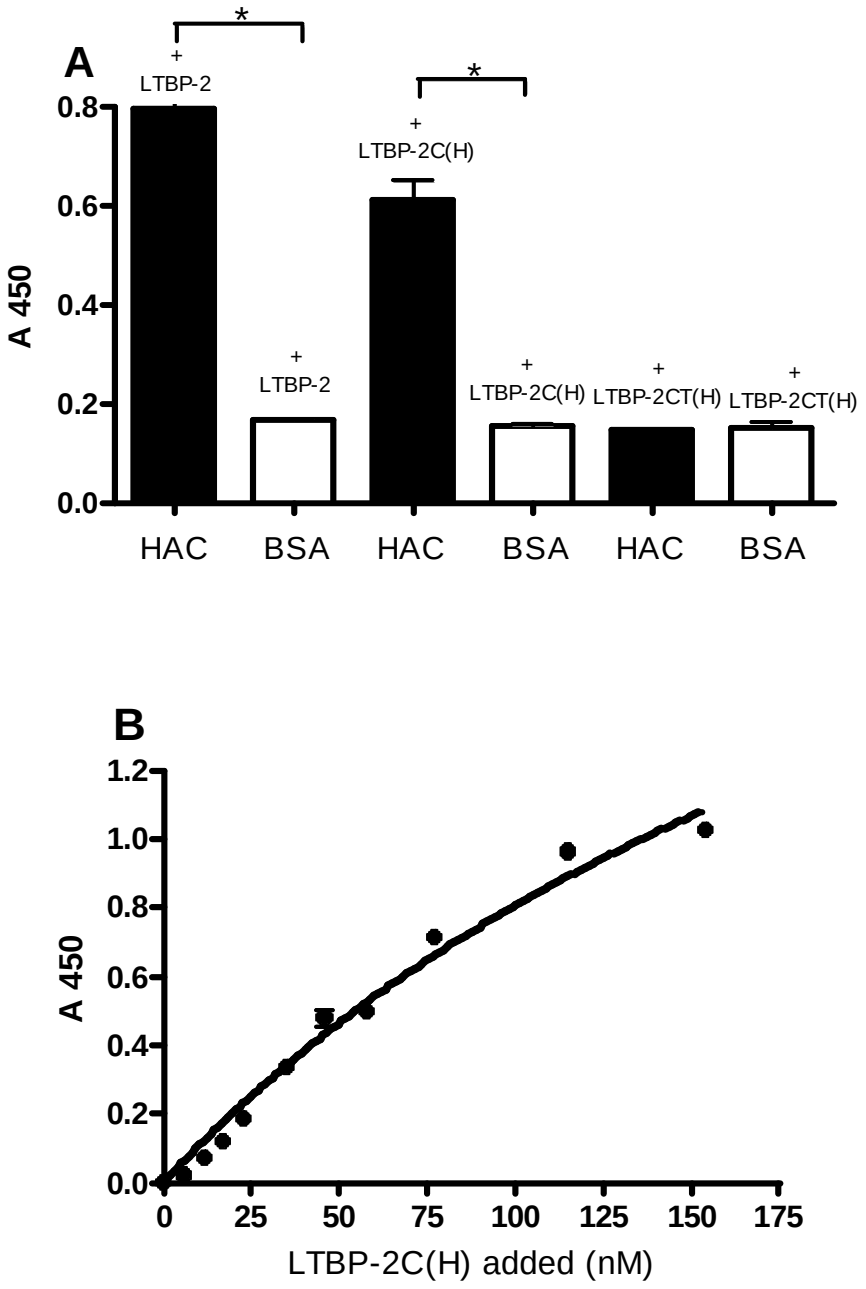

Figure 4.2. Heparin binds specifically to rLTBP-2C(H). **A,** Full length rLTBP-2 and rLTBP-2 fragments; rLTBP-2C(H) and rLTBP-2CT(H) in solution were incubated with immobilised heparin (HAC) or similar molar equivalent of BSA. Anti-(tetra-his) antibody (0.1μg/ml) was then used for binding detection. **B,** Solid phase binding curve of the interaction of rLTBP-2C(H) with heparin. Increased molar concentration of rLTBP-2C(H) (0-154nM) in solution was incubated with constant amount of heparin (HAC) (2.8pmol) or same molar equivalent of BSA coated on the wells. The resulting curve is after subtraction of BSA. * indicates statistical significance of $P \leq 0.05$. *, P= 0.0002.

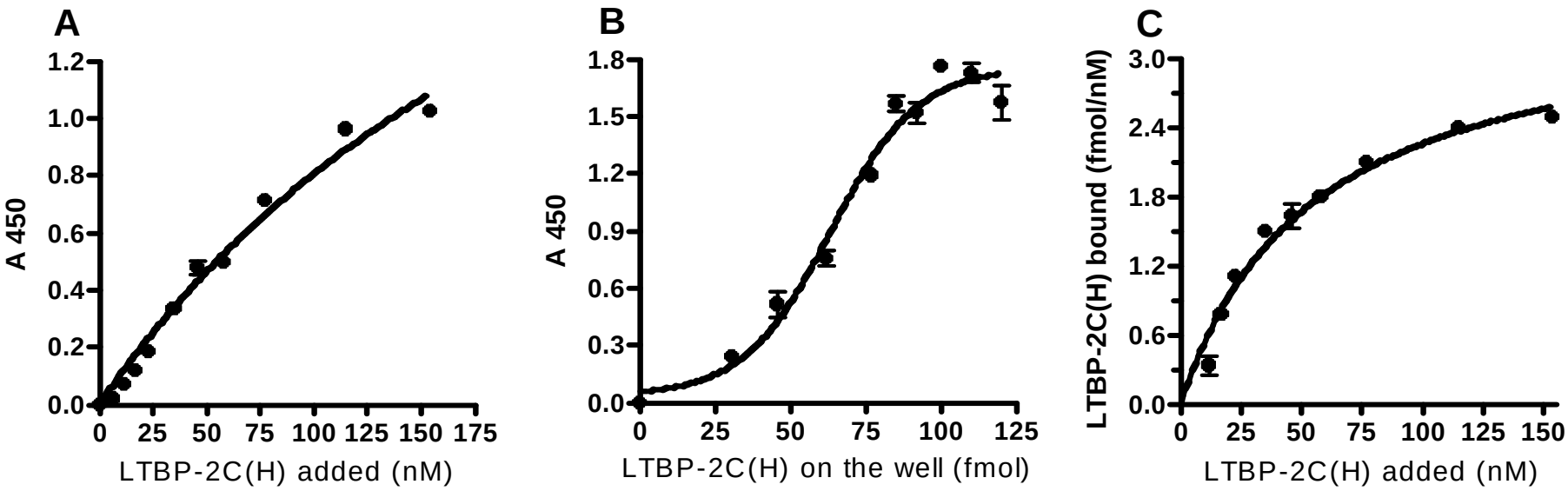

Figure 4.3. Kinetic analysis of the interaction between central fragment of LTBP-2 and heparin using solid phase binding assay. **A,** Saturation binding curve for rLTBP-2C(H) and heparin (HAC) after subtraction of the background BSA. Increasing molar concentration of rLTBP-2C(H) (0-154nM) in solution was incubated with constant molar amount of heparin (HAC) or molar equivalent of BSA coated on the wells. **B,** Standard ELISA curve for LTBP-2 after subtraction of the background. Increasing molar amount of rLTBP-2C(H) (0-0.12pmol) was coated on the wells overnight and signal levels for each specific quantity was determined using anti-(tetra-his) antibody (0.1μg/ml). **C,** LTBP-2C(H)-heparin (HAC) binding curve used to calculate K_d. The total molar concentration of rLTBP-2C(H) added in solution in **A** was plotted against the molar amount bound determined in **B**. The K_d was calculated to be 52.2±6.9nM, suggesting the heparin binding site in the central region of LTBP-2 is of strong affinity.

CHAPTER 5
LTBP-2 INTERACTIONS WITH PERLECAN AND SYNDECANS

The interaction of rLTBP-2 with heparin as demonstrated in chapters 3 and 4, reflects the interaction of LTBP-2 with HS-associated PGs in the ECM or at the surface of cells in tissue. HSPGs found in the ECM include perlecan, agrin and collagen type XVIII (Ackley *et al.*, 2003; Batmunkh *et al.*, 2007; Dong *et al.*, 2003; Iozzo, 1998; Tsen *et al.*, 1995). Perlecan was a candidate HSPG for investigation for interaction with LTBP-2 since perlecan is a constituent of BM of all human tissues (Murdoch *et al.*, 1994), while agrin is less widespread being a major HSPG of neuromuscular junctions and renal BMs (Denzer *et al.*, 1995; Tsen *et al.*, 1995).

Cell surface HS are mostly members of two major groups of membrane-bound protein groups, syndecans and glypicans (Bernfield *et al.*, 1999). Syndecans are expressed on the surface of all adherent cells, while glypicans are expressed predominantly in the central nervous system (David *et al.*, 1992). Therefore, syndecans were also candidate HSPGs to be tested for interaction with LTBP-2.

5.1 LTBP-2 interacts with Perlecan

Solid phase binding assays were used to determine if LTBP-2 interacts with perlecan. When rLTBP-2 in solution was incubated with perlecan coated on wells, a strong signal was detected with anti-LTBP-2 antibody (LTBP-2C) (**figure 5.1A**). In addition, a minimal non-specific binding signal was detected for the interaction of rLTBP-2 with BSA control wells. This result indicated that LTBP-2 specifically interacts with perlecan. To confirm the interaction, a binding curve was established where a constant concentration of rLTBP-2 in solution was incubated with increasing amounts of immobilised perlecan. The binding relationship was linear, showing that the interaction of rLTBP-2 with perlecan was proportional to the amount of perlecan coated on the wells (**figure 5.1B**). The binding between rLTBP-2 and perlecan did not reach saturation even when the highest amount of perlecan coated on the wells was incubated with rLTBP-2 in solution. This may have been due to the presence of excess rLTBP-2 compared with perlecan. With limited availability of purified perlecan (a gift from Professor John Whitlock, University of New South Wales), we were unable to repeat the experiment with a lower ratio of rLTBP-2 to perlecan to achieve saturation of the interaction. For the purposes of this work the established graph was

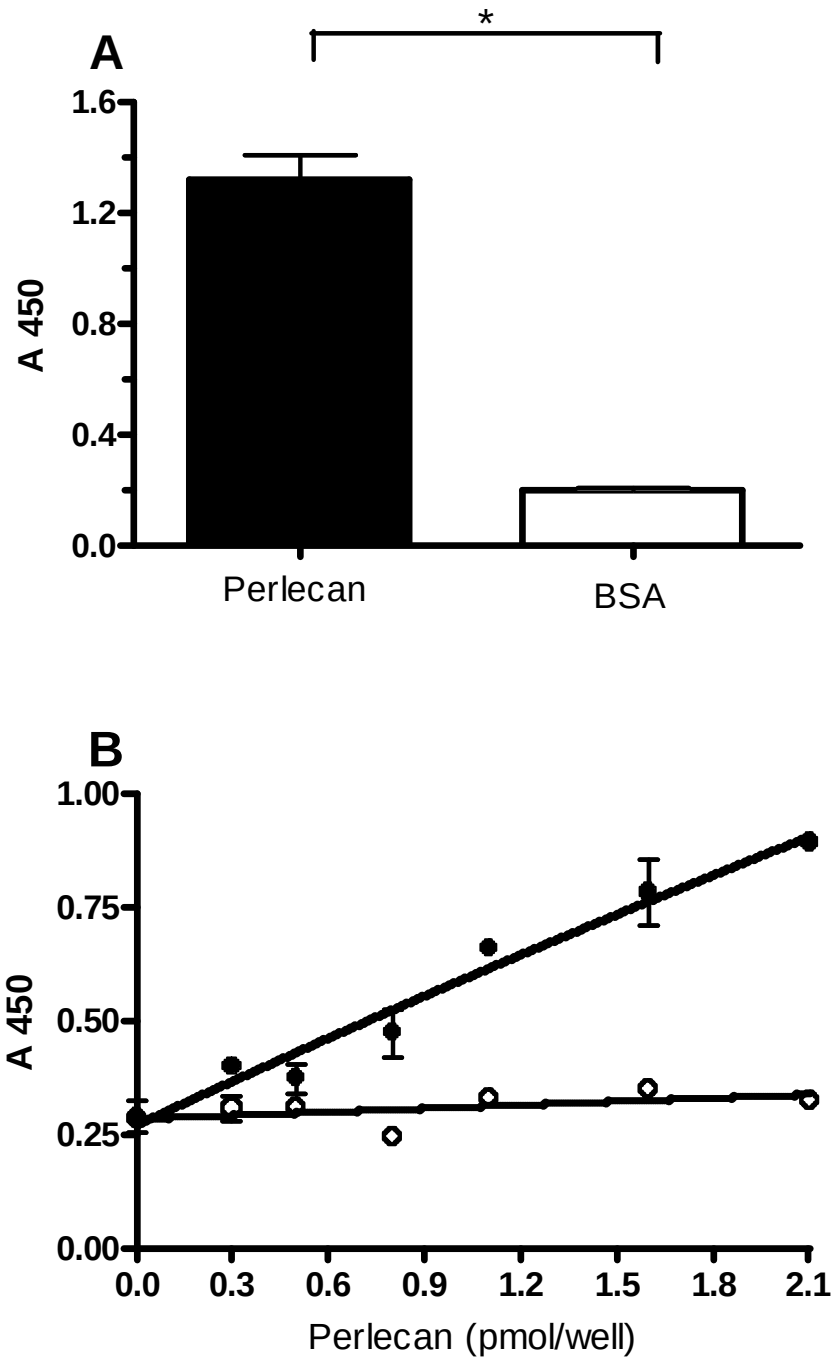

Figure 5.1. LTBP-2 interacts specifically with perlecan. **A,** rLTBP-2 (10nM) in solution was incubated with immobilised perlecan (2.1pmol) or molar equivalent of BSA. Specific binding was detected using anti-LTBP-2 antibody (LTBP-2C) (0.1μg/ml). **B,** Binding curve for the interaction of rLTBP-2 with perlecan. Constant concentration of rLTBP-2 in solution (10nM) was incubated with increasing amount of perlecan (0-2.1pmol) on the wells, *black circles*, or with molar equivalent of BSA, *white circles*, which had been coated on the wells. Anti-LTBP-2 antibody (LTBP-2C) (0.1μg/ml) detection of binding indicates that, the interaction of rLTBP-2 with perlecan is proportion to the amount of perlecan present. * indicates statistical significance of $P \leq 0.05$. *, P= 0.0003.

sufficient in showing that the interaction between LTBP-2 and perlecan was specific and it was not just a non-specific protein-protein interaction.

5.2 The interaction of LTBP-2 with perlecan is via the heparan sulphate side chains

The findings from previous chapters suggest the interaction of LTBP-2 with perlecan was likely to be via its HS-side chains. To verify this possibility, free heparin was added to inhibit this interaction. Using a solid phase binding assay, rLTBP-2 in solution was incubated with heparin at ten-times the molar concentration of perlecan prior to incubation with perlecan-coated wells. A positive control where the interaction of rLTBP-2 with perlecan was tested in the absence of added heparin was included in addition to a negative control where a molar equivalent of BSA was substituted for perlecan-coated wells. A strong signal was observed for the interaction between rLTBP-2 and perlecan (**figure 5.2**), whereas a significant reduction in binding signal was observed when rLTBP-2 was pre-incubated with heparin, therefore suggesting free heparin completely blocked the interaction of rLTBP-2 with perlecan. The presence of heparin did not significantly affect the level of non-specific interaction of rLTBP-2 with the BSA-coated wells. If LTBP-2 contained binding regions to the protein core component of perlecan, then the presence of free heparin should not have completely inhibited the binding of rLTBP-2 with perlecan. Therefore, it was evident that LTBP-2 interaction with perlecan is predominantly via the HS-side chains.

To confirm that LTBP-2 lacks binding affinity for the core protein of perlecan, isolation of the core protein was pursued by digesting the GAGs. Initially, methods adopted from Hayashi *et al.,* (1992) were used for the preparation of the core protein by digestion with heparitinase (section 2.13.6) which cleaves N-sulphated glucosaminidio-L-iduronic acid linkages of heparin. After digestion was completed, the enzyme was not denatured, since the native structural conformation of perlecan was required for future solid phase binding assays. The digested perlecan was compared to undigested perlecan on SDS-PAGE. After Coomassie Blue staining of the 10% gel, the undigested perlecan could not be detected on the gel (**figure 5.3**). This may have been due to the large size of the HSPG which prevented it from entering the polyacrylamide gel. In contrast, the digested perlecan appeared as several bands with high molecular weights, which suggested degradation of the core protein. It should be noted that an additional band at 66 kDa was also detected and this band was the heparitinase that was stained with Coomassie Blue staining.

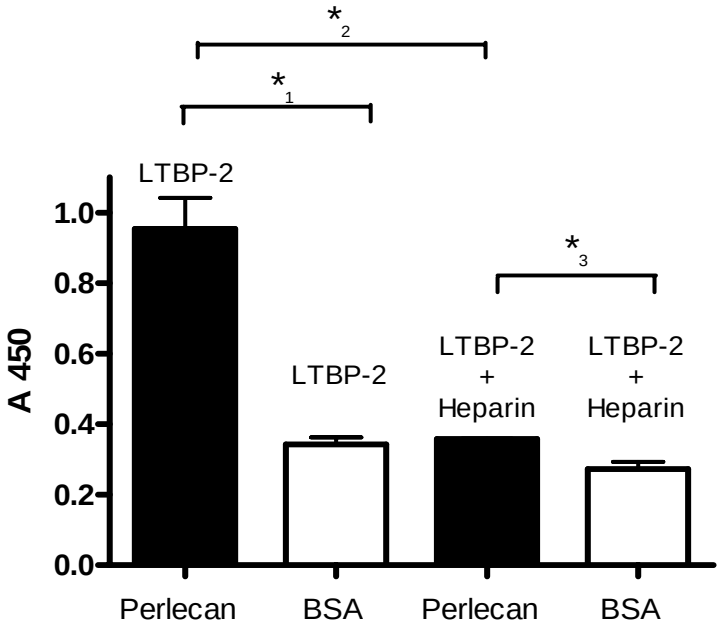

Figure 5.2. Perlecan interacts with LTBP-2 via its HS-side chains. Recombinant LTBP-2 (10nM) in solution or with the addition of free heparin (125nM) were pre-incubated for 15 minutes prior to incubation with perlecan (1.25pmol) or molar equivalent of BSA on the wells. The interaction of rLTBP-2 with perlecan was completely inhibited by free heparin. * indicates statistical significance of $P \leq 0.05$. $*_1$, P= 0.0004. $*_2$, P= 0.0003. $*_3$, P= 0.02.

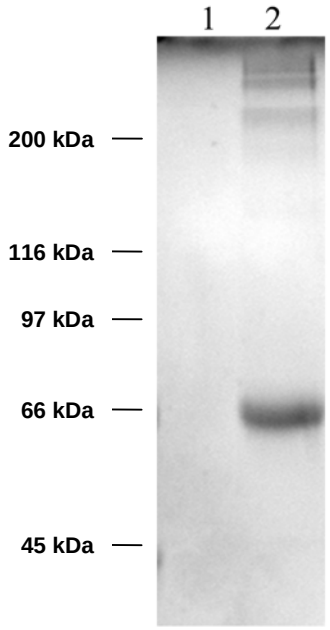

Figure 5.3. Preparation of the perlecan core protein. Perlecan (12.5µg) was digested with (0.042U) of heparitinase. Samples of the undigested **(lane 1)** and the digested perlecan **(lane 2)** were analysed by SDS-PAGE and Coomassie Blue staining.

5.3 The interaction of LTBP-2 with perlecan is cation dependent

Calcium ions were shown to enhance the interaction between rLTBP-2 and heparin (HAC) in section 3.3.4. From this we can speculate that calcium is also required for the interaction of LTBP-2 with perlecan. In this study, the calcium dependence of the interaction between LTBP-2 and perlecan was investigated. A solid phase binding assay was performed to examine the interaction between rLTBP-2 and perlecan in the presence of 2mM calcium ions or 5mM EDTA. A strong signal was detected for the interaction of rLTBP-2 and perlecan in the presence of 2mM calcium ions, while a low signal was detected for the interaction performed in the presence of 5mM EDTA (**figure 5.4**). The obtained result suggested that a metal cation, probably calcium, plays a role in the interaction of LTBP-2 with perlecan, either directly or indirectly through conformation changes in the LTBP-2 molecule.

5.4 LTBP-2 interacts with syndecan-4 but not syndecan-2

To expand the spectrum of HSPGs examined as possible binding ligands of LTBP-2, the cell surface HSPG syndecans were investigated for binding to LTBP-2. Possible cell adhesion properties have been predicted for fibrillin through its interaction with heparin (Bax et al., 2007; Cain *et al.*, 2008). Thus, similar functions may be possible for LTBP-2 through interaction with syndecans. The syndecan family consists of four transmembrane HSPG proteins syndecan -1 to -4 (Rapraeger, 2000). All members of the syndecan family except syndecan-3 have been purified from vascular sources (Kojima *et al.*, 1992; Mertens *et al.*, 1992). Syndecan-1 is the major syndecan of epithelial cells including vascular endothelium (Cizmeci-Smith *et al.*, 1997; Gallo *et al.*, 1996; Kojima *et al.*, 1992). Syndecan-2 is mostly present in mesenchymal, neuronal and smooth muscle cells (Cizmeci-Smith *et al.*, 1997; Pierce *et al.*, 1992), while syndecan-3 is the major syndecan of the nervous system (Chernousov and Carey, 1993; Hienola *et al.*, 2006). Syndecan-4 is ubiquitously expressed but at lower levels than the other syndecans (Tkachenko *et al.*, 2005; Yoneda and Couchman, 2003). In this study, r-syndecan-2 and -4 were tested for interaction with rLTBP-2 (section 2.13.1). A solid phase binding assay was used where rLTBP-2 in solution was incubated with the syndecan coated on the wells. The result was the detection of a strong specific signal for the interaction of rLTBP-2 with r-syndecan-4, using the anti-(LTBP-2) antibody (LTBP-2C) compared with the background signal that was detected between rLTBP-2- and BSA-coated wells (**figure 5.5**). In contrast, the antibody detected a weak signal for the interaction between rLTBP-2 and r-syndecan-2 (**figure 5.5**), which was not significant. The data obtained from the solid phase assay suggests that rLTBP-2 interacts with r-syndecan-4 but not with r-syndecan-2. This result suggests that LTBP-2 does not bind to all HS-side chains.

It is possible that heterogeneity in the HS sequences may result in HS having binding specificity for LTBP-2.

The results of the solid phase binding assays identified two potential biological ligands for LTBP-2, one a BM HSPG and the other a cell surface HSPG. Both HSPGs interact with LTBP-2 though their HS-GAG chains. Overall, LTBP-2 potentially interacts with a specific protein-interacting sequence in HS.

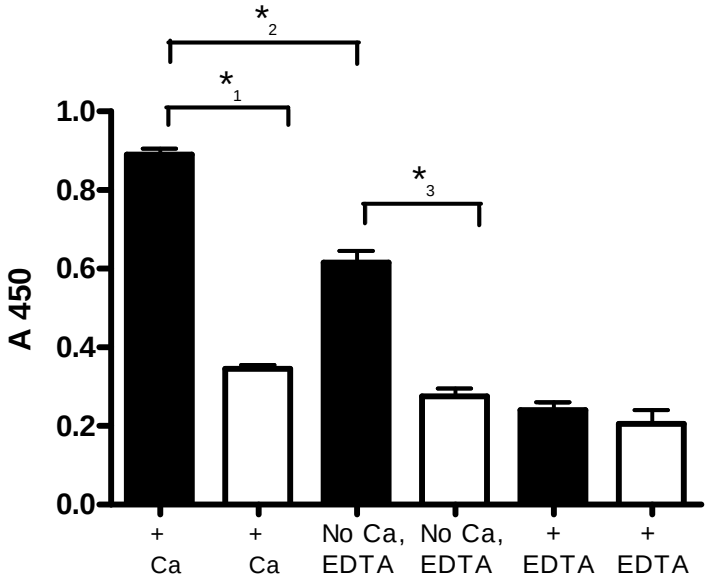

Figure 5.4. The interaction of perlecan with LTBP-2 is cation dependent. Recombinant LTBP-2 (10nM) in three alternative solution including TBS plus calcium ions, TBS only and TBS plus EDTAwas incubated with immobilised perlecan (1.1pmol) or molar equivalent of BSA. The interaction between LTBP-2 and perlecan in the alternative solutions was detected by anti-LTBP-2 antibody (LTBP-2C) (0.1μg/ml). The presence of EDTA completely blocked the interaction of rLTBP-2 with HS-side chains of perlecan. * indicates statistical significance of $P \leq 0.05$. $*_1$, P= 0.001. $*_{2 \text{ and } 3}$, P= 0.01.

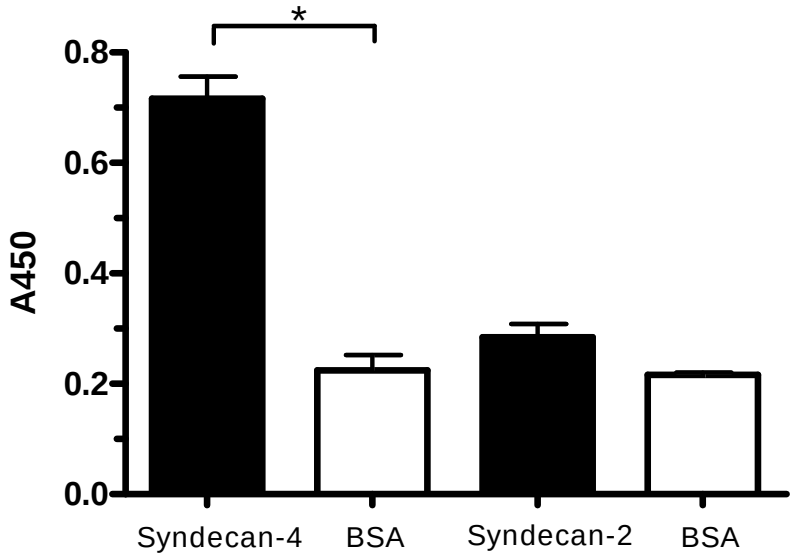

Figure 5.5. LTBP-2 interacts with syndecan-4 but not with syndecan-2. Recombinant LTBP-2 in solution (10nM) was incubated with r-syndecan -2 and -4 (27pmol) and molar equivalent of BSA coated on the wells. Binding was detected with anti-LTBP-2 antibody (LTBP-2C) (0.1μg/ml). * indicates statistical significance of $P \leq 0.05$. *, P= 0.0005.

CHAPTER 6
IMMUNOHISTOCHEMICAL ANALYSIS OF HUMAN FOETAL AORTA INDICATES LTBP-2 HAS AREAS OF COLOCALISATION WITH PERLECAN

The data in chapter 5 showed that LTBP-2 interacts with HS-side chains of perlecan *in vitro*. However, unlike the *in vitro* systems where optimal conditions are created to provide the best environment for interactions to occur, this is not necessarily true *in vivo*. Previously, it has been shown that LTBP-2 has widespread localisation with fibrillin-microfibrils in human foetal aorta (Gibson *et al.,* 1995; Hirani *et al.,* 2007), while perlecan has been documented to be the predominant HSPG found in all vascular BM (Murdoch *et al.,* 1994). Therefore, LTBP-2 and perlecan are expressed in the same tissue at similar developmental stages. It is unclear if LTBP-2 and perlecan are only found in association with fibrillin-microfibrils and BMs respectively, or if they are found independent of these major structures or lie on similar structures. Furthermore, the possibility of an interaction between LTBP-2 and other components of the matrix, independent of microfibrils, has not fully been explored. Therefore, immunohistochemical analysis was undertaken to examine the localisation of LTBP-2 and perlecan in developing human thoracic aorta and to determine if they are found in close proximity to allow interaction between the two matrix components. The developing human aorta was selected as the tissue of choice as it has a high elastic fibre and BM content.

6.1 Localisation of LTBP-2 on microfibrils and perlecan on basement membrane in human foetal aorta

6.1.1 LTBP-2 localises on fibrillin-1-microfibrils in the human foetal aorta

To investigate the immunolocalisation of LTBP-2 in the aorta, developing human aorta from a 20-week-old foetus was obtained under clearance from the Human Ethics Committee of University of Adelaide and the Women's and Children's Hospital, Adelaide, with the informed consent of the patient, mother. The tissue was immediately snap-frozen and stored at -80˚C. Cryostat sections of the foetal aorta were prepared (section 2.14) and were then immunostained with anti-(LTBP-2) antibody (LTBP-2C) and anti-(fibrillin-1) antibody (MAB1919) (**appendix C**). Specific antibodies to LTBP-2 and fibrillin-1 were used firstly to determine the localisation of LTBP-2 and to highlight fibrillin-1-microfibrils in the thoracic aorta, and secondly to establish whether all of LTBP-2 found in the aorta localised on the fibrillin-microfibrils. Control sections incubated with pre-immune mouse or rabbit IgG

were included to indicate non-specific background staining of the polyclonal and the monoclonal antibodies respectively.

To determine any overlap in the distribution patterns of these proteins, stained sections were analysed by Leica SP5 spectral scanning confocal microscope, using secondary antibodies conjugated to fluorophores Alexa488 and Cy5 (**appendix C**). These antibodies were chosen since the wavelengths used to excite the fluorophores were the furthest apart in the emission spectrum allowing distinct visualisation of the stained proteins with minimal bleed-through of the fluorescent signal between the two channels used for analysis.

Confocal microscope analysis of tissue sections stained with anti-(LTBP-2) antibody, (LTBP-2C), showed strong staining of LTBP-2 within the medial and intimal layers of the developing aorta, whilst LTBP-2 staining was observed to be absent in the adventitia layer of the aorta (**figure 6.1A**). The staining pattern indicated that LTBP-2 is highly expressed only in the inner two layers of the thoracic aorta at this stage of development. Examination of the control sections incubated with rabbit IgG showed a minimal, generalised cellular staining which indicated that non-specific background staining was low (**figure 6.1D**), and confirmed that the staining pattern for LTBP-2 in the aorta was specific. Similar LTBP-2 staining has been previously reported in the medial layer of developing human aorta using this anti-(LTBP-2) antibody (LTBP-2C) (Hirani *et al.,* 2007). In contrast to our findings, Hirani *et al.,* (2007) described a lack of LTBP-2 staining in the intimal region. The discrepancy between the staining of the intimal layer is perhaps due to the different developmental stages of the aorta used in the two studies. Our study looked at expression of LTBP-2 in a 20-week-old human foetal aorta, while immunohistochemical studies undertaken by (Hirani *et al.,* 2007) examined LTBP-2 expression at 25-36 weeks.

Staining with fibrillin-1, anti-(fibrillin-1) antibody (MAB1919) produced a widespread specific staining in all three intimal, medial and adventitial layers of the aorta (**figure 6.1B**). The specificity of the MAB1919 staining pattern was confirmed by the negligible background staining in control sections treated with pre-immune mouse IgG (**figure 6.1D**). Overall, the immuno-staining results indicated that in the developing aorta there is an extensive co-distribution of LTBP-2 and fibrillin-1. However, LTBP-2 is not present in the adventitial layer.

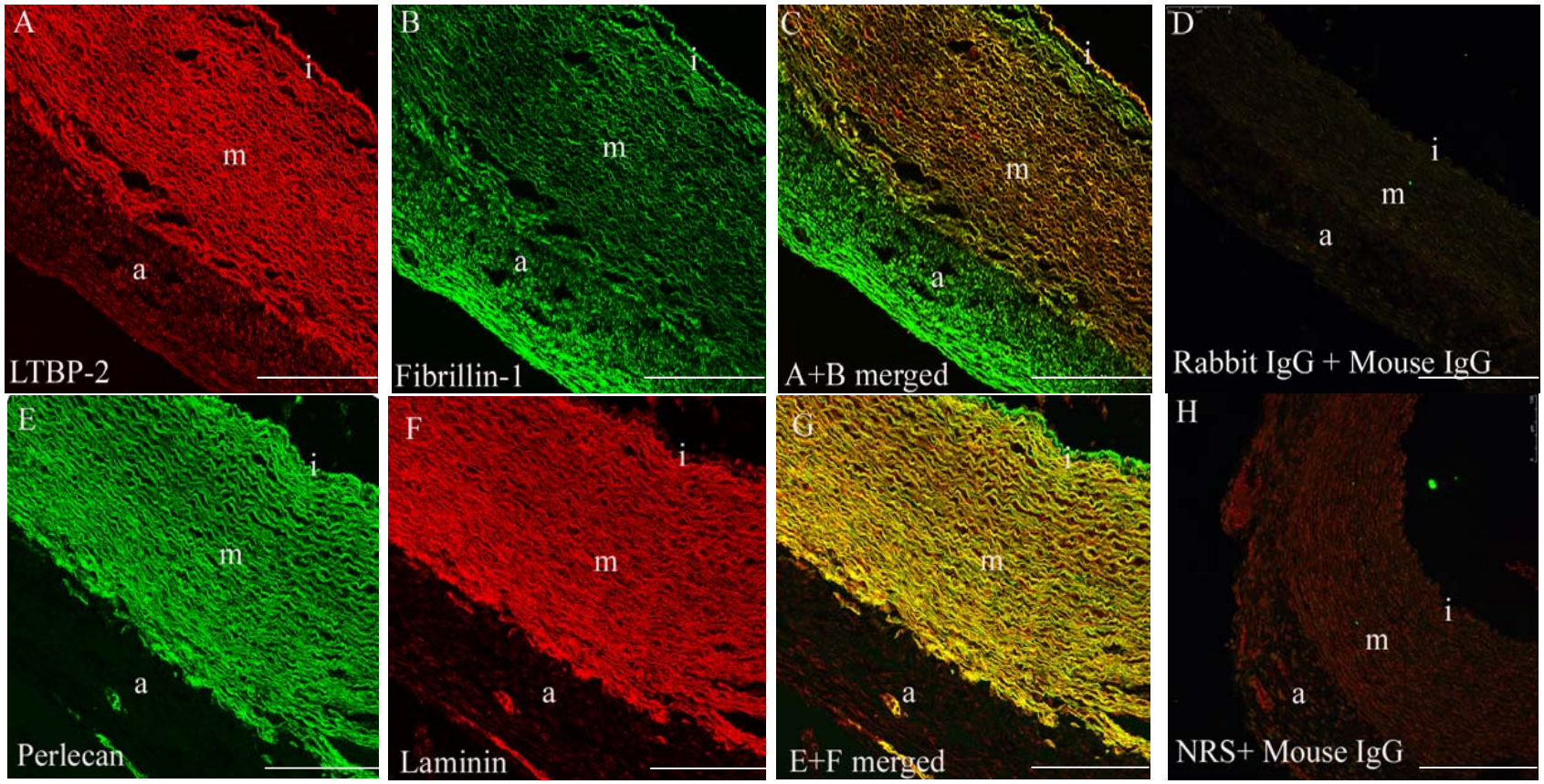

Figure 6.1. The distribution of LTBP-2, fibrillin-1, perlecan and laminin in the foetal aorta. Cryostat sections of human foetal aorta (20 weeks) were incubated with anti-(LTBP-2) antibody (LTBP-2C) (15µg/ml) (**A** and **C**); anti-(Fibrillin-1) antibody (MAB1919) (5µg/ml) (**B** and **C**); anti-(perlecan) antibody (7A5cc) (1:100 dilution) (**E** and **G**); and anti-(EHS Laminin) antibody (Rabbit 47) (1:10 dilution) (**F** and **G**). Control sections were incubated with matched concentration of rabbit IgG (15µg/ml) and mouse IgG (5µg/ml) (**D**) and normal rabbit serum (1:10 dilution) and mouse IgG (15µg/ml) (**H**). Primary antibody binding was detected using an appropriate secondary antibody conjugated to florophore Alexa488 or Cy5, prior to analysis on the Leica SP5 spectral scanning confocal microscope with a 20×objective. **A** and **B** are merged in **C**, **E** and **F** are merged in **G**. Magnification bars, **A**-**H** = 100µm. a, adventitia; m, media; and i, intima.

To determine whether in the developing aorta LTBP-2 is only found in association with fibrillin-microfibrils or if it is found independent of these structures, overlay analysis of the dual labelled cryostat sections was carried out. The resulting overlay showed that most of LTBP-2 staining in the intimal and the medial layers of the aorta coincided with fibrillin-1 staining (visualised as yellow areas within **figure 6.1C**). Therefore, the staining pattern confirmed that almost all of the LTBP-2 protein found in the aorta is associated with fibrillin-1-microfibrils.

6.1.2 Perlecan is predominantly associated with smooth muscle BM in foetal aorta

Perlecan is predominantly found in most if not all BM (Bix and Iozzo, 2008; Mohan and Spiro, 1991). Thus, it can be assumed that in the developing aorta perlecan will be localised on BM. However, it is not known if perlecan may also be found independent of BM in this tissue. To determine if perlecan can be found associated with alternative structures other than the BM, dual labelling of cryostat sections with anti-(perlecan) antibody (7A5cc), and anti-(EHS Laminin, α-chain) antibody, Rabbit 47 (**appendix C**) was performed (section 2.14). Laminin is a major BM component (LeBleu *et al.*, 2007), therefore tissue sections were stained for laminin α-chain to highlight the BM in the foetal aorta. Control sections were incubated with the appropriate mouse IgG and normal rabbit serum to determine the level of non-specific background staining.

When cryostat sections were incubated with anti-(perlecan) antibody (7A5cc) staining was detected evenly throughout the medial, and intimal layer of the developing aorta, while perlecan staining was largely absent in the adventitia (**figure 6.1E**). Control sections stained with pre-immune mouse IgG showed a negligible signal (**figure 6.1H**).

Staining for laminin using anti-(EHS Laminin, α-chain) antibody (Rabbit 47) produced a similar pattern to perlecan (**figure 6.1F**). However, the laminin antibody also showed weak non-specific cellular staining detected in the adventitia of foetal aorta sections. The cellular staining was considered non-specific as a similar staining pattern was also observed for control sections stained with normal rabbit serum (**figure 6.1H**). The results therefore indicate that perlecan and laminin are extensively expressed in the inner two layers of the developing aorta.

Overlay analysis of dual-labelled cryostat sections with perlecan- and laminin-specific antibodies, showed perlecan staining considerably overlapped with that of laminin in the media, intima and the outer region of the adventitia (visualised as yellow areas within **figure 6.1G**), confirming an extensive colocalisation of perlecan with BM. Interestingly, in the intimal region it appeared that some perlecan staining occurs independently of BM (**figure 6.1G**). There also appeared to be some laminin staining independent of perlecan in

the medial layer that is visualised as faint red areas. However, this staining was most likely due to non-specific cellular staining by the antibody, as similar staining was also seen in the normal rabbit serum treated control section. As anticipated, normal rabbit serum produced a higher overall background cellular staining compared to mouse IgG (red staining indicates normal rabbit serum in **figure 6.1H**) in control sections. The higher level of background signal observed is due to the presence of impurities in the anti-(EHS Laminin, α-chain) antibody (Rabbit 47) and in normal rabbit serum, since they were collected serums from rabbit bleeds which had not been affinity purified. Overall, the results indicated that the majority of perlecan is found in association with BM in the foetal aorta.

In summary, although LTBP-2 can be expressed independently of fibrillin-microfibrils in some tissues, for example the testis (Shipley *et al.*, 2000), when staining the developing aorta almost all of the LTBP-2 resides on the fibrillin-microfibrils (**figure 6.1C**). Similarly, the majority of the expressed perlecan in human foetal aorta is found on the BMs (**figure 6.1G**). With the establishment of LTBP-2 and perlecan on distinct structures in the foetal aorta, the localisation of microfibrils in relation to BM in the aorta was investigated. Determining whether the two matrix components are found close enough in the foetal aorta to interact with each other could indicate if LTBP-2 has additional roles in microfibril-basement membrane interaction.

6.1.3 Colocalisation of fibrillin-1 with perlecan

For comparing the distribution patterns of microfibrils and BMs in a 20-week-old human foetal aorta, cryostat sections were labelled with dual combinations of anti-(fibrillin-1) antibody (Fib-1A) and anti-(perlecan) antibody (7A5cc) (**appendix C**). Sections incubated with the appropriate mouse or rabbit IgG were also included as controls (section 2.14).

Overlay analysis of cryostat sections stained with specific antibodies to both perlecan (**figure 6.2A, C, E, & G**) and fibrillin-1 (**figure 6.2B-C & F-G**), showed distinct staining patterns for the two antibodies. Generally, each protein appeared to be localised independently from the other (**figure 6.2C**). However, there were patchy areas in the outer regions of the medial layer where fibrillin-1 colocalised with perlecan (visualised as yellow staining in **figure 6.2C**). Control sections incubated with rabbit IgG and mouse IgG showed negligible background staining (**figure 6.2D**), confirming the specificity of the staining patterns for fibrillin-1 and perlecan in the aorta.

Higher power examination of the medial layer confirmed the patchy overlapping distribution of fibrillin-1 with perlecan (seen as yellow staining, **figure 6.2G**). A number of the areas where fibrillin-1 and perlecan potentially interact have been marked by arrows in **figure 6.2G** and magnified in figure 6.2G *e* & *f*. The results indicate that fibrillin-1 and

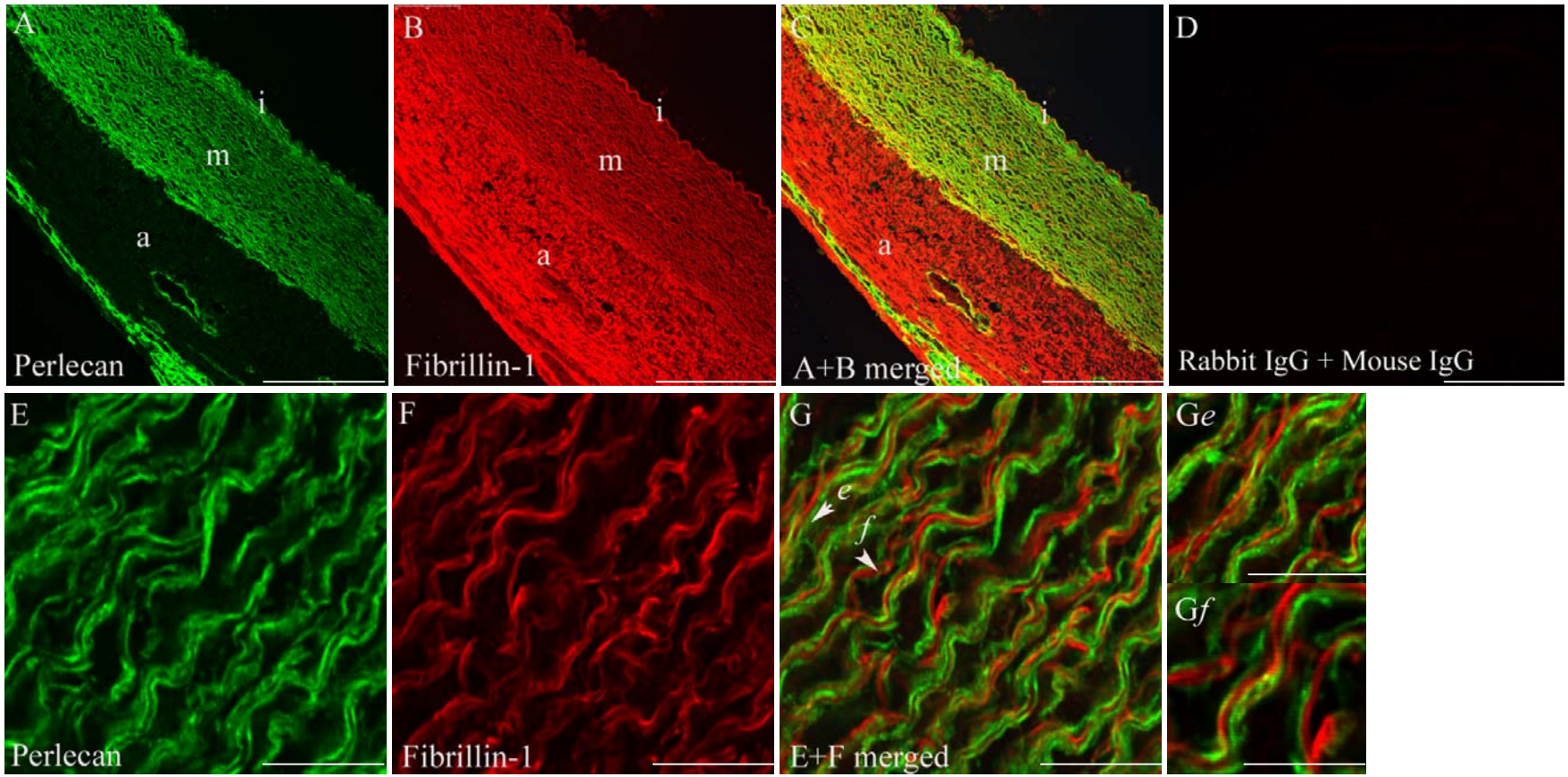

Figure 6.2. Fibrillin-1 and perlecan have potential areas of colocalisation within the medial layer of human foetal aorta. Cryostat sections (5µm) from 20-week-foetal aorta were incubated with anti-(perlecan) antibody (7A5cc) (1:100 dilution) (**A, C, E** and **G**) and anti-(fibrillin-1) antibody (Fib-1A) (1:10 dilution) (**B, C, F** and **G**). Primary antibody binding was detected using an appropriate secondary antibody conjugated to flurophore Alexa488 or Cy5, prior to analysis on a Leica SP5 spectral scanning confocal microscope with 20×objective (**A-G**) and 4.04×zoom (**E-G)**. Control sections were incubated with rabbit IgG (15µg/ml) and mouse IgG (15µg/ml) (**D**). **A** and **B** are merged in **C**. **E** and **F** are merged in **G**. In **C** and **G**, red staining indicates fibrillin-1, green staining indicates perlecan and the patchy areas where fibrillin-1 colocalises with perlecan are seen as yellow regions. The overlapping areas are marked by arrows in **G**, and are magnified in *e* and *f*. Magnification bars **A-D**= 100µm; **E-G** 25µm and *e* and *f*= 5µm.

perlecan have a limited co-distribution pattern in the foetal aorta, this perhaps occurring where the BM surrounding the smooth muscle cells and elastic fibres are close to each other. The results support previous reports of perlecan colocalising with fibrillin-1-microfibrils close to BM zones (Tiedemann *et al.,* 2005). Furthermore, our findings and those of Tiedemann *et al.,* (2005) identified that in both elastin and elastin-free tissues fibrillin-1 may directly link microfibrils to BMs.

6.1.4 Colocalisation of LTBP-2 and perlecan in the foetal aorta

Co-localisation of LTBP-2 and perlecan was performed on cryostat sections dual-labelled with anti-(perlecan) antibody (7A5cc) (**figure 6.3A, C, E & G**) and anti-(LTBP-2) antibody (LTBP-2C) (**figure 6.3B, C, F & G**) (section 2.14). Analysis of the immuno-stained tissue sections showed that LTBP-2 and perlecan generally have uniform and strong staining for both molecules detected in the intimal and medial regions (**figure 6.3A-C**). In addition, perlecan also appeared to localise to the blood vessels in the adventitia (**figure 6.3A & C**). Control sections showed negligible background staining (**figure 6.3D**), indicating that the staining for perlecan and LTBP-2 was specific. The overlay analysis of the staining patterns for LTBP-2 and perlecan confirmed the mainly independent localisation of perlecan and LTBP-2 in the intimal and medial layers (**figure 6.3C**). Interestingly, there were patchy areas in the medial region, particularly towards the outer regions where staining for LTBP-2 coincided with perlecan staining (seen as yellow areas in **figure 6.3C**). This pattern was similar to that observed for fibrillin-1 and perlecan (section 6.1.3). These areas were therefore chosen for examination at higher magnification.

Examination at higher magnification of the medial layer revealed scarce areas of colocalisation of LTBP-2 and perlecan on the microfibrillar network (**figure 6.3G**). A number of these areas are magnified in **figure 6.4G a-d**. Elastin autofluorescence has also been included to indicate the location of elastic fibres (visualised as blue staining in **figure 6.3G**). The confocal analysis of the distribution patterns of LTBP-2 and perlecan therefore suggested a potential but limited *in vivo* interaction between the two proteins.

In conclusion, it appears that LTBP-2 has the potential to play a role in the connection of microfibrils with BMs through the interaction with perlecan. The potential role of LTBP-2 as a linker molecule between microfibrils and BMs is further discussed in chapter 8.

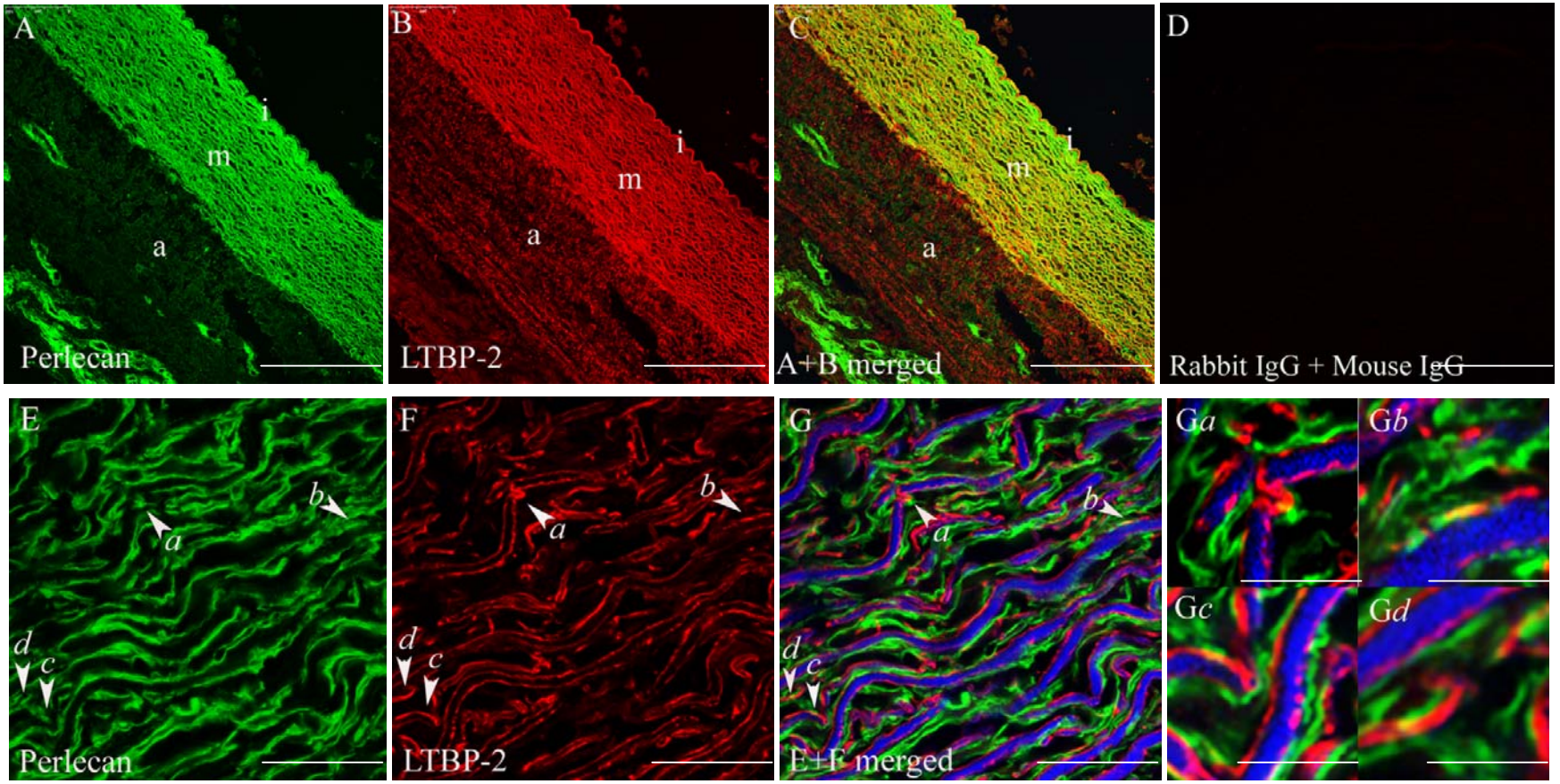

Figure 6.3. Regions of partial colocalisation of LTBP-2 and perlecan within the medial layer of foetal aorta. Cryostat sections of human foetal aorta (20-week) were incubated with anti-(perlecan) antibody, 7A5cc, (1:100 dilution) (**A,C, E** and **G**) and anti-(LTBP-2) antibody (LTBP-2C) (15µg/ml) (**B, C, F,** and **G**). Control sections were incubated with rabbit IgG (15µg/ml) and mouse IgG (15µg/ml) (**D**). Primary antibody binding was detected using an appropriate secondary antibody conjugated to florophore Alexa488 or Cy5, prior to analysis on a Leica SP5 spectral scanning confocal microscope with 20×objective (**A-G**) and 4.04×zoom (**E-G**). Elastin autofluorescence analysed under distinct channel, seen as blue staining in (**G**). **A** and **B** are merged in **C**. **E** and **F** are merged in **G**. Magnification bars, **A-D** = 100µm; **E-G** = 25µm; and ***a-d*** = 5µm. a, adventitia; m, media; and i, intima. Perlecan is visualised as green staining of BMs, LTBP-2 is visualised as red staining of elastic fibres and areas where BMs and elastic fibres potentially meet are visualised as yellow staining. Arrows indicate the areas where LTBP-2 colocalises with perlecan. These regions areas are viewed in higher magnification field in ***a-d***.

CHAPTER 7
IDENTIFICATION OF MATRIX MOLECULAR BINDING PARTNERS OF βig-h3 AND LTBP-2 USING AFFINITY BINDING AND PROTEOMICS TECHNIQUES

βig-h3 and LTBP-2 are matrix components that are associated with two distinct microfibrillar structures of the matrix: collagen VI microfibrils and fibrillin-microfibrils respectively (Gibson *et al.,* 1995; Gibson *et al.,* 1997; Hanssen *et al.,* 2003). Previous studies have found βig-h3 and LTBP-2 to be present in ECM of most tissues (Escribano *et al.,* 1994; Gibson *et al.,* 1997; LeBaron *et al.,* 1995; Moren *et al.,* 1994; Shipley *et al.,* 2000; Skonier *et al.,* 1994). Their importance has been demonstrated by their involvement in certain phenotypes, for example, in mutations of the human βig-h3 gene (TGFβI) which have been the cause of several phenotypically different corneal dystrophies (Klintworth, 2003; Munier *et al.,* 1997). Also, there have been reports of involvement of βig-h3 with certain cancers including colorectal carcinoma, lung carcinoma, renal cell carcinoma (Kitahara *et al.,* 2001; Sasaki *et al.,* 2002; Yamanaka *et al.,* 2008). Furthermore, Shipley *et al.,* (2000) demonstrated that knockout of the LTBP-2 gene in mice is embryonic lethal, suggesting that LTBP-2 is an important molecule in the development of embryos possibly during implantation. Additionally, LTBP-2 has been implicated in the development of degenerative and inflammatory pathologies (Bujan *et al.,* 2003).

Given the recognition of the importance of these matrix proteins, the full extent of the physiological functions of βig-h3 and LTBP-2 has not yet been characterised. Therefore, to better understand the possible roles of these matrix proteins, binding partners for βig-h3 and LTBP-2 need to be identified. With the expression and purification of rLTBP-2 described in section 3.1, this chapter firstly describes the expression and purification of rβig-h3 followed by subsequent experiments to identify potential binding partners for rβig-h3 and rLTBP-2.

Some insight has been forthcoming into the potential binding ligands of βig-h3 and LTBP-2 from previous studies. Firstly integrin binding motifs of βig-h3 and LTBP-2 have been identified (Kim *et al.,* 2000; Saharinen *et al.,* 1999; Skonier *et al.,* 1992). Secondly, analysis of tissue extracts has shown βig-h3 and LTBP-2 to be associated with collagenVI and fibrillin-microfibrils respectively (Gibson *et al.,* 1995; Gibson *et al.,* 1989; Gibson *et al.,* 1997; Hanssen *et al.,* 2003). A number of *in vitro* binding studies using rβig-h3 have also identified fibronectin, decorin and biglycan as binding partners of βig-h3 (Billings *et al.,* 2002; Reinboth *et al.,* 2006).

In vitro solid phase binding assays using rLTBP-2 have identified binding of LTBP-2 to the N-terminal of fibrillin-1, while no binding was detected for fibrillin-2, MAGP, elastin, collagen types I, III, V and VI (Hirani *et al.,* 2007). However, the range of purified matrix proteins available to be screened individually by *in vitro* binding assays for identifying additional binding partners of βig-h3 and LTBP-2 represents only a small spectrum of matrix proteins with the potential to interact with either βig-h3 and LTBP-2. To more systematically identify new binding partners, a different approach was required.

Previously in our laboratory a yeast-two-hybrid system was tested with βig-h3 as bait. However, many false positives were identified due to inappropriate formation of disulphide bonds between the bait and the retrieved target protein in the yeast cytoplasm (Hew and Gibson, unpublished observations). Therefore an approach using affinity chromatography combined with proteomics techniques was tested, using both rβig-h3 and rLTBP-2. Two basic techniques, 2-DGE and mass spectrometry were used to identify the binding partners.

Peptide mass finger-printing is the analytical technique used for bound protein identification. In this method, the unknown protein of interest is cleaved into smaller peptides, and the masses of the produced peptides are accurately measured by MALDI-TOF-MS. These masses are then in silico are matched against protein sequence databases such as in-house Mascot server, SwissPort, MSDB or NCBI to determine the protein's identity. The results are statistically analysed to find the best match. This approach has great promise for improved sensitivity, increased throughput, increased resolution and mass accuracy (Bergquist *et al.,* 2002)

Initially, suitable affinity matrices needed to be made, and an appropriate mixture of matrix proteins needed to be prepared. The conditions of the affinity chromatography needed to be optimised in order to isolate proteins (from the prepared extract) that specifically bound to the affinity matrices. Bound proteins were then to be resolved using SDS-PAGE, or 2-DGE if sufficient resolution was not achieved by the former method. The identities of each protein band would be determined by tryptic digestion and peptide mass finger-printing.

7.1 Expression and purification of recombinant βig-h3

The expression and purification of full length human rβig-h3 has been described previously (Hanssen *et al.,* 2003). Briefly, human βig-h3 cDNA was cloned into pGEMT-easy vector and clones containing authentic βig-h3 cDNA were selected for subcloning of the cDNA into episomal expression vector pCEP-4. The pCEP-4 vector carries an ampicillin resistance gene for the selection in bacteria and hygromycin B resistance gene for selection in mammalian cells.

For purification of human rβig-h3, a his_6-tag was introduced close to the N-terminus, 27 amino acids in the peptide sequence to allow for purification on Ni-sepharose. The recombinant expression construct (pCEP/BH18) was transfected into 293-EBNA cells and the resultant recombinant βig-h3 protein was purified from the serum-free DMEM medium using Ni-sepharose chromatography (section 2.4). The purified recombinant protein when analysed by SDS-PAGE and Coomassie Blue staining (section 2.6) appeared to migrate as a triplet of bands under reducing conditions, with the major band corresponding to apparent molecular mass of 66 kDa, while the minor two bands migrated close together at 71 kDa (**figure 7.1A, lane1**). Tissue βig-h3 migrates at 76-78 kDa in size on gels (Gibson *et al.,* 1996; Gibson *et al.,* 1989) but processing also yields a 68-70 kDa isoform (Skonier *et al.,* 1994). The major band at 66 kDa and two of the minor bands migrating close to 71 kDa, corresponded in size to purified rβig-h3 produced previously (Hanssen *et al.,* 2003).

In addition to the expected 66 kDa rβig-h3, a smaller protein migrating as a band at 54 kDa was also purified from the medium (**figure 7.1A, lane 1**). When the purified protein(s) were analysed by immunoblotting (section 2.6), all four bands reacted with anti-(βig-h3) antibody (MP78/70) (**figure 7.1A, lane 2**), thus confirming that all of the bands were βig-h3-related species and not contaminants. The yield of rβig-h3 was approximately 0.2μg/ml of DMEM medium and in total 1.2mg of rβig-h3 was purified.

7.2 Preparation of the affinity column; coupling of rβig-h3 and rLTBP-2 to CNBr-activated sepharose-4B

Several factors were considered when selecting an appropriate matrix for affinity chromatography. Firstly, the entire protein needed to be considered as a bait protein since potential binding sites were not defined. Secondly, the reusability of the coupled column was important because purified recombinant proteins were limited in quantity and preparation of a fresh column for each experiment would be time consuming and laborious. Thus the bait needed to be immobilised covalently to the sepharose support. For these reasons, CNBr-activated sepharose was chosen as the appropriate support. CNBr-activated sepharose reacts readily with primary amines to form a covalent coupling of the bait protein to the agarose matrix and to allow multi-point attachment of the protein for good chemical stability. Furthermore it immobilises the bait protein in a variety of orientations since the coupling occurs at random sites on the protein.

Due to the potential loss of activity of the bait as a result of repeated contact with the denaturant, 6M urea, only small quantities of the rβig-h3 protein e.g.613μg/7.8ml, or rLTBP-2 e.g. 1mg/7.5ml, were immobilised to CNBr-activated sepharose (200μl). This allowed the use of fresh affinity columns for each target protein mixture.

For the coupling of rβig-h3 and rLTBP-2 to CNBr-activated sepharose, the purified recombinant proteins were first dialysed into a coupling buffer (section 2.15). Dialysis was performed at 4°C to minimize degradation of the proteins by proteases. The dialysed recombinant proteins were analysed on a 15% polyacrylamide gel to confirm there was no substantial loss of proteins during dialysis (section 2.6). The concentrations of the dialysed proteins were determined by densitometry against known amounts of standard proteins.

Analysis of the Coomassie Blue-stained gel of rβig-h3 sample prepared for sepharose coupling showed the presence of additional bands which migrated at 128 kDa, 120 kDa, 54-kDa, 46 kDa and 42 kDa on 15% SDS-PAGE (**figure 7.2A, lane 1**). Immuno-reactivity of these bands with anti-(βig-h3) antibody (MP78/70) suggested that they appear to be degradation and aggregation products of the recombinant protein. Both rβig-h3 and rLTBP-2 were successfully coupled to the CNBr-activated sepharose, with approximately 3% of rβig-h3 and 5% of rLTB-2 remaining unbound to the CNBr-activated sepharose after two rounds of incubation (section 2.15). This was evident from the faint staining of the recombinant proteins detected in the coupling solution after the incubation with CNBr-activated sepharose (**figure 7.2, lanes 2**). Therefore a third incubation with the CNBr-activated sepharose was not necessary. The coupled columns were then equilibrated for subsequent affinity chromatography.

7.3 Selection of tissue extracts for identification of binding partners for rβig-h3 and rLTBP-2

When selecting a protein mixture to incubate with the prepared affinity columns, it was crucial to ensure that the extracted proteins were from a tissue that contained either βig-h3 or LTBP-2, if not both. It was reasoned that, when the bait protein is present in the tissue, then the proteins isolated with the affinity columns were more likely to be valid binding partners. One such tissue was bovine nuchal ligament, as both proteins were originally characterised from this tissue (Gibson *et al.,* 1995; Gibson *et al.,* 1989; Gibson *et al.,* 1997; Hirani *et al.,* 2007). Moreover, successful protein extraction protocols have previously been established for bovine nuchal ligament, with the extracted protein populations relatively well characterised (Gibson *et al.,* 1989). Furthermore, a number of proteins within bovine nuchal ligament have previously been identified as binding partners for βig-h3 or LTBP-2 (Gibson *et al.,* 1995; Hanssen *et al.,* 2003; Hirani *et al.,* 2007; Reinboth *et al.,* 2006).

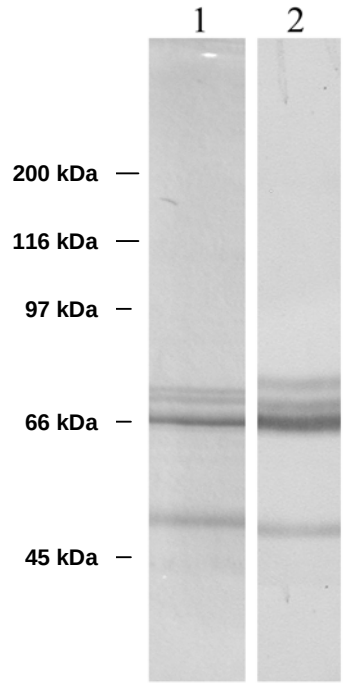

Figure 7.1. Purification of rβig-h3. Recombinant βig-h3 (15µl) was resolved by 8% SDS-PAGE followed by **lane 1**, Coomassie Blue staining or **lane 2**, immunoblotting with anti-(βig-h3) antibody (MP78/70). Recombinant βig-h3 migrated as a triplet with the major band at approximately 66 kDa and a partially degraded fragment at 54 kDa**.**

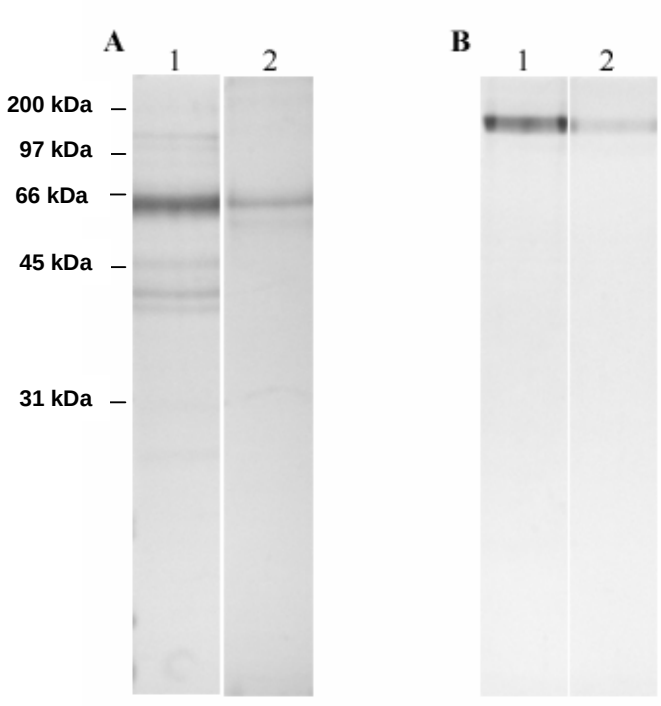

Figure 7.2. Determination of the extent of coupling of rβig-h3 or rLTBP-2 to CNBr-activated sepharose. **A**, rβig-h3 and **B,** rLTBP-2 were incubated with CNBr-activated sepharose and unbound materials were analysed by 15% SDS-PAGE and Coomassie Blue staining. Recombinant proteins (50µl) present **lanes 1**, before and **lanes 2**, after coupling. Approximately 3% of rβig-h3 and 5% of rLTBP-2 remained unbound to CNBr-sepharose.

Bovine nuchal ligament tissue from a foetal calf of 230-day gestation was chosen for protein extraction, as there is an increase in the amount of elastic fibre and collagen production in the last two months of foetal development (Cleary *et al.,* 1967). The tissue was sequentially extracted with 0.1% NP-40 detergent, 1M NaCl and 6M Guanidine hydrochloride (GuHCl). Readily soluble proteins such as serum albumin were extracted by the initial treatments, saline plus detergent Nonidet P-40 and 1M NaCl, while a different population of polypeptides was solubilised by 6M GuHCl (Gibson *et al.,* 1989). Bovine nuchal ligament protein mixtures extracted with 1M NaCl (BNLPM-1M NaCl) and 6M GuHCl (BNLPM-6M GuHCl) were selected for subsequent affinity binding experiments.

7.4 The use of BNLPM-1M NaCl for identification of novel binding partners

7.4.1 Selecting a suitable binding buffer

Initially the solubilised BNLPM-1M NaCl was investigated for potential binding to rβig-h3 and rLTBP-2. BNLP-1M NaCl appeared to be more readily soluble in solutions at or close to physiological conditions compared with proteins extracted with 6M GuHCl. Before the extract was incubated with the coupled rβig-h3 and rLTBP-2 columns, it needed to be equilibrated into a suitable buffer. One molar NaCl was a much higher salt concentration compared with physiological salt concentration (0.15M), hence this could interfere with binding of proteins to the ligands. To ensure binding, it was necessary to perform the experiment as close to physiological conditions as possible. Therefore the solubility of the BNLPM-1M NaCl was tested in TBS and TBS/0.5M NaCl using SDS-PAGE and Coomassie Blue staining (section 2.6). **Figure 7.3** illustrates the proteins that remained soluble following the different treatments. The BNLPM-1M NaCl was also included for comparison (**figure 7.3, lane 1**). Analysis of the proteins that remained soluble in TBS (**figure 7.3, lane 2**) and proteins that precipitated out of solution in TBS (**figure 7.3, lane 3**), revealed the presence of three protein bands around 40 kDa of similar staining intensity in both the supernatant and the precipitate. This suggested a partial precipitation of some BNLPs in TBS. In addition, there was relatively strong staining of several protein bands migrating below 35 kDa in the precipitated sample (**figure 7.3, lane 3**) compared to the supernatant (**figure 7.3, lane 2**). The intensity of staining of these precipitated protein bands was similar to that of the same bands present in the original 1M NaCl solution (**figure 7.3, lane 1**), thus confirming the almost complete precipitation of these proteins in TBS. Since there was potential for several proteins to migrate to the same position during polyacrylamide gel electrophoresis, each band on the gel could potentially represent more than one protein and the absence of each band in the supernatant could mean the loss of several proteins. Thus TBS was not considered as an optimal buffer for the study.

The staining of the protein bands in TBS/0.5M NaCl solution was similar to the staining detected in BNLPM-1M NaCl, indicating that most if not all of the proteins are soluble in the TBS/0.5M NaCl buffer. There were also a number of proteins migrating between 45-97 kDa, which appeared in both the supernatant (**figure 7.3, lane 4**) and the precipitate (**figure 7.3, lane 5**), showing a small degree of precipitation. There appeared to be a population of proteins that precipitated out of solution, which were larger than 97 kDa (**figure 7.3, lane 5**). The observed banding pattern of these proteins was different to the banding patterns of proteins with similar molecular weights that stayed soluble in solution or present in the original 1M NaCl solution. This was due to the analysis of different quantities of the precipitated proteins compared with the proteins that remained in the supernatant. While out of the total volume of BNLPM (1ml), only a small fraction of the mixture (60µl) was analysed by SDS-PAGE for examination of the soluble proteins, precipitated proteins from 1ml of BNLPM were used for comparison. Therefore the bands present in the precipitated sample which were not present in the supernatant sample or the sample from the original solution, represented protein populations with low concentrations, which were unable to be detected by Coomassie Blue in the comparison samples tested. Therefore from the results it was concluded that there was only minor precipitation of protein bands from BNLPM in TBS/0.5M NaCl. Hence, TBS/0.5M NaCl was selected for subsequent affinity chromatography experiments.

7.4.2 Incubation of BNLPM with a sepharose column for detection of non-specific interactions

Prior to the incubation of BNLPM with the prepared affinity columns, the level of non-specific interaction of the proteins with the sepharose was investigated. For that, BNLPM in TBS/0.5M NaCl was incubated with sepharose CL-4B and bound proteins were analysed by SDS-PAGE and Coomassie Blue staining, in order to determine the amount of non-specific binding of proteins to the sepharose CL-4B (section 2.6). Comparison of the BNLPM before and after incubation with sepharose CL-4B showed no major loss of proteins (**figure 7.4, lane 1& lane 2**). However, there were a number of band proteins with molecular weights that ranged from 45-200kDa which appeared to be non-specifically binding to sepharose CL-4B (**figure 7.4, lane 3**). The staining intensity of these non-specific binding protein bands was either the same or lower compared with that of the same bands remaining in solution after incubation (**figure 7.4, lane 2**). The results therefore suggested that the non-specific interactions with the sepharose CL-4B were minimal. Moreover, there was no loss of specific protein sub-populations due to the non-specific interactions. It would be ideal to have

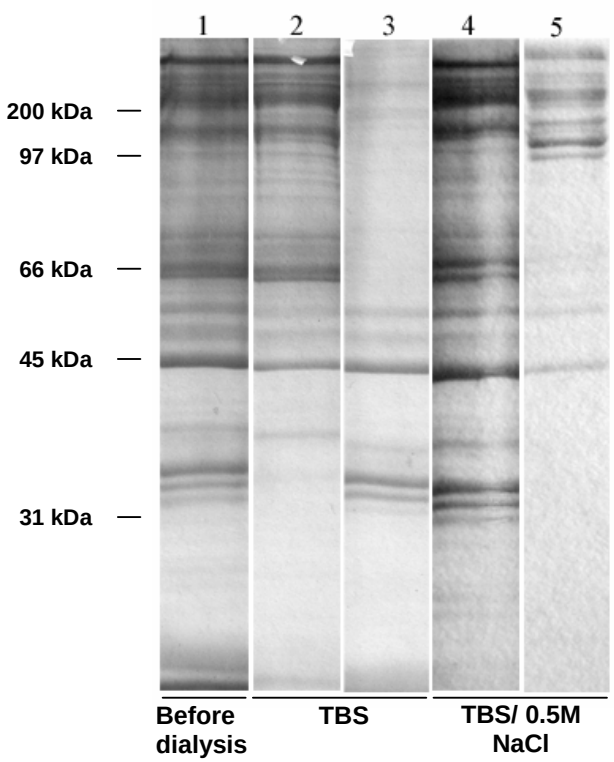

Figure 7.3. Solubility of BNLPM-1M NaCl following different treatments. **Lane 1**, BNLPM-1M NaCl (30µl). **Lanes 2 & 3**, BNLPM in TBS (60µl). **Lanes 4 & 5** BNLPM in TBS/0.5M NaCl, supernatant (30µl) and precipitate (1ml). Samples were centrifuged and **lanes 2 & 4,** each supernatant and **lanes 3 & 5,** each pellet were analysed by 12% SDS-PAGE and Coomassie Blue staining.

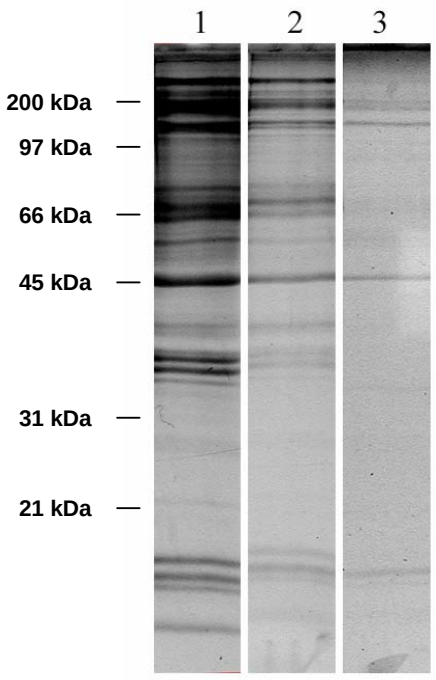

Figure 7.4. BNLPs interacting with sepharose-CL-4B. BNLPM (1mg/ml) in TBS/0.5M NaCl was incubated with sepharose CL-4B. Bound and unbound proteins were analysed by SDS-PAGE on 12% gel and Coomassie Blue stained. **Lane 1**, mixture prior to incubation (50µl). **Lane 2**, unbound proteins (50µl). **Lane 3**, bound proteins eluted with 6M urea (500µl). Only minor non-specific interaction with sepharose was observed.

no non-specific binding to sepharose, and further reductions may be possible by increasing the salt concentration in the buffer. However, by so doing, possible authentic interactions with the target proteins could be compromised. Thus the small amount of background binding was considered acceptable for subsequent affinity chromatography.

7.5 Identification of potential binding partners for rβig-h3 from the BNLPM-1M NaCl

7.5.1 Analysis of the binding proteins using Coomassie Blue staining

Novel binding partners for rβig-h3 were investigated using a solubilised BNLPM. After incubation of BNLPM with rβig-h3 coupled to CNBr-activated sepharose (rβig-h3-sepharose) and sepharose CL-4B (sepharose-control), bound proteins were eluted and analysed by SDS-PAGE and Coomassie Blue staining (section 2.15 and 2.6). A sample of BNLPM prior to incubation with the affinity columns was also included for comparison (**figure 7.5, lane 1**). From examination of the eluted proteins, it appeared that there were several more protein bands present in the eluate from the rβig-h3-sepharose (**figure 7.5, lanes 2**), when compared with the eluate from sepharose-control (**figure 7.5, lane 3**).

On close inspection of the resolved protein bands, it appeared that there were several bands which were common to both the eluates from the rβig-h3-sepharose and sepharose-control. These proteins migrated at 14 kDa, 14.7 kDa, 45 kDa, and 54 kDa, as well as two other bands above 97 kDa on both 15% polyacrylamide gels. All of the above mentioned protein bands appeared to be major components of the original extract (**figure 7.5, lane 1**). Greater staining intensity of these protein bands was detected in the eluates from the rβig-h3-sepharose compared with those from the sepharose-control. Therefore these proteins were considered to be possible candidate binding partners for rβig-h3.

A protein band with an apparent molecular weight of 12.5 kDa was intensely stained in the eluates from the sepharose-control (**figure 7.5, lane 3**), suggesting that the protein interacted non-specifically with sepharose. In contrast, there was a moderately strong staining of a 15 kDa protein band in the eluate from rβig-h3-sepharose (**figure 7.5, lane 2**), which was also present in the extract. This band was therefore defined as a novel candidate binding partner of rβig-h3. A repeat of the experiment further confirmed the specificity of the interaction between this particular protein and rβig-h3 protein (data not shown). As good practice, upon confirmation of the candidacy of the protein, it was decided to ensure the candidate protein was not a βig-h3-related species prior to protein identification by mass spectrometry (section 7.5.2).

A prominent band identified as a candidate binding partner for βig-h3 had the same size (66 kDa) as the main band of purified rβig-h3 (**figure 7.5, lane 2**). In order to determine

if this band was βig-h3, eluates were tested for reactivity to specific antibodies to rβig-h3. It was possible that βig-h3 had been pulled out from the BNLPM by homeotypic interaction with rβig-h3-sepharose or that rβig-h3 had leaked from the sepharose. Another reason for testing the eluates for reactivity to rβig-h3-specific antibodies was to identify additional bands that could be fragments of βig-h3.

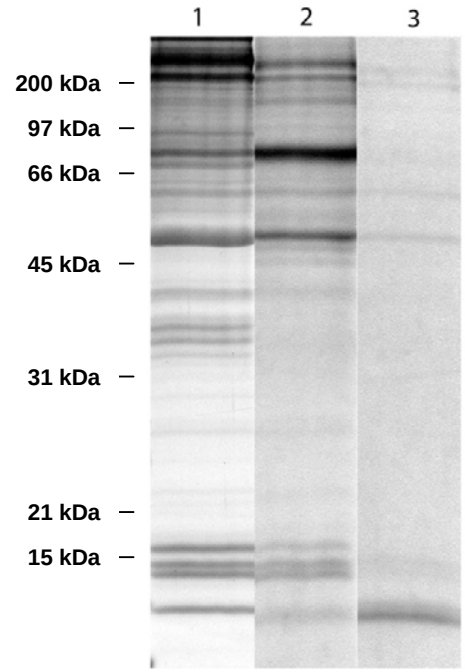

Figure 7.5. BNLPs interacting with rβig-h3-sepharose. BNLPM was incubated with rβig-h3-sepharose and sepharose-control. Bound proteins were analysed by SDS-PAGE on a 15% gel and Coomassie Blue stained. **Lane 1,** BNLPs before incubating with the columns (50µl). **Lane 2,** bound proteins eluted from rβig-h3-sepharose (500µl). **Lane 3,** bound proteins eluted with 6M urea from sepharose-control (500µl).

7.5.2 Detection of βig-h3 in proteins eluted from rβig-h3-sepharose

The proteins binding to the rβig-h3-sepharose and sepharose-control, plus BNLPM-1M NaCl were tested for reactivity to anti-(βig-h3) antibody (MP78/70) and anti-(tetra-his) antibody by western blot analysis (section 2.6). A number of protein bands (molecular weight 31 kDa to above 200 kDa) were stained with anti-(βig-h3) antibody (MP78/70) in the sample of BNLPM (**figure 7.6A, lane 1**) and in the eluate from rβig-h3-sepharose (**figure 7.6A, lane 2**). The higher molecular weight bands were 1.5-3 times larger in size than the βig-h3 monomer. Unpublished work by Dr. Hanssen suggested βig-h3 aggregates are present in bovine nuchal ligament, thus supporting the idea that these proteins were βig-h3 aggregates. There was no Coomassie Blue staining of the candidate 15 kDa band identified in **figure 7.5** and no reactivity was detected in the eluates from the sepharose-control (**figure 7.6A, lane 3**).

When a sample of BNLPM was immuno-blotted with anti-(tetra-his) antibody, no strongly staining bands were detected (**figure 7.6B, lane 1**), although some minor immuno-reactive proteins were present. Staining of the eluates from βig-h3-sepharose with anti-(tetra-his) antibody (**figure 7.6B, lane 2**), produced staining of similar band proteins previously stained with anti-βig-h3 antibody (MP78/70) (**figure 7.6A, lane 2**). The staining results therefore identified the major immuno-reactive bands as rβig-h3, not tissue-extracted βig-h3, which was leaching from the column. It was therefore deduced that regular replacement of the column would be required due to the significant loss of the coupled protein with each experiment. As expected, there was no staining detected in the sepharose-control (**figure 7.6B, lane 3**). Overall, the majority of the proteins in the eluates from βig-h3-sepharose were rβig-h3, which had been coupled to the sepharose. Therefore, the findings indicated that rβig-h3 was not completely linking to the sepharose.

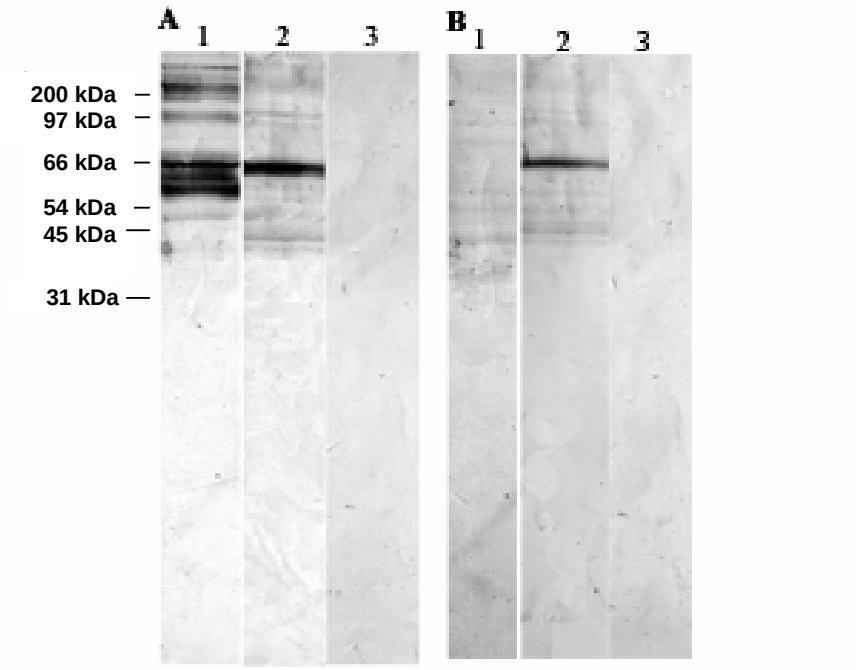

Figure 7.6. Identification of rβig-h3 in the eluted protein fractions. Proteins bound to rβig-h3-sepharose and sepharose-control were eluted with 6M urea and eluates were analysed by 15% SDS-PAGE and immunoblotting with **A,** anti-(βig-h3) antibody (MP78/70) or **B**, anti-(tetra-his) antibody, specific for rβig-h3. **Lane 1**, BNLPM before incubation with the columns (60µl). **Lane 2**, proteins binding to rβig-h3-sepharose (125µl). **Lane 3**, proteins binding to sepharose-control (125µl).

Immunoblotting analysis of the eluates from βig-h3-sepharose identified the majority of the candidate bands as βig-h3 species or aggregates of βig-h3, except for the protein band with the apparent size of 15 kDa. To identify the 15 kDa species, the band was prepared for

mass spectrometry. The mass spectrometric analysis was performed at Protein Core Facility at the Hanson Institute by Dr. Ian R. Milne using tryptic digestion. The mass spectrometry analysis identified the band as a human keratin contaminant in the sample. Keratin-like proteins are one of the most common contaminations found during a protein identification process by mass spectrometry. Keratin proteins can come from virtually anywhere, from the air, dandruff from the hair and skin, and those already present in the extract. The keratin protein can have a molecular weight ranging from 20 kDa to 70 kDa, but the size may vary depending on the point of the experiment at which it was introduced. Keratin contamination affects identification of potential protein bands depending on the keratin: protein ratio of the excised band. Even with stringent conditions of cleanliness complete avoidance is hardly possible. Steps were introduced to minimize future contamination, including washing of all containers with 0.1M NaOH prior to use, keeping contact of the samples and gels with air to the minimum by making sure lids were always on the test tubes and containers during all steps of the experiment, and ensuring face masks were worn when inspecting and analysing the stained gels.

7.5.3 Detection of the potential binding proteins for rβig-h3 using silver staining

The results in section 7.5.2 demonstrated that most of the intensely-stained bands in the eluate from the βig-h3-sepharose were identified as rβig-h3 derivatives. The BNLPM contains many proteins at various concentrations that may interact with rβig-h3 with varying affinities. These factors may affect the chance of detecting an interaction with rβig-h3 since only minute amounts of the ligand may be present in the eluates. Therefore, rare interacting molecules may not be detected by Coomassie Blue staining after separation by SDS-PAGE. In order to visualise a wider spectrum of proteins binding to rβig-h3, a more sensitive method of detection was considered. One such technique was silver staining. Silver staining has a sensitivity of 0.3-10ng/band (Switzer *et al.,* 1979), compared with Coomassie Blue R-250 which has a sensitivity of 50-100ng/band. Initially the modified silver staining protocol from Cheng *et al.,* (1994) was adapted to detect proteins eluted from rβig-h3-sepharose (section 2.7). However, this method resulted in almost instantaneous development of the protein bands and the background gel, making it difficult to distinguish individual protein bands separated in the polyacrylamide wells. The high sensitivity of this silver staining method did not allow comparison to be made between the samples (data not shown). However, there was a significant increase in the overall number of bands detected on the gel compared to Coomassie Blue staining. Modifications were therefore made to reduce the background staining and to permit more control over the rate of staining. The first modification was the addition of a washing step after silver nitrate incubation, for up to 10 minutes, instead of a

quick rinse. This washing step after incubating the polyacrylamide gel with silver nitrate did not however improve the contrast between the protein bands and the background as it washed away the silver nitrate from the gel and hence no staining was detected (results not shown). The second modification included diluting the developing solution. It was found that development of protein bands using a diluted developing agent slightly reduced the overall background staining, but not to required levels (results not shown). Also, this did not improve the rate of protein band development versus background development. Addition of a washing step after incubating the polyacrylamide gel with silver nitrate did not help as it washed away the silver nitrate from the gel and hence no staining was detected.

Due to the above problems, a second method for silver staining was adapted from Gromova, (2006) (see section 2.7). Initial modifications were made to the protocol to suit the thin polyacrylamide gels used for the separation of the proteins. A quick rinse of 10 seconds with distilled water replaced the 3×5min and 2×1min washes after sensitising the gel with sodium thiosulphate, and after incubation of the gel with silver nitrate respectively. The result was minimal background staining and greater control over the staining intensity of the developing protein bands. This method was used for all subsequent silver staining. **Figure 7.7** illustrates the pattern of proteins bound to the rβig-h3-sepharose and sepharose-control. Numerous protein bands were detected in the eluates from both rβig-h3-sepharose (**figure 7.7, lane 1**) and sepharose-control (**figure 7.7, lane 2**) by silver staining when compared to Coomassie Blue staining previously described (**figure 7.5, lane 2 & lane 3**). Therefore as expected, a larger spectrum of proteins potentially interacting with the rβig-h3 was revealed due to this higher sensitivity.

Bands present in the eluates from both rβig-h3-sepharose and sepharose-control were disregarded. However, a substantial number of protein bands remained that were candidate binding partners of βig-h3. However, we were interested in focusing on one or two stained bands which represented major new binding partners for rβig-h3 in BNLPM rather than previously identified binding partners. Therefore, measures were taken in order to identify more specific binding partners for rβig-h3 using silver staining.

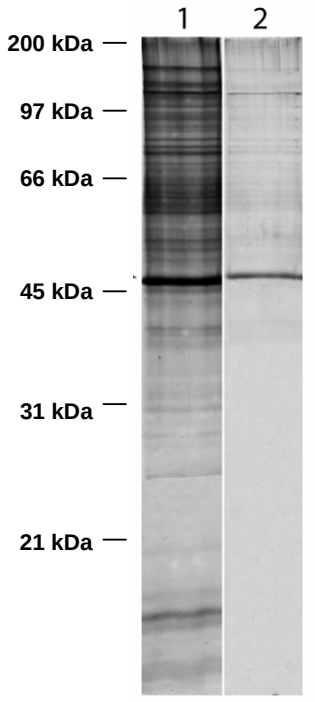

Figure 7.7. Detection of BNLPs binding to rβig-h3-sepharsose using silver staining. Bound proteins were eluted with 6M urea and subsequently analysed by 15% SDS-PAGE and silver staining. **Lane 1**, eluted proteins from rβig-h3-sepharose (200µl). **Lane 2**, proteins eluted from sepharose-control (200µl). This stain improved the sensitivity for detection of proteins, exposing more protein bands that appear to interact with rβig-h3.

7.5.4 Isolation of potential binding partners of βig-h3 using immobilised-Metal Affinity chromatography

The rβig-h3 contains a Ni-binding his_6-tag and thus Ni-sepharose chromatography can potentially be used to pull out rβig-h3 together with proteins that are bound specifically to it. An advantage of using Ni-sepharose is that the bait protein binds to the Ni-sepharose by its his-tag compared with the randomly cross-linking of rβig-h3 to the CNBr-activated sepharose. Therefore the use of Ni-sepharose allows the entire rβig-h3 molecule to be available to bind its ligands. This may maximise the identification of specific binding partners.

In section 7.4.1 TBS/0.5M NaCl was considered as an optimal buffer for BNLPM for subsequent affinity binding to rβig-h3-sepharose. However, it is possible that the presence of 0.5M NaCl may interfere with binding of rβig-h3 to some ligands. Consequently, binding studies were carried out under physiological conditions. However, two factors needed to be considered before carrying out the experiment. Firstly, as previously shown in section 7.4.1, there is a complete loss of the lower molecular weight proteins when BNLPM-1M NaCl is dialysed into TBS. Loss of these proteins due to precipitation potentially meant loss of possible binding ligands. However, BNLPM was considered to contain a number of

unidentified proteins with the potential to interact with βig-h3. Thus loss of a small portion of these proteins would still leave many other interactions to be identified under physiological conditions. To prevent the precipitation of rβig-h3 in TBS, it was necessary to bind rβig-h3 to Ni-sepharose prior to incubation with the BNLPM in a physiological buffer (TBS). In addition, Ni-sepharose was used as a control (section 2.16).

Bound proteins were eluted with 500mM imidazole, resolved by SDS-PAGE and detected by silver staining. A number of intensely stained bands, such as those migrating at 26 kDa, 42 kDa, 46 kDa, 54 kDa, 66 kDa, 97 kDa, 120 kDa, 128 kDa and 200 kDa, were detected in the eluate from the rβig-h3-Ni-sepharose (**figure 7.8A, lane 1**) which was not as strongly stained in the Ni-sepharose-control (**figure 7.8A, lane 2**). However, there also appeared to be more non-specific interaction of proteins with the Ni-sepharose-control, compared to previous sepharose-control. Most of the non-specifically interacting proteins were of very high molecular weight for one protein band migrating at 46 kDa. To identify rβig-h3 protein and its isoforms verses the mixture of candidate binding partners, the eluates from both rβig-h3-Ni-sepharose and Ni-sepharose-control were immunoblotted with anti-(tetra-his) antibody and anti-(βig-h3) antibodies (MP78/70) and Rabbit 45 (section 2.6). A sample of purified rβig-h3 was also included for positive identification of rβig-h3. Two specific antibodies to βig-h3 were used as they recognised different epitopes. The Rabbit 45 is made to a peptide in fasciclin-1 domain of βig-h3, while (MP78/70) recognises mainly regions of fasciclin-2 and fasciclin-4 domains of βig-h3 (Gibson, M. A., unpublished REFERENCE_TYPE>0</REFERENCE_TYPE><REFNUM>7</REFNUM><ACCESSION_NUMBER>12719415</ACCESSION_NUMBER><VOLUME>278</VOLUME><NUMBER>27</NUMBER><YEAR>2003</YE**AR><DATE>Jul 4</D**ATE><TITLE>Covalent and non-covalent interactions of betaamples from the Ni-sepharose-control (**figure 7.8B, lane 2**). Therefore, the results indicated that tissue βig-h3 does not bind non-specifically to Ni-sepharose. Anti-(tetra-his) antibody staining of the purified rβig-h3 sample showed staining of a major band at 66 kDa and the triplet band at 56 kDa (**figure 7.8B, lane 3**). It should be noted that due to the difference in quantity of rβig-h3 present in the eluate from rβig-h3-Ni-sepharose and the purified sample, it was not possible to confirm the identity of the other identified band proteins in **figure 7.8B lane 1**. Similarly anti-(βig-h3) antibody (MP78/70) identified the prominent bands at 42k-66 kDa, 120 kDa, 128 kDa and 200 kDa, but not the bands at 26 kDa and 97 kDa as βigh-3 in the rβig-h3-Ni-sepharose eluate (**figure 7.8C lane 1**). There was no staining detected in the eluted samples from the Ni-sepharose-control (**figure 7.8C, lane 2**). The immunoreactivity of a 97 kDa band protein in the purified rβig-h3 sample (**figure 7.8C, lane3**), suggested that the similar sized protein band observed by silver staining could potentially be related to rβig-h3. Anti-(βig-h3) antibody Rabbit 45 staining of the

fractionated samples by SDS-PAGE identified similar bands migrating at 42-66 kDa, 128 kDa and 200 kDa in the eluate from rβig-h3-Ni-sepharose (**figure 7.8D, lane 1**). There was no staining detected in the eluted sample from the Ni-sepharose-control when tested with the anti-(βig-h3) antibody, Rabbit 45 (**figure 7.8C lane 2**). Furthermore, band proteins stained with anti-(βig-h3) antibody (MP78/70) in the sample of purified rβig-h3, also showed reactivity to anti-(βig-h3) antibody, Rabbit-45 (**figure 7.8D, lane 3**). Overall from these results it was concluded that the majority of the prominent bands detected in the silver stained eluate from rβig-h3 coupled to Ni-sepharose were βig-h3. The exception was the silver-stained band with molecular weight of 26 kDa, in the eluate from βig-h3-Ni-sepharose which did not immuno-react with either of the antibodies and therefore, may be a potential binding partner of βig-h3. To confirm the protein band as a unique candidate binding partner for βig-h3, the BNLPM was also tested for immuno-reactivity to anti-(tetra-his) antibody, and anti-βig-h3 antibodies (MP78/70) and Rabbit 45). No reactivity of the candidate protein band to anti-(tetra-his) antibody and anti-βig-h3 antibody (MP78/70) was detected (data not shown). However, the candidate protein showed reactivity to anti-βig-h3 antibody, Rabbit 45 suggesting the possibility that the candidate band may be related to βig-h3 (**figure 7.8D, lane 4**). In addition the major βig-h3 species at 66 kDa was detected as a doublet in the BNLPM compared to the βig-h3 coupled and eluted from Ni-sepharose.

From the collected data no certain candidate binding partners were identified as it was concluded that rβig-h3 interfered with gel analysis of potential binding partners. Therefore, this alternative approach of nickel affinity chromatography under physiological conditions did not appear to improve the detectability of protein interactions with rβig-h3.

From the results of sections 7.5.1-7.5.3, it was apparent that a lot more proteins in the BNLPM were bound to rβig-h3-sepharose than to sepharose-control. Some of these proteins may be authentic binding ligands of βig-h3. However, identification of a few specific βig-h3 ligands was not achieved using the methods described above, nor was it possible to narrow down and select with confidence the potential candidate binding partners amongst the rest of the eluted proteins. To reduce problems in the system, different aspects of the system had to be tested. Given that a substantial number of BNLPs were binding to the affinity columns, BNLPM was tested to determine if the BNLPs were sticky in nature. For this, the approach taken was changing of the bait protein, to see whether the same degree of non-specific interaction between BNLPs and a different bait protein still occurred. Therefore, rLTBP-2 was chosen as an alternative bait protein for separation of potential binding ligands from BNLPM (described in more detail in section 7.6).

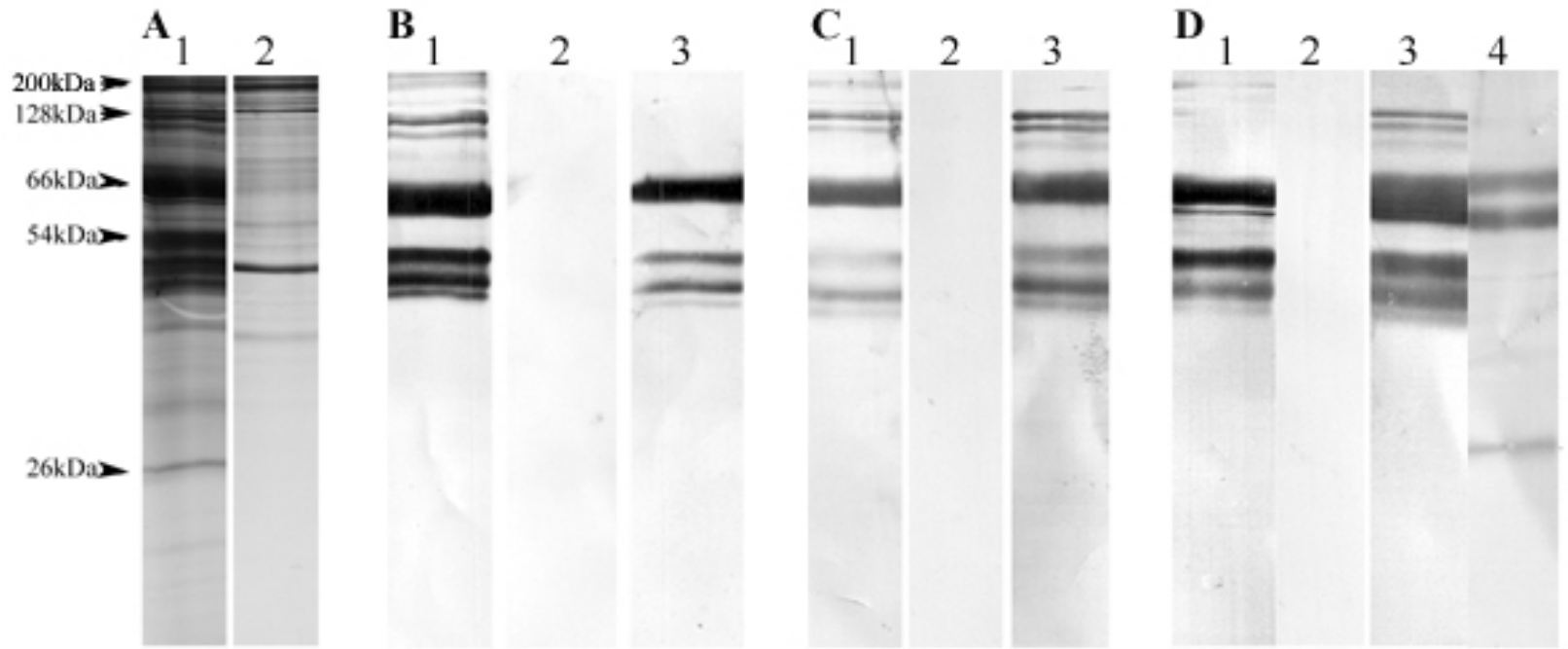

Figure 7.8. Affinity chromatography on columns of rβig-h3 bound to Ni-sepharose. BNLPM was incubated with rβig-h3 (30µg) coupled to Ni-sepharose or Ni-sepharose-control. Bound proteins were eluted with 500mM imidazole and eluates (50µl) were analysed by SDS-PAGE on a 15% gel, followed by **A**, silver staining, or immunoblotting with **B**, anti-(tetra-his) antibody, or anti-(βig-h3) antibody; **C**, MP78/70 and **D**, Rabbit 45. **Lane 1**, rβig-h3 plus BNLPs eluted from Ni-sepharose (50µl). **Lane 2**, BNLPs eluted from Ni-sepharose-control (50µl). **Lane 3**, purified rβig-h3 (0.6µg). **Lane 4**, BNLPM extract (20µl). The majority of the unique bands identified were rβig-h3 that bound to Ni-sepharose. Arrows in **A** indicate molecular weights of some of the eluted proteins from the Ni-sepharose.

7.6 Identification of binding partners for rLTBP-2 from BNLPM using silver staining

The interaction of rLTBP-2 with BNLPMs was investigated to identify novel binding ligands for LTBP-2, and to observe how the banding pattern of proteins eluted from rLTBP-2-sepharose compared with that for rβig-h3. A BSA-coupled sepharose was added as a control to identify non-specific protein-protein interactions that might be occurring in the affinity chromatography system. Analysis of proteins eluting from rLTBP-2-sepharose and BSA-sepharose-control following incubation with BNLPM in TBS/0.5M NaCl, showed more protein bands in the eluate from rLTBP-2-sepharose (**figure 7.9A, lane 1**) compared to the eluate from BSA-sepharose-control (**figure 7.9A, lane 2**). Comparison of the eluates from rLTBP-2-sepharose with gels from previous experiments using rβig-h3-sepharose (**figure 7.7, lane 1**) showed that both have very similar banding patterns, therefore suggesting that the isolated proteins binding non-specifically. When the silver stained eluate from the sepharose-control (**figure 7.7 lane 2**) and BSA-sepharose-control (**figure 7.9A lane 2**) were compared, it appeared that there were more band proteins present in the eluate from sepharose-control, although it appeared that there was an overall increased quantity of proteins present in the eluate from BSA-sepharose-control. This was evident from the stronger staining of the band ation</KEYWORD><KEYWORD>*Heart Catheterization</KEYWORD><KEYWORD>*Pulmonary Valve Stenosis</KEYWORD></KEYWORDS><UR-control represent a wider spectrum of non-specifically interacting proteins making sepharose-control a more appropriate control for identification of potentially interacting BNLPs. The detection of large number of proteins in the eluate from rLTBP-2-sepharose reflects the previous observations made for eluates from rβig-h3-sepharose, i.e. that the large number of proteins isolated from BNLPM by rβig-h3-sepharose and rLTBP-2-sepharose could be due to the adhesive property of the BNLPs. Thus, usage of an alternative protein mixture may perhaps be more successful for identification of potential binding partners with βig-h3-sepharose and LTBP-2-sepharose.

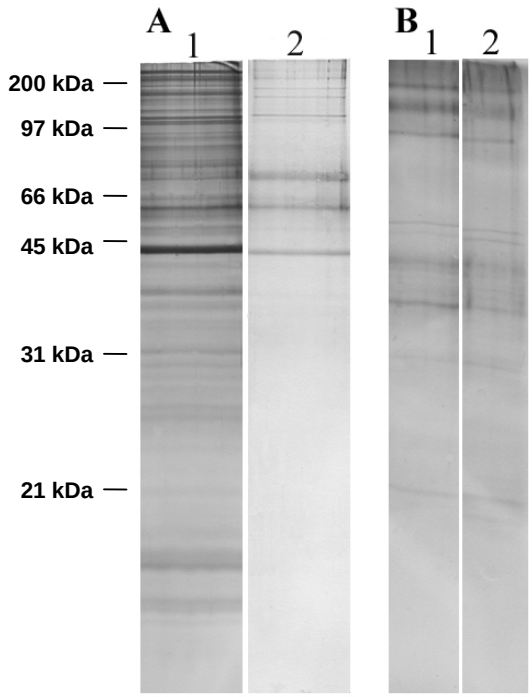

Figure 7.9. Identification of matrix proteins potentially interacting with LTBP-2. Matrix protein mixtures; **A,** BNLPM or **B,** BM-rich matrigel mixture (1mg/ml) were incubated with rLTBP-2-sepharose and BSA-sepharose-control. Bound proteins were eluted with 6M urea and eluates were analysed by 15% SDS-PAGE and silver staining. **Lanes 1**, proteins bound to rLTBP-2-sepharose (200µl). **Lanes 2**, bound proteins to BSA-sepharose-control (200µl).

7.7 Isolation of binding partners for rLTBP-2 from a basement membrane-rich mixture

Since the distribution of LTBP-2 in all tissues is not yet defined, and LTBP-2 expression has been reported in BM-rich tissues such as placenta (Moren *et al.*, 1994), there is a possibility that LTBP-2 may have some association with BM. Therefore, it was decided to search for binding partners for LTBP-2 amongst BM components. If isolation of binding ligands for LTBP-2 was successful, searching for βig-h3 binding partners in a BM mixture would then be considered, since βig-h3 expression has previously been reported in the BM of proximal tubules of kidney (Park, 2004). The commercially available BM preparation, matrigel (BD Biosciences, San Jose, CA) was used for the experiments. Matrigel BM mix is a solubilised BM preparation extracted from the EHS mouse sarcoma, a tumour rich in these components. Its major component is laminin, followed by collagen IV, HSPG and nidogen. It also contains TGF-β and other growth factors which occur naturally in the EHS tumours.

After the incubation of matrigel at 1mg/ml in TBS with rLTBP-2-sepharose and BSA-sepharose-control, eluates were analysed by SDS-PAGE and silver staining (section 2.15, 2.6 and 2.7). Several protein bands appeared to be interacting non-specifically with both rLTBP-2-sepharose (**figure 7.9B, lane 1**) and BSA-sepharose-control (**figure 7.9B, lane 2**). Thus,

the results of incubating rLTBP-2-sepharose with matrigel were very similar to that of incubating rLTBP-2-sepharose with BNLPM, in that a large number of proteins from both mixtures bound non-specifically to rLTBP-2. Therefore, it appeared that, similar to BNLPs, the BM proteins contain strong adhesive properties. In addition, it can be concluded from the combined results that LTBP-2 also has extensive adhesive properties that contribute to its non-specific interaction with BNLPs and proteins found in matrigel. Similar adhesive characteristics also appear to exist for βig-h3, although alternative tissue extracts or protein mixtures need to be tested to confirm this observation.

From the results of the affinity chromatography thus far, it was evident that the general adhesive characteristics of matrix proteins including βig-h3 and LTBP-2 were major problems for the isolation of binding partners from various extracts at or close to physiological conditions. With this in mind, modifications to the affinity chromatography system were necessary and hence considered in an attempt to reduce the non-specific protein-protein interactions of rβig-h3 and rLTBP-2.

7.8 Affinity chromatography improvements for isolation of binding ligands for βig-h3 and LTBP-2 from BNLPM

7.8.1 Dilution of BNLPM

To reduce non-specific binding, alterations to the affinity chromatography system were considered for identifying binding partners for rβig-h3 and rLTBP-2. BNLPM was chosen over matrigel since BNLPs interacted non-specifically with sepharose-control and BSA-sepharose-control to a lesser extent than the proteins in the matrigel mixture.

Initially, the concentration of BNLPs incubated with the columns was decreased to investigate its effect on the specificity of the interaction with rβig-h3 and rLTBP-2. Previously a total of 1mg/ml of solubilised BNLPM in TBS/0.5M NaCl was incubated with each column. Since the mixture contains a diverse population of proteins, the concentration of the individual proteins will be quite low compared to concentration of the bait protein. Thus it was predicted that excess bait protein would be available to interact non-specifically at a lower affinity with various proteins instead of specifically with its high affinity binding partners. These non-specific binding proteins may also have precipitated on the column contributing to the high level of background observed in previous experiments. It was considered that dilution of the BNLPM may result in an increased chance of specific protein-protein interactions occurring during the incubation period.

A 1/10 dilution of BNLPM (100μg/ml), was incubated with rβig-h3-sepharose, rLTBP-2-sepharose and sepharose-control. Silver staining of the eluted proteins from the columns indicated that more BNLPs bound to rβig-h3-sepharose (**figure 7.10, lane 1**) and

rLTBP-2-sepharose (**figure 7.10, lane 2**) compared to the sepharose-control (**figure 7.10, lane 3**). The protein patterns from rβig-h3-sepharose and rLTBP-2-sepharose appeared to be similar, though the intensity of the staining of the bands was greater in the eluate from the rLTBP-2-sepharose. The reduction in the concentration of the extract did not appear to increase the specificity of the interaction between rβig-h3 and rLTBP-2 with the BNLPs. The dilution of the BNLPM also appeared to make no significant difference to the pattern of bands in the non-specific binding to the sepharose-control column, compared to the undiluted extract (**figure 7.7, lane 2**). However, a general increase in the staining intensity of the protein bands was noted, suggesting dilution of the BNLPM actually increased the background binding.

7.8.2 Reducing the size of the 'bait' protein columns

The size of the rβig-h3-sepharose, rLTBP-2-sepharose, BSA-sepharose-control and sepharose-control columns (40µl) was reduced 5-fold with respect to the amount of BNLPM. Silver staining of the eluted proteins from the smaller columns revealed a different pattern of bands with a total of only four bands identified in the eluates from all four columns. These were rβig-h3-sepharose (**figure 7.11, lane 1**), rLTBP-2-sepharose (**figure 7.11, lane 2**) and BSA-sepharose-control (**figure 7.11, lane 3**). No protein bands were detected in the sepharose-control (**figure 7.11 lane 4**). These results showed that decreasing the amount of bait protein, by reducing size of the columns, did not increase the interaction with specific binding partners in the BNLPM.

Despite altering the concentration of the BNLPM, or the size of protein-sepharose columns and the use of different protein mixtures (BNLPM, matrigel), a large number of proteins in the mixtures continued to bind to both the rβig-h3-sepharose and rLTBP-2-sepharose. This suggested that most interactions were of a non-specific nature. Due to our continuing inability to reduce the non-specific interaction of the proteins in tissue extracts with the recombinant proteins, a different approach needed to be considered. Better controls were needed for distinguishing the proteins binding specifically to the bait-sepharose columns compared with those that bound non-specifically. Hence, the eluates from rβig-h3-sepharose and rLTBP-2-sepharose were chosen to act as controls for the other since most proteins appeared to be non-specifically binding to both rβig-h3 and rLTBP-2. Identification of proteins that bind uniquely to only one of the two bait proteins would suggest a specific interaction.

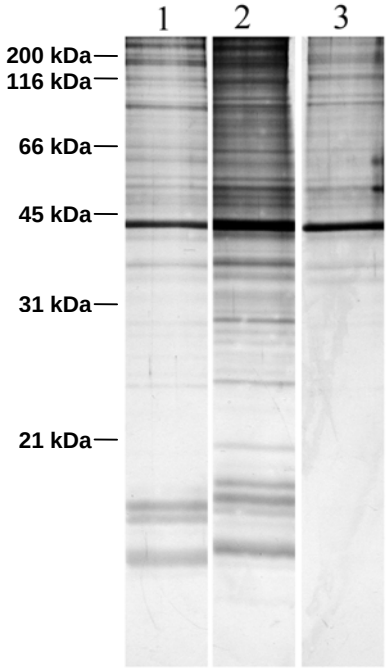

Figure 7.10. Effect of decreased concentration of BNLPM on isolating binding ligands for rβig-h3 and rLTBP-2. BNLPM at 100μg/ml was incubated with rβig-h3-sepharose and sepharose-control. Bound proteins were eluted with 6M urea and eluates were analysed by 15% SDS-PAGE and silver staining. **Lane 1**, rβig-h3-sepharose (200μl). **Lane 2**, rLTBP-2-sepharose (200μl). **Lane 3**, sepharose-control. The pattern of proteins eluted from rβig-h3 and sepharose column appeared to be very similar.

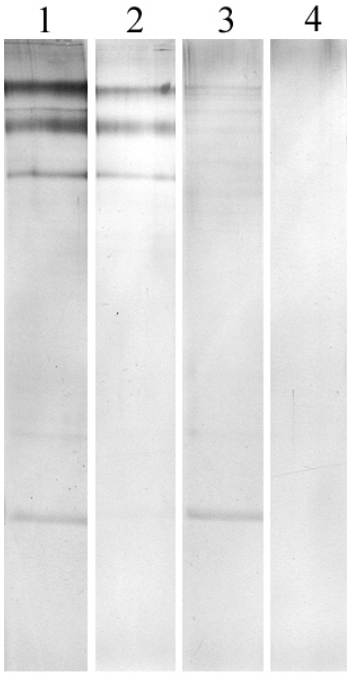

Figure 7.11. Effect of reducing the size of the sepharose affinity columns on non-specific background binding. The amount of rβig-h3-sepharose and rLTBP-2-sepharose incubated with BNLPM was reduced from 200μl to 40μl. Bound proteins were analysed by 15% SDS-PAGE and silver staining. **Lane 1**, rβig-h3-sepharose (200μl). **Lane 2**, rLTBP-2-sepharose (200μl). **Lane 3**, BSA-sepharose-control (200μl). **Lane 4**, sepharose-control (200μl).

7.9 Separation of proteins eluted from rβig-h3- and rLTBP-2-sepharose by 2-D Gel Electrophoresis (2-DGE)

7.9.1 Silver staining detection of proteins separated by 2-DGE

The large number of proteins that bound to rβig-h3 and rLTBP-2 made it difficult to identify specific binding partners, especially when the eluates from both rβig-h3-sepharose and rLTBP-2-sepharose gave very similar banding patterns. Considering that the proteins are associated with different structures within the tissue it was unlikely that they shared a large number of binding partners. Therefore the results thus far indicated that the adhesive natures of βig-h3 and LTBP-2 contributed to the similar banding patterns seen when the eluates from both columns were separated on a polyacrylamide gel. There were potential differences in the proteins that bound to the two sepharose columns; however, they may have been masked by insufficient separation of the eluted proteins by SDS-PAGE. It was considered that further separation of the proteins might aid in identification of distinct binding partners of rβig-h3 and/or rLTBP-2. For additional separation, affinity-purified proteins were analysed by 2-dimensional gel electrophoresis (2-DGE) (section 2.17). Two-DGE is a widely used separation technique in which proteins are separated according to isoelectric point by isoelectric focusing in the first dimension, and according to molecular weight by SDS-PAGE in the second dimension (O'Farrell, 1975). 2-DGE has a high capacity for resolution of complex mixtures of protein, permitting visualisation and analysis of hundreds of protein spots (Tannu and Hemby, 2006).

BNLPM was applied to both the rβig-h3-sepharose and rLTBP-2-sepharose and bound proteins were eluted and the total protein concentrations were determined using the Bradford assay (section 2.15). A sample of the eluate, (5.5µg) was made up in standard solubilisation buffer (section 2.17) which was a modification of O'Farrell's lysis buffer (O'Farrell, 1975). These modifications included change of the total urea concentration from 9.5M urea to 6M, substituting 5% β-mercaptoethanol for 50mM dithiothreitol and 2% (w/v) NP-40 for 4% CHAPS (as recommended by Bio-Rad Laboratories, Hercules, CA). This was then followed by passive loading of the sample on to the 7cm IPG strip pH 3-10. Proteins were separated by isoelectric focusing using a slow ramping preset program (section 2.17). After completion of the isoelectric focusing, the IPG strip was then treated sequentially with dithiothreitol and iodoacetamide equilibration buffers (**appendix B**) and electrophoresed on a 10% polyacrylamide gel (section 2.6). The protein spot patterns of eluates from rβig-h3-sepharose and rLTBP-2-sepharose, were visualised by silver staining (section 2.7) (**figure 7.12**). Compared to the protein spots detected on the gel of the eluate from rβig-h3-sepharose (**figure 7.12A**), there appeared to be less protein detected on the gel of the eluate from

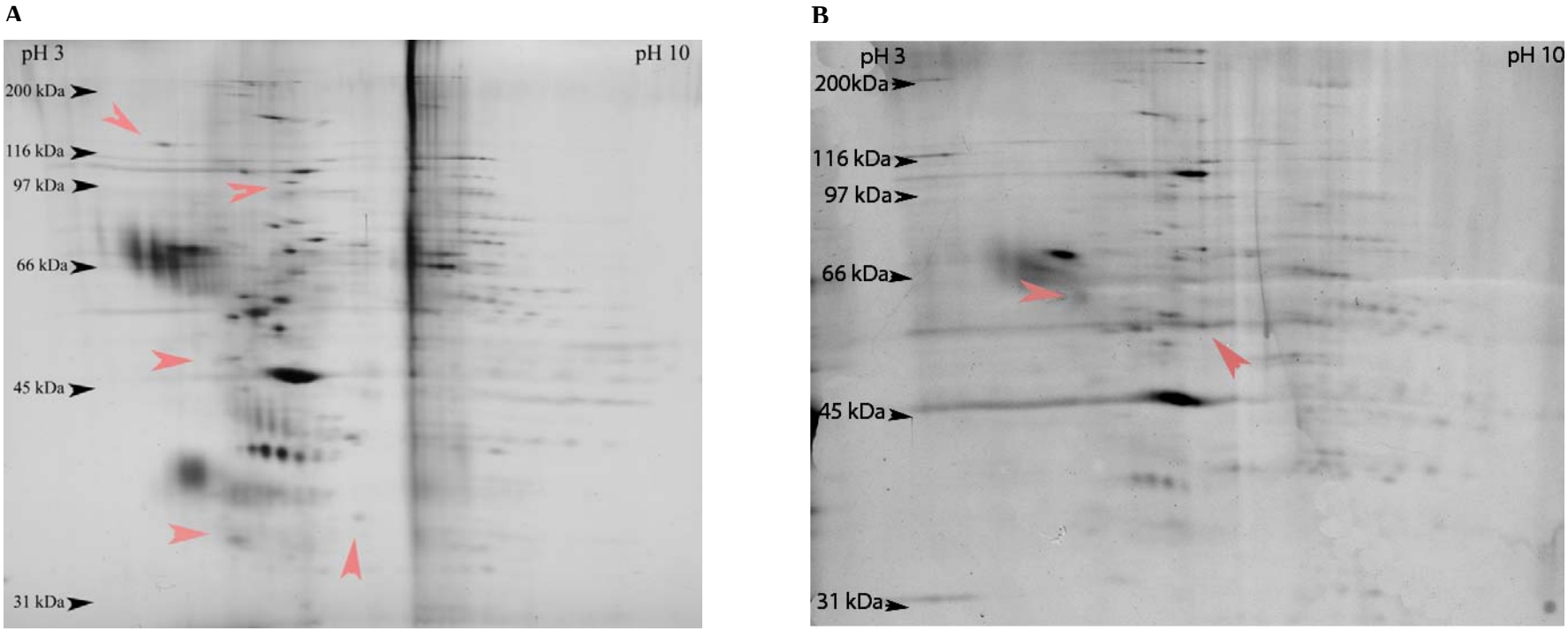

Figure 7.12. 2-DGE analysis of BNLPs bound to rβig-h3 and rLTBP-2. Eluates from rβig-h3-sepharose and rLTBP-2-sepharose were separated in the first dimension by isoelectric focusing on a pH 3-10 IPG strip, followed by 10% SDS-PAGE separation and silver staining. **A,** Proteins bound to rβig-h3-sepharose (5.5µg). **B,** Proteins bound to rLTBP-2-sepharose (5.5µg). The arrows indicate unique spots to each protein.

rLTBP-2-sepharose (**figure 7.12B**). There were a number of spots that seemed specific to the individual bait proteins which were marked by arrows in **figure 7.12**, but it was difficult to confirm their candidacy due to inequality of loading between the two gels. The reduced amount of protein present on the SDS-PAGE of the sample from the rLTBP-2-sepharose may have been caused by insufficient sample entering the IPG strip or by the loss of proteins during dialysis prior to application to the strip. In addition to the difference in the amount of total protein present on the gels, there were horizontal steaks associated with some protein spots which were more apparent in the gel of the sample eluted from the rLTBP-2-sepharose. The horizontal streaking associated with protein spots indicated incomplete focusing of the protein spots. This might have been caused by samples having incomplete solubilisation prior to application or by the presence of ionic impurities in the sample. In contrast to the LTBP-2 gel, there was a prominent vertical streak observed close to pH 7 in the sample eluted from rβig-h3-sepharose. The vertical streak was probably due to high salt in the mixture, perhaps due to inefficient removal of salts by dialysis. Furthermore, as described by (Gorg *et al.*, 1988), vertical streaking is related to the second dimension, and may be caused by insufficient equilibration prior to SDS-PAGE (Gorg *et al* 1988). In summary, an increase in solubility of the proteins in the samples was required to improve the entry of the proteins into the IPG strip, as well as improving the focusing of the proteins in the strip by altering the isoelectric focusing run. These are further discussed section 7.9.2.

7.9.2 Improving the resolution of 2-DGE

From the evidence in section 7.9.1, the separation of the BNLPs eluting from rβig-h3-sepharose and rLTBP-2-sepharose needed to be optimised for comparison and identification of specific ligands with adequate certainty. Firstly, the total protein concentrations of both samples needed to be equal to compare the samples properly. Therefore, extra care was taken during preparation of the sample for isoelectric focusing, i.e. during dialysis of the samples into 6M urea and during rehydration of the IPG strip, to minimize protein loss. Furthermore, to further improve the entry of the proteins into the IPG strip during passive rehydration, and to improve their focusing on the strip, the solubility of the eluates could be improved by dialysis into enhanced solubilisation solution. This was designed to increase both the uptake of the proteins by the strip and the protein resolution by allowing complete dis-aggregation, denaturation, and reduction of proteins due to disruption of all protein-protein interactions (Herbert, 1999; Rabilloud, 1996). A typical solubilisation solution contains 1) a chaotropic agent such as urea and/or thiourea for denaturation of proteins (Galvani *et al.*, 2001; Rabilloud *et al.*, 1997), 2) detergents for forming stable solubilised complexes with exposed hydrophobic residues during focusing, 3) reducing agents for reduction of disulphide bonds

to ensure complete protein solubilisation, and 4) carrier ampholytes to keep the separated proteins in a charged state (Lalwani *et al.,* 2005). Compared to the original solubilising solution, the enhanced solubilising solution contains the additional non-detergents sulfobetaine 3-10, and the chaotropic agent thiourea and replaces of dithiothreitol with the reducing agent tributylphosphine. A urea-thiourea mixture has been reported to improve the solubility and resolution of proteins on IPG strip compared with urea alone. Also tributylphosphine is known to be a more selective and efficient reducing agent than dithiothreitol, as it retains its reducing power at acidic pH 5 and at pH levels above 7.5 (Herbert *et al.,* 1998). The addition of the zwitterionic surfactant, sulfobetaine 3-10 has been reported to improve protein solubility at or near its isoelectric point (Esteve-Romero *et al.,* 1996).

Secondly, the isoelectric focusing resolution needed to be improved for differentiation of the fainter proteins spots. Therefore, several aspects of the isoelectric focusing were altered in an attempt at improving the focusing of the protein mixture. One of the isoelectric focusing alterations that were considered was the time of the conditioning step. This step was increased from 15 minutes to 3 hours to allow more time for the salts and other contaminants to be removed prior to focusing the proteins. Salts increase the ionic strength of the solution and thus produce a high current which is not desired when high voltages need to be reached during the isoelectric focusing (Vincourt *et al.,* 2006). An additional clean up step to further remove salt from the samples was considered, but additional steps needed to be kept to a minimum to limit losses of the protein sample.

To observe whether salts and contaminants were the reason for insufficient focusing of the proteins, a sample of eluate from rβig-h3-sepharose (5.5µg) was loaded on to a IPG pH 3-10 strip through passive rehydration and was isoelectric-focused with a 3 hrs conditioning step and several changes of the electrode filter paper electrode strips. Silver staining of the 2-D pattern, showed reduction in the vertical smearing (**figure 7.13A**) previously present. However, there also appeared to be a marked reduction in the total amount of protein resolved on the gel. Thus it was difficult to establish how the prolonged voltage step aided in the focusing of the proteins. There did appear to be a slight change in one of the prominent spots migrating at 47 kDa. This spot seemed to focus as three spots, instead of one as previously, but this result may have been caused by protein carbamylation. Protein carbamylation changes a protein's isoelectric point and is caused by reaction with isocyanate, a urea degradation product. However, the proteins migrating at 37 kDa have consistently clustered very close together, therefore these protein spots might be normal modifications of the same protein within the extract and may not be modifications due to urea carbamylation.

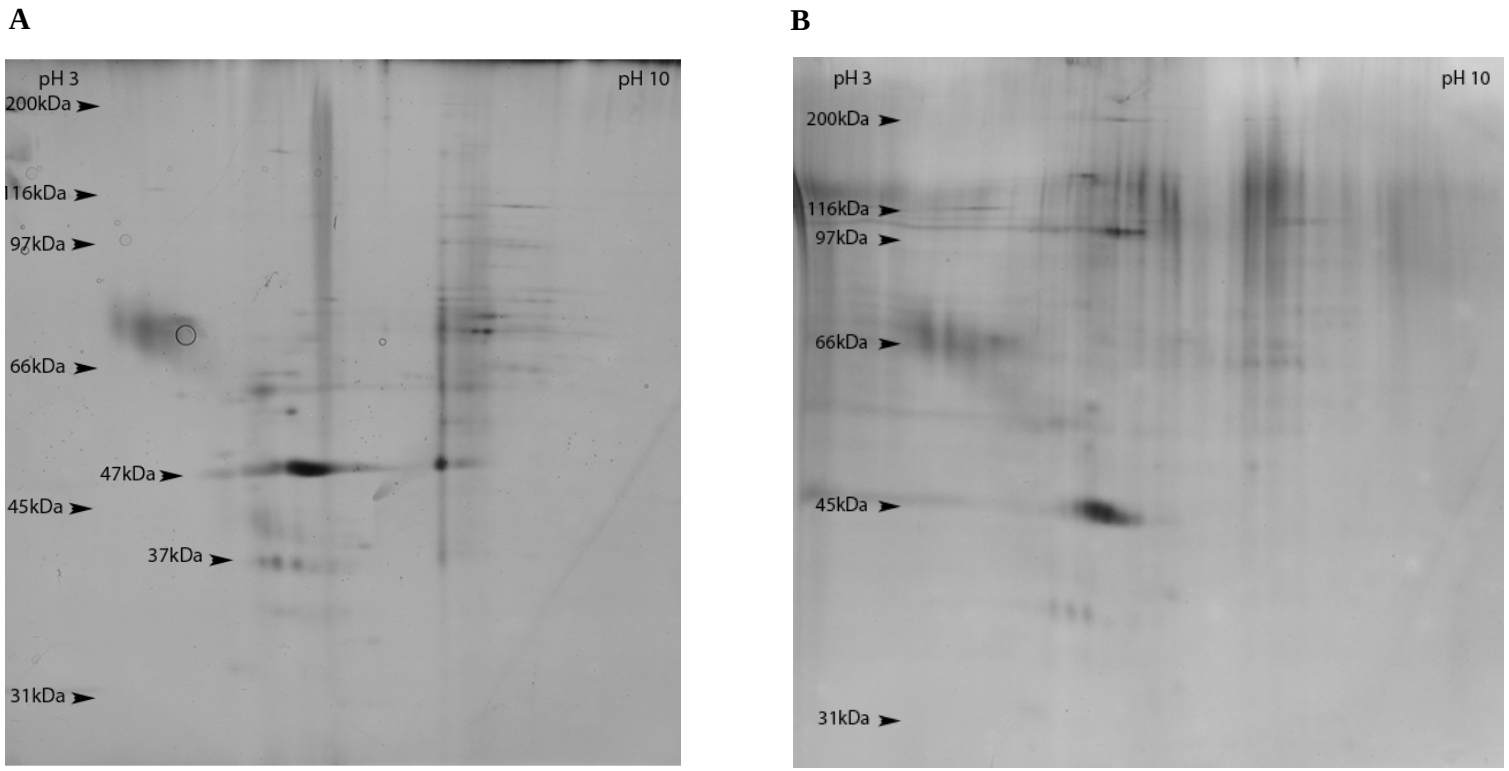

Figure 7.13. The effect of a prolonged conditioning step or different solubilisation solution on isoelectric focusing of proteins. Proteins bound to rβig-h3-sepharose (5.5µg) were separated by 2-DGE under different conditions and silver stained for analysis. In **A,** the conditioning step was for 3 hours during the isoelectric focusing run, while in **B,** bound protein was dialysed into multiple surfactant solubilisation solution prior to passive rehydration. Fewer proteins were observed on the gels.

To investigate whether enhanced solubilisation solution improved the uploading of the proteins onto the strip and their focusing, the eluted proteins from rβig-h3-sepharose (5.5µg) were dialysed into a multiple surfactant solubilisation solution, loaded passively onto the IPG strip and analysed by for 2-DGE. Silver staining of the 2-D gel revealed once again reduced amounts of total proteins present on the gel (**figure 7.13B**), when compared with the original conditions used. The protein spots that were detectable on the gel did not appear better focused. They looked blurred and had vertical smears still associated with a number of the spots. The results therefore indicated that under our standard conditions the use of multiple surfactant solubilisation solution did not improve the focusing of the proteins on the IPG strip during isoelectric focusing. Similar findings were reported by Lee, (2009) where direct correlation between the effects of buffers with changes in protein solubilisation was investigated. Lee, (2009) reported that neither the replacement of dithiothreitol with tributylphosphine nor the addition of detergent improved the solubility and resolution of the protein sample tested. In contrast, solubilisation of proteins with buffer containing 1.5% dithiothreitol and 4% CHAPS increased spot numbers, density and resolution (Lee, 2009). Therefore it appeared that the original solubilisation solution and the initial focusing program were more appropriate for use for isoelectric focusing.

From the results it was concluded that one of the contributing factors to the lack of identification of specific binding ligands for βig-h3 and LTBP-2 was poor reproducibility of protein spot patterns. This perhaps was caused by the lack of consistent uptake of the protein sample into the IPG strip. Therefore an alternative approach which included cup loading was considered to improve sample loading. Cup loading is an alternative approach to passive rehydration and it is commonly used to improve resolution when separating basic proteins (Görg *et al.,* 2000). For this, samples were actively loaded using a cup onto a pre-hydrated IPG strip and separated by 2-DGE (sections 2.17). The resulting spot pattern however, showed no improvements in the amount or resolution of proteins entering the gel (data not shown).

Optimal conditions for solubility and resolution of protein samples vary somewhat with the type of sample under examination. Thus far, the problems of insufficient sample entering the gel and incomplete focusing of spots were unable to be eliminated by various modifications of the 2-DGE method. It was considered that, working with such low concentrations of protein in association with complicated sample preparation may be affecting the total protein that is resolved on the gel. Because of such low amounts of proteins being available for analysis, silver staining appeared to be of limited value for identifying protein spots from artefacts on the gels. Therefore, increasing the sensitivity of the staining would overcome the lack of detection of scarce protein spots and allow for

adequate comparison between the eluates from the rβig-h3-sepharose and rLTBP-2-sepharose. The detection of minute amounts of proteins may even compensate for the insufficient focusing of the proteins on the IPG strip. Another contributing factor to the inability of positive identification of unique protein spots was the variability seen within two gels after 2-DGE, making it difficult to match protein spots in the two gels. The variability associated with 2-DGE, including sample preparation and sample separation, was approximately 20-30% from gel-to-gel. Therefore better methods needed to be considered in order to eliminate gel-to-gel variation.

7.9.3 Detection of proteins separated by 2-DGE using 2-D-DIGE technology

7.9.3.1 Labelling of the proteins with CyDye DIGE Fluor minimal dye

The silver stained 2-DGE protein spot patterns were difficult to analyse, compare and contrast. This was mostly due to inconsistent concentration of sample protein entering the IPG strip due to loss of protein during sample preparation. Additionally, there was gel-to-gel variation which also contributed to the difficulty in trying to distinguish real differences between unique proteins and non-specifically binding proteins that bound to rβig-h3-sepharose and rLTBP-2-sepharose. Hence 2-D SDS-PAGE using fluorescence 2-D difference gel electrophoresis (2-D-DIGE) technology was employed for detection of minute amounts of protein being analysed and to improve comparability between eluates from rβig-h3-sepharose and rLTBP-2-sepharose. The advantage of this technology is that it allows the analysis of both samples on the one gel, eliminating gel to gel variation.

2-D DIGE uses molecular weight- and isoelectric point-matched, spectrally resolvable cyanine dyes (Unlu *et al.*, 1997) to label two or three protein samples prior to 2-DGE. It is the use of different dyes to separately label BNLPs eluted from rβig-h3-sepharose and rLTBP-2-sepharose that allows for co-separation of the samples in a single 2-D polyacrylamide gel. Firstly, CyDye DIGE fluor minimal dyes, Cy3 and Cy5 were used for labelling of the bound proteins. The sensitivity of CyDye DIGE dyes Cy3 and Cy5 is 0.025ng compared with silver staining which has a sensitivity of 1ng (Marouga *et al.*, 2005). The labelling reaction was designed to ensure labelling of approximately 1-2% of the lysine residues of the protein sample (Marouga *et al.*, 2005; Tannu and Hemby, 2006). Therefore, for comparison of protein spot pattern between proteins bound to rβig-h3-sepharose and rLTBP-2-sepharose, 5µg of eluates from both sepharose columns were labelled with CyDye DIGE fluor minimal dyes Cy3 and Cy5 respectively.

After the CyDye-labelled proteins had been fractionated by 2-DGE, the gels were scanned and analysed by a Typhoon Trio+ variable mode imager (GE Healthcare, Uppsala, Sweden). The resulting spot patterns for the eluates from rβig-h3-sepharose (**figure 7.14A &**

C) and rLTBP-2-sepharose (**figure 7.14B & C**) appeared to be very similar and the inconsistency between the concentrations of the two eluates appeared to have been eliminated. However, there appeared to be fewer protein spots detected when samples were labelled with the CyDye DIGE fluor minimal dyes than when previously stained with silver. This suggested that the labelling reaction was not efficient. Furthermore, the labelled proteins were not focused sufficiently, as they all appeared to be migrating as a block in the second dimension. In addition, instead of protein spots horizontal smears dominated the gel, which further suggested that the isoelectric focusing step was not optimised. In spite of these problems, the overlay of the two staining patterns revealed several protein spots that appeared to be unique to rβig-h3-sepharose or rLTBP-2-sepharose which were marked by arrows in **figure 7.14C**. To confirm the authenticity of the unique spots, the experiment was repeated. **Figure 7.15** illustrates the spot pattern achieved for each of the fractionated samples. In this experiment the labelling reaction appeared to be more successful as there were more total protein spots present, most of which appeared to have localised in the centre of the gel close to neutral pH (**figure 7.15**). No obvious unique protein spots were identified by comparing the separated BNLPs eluted from the rβig-h3-sepharose (**figure 7.15A & C**) with rLTBP-2-sepharose (**figure 7.15B & C**). However, from the overlay analysis of the spot patterns, several protein spots were identified as possible unique binding partners for both rβig-h3 and rLTBP-2 (**figure 7.15C**). The unique protein spots identified previously were no longer detectable, perhaps due to better labelling of the proteins in the samples, thus indicating that they were not true unique protein spots. However, they were neither sufficiently convincing nor abundant to be taken for protein identification.

From the results of CyDye DIGE fluor minimal dye labelling of the eluates, it appeared that there was inconsistency with the labelling of the protein samples under analysis. Consistency was necessary for labelling of the protein samples and subsequent binding ligand identification. Since each CyDye DIGE fluor minimal dye labels only a small percentage of the total protein present in the sample (Marouga *et al.,* 2005), the next approach was to use CyDye DIGE fluor saturation dyes for labelling. CyDye DIGE fluor saturation dye labelling, labels the majority of the total proteins present in the samples, which improves the sensitivity of spot detection (Shaw *et al.,* 2003).

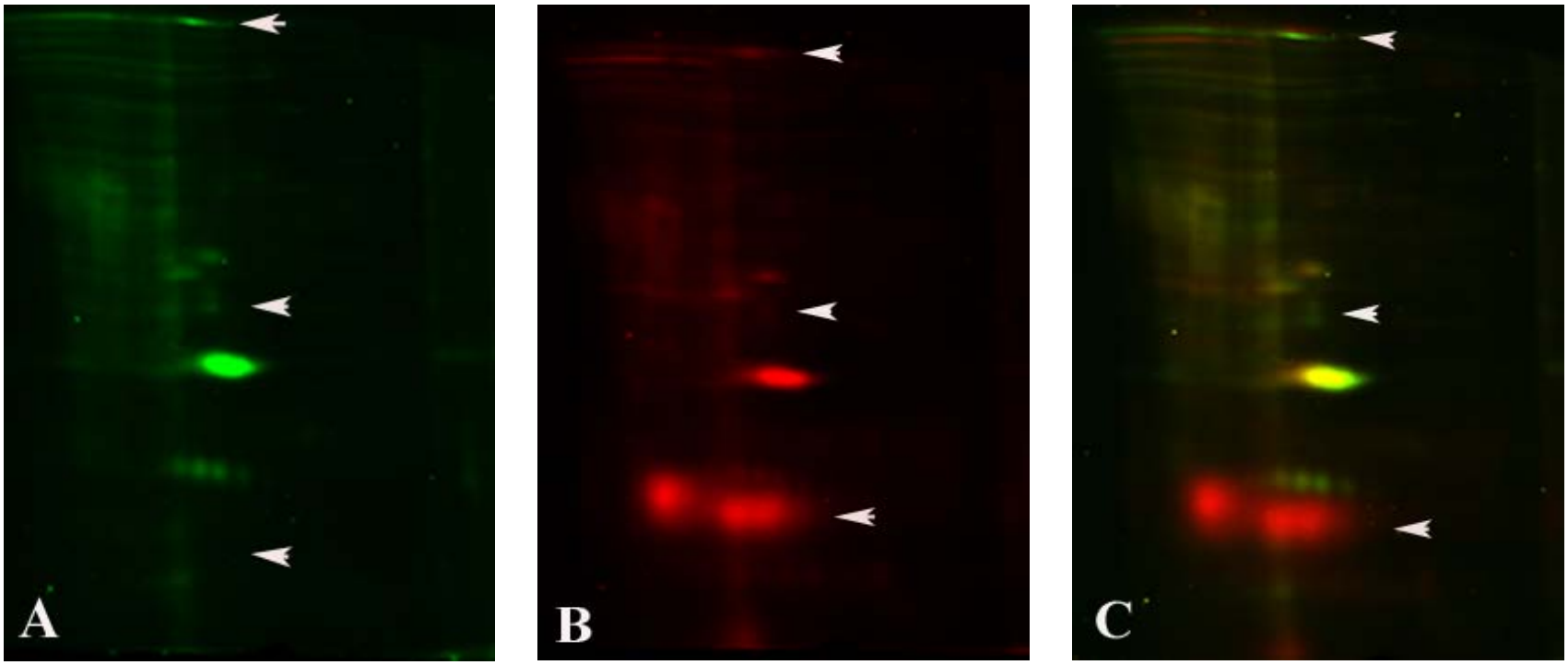

Figure 7.14. Comparison of the bound proteins to rβig-h3 and rLTBP-2 using 2-D-DIGE technology. CyDye DIGE fluor minimal dye labelling of the eluates from **A,** rβig-h3-sepharose (5μg) and **B,** rLTBP-2-sepharose (5μg), prior to 2-DGE. **A** and **B** are superimposed in **C**. Arrows indicate the specific spots for each protein. Proteins specifically binding to rβig-h3 are visualised as green spots, while red spots are proteins binding specifically to rLTBP-2. Yellow spots indicates proteins binding to both rβig-h3 and rLTBP-2.

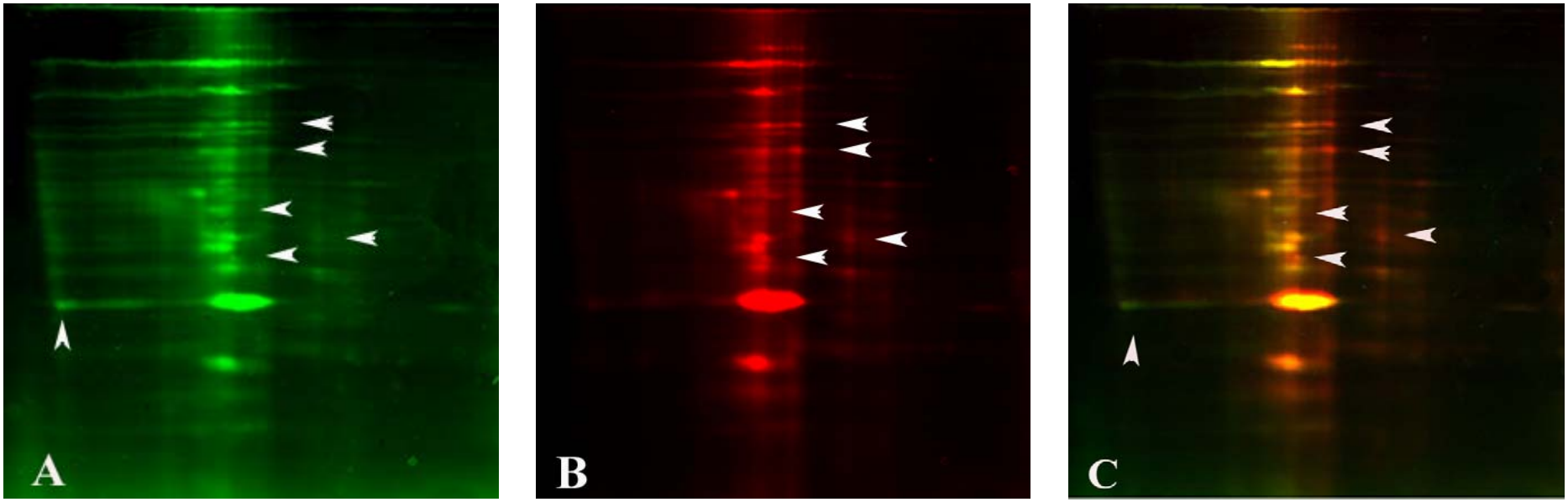

Figure 7.15. Repeat of CyDye DIGE fluor minimal labelling of bound proteins to rβig-h3 and rLTBP-2. A sample of the eluates from **A,** rβig-h3-sepharose (5μg) and **B,** rLTBP-2-sepharose (5μg) were labelled with Cy3 and Cy5 respectively, prior to 2-DGE. **A** and **B** are superimposed in **C**. Arrows indicate specific spots to each protein. There were more proteins spots present on the gel compared with initial CyDye DIGE fluor minimal labelling of bound proteins to the coupled sepharose columns.

7.9.3.2 Labelling of the proteins with CyDye DIGE fluor saturation dyes

The CyDye DIGE fluor saturation dyes label all reduced cysteine thiols of proteins, and are even more sensitive than minimal dyes in detecting amounts as low as 15pg (Marouga *et al.,* 2005). It was hoped that this system would increase the number of protein spots detected and the intensity of the detected protein spots. In previous experiments, only the abundant proteins were detected and these appeared to be present in eluates from both rβig-h3-sepharose and rLTBP-2-sepharose. Visualsing the larger spectrum of proteins present in the samples would increase the chance of identifying authentic candidate partners.

Similar to CyDye DIGE fluor minimal dye labelling, 5μg of bound proteins eluted from rβig-h3-sepharose and rLTBP-2-sepharose were labelled with Cy3 and Cy5 respectively. After labelling of the bound proteins, they were combined and were loaded on the IPG strip through passive rehydration (section 2.17). Upon completing the fractionation of the labelled proteins by size, the gel was scanned and analysed once again by a Typhoon Trio+ variable mode imager (GE Healthcare, Uppsala, Sweden). The resulting image was a black gel with no traces of labelled protein spots and a dye front at the bottom of the polyacrylamide gel (data not shown). The results indicated that the labelling reaction was unsuccessful, and no proteins were labelled despite following the manufacturer's instructions (see section 2.17). The experiment was repeated, this time paying extra attention to the pH of the sample prior to commencing labelling, since it is essential for the protein samples to be at pH 8.0 for efficient labelling with CyDye DIGE fluor saturation dyes. Analysis of the gel using Typhoon Trio+ again revealed no labelled spots, suggesting unsuccessful labelling of the proteins with CyDye DIGE fluor saturation dyes. Several possible factors may have contributed to the unsuccessful CyDye DIGE fluor saturation dye labelling of the bound proteins, including the loss of BNLPs during sample preparation for labelling and fractionation by 2-DGE. Furthermore, even though care was taken to ensure an optimised condition for successful labelling, the conditions may have still been sub-optimal for labelling, perhaps due to contaminants being carried over or perhaps due to over-estimation of the amount of proteins in the eluates.

Identification of the novel binding ligands for βig-h3 and LTBP-2 from protein mixtures proved to be difficult using affinity chromatography and proteomics techniques. The non-specific interaction of proteins with the affinity columns and low concentration of eluates remained major problems despite various modifications. The small quantities of purified recombinant proteins available for column preparation were also a limiting factor for this project, and preparation of affinity columns with more 'bait' proteins should be considered for similar experiments in the future. The amount of 'bait' protein available was one of several limiting factors in the isolation of novel binding partners of rβig-h3 and

rLTBP-2 using affinity chromatography. Details of these and possible alternatives for future experiments are outlined and discussed in section 8.2.2.

CHAPTER 8
DISCUSSION AND FUTURE DIRECTIONS

8.1 Discussion

LTBP-2 belongs to the fibrillin/LTBPs superfamily of ECM proteins. The members of this superfamily share similar protein composition and structure. The full extent of LTBP-2 functions within the ECM is still unclear. The involvement of LTBP-2 in elastic fibre assembly has been suggested following tissue extraction and immunohistochemical analysis of bovine nuchal ligament, where LTBP-2 was identified as an associated component of fibrillin-microfibrils (Gibson *et al.,* 1995). In Dr. Gibson's laboratory, to further characterise the function of LTBP-2 in the structure and assembly of elastic fibres, the identification of LTBP-2 interactions with associated components of fibrillin-microfibrils has been ongoing. Binding and immunohistochemical studies have been used previously to demonstrate the interaction between LTBP-2 and fibrillin-1 (Hirani *et al.,* 2007). No direct interaction with other elastic fibre-associated proteins, namely fibrillin-2, tropoelastin, MAGP-1, -2, dermatan sulphate-PGs, decorin and biglycan, was identified (Hirani *et al.,* 2007).

In recent years the interaction of fibrillin-1 with unidentified HSPGs has been reported to have an essential influence on the assembly of microfibrils and elastic fibres (Cain *et al.,* 2005; Cain *et al.,* 2008; Ritty *et al.,* 2003a; Tiedemann *et al.,* 2001). In elastic tissues HSPGs are found mainly on cell surfaces for example, syndecans and glypican or in BM for example, perlecan. This suggested the importance of HSPG and instigated the investigation of possible HSPG interactions with LTBP-2.

To commence with, conjugated heparin was used to represent HSPG in the solid phase binding studies with LTBP-2. One of the reasons for this use was the limited availability of rHSPG. Recombinant HSPG of interest were either not available (perlecan) or were very expensive in small quantities (syndecans). Tissue extraction of HSPGs is possible, but it is difficult and it usually results in low yields of impure product. On the other hand, heparin was readily available commercially in large quantities. The most important factor however, is the structural similarity that is shared between heparin and HS which allowed heparin to be suitable for the binding studies (**table 1.1**). Solid phase binding assay was the method of choice for determining direct interactions between LTBP-2 and heparin. Other methods such as co-culture systems in conjunction with immunofluorescence staining can be used to identify interactions between two matrix proteins. However, colocalisation does not

necessarily indicate that there is a direct interaction between the proteins, as was found for fibronectin and LTBP-1 (Chen *et al.*, 2007).

Solid phase binding studies revealed that full length rLTBP-2 contains a moderately strong binding affinity for heparin (section 3.3.5). To ensure the interaction was not merely charge-related, it was important to test the interaction of LTBP-2 with C-6-S, another highly sulphated GAG, which is found in the matrix attached to other PG. Sulphate groups are attached to a number of hydroxyl or amino groups on GAG and they contribute considerably to the GAG polyanionic properties (Zhang *et al.*, 2005). The inability of C-6-S to block the interaction between LTBP-2 and heparin suggests that the heparin-binding region(s) in LTBP-2 are specific for heparan sulphate (section 3.3.3). Similar results were found by Tiedemann *et al.*, (2001), where inhibition assays were used to demonstrate the lack of binding inhibition between heparin and fibrillin-1 with chondroitin -4-sulphate, C-6-S or dermatan sulphate, thus confirming the specificity of heparin binding to fibrillin-1. Furthermore, (Kozel *et al.*, 2004) demonstrated that HS, but not chondroitin sulphate was able to decrease the deposition of tropoelastin into fibres in an *in vitro* model.

The interaction of LTBP-2 with heparin was found to be largely cation (calcium) dependent, similar to the interaction of heparin with other relevant ECM proteins, for example, fibrillins (Jensen *et al.*, 2001; Kielty and Shuttleworth, 1993; Reinhardt *et al.*, 1997a; Reinhardt *et al.*, 1997b) and fibulins (Yanagisawa *et al.*, 2002). Depletion of calcium ions prevented the binding of LTBP-2 to heparin (section 3.3.4), although the mechanism by which the binding was affected is not clear. Two possible ways in which the binding of LTBP-2 to heparin may have been affected are (a) directly, if one of the many cbEGF-like domains present in LTBP-2 calcium was involved in the binding site itself perhaps on or (b) indirectly, where removal of calcium ions may alter the structural conformation of the cbEGF-like domains on LTBP-2, consequently disrupting the heparin binding site. Similar enhancement of binding to heparin in the presence of calcium ions has been previously demonstrated for other relevant molecules, for example MAGP-1 to fibrillin-1 (Jensen *et al.*, 2001). Furthermore, (Yanagisawa *et al.*, 2002) demonstrated that the binding of fibulin-5 to tropoelastin is inhibited in the presence of 10mM EDTA. In general, it appears that calcium chelation with 5mM EDTA or 5mM EGTA does not permanently affect the integrity or the function of proteins. Indeed, Kielty and Shuttleworth (1993), demonstrated that the effects of calcium chelation can be rapidly reversed when isolated fibrillin-microfibrils were incubated with 5mM EDTA or 5mM EGTA prior to incubation with calcium (5mM $CaCl_2$). However, the effects of 25mM EDTA or 25mM EGTA were not completely reversed by subsequent incubation with calcium (25mM $CaCl_2$). Disrupted regions within individual microfibrils were still observed in these treated microfibrils (Kielty and Shuttleworth 1993).

To aid further functional analysis of LTBP-2, it was planned to identify the location of the heparin binding sites on LTBP-2. Recombinant central and carboxy-terminal fragments of LTBP-2 were tested for heparin binding. The C-terminal fragment of LTBP-2 lacked heparin binding. Since LTBP-2 interacts with fibrillin-1 through its carboxyl region (Hirani *et al.,* 2007), the absence of a binding site for heparin in this region implies that LTBP-2 interaction with heparin/HSPGs is unlikely to directly interfere with LTBP-2 binding to fibrillin-1-microfibrils. A relatively low-affinity binding site was identified in the central region of LTBP-2. The difference in the strength of heparin binding to the full length LTBP-2, compared with the central region of this molecule, suggested additional heparin binding site(s) may be present in the amino-terminal region of LTBP-2. Subsequent binding studies from our laboratory have revealed three heparin binding-sites in the N-terminal region of LTBP-2 (J Adams and M Gibson).

Thus far five heparin binding sites have been identified on fibrillin-1 (Cain *et al.,* 2005; Cain *et al.,* 2008; Tiedemann *et al.,* 2001).There are two in the N-terminal region and one in the C-terminal region, which are considered to regulate linear assembly of microfibrils, perhaps by acting as a template for the newly-secreted fibrillin-1 or for alignment and concentration of fibrillins-1 (Cain *et al.,* 2008). Earlier cell culture experiments had shown that exogenous heparin disrupts microfibril deposition, but has no effect on the secretion of these macromolecules (Tiedemann *et al.,* 2001). Interestingly, heparin was found to inhibit the binding of MAGP-1 to the N-terminal region of fibrillin-1, but was found not to affect the head to tail binding of fibrillin-1 (Ritty *et al.,* 2003a). Thus N-terminal HS binding is likely to be a critical determinant of fibrillin-1 polymerisation during microfibril assembly and of MAGP-1 binding during elastic fibre assembly (Cain *et al.,* 2005). The heparin binding site at the C-terminal region of fibrillin-1 overlaps with the tropoelastin binding site on fibrillin-1, and binding assays have been used to demonstrate that heparin inhibits the interaction of tropoelastin with fibrillin-1 C-terminal regions (Cain *et al.,* 2008). Tropoelastin has another binding site in the central region of fibrillin-1 (Rock *et al.,* 2004). Competitive binding between heparin and tropoelastin for the fibrillin-1 central region has also been demonstrated. Therefore, HS attachment to fibrillin-1 at sites overlapping with tropoelastin has been suggested to regulate the deposition of elastin onto the microfibrils (Cain *et al.,* 2005; Cain *et al.,* 2008). A heparin binding site in central region of fibrillin-1 has also been shown to bind perlecan (Tiedemann *et al.,* 2005). This interaction is proposed to be involved in anchorage of microfibrils to BM (Tiedemann *et al.,* 2005). With the identification of multiple heparin binding sites on fibrillin-1, it can be speculated that heparin/HS binding ability of LTBP-2 may modulate the binding of HSPGs with various sites on fibrillin-1 (see below).

To investigate the implications of LTBP-2 interaction with heparin for microfibril and elastic fibre assembly, the immunolocalisation of LTBP-2 in elastic tissues was examined (Chapter 6). In the human foetal aorta, the majority of LTBP-2 was revealed to be associated with elastic fibres in the medial layer and not with elastin-free microfibrils in the adventitia. These findings suggest that LTBP-2 interaction with fibrillin-1 is not essential for the assembly of microfibrils. Therefore, it appears that LTBP-2 is more important for elastic fibrillogenesis, rather than microfibrillogenesis, and the interaction of LTBP-2 with HSPG is more likely to involved in this process.

It can be speculated that the interaction between LTBP-2 and heparin may be involved in the deposition of elastin on fibrillin-1 microfibrils. A recent study has implicated LTBP-2 in promoting elastin deposition on fibrillin-1-containing microfibrils during elastic fibre assembly (Hirai *et al.,* 2007). Hirai *et al.,* (2007) demonstrated that the fibulin-5-targeting role of the LTBP-2 is mediated by the interaction of N-terminal region of LTBP-2 with fibulin-5, a protein well documented for its involvement with deposition of elastin on microfibrils during elastic fibre assembly (Freeman *et al.,* 2005). It is possible that, during targeting of the fibulin-5/elastin complex to fibrillin-1 microfibrils, LTBP-2 binding to HS-side chains of HSPG displaces it from fibrillin-1-microfibrils allowing deposition of the elastin. This speculation is supported by the inhibition studies showing that heparin binding to fibrillin-1 prevents tropoelastin from binding to fibrillin-1 (Cain *et al.,* 2008). Therefore, LTBP-2 binding HSPGs may regulate elastic deposition on microfibrils during elastic fibre assembly.

An alternative way that the HSPGs binding to LTBP-2 may play a role in elastic fibre assembly is through regulating the interaction of LTBP-2 with fibulin-5. HS-chains of HSPGs binding to LTBP-2 may instigate conformational changes to the LTBP-2 protein structure. This may in turn have either a positive or a negative influence on LTBP-2 binding with fibulin-5, depending on whether it enhances or inhibits the interaction.

There is strong evidence that fibrillin-microfibrils intersect with BM in various tissues (Sakai *et al.,* 1986; Tiedemann *et al.,* 2005). In human tissues, studies have shown the colocalisation of perlecan with fibrillin-1-microfibrils (Tiedemann *et al.,* 2005). In addition, *in vitro* binding studies have shown that fibrillin-1 interacts with high affinity to domain V of perlecan core protein and with relatively low affinity with the HS-chains attached to domain I of the protein core (Tiedemann *et al.,* 2005). This raises the question whether there are other associated components of fibrillin-microfibrils, which have the potential to serve as “linker” molecules, between microfibrils and BM. One such molecule could be LTBP-2.

On the molecular level we have shown that LTBP-2 interacts with the HS-side chains of perlecan (section 5.1). The presence of exogenous heparin was found to greatly inhibit the

interaction between LTBP-2 and perlecan, indicating the prominent binding was to the HS-chains. However, protein-protein interaction between LTBP-2 and the protein core component of perlecan cannot be completely ruled out, and further experiments investigating the binding interaction with the perlecan protein core are needed. At the tissue level, LTBP-2 and perlecan have been found to partially colocalise in the medial layer of the foetal aorta (section 6.1.4). The identified interaction between LTBP-2 and perlecan suggests a potential role of LTBP-2 in connecting microfibrils to BMs. Previously, (Tiedemann et al., 2001) demonstrated by double immunofluorescence and immunogold labelling that fibrillin-1 and perlecan were colocalised in close vicinity with various dermal and ocular BM. In the present study it is of interest that perlecan was found to colocalise with fibrillin-1 in the medial layer of the developing foetal aorta, in areas where microfibrils and BM are in close contact. The distribution patterns of fibrillin-1 and perlecan in the foetal aorta were found to be similar to that of LTBP-2 and perlecan. This similar pattern of overlap suggests that LTBP-2 may play a part in the interaction of fibrillin-1-microfibrils and perlecan in the aorta. The role of LTBP-2 could be to stabilise the interaction between fibrillin-1 and the core protein of perlecan by interacting with the HS-chains of perlecan. The interaction of fibrillin-1 with perlecan in the foetal aorta still remains to be confirmed as does the interaction of LTBP-2 with perlecan in this tissue. In order to confirm these interactions *in vivo*, electron microscopy analysis of these regions is required. Post-embedded electron microscopy staining of tissue samples was attempted to identify the structures associated with LTBP-2, fibrillin-1 and perlecan in the developing aorta. However, analysis of the sections was uninformative due to lack of staining. This may be due to the large size of the gold particles not being able to penetrate the tissue after embedding. To overcome this problem, pre-imbedding staining of fresh samples needs to be considered. Further studies on the role of LTBP-2 in microfibril-BM interactions are suggested in section 8.2.1.

It has been reported that knockout of mouse *ltbp-2* results in embryonic lethality between E-3.5 and E-6.5 (Shipley *et al.,* 2000). In the study it was reported that the expression of *ltbp-2* mRNA is detected at E-3.5, is switched off by E-6.5 and reinitiates again at E-13.5. The absence of elastic fibres or fibrillin microfibrils in a developing embryo at E-3.5 indicates any role of LTBP-2 in early mouse development must be independent of these structures. Such novel functions of LTBP-2 have yet to be investigated.

During early embryogenesis, the only ECM structure to exist is BM surrounding the developing blastocoelic cavity, and perlecan is present within this structure (Arikawa-Hirasawa *et al.,* 1999; Costell *et al.,* 1999). The BM plays a critical role during early stages of the developing embryo (Miner and Yurchenco, 2004). Disruption in initial stages of BM development can have severe consequences for the state of the embryo, usually causing

embryonic lethality (Miner and Yurchenco, 2004). For instance, knockout of the laminin γ1 subunit, the most expressed laminin subunit of the first BM in the embryo, causes lethality during the same period reported for LTBP-2 null lethality (E-5) (Miner *et al.,* 2004; Smyth *et al.,* 1999). The death of the embryo is due to the absence of BM (Smyth *et al.,* 1999). We can speculate that LTBP-2 associates with the BM by interacting with perlecan, and thus it plays a role in early embryo development which is independent from elastic fibres. The possibility that the interaction of LTBP-2 with perlecan is necessary for proper development of the embryo deserves further investigation.

In addition to the interaction with perlecan, we have established that LTBP-2 interacts with the cell surface HSPG syndecan-4 but not with another member of the syndecan family, syndecan-2, hence suggesting LTBP-2 may possess novel cell interaction. A previous study has demonstrated that LTBP-2 supports melanoma cell adhesion and migration (Vehvilainen *et al.,* 2003), which appears to be dependent on α3β1 and α6β1 integrins, and that soluble heparin was able to inhibit this adhesion to LTBP-2. Syndecan-4 could therefore be a natural modulator of LTBP-2 interactions.

Cell adhesion is a central, regulated cascade of events during development (Gumbiner, 1996). The interaction of cells with the ECM contributes to modifications in cell proliferation, morphogenesis and survival and HSPGs allow this interaction to occur (Wilcox-Adelman *et al.,* 2002). During embryo development syndecan-4 is mainly expressed in the embryonic ectoderm of the post-implantation embryo (Sutherland *et al.* 1991). It is possible that LTBP-2 interacting with syndecans-4-expressing cells may be involved in some of these cell processes during development, after implantation of the embryo. Further analysis of the interaction of LTBP-2 with syndecan-4, identifying syndecan-expressing cells and establishing the distribution patterns in developing embryos may produce rewarding data.

In addition to the solid phase binding studies we were interested in employing an alternative approach for isolating binding partners for LTBP-2 and also matrix protein βig-h3 from tissue extracts or other protein mixtures using affinity chromatography. The advantage of this method was that it was not limited to the availability of purified candidate proteins. In addition to the LTBP-2 work, identifying βig-h3 interaction with associated components of collagen type-VI microfibrils has been ongoing in Dr. Gibson's laboratory. Furthermore, isolating binding ligands of βig-h3 independent of collagen-VI microfibrils will provide insight into the possible novel function of this molecule in the matrix. During attempts to identify binding ligands for LTBP-2 and βig-h3, it was found that the highly adhesive nature of the two proteins contributed to non-specific interactions with the BNLPs, making it difficult to identify specific partners for these proteins by SDS-PAGE. Modifications to the

affinity chromatography system were carried out to improve detectability of specific interactions of proteins with the rβig-h3- and rLTBP-2 attached to sepharose columns.

The presence of large numbers of proteins present in the eluted fractions from the columns made separation by SDS-PAGE alone an inadequate method. Thus 2-DGE was necessary for sufficient separation of the proteins. Two-Dimensional Gel Electrophoresis is a powerful technology for the study of a highly diverse protein sample. In general, 2,000 protein spots can be visualised on a gel depending on the staining technique, the pI range of the first dimension and the size of the 2-DGE (Tannu and Hemby, 2006).

The separation of the bait-column eluates by 2-DGE and subsequent silver staining did little to help identify candidate binding partners of rβig-h3 and rLTBP-2. This was due to several contributing factors, including the inconsistency of the amount of proteins entering the gels, most likely due to loss of proteins during sample preparation, and the use of small amounts of material. Some loss of protein during sample preparation is inevitable, but commencing with amounts as low as 5µg makes any loss significant. It should be noted that there are specific limitations to 2-DGE which depend on the characteristics of the proteins to be visualised. For instance, many hydrophobic proteins or extreme acidic or basic proteins are not able to enter the IPG strip used for first dimensional separation (Van den Bergh *et al.,* 2003). The detection of low numbers of protein spots on a gel made confirming possible candidate binding partners difficult. Even though silver staining is a highly sensitive method for protein staining (Steinberg *et al.,* 2000), it can easily over-develop and speckled background staining also occurs (unpublished observation). In order to visualise less abundant proteins without compromising visualisation of more abundant proteins, 2-DGE in conjunction with CyDye DIGE fluor minimal and saturation dyes was considered. CyDye DIGE fluor minimal and saturation dyes and 2-DGE are proven tools for identification of ligands since in combination they provide sensitivity and allow analysis of multiple samples on one polyacrylamide gel.

CyDye DIGE fluor minimal and saturation dyes are much more sensitive than Coomassie Blue staining and are quantitative, unlike silver staining. However, there was a lack of reproducibility in the labelling of the proteins with the CyDye DIGE fluor minimal dyes, even though labelling of the proteins was achieved. To overcome this difficulty, CyDye DIGE fluor saturation dyes were used to label up to 5µg of total protein and generate 2-D images with 1,500 protein spots (Kondo *et al.,* 2003). However, we were again unable to optimise the conditions for the labelling of proteins with CyDye DIGE fluor saturation dyes, and this was the main factor in the lack of adequate protein labelling which contributed to low numbers of proteins detectable on the gels.

Even though a suitable separating method and sensitive detection techniques were developed, higher initial concentrations of protein samples appeared to be the key to overcoming the above problem. The rationale for this is a) less manipulation is needed for sample preparation, for example various sample concentration steps will be eliminated, and b) several experiments can be carried out from the same column eluates and thus reproducibility will be improved. The higher concentrations will thus improve detection of possible candidate binding partners for rβig-h3 and rLTBP-2.

8.2 Future Directions

8.2.1 Experiments for the comprehensive understanding of LTBP-2 interactions with HSPG

The recognition of heparin binding sites on fibrillin-1 has shed new light on its interaction with other ECM structures and the complexity of microfibril assembly (Cain *et al.,* 2005; Tiedemann *et al.,* 2001; Tiedemann *et al.,* 2005). More recently, LTBP-4 interaction with heparan sulphate has been shown to play a role in TGF-β storage and cell adhesion (Kantola *et al.,* 2008). In this thesis, the interaction of LTBP-2 with heparin/HSPGs including perlecan and syndecan-4 has been demonstrated. However, more studies are needed for confirmation of the functional role of these binding interactions with LTBP-2. Defining the affinities of the LTBP-2 interactions with perlecan and syndecan-4 *in vitro* will indicate the strength of the interaction, and whether it is likely to be transient or more permanent. Results obtained in section 5.2 indicated the interaction between LTBP-2 and perlecan is through its HS-side chains. To determine if perlecan interacts only via its GAG-side chains, solid phase binding assay using perlecan core protein will determine if there are additional LTBP-2 binding sites on perlecan.

To understand the physiological significance of the identified interactions, determination of the range of tissues where LTBP-2 colocalises with perlecan or syndecan-4 is required using immunohistochemisty. The use of this technique may also confirm any identified *in vitro* interaction to be biologically relevant. Both LTBP-2 and perlecan are expressed in tissues such as the aorta, lung, and kidney and these are possible tissues for further investigation. Colocalisation of LTBP-2 with HSPGs perlecan and/or syndecan-4 during different stages of normal mouse embryonic development is another area of interest for understanding the possible functions of LTBP-2 in embryo development. Perlecan plays a role in the adaptive modification of the uterine micro-environment to receive and implant the embryo (San Martin *et al.,* 2004). The role of LTBP-2 in this process needs further characterisation using immunohistochemistry techniques to look at the distribution patterns of the pre-implanted embryo and the uterine tissue. Furthermore, since syndecan-4 is mainly expressed in both the embryo and the uterine tissue after the embryo is implanted (San

Martin *et al.,* 2004), distribution patterns of LTBP-2 and syndecan-4 in embryos and uterine tissues after implantation are worthy of investigation.

8.2.2 Possible alternatives for the identification of binding partners for βig-h3 and LTBP-2

Determining protein-protein interaction is an important component in assigning function and understanding the biological relevance of βig-h3 and LTBP-2 within a physiological context. The actual detection of protein interaction is complicated by the fact that proteins themselves are chemically distinct entities with differing charges, numerous secondary and tertiary structural folds, and may include a wide variety of parameters, for instance concentration of protein, ionic strength, and dissociation constants, all of which can influence molecular interactions (Howell *et al.,* 2006; Kantola *et al.,* 2008). Hence, selection of the most appropriate experimental techniques is important to ensure that the interaction is detected.

Several methods can be used to study protein-protein interactions. Affinity chromatography was the first method of choice for detection of specific protein interaction with rβig-h3 and rLTBP-2 which were coupled to sepharose. The method was chosen because affinity chromatography has been used very successfully to identify specifically interacting proteins (Howell *et al.,* 2006). Many efforts were made to identify specific partners from BNLPMs for rβig-h3 and rLTBP-2 attached to sepharose. The high background binding made the direct identification of potential interactions difficult using this method. Further alterations (to the method) may be made to improve the identification of specific binding partners for rβig-h3 and rLTBP-2 using this method. One of the alterations may be performing binding studies between rβig-h3-sepharose or rLTBP-2-sepharose in the presence of a mild detergent such as Nonidet P-40, Lubrol PX, octylglucoside, CHAPS, tween-20 or triton X-100, to aid in minimizing non-specific interactions of hydrophobic domains of proteins with βig-h3 and LTBP-2 coupled to sepharose. Alternatively, testing alternative eluting buffers for the elution of bound proteins may improve the isolation of candidate binding partners of βig-h3 and LTBP-2. Rather than using a strong denaturant (6M urea) for elution of all of the bound proteins, a gradient of denaturants can be used for the gradual elution of proteins interacting with different affinities from the columns. Alternatively, fractionation of the BNLPM using gel filtration chromatography prior to incubation with rβig-h3-sepharose and rLTBP-2-separose would be another appropriate approach for reducing the background binding problem.

In addition to alterations of binding conditions, increasing the size of the coupled columns used in affinity chromatography, by coupling more rβig-h3 and rLTBP-2 to CNBr-activated sepharose, may have improved the analysis of the proteins binding to rβig-h3-

sepharose and rLTBP-2-sepharose. An increase in the size of the affinity columns should correlate with an increase in the amount of proteins eluted from the columns. Thus analysis of the bound proteins using Coomassie Blue staining would have been possible with minimal handling of the samples. However, an increase in the size of the columns also risks an increase in the amount of non-specific interaction with the columns. In 2-DGE, starting with a higher concentration of protein sample would mean that there would be a greater chance of retaining rarer proteins during sample preparation and thus more of these proteins would be visibly represented on the gel.

Another procedure similar in principle to the affinity columns used for interaction studies is affinity blotting. With affinity blotting, BNLPs eluted from rβig-h3 sepharose and rLTBP-2 sepharose can be fractionated by either SDS-PAGE or 2-DGE and transferred to nitrocellulose membrane. Specific interactors can then be identified by their ability to bind the probe (rβig-h3 or rLTBP-2). The appropriate probes can subsequently be detected either with antibodies specific to each protein or by anti-(tetra-his) antibody specific for the his_6-tag of the recombinant proteins. Affinity blotting was used previously to identify the specific interaction of MAGP-1 with the α3 (VI) chain of pepsin type VI collagen (Finnis and Gibson, 1997). Considerations in affinity blotting include the recovery of the biological activity of the proteins after separation under denaturing conditions and the activity of the probes added to the membrane.

Other methods such as co-immunoprecipitation (CoIP) can be used for detection of potential ligands of βig-h3 and LTBP-2. CoIP uses bait-specific antibody to co-precipitate the bait protein along with any target protein for identification of specific interactors, for example of βig-h3 and LTBP-2. The CoIP method has the advantage of identifying less tightly bound targets due to the specificity of the antibody for antigen. This allows interaction experiments to be carried out under less stringent conditions, more closely mimicking *in vivo* conditions. For example, successful identification of LTBP-2 interaction with fibulin-5 from cultured media of bovine aortic smooth muscle cells using CoIP has been recently reported Hirai *et al.,* (2006). A disadvantage of this method is that it is not suitable for low abundance proteins (Howell *et al.,* 2006).

The most common biochemical technique used to identify protein-protein interactions include affinity purification procedures. Either using antibodies to endogenous proteins or using exogenous expression of tagged recombinant protein baits. Mass spectrometry has become established as method of choice for identifying purified proteins because of its high sensitivity. However, the majority of these proteins usually represent contaminants, including proteins that bind non-specifically to the affinity matrix (Boulon *et al.,* 2010). Thus, despite many technical improvements made in recent years, the unambiguous discrimination between

genuine protein interaction partners, either stable or transient and co-purifying contaminants remains one of the major challenges in the field. Most researchers have sought to identify specific protein interactors by reducing or eliminating the background of non-specific proteins through either biochemical or data analysis strategies (Boulon *et al.,* 2010). In this project eliminating non-specific interactors was attempted at the biochemical level however, our groups have eliminated background binding through data analysis strategies.

Recently, affinity capture liquid chromatography tandem mass spectrometry has been used by others successfully to identify ECM molecular interactions (Cain *et al.,* 2009). A range of purified recombinant human elastic fibre molecules containing four his_6-tags were incubated with cells in culture or with the solubilised matrix. This was followed by purification of protein complexes formed with the recombinant proteins using a HisTrap FF column. Mass spectrometry analysis of the eluates from the affinity column revealed that abundant proteins were purified though this protocol. Amongst the proteins binding specifically to the bait proteins, keratin contaminants were also present and were estimated to have a protein-protein association probability of greater than 40% (Cain *et al.,* 2009). These proteins were therefore removed from further analysis. It appears that the presence of non-specific contaminants is inevitable. An alternate to the attempts of eliminating non-specific binding of proteins to the affinity columns, is discarding them from future analysis similar to the works of Cain *et al.,* (2009).

In addition, the combination of quantitative mass spectrometry and differential labelling of proteins with heavy isotopes, especially with stable isotope labelling with amino acids in cell culture (SILAC) (Ong *et al.,* 2002; Ong and Mann, 2006) can also help to distinguish between specific and non-specific binding proteins in an affinity experiment. Differentiation between specific and non-specific binding of proteins is achieved through the inclusion of an integral negative control. The presence of a negative control allows for direct comparison between the relative levels of each protein present in the control and experimental samples. SILAC thus objectively identifies proteins that can bind non-specifically to the affinity matrix or the fusion tag protein and highhights by comparison proteins that bind specifically to the bait protein (Vermeulen *et al.,* 2008). For instance, HeLa cells expressing a tagged protein were metabolically labelled by culturing in heavy media containing 13C-isotopes of arginine and lysine, while the parental HeLa cells were grown in light media containing the 12C-isotopes of arginine and lysine. Whole cell extracts were then prepared and pre-cleared on sepharose beads. The pre-cleared extracts were mixed in equal amounts prior to affinity purification of the tagged protein. This was followed by elution of the protein from the beads and size fractionation by SDS-PAGE for digestion and liquid chromatography tandem mass spectrometric analysis. The advantage of SILAC is that it

identifies components of protein complexes purified under lower stringency conditions, which preserves more specific interactions (Trinkle-Mulcahy *et al.,* 2008).

Overall, we have characterised LTBP-2 as a heparin/HSPG binding molecule. *In vitro* binding assays demonstrated LTBP-2 binds basement membrane HSPG perlecan and transmembrane cell-signalling HSPG syndecan-4. These findings suggest LTBP-2 has a more complex function in elastic fibre assembly, than previously anticipated. As described in section 1.1.2 tropoelastin aggregates on cell surfaces and it remains attached to cell surface heparan sulphate, prior to its release onto preformed microfibrils. Since unknown HSPGs play a critical role in elastic fibre assembly, it may be that LTBP-2 binding to heparan sulphate enhances displacement of the fibulin-5/elastin complex from the cell surface HSPGs. In addition, the binding of LTBP-2 to GAG-side chains of HSPGs may be involved in the detachment of elastin from fibulin-5 during its deposition on fibrillin-microfibril scaffold. Syndecan-4 is a strong candidate for a HSPG involved in the above mechanisms. The interaction of LTBP-2 with syndecan-4 may also be important for other processes. Generally, LTBP-2 is known as an antiadhesive molecule with poor interaction with integrin receptors. However, the findings presented within this thesis suggest that syndecan-4 may be a novel mediator of LTBP-2-cell signalling. In addition, it would be interesting to investigate whether LTBP-2 binding to syndecan-4 influences heparin sulphate-dependent growth factor signalling e.g, fibroblast growth factor-2, which requires the formation of a ternary complex with its high affinity receptors (FGFR1-FGFR4) and HSPGs to initiate its signalling cascade (Eswarakumar *et al.,* 2005; Jaye *et al.,* 1992). Identification of novel binding partners for LTBP-2 has helped in understanding the function of this intriguing matrix molecule. Further studies into revealing the full spectrum of LTBP-2-binding proteins is an exciting area of continuing research that will lead to disclosure of additional unknown biological roles of LTBP-2.

APPENDIX A

Primer sequences used for cloning of recombinant LTBP-2NT(H) and LTBP-2C(H). Prime sequences are written 5'-3'. Primer sequences are based upon Genbank™ published sequences, accession numbers and base numbers where the primers bind are included.

	Sequence (5'-3')	**Bases**	**Genbank™ accession code**
***HindIII* +LTBP-2 NT Forward**	CAC CAA GCT TCC AAA GGG ACC CCG T	492-506	NM_000428
LTBP-2 NT Reverse+ *HindIII*	GGC CAA GCT TAG AGT CAC CCT TGT C	2749-2763	NM_000428
LTBP-2 Central Forward	CTG AAA GCT TGG ACT CTC AGG CTG GCC AGG	2758-2776	NM_000428
LTBP-2 Central Reverse	TTT TAA GCT TGA TGT CCA TGT GGA TGT CGT	5123-5142	NM_000428
M13F	GTTTTCCCAGTCACGAC		
M13R	CAGGAAACAGCTATGAC		
HLTBPF3	CAG CCC CCT GGG TGA CTC CT	2141-2148	NM_000428
LTBP-R2	TCA CAG AGC GCG GCC CCA CAT AC	4450-4472	NM_000428

APPENDIX B

Solution formulation

10×PCR reaction buffer (Stratagene, La Jolla, CA)
200mM Tris-HCl (pH 8.8)
20mM $MgSO_4$
100mM KCl
100mM $(NH_4)_2SO_4$
1% Triton X-100
1mg/ml nuclease-free BSA

6× load buffer for DNA gels
5mL Glycerol
2mL 50× TAE buffer (see below)
2mL Bromophenol Blue (saturated) (see below)
Adjust volume to 10mL using ddH_2O, aliquot and store at -20˚C

50× TAE
2M Tris-HCl
57.1mL Glacial acetic acid
0.1M $Na_2EDTA.2H_2O$
Adjust to 1L volume using ddH_2O

Soc medium
2g bacto-tryptone
0.5g bacto yeast extract
10mM NaCl
2.5mM KCl
Dissolve in 100mL ddH_2O, autoclave and cool to room temperature. Add 20mM Mg^{2+} (1mL of 2M Mg^{2+} stock containing 1M $MgCl_2$ and 1M $MgSO_4$) and 20mM glucose. Filter through 0.2µm filter to sterilize store at room temperature in 25-50mM aliquots.

Luria Broth
10g Bacto-tryptone (BD Biosciences, Sparks, MD)
5g Bacto-yeast extract (BD Biosciences, Sparks, MD)
86mM NaCl
Dissolve in 1L ddH_2O, adjust pH to 7.5 with NaOH and autoclave to sterilize. For LB plates, include 15g bacto-agar (BD, Sparks, MD) prior to autoclaving.
Allow solutions to cool to 55˚C prior to adding amplicillin.

Dulbecco's Modification of Eagles Medium (DMEM)
13.05g/1L Powdered DMEM
3.7g/1L $NaHCO_3$
pH 7.2
0.22µm filter sterilized

Dulbecco's PBS
0.14M NaCl
2.7mM KCl
3.2mM $Na_2HPO_4.12H_2O$
1.5mM KH_2PO_4
pH 7.4
Filter sterilize using 0.22µm filter

8×Phosphate Buffer
80mM $Na_2HPO_4.12H_2O$
80mM $NaH_2PO_4.2H_2O$
4M NaCl
pH 7.4

2M Imidazole
2M imidazole
pH 7.4
Filter through 0.45µm filter

0.1M $NiSO_4$ (nickel sulphate)
0.1M $NiSO_4.6H_2O$
Dissolve in ddH_2O and filter through a 0.2µm filter.

10mM Imidazole Buffer
1× Phosphate buffer
10mM Imidazole
pH 7.4-7.6

500mM Imidazole Buffer
1×Phosphate buffer
500mM Imidazole
pH 7.4-7.6

0.05M EDTA Solution
0.02M Na_2HPO_4
0.5M NaCl
0.05M EDTA
Add ddH_2O to 100mls, filter through 0.2µm filter

1M NaOH Solution
4g NaOH
Dissolve in 100mLs of ddH_2O, filter through 0.2µm filter

Tris Buffered Saline (TBS)/ 0.5M NaCl
20mM Tris
0.5M NaCl
0.005% Thimerosal
pH 7.4
Dissolve in ddH_2O, adjust pH 7.4

Freezing solution A
50% (v/v) Foetal Calf Serum
50% (v/v) DMEM

Freezing solution B
15% (v/v) Dimethyl sulphoxide (DMSO)
85% (v/v) DMEM
Dilute DMSO into DMEM then filter sterilize the solution through 0.2µm.

Stock 30% Acrylamide Solution
4.22M (30%) acrylamide
52mM (0.8%) Bis-acrylamide (N-N,Methylenebisaceylamide)

Dissolve in ddH_2O, filter using whatman paper, store in a dark bottle at 4˚C

Separating Gel
25mL separating gel buffer
x mL Stock 30% acrylamide solution (amount depends on the strength of the separating gel)
10mg Ammonium persulphate
22.5µL TEMED (Sigma-Aldrich, St. Louis, MO)
Dissolve in ddH_2O to total volume of 50mL, the ammonium persulphate and TEMED should only be added just before gels are to be set

3% Stacking Gel
12.5mL Stacking Gel Buffer
2.5mL Stock acrylamide solution
18.8mg Ammonium Peroxide
11µL TEMED
Dissolve in ddH_2O to total volume of 25mL, the ammonium persulphate and TEMED should be added just before gels are to be set

Protein sample Loading Buffer
10mL Glycerol (add last)
25mL Stacking gel buffer (see above)
2M Urea
20mL of 10% (w/v) SDS solution
20mg phenylmethylsulphonyl fluoride (PMSF) (dissolve in of ethanol added dropwise) (Sigma-aldrich, St Louis, MO)
5mL Bromophenol Blue (saturated) (see below)
Dissolve in 100mL ddH_2O until dissolved, aliquot and store at -20˚C.

Saturated Bromophenol Blue
0.1g Bromophenol Blue
Dissolve in 20mL ddH_2O by stirring overnight at 37˚C

Chamber Buffer
25mM Tris
195mM Glycine
3.5mM SDS
Dissolve in ddH_2O, do not pH

Coomassie Brillian Blue R-250
Dye content of coomassie Blue should be ~50%

0.3% (w/v) Coomassie brilliant Blue R-250
45% (v/v) Methanol
9% (v/v) Acetic Acid
Dissolve in ddH_2O, stir solution well, filter using Whatman paper before use.

40% Methanol/ acetic acid solution
40% (v/v) Methanol
7% (v/v) Acetic Acid
Dissolve in ddH_2O

7.5% Methanol/ acetic acid solution
7.5% (v/v) Methanol
7% (v/v) Acetic Acid
Dissolve in ddH_2O

Tris/Glycine Buffer
6mM Tris
48mM Glycine
pH 8.3

Tris Buffered Saline (TBS)
20mM Tris
0.13M NaCl
0.0005% (w/v) Thimerosal
Dissolve in ddH_2O, adjust pH to 7.4 with HCl and autoclave if sterile solution required

Blocking solution for western blots
10% (w/v) non-fat skim milk in TBS
3% (w/v) BSA in TBS for anti-(his tag) antibodies

Antibody solution for western blots
2% (w/v) non-fat milk in TBS
3% (w/v) BSA in TBS for anti-(his tag) antibodies

Tris/ Tween-20/ Triton X-100
20mM Tris
500mM NaCl
0.05% (v/v) Tween-20
0.2% (v/v) Triton X-100
0.005% Thimerosal
Dissolve Tris, NaCl, and thimerosal in ddH_2O and then add tween-20 and triton X-100, adjust pH to 7.5

Substrate Buffer
100mM Tris
100mM NaCl
50mM $MgCl_2$
pH 9.5

Developing solution for revealing western blots
10mL Substrate Buffer
100µL BCIP (see below)
100µL NBT (see below)
mix and use immediately

5-Bromo-4Chloro-3-indolyl-phosphate (BCIP)
(Diagnostic Chemicals Ltd, Charlottetown, PEI)
25mg BCIP
0.5ml H_2O
0.5ml N, N-Dimethylformamide (DMF)

Nitro Blue Tetrazolium (NBT)
(Boehringer Mannheim GmbH, Mannheim, Germany)
50mg NBT
0.3ml H_2O
0.7ml N, N-Dimethylformamide (DMF)

H_2SO_4/Sodium Tetreborate
0.0125M Tetraborate in conc. H_2SO_4.

Phosphate buffered Saline (PBS)
20mM $NaH_2PO_2.2H_2O$
0.13M NaCl
0.005% Thimerosal

Coupling Buffer
0.1M $NaHCO_3$
0.5M NaCl
pH 4

Blocking Buffer
0.1M Ethanolamine
pH 8

Rehydration Buffer
6M Urea
50mM Dithiothreitol
4% CHAPS
0.2% Bio-Lyte 3/10 ampholytes
0.0002% Bromophenol Blue

Dithiothreitol Equilibration Buffer
6M Urea
2% (v/v) SDS
0.05M Tris pH8.8
20% (v/v) Glycerol
2% (w/v) Dithiothreitol

Iodoacetamide Equilibration Buffer
6M Urea
2% (v/v) SDS
0.05M Tris pH8.8
20% (v/v) Glycerol
2.5% (w/v) Iodoacetamide

Lysis Buffer
7M Urea
2M Thiourea
4%CHAPS
30mM Tris
pH 8.5 for minimal labelling
pH 8.0 for saturation labelling

APPENDIX C

Antibody concentrations for various experiments conducted are listed in the table below. Concentrations for each antibody are indicated as working dilutions from stock antibody solution ane are specified for western blots, solid phase assays and tissue section immunofluorescence.

Antigen	**Antibody**		**Concentration for blot**	**Concentration for solid phase**	**Concentration for immumo-fluorescence**
his_6-tag	Tetra-his at 100µg/mL (Qiagen)	Mouse ascites Monoclonal	1:1000	1:1000-1:2000	
LTBP-2	LTBP-2C (affinity purified at 500µg/mL)	Rabbit polyclonal	1:500	1:5000	1:20
Fibrillin-1	MAB1919-Fib1N(H) 2mg/mL (Chemicon)	Mouse ascites monoclonal	1:2000		1:200
Fibrillin-1	Fib-1A	Rabbit Polycolonal			1:10
Perlecan	7A5CC	Mouse Monoclonal			1:100
EHS Laminin, α-chain	Rabbit-47 "14/9/87"	Rabbit Polyclonal			1:10
βig-h3	MP78/70	Polyclonal	1:500		
βig-h3	Rabbit-45	Polyclonal	1:5000		
	Goat anti-rabbit conjugated to alkaline phosphatase or horseradish peroxidase (Bio-Rad)	Goat secondary	1:2000	1:2000	
	Goat anti-mouse conjugated to alkaline phosphatase or horseradish peroxidase	Goat secondary	1:2000 1:5000 (for detecting 6His-specific antibodies)	1:2000	
	FITC 1.5mg/mL (Jackson Immuno-	Donkey secondary			1:25

	reseach)				
	Alexa488 2mg/mL (Molecular Life Sciences)	Donkey secondary			1:25
	Cy5 1.5mg/mL (Molecular Life Sciences)	Donkey secondary			1:25

REFERENCES

Ackley, B.D., Kang, S.H., Crew, J.R., Suh, C., Jin, Y. and Kramer, J.M. (2003) The basement membrane components nidogen and type XVIII collagen regulate organization of neuromuscular junctions in Caenorhabditis elegans. *J Neurosci*, **23**, 3577-3587.

Aebersold, R. and Mann, M. (2003) Mass spectrometry-based proteomics. *Nature*, **422**, 198-207.

Alexopoulos, L.G., Setton, L.A. and Guilak, F. (2005) The biomechanical role of the chondrocyte pericellular matrix in articular cartilage. *Acta Biomater*, **1**, 317-325.

Alexopoulos, L.G., Youn, I., Bonaldo, P. and Guilak, F. (2009) Developmental and osteoarthritic changes in Col6a1-knockout mice: biomechanics of type VI collagen in the cartilage pericellular matrix. *Arthritis Rheum*, **60**, 771-779.

Alexopoulou, A.N., Multhaupt, H.A. and Couchman, J.R. (2007) Syndecans in wound healing, inflammation and vascular biology. *Int J Biochem Cell Biol*, **39**, 505-528.

Ali, M., McKibbin, M., Booth, A., Parry, D.A., Jain, P., Riazuddin, S.A., Hejtmancik, J.F., Khan, S.N., Firasat, S., Shires, M., Gilmour, D.F., Towns, K., Murphy, A.L., Azmanov, D., Tournev, I., Cherninkova, S., Jafri, H., Raashid, Y., Toomes, C., Craig, J., Mackey, D.A., Kalaydjieva, L., Riazuddin, S. and Inglehearn, C.F. (2009) Null mutations in LTBP2 cause primary congenital glaucoma. *Am J Hum Genet*, **84**, 664-671.

Anderson, D.R. (1981) The development of the trabecular meshwork and its abnormality in primary infantile glaucoma. *Trans Am Ophthalmol Soc*, **79**, 458-485.

Annes, J.P., Munger, J.S. and Rifkin, D.B. (2003) Making sense of latent TGFbeta activation. *J Cell Sci*, **116**, 217-224.

Appleton, C.T., Pitelka, V., Henry, J. and Beier, F. (2007) Global analyses of gene expression in early experimental osteoarthritis. *Arthritis Rheum*, **56**, 1854-1868.

Arikawa-Hirasawa, E., Rossi, S.G., Rotundo, R.L. and Yamada, Y. (2002) Absence of acetylcholinesterase at the neuromuscular junctions of perlecan-null mice. *Nat Neurosci*, **5**, 119-123.

Arikawa-Hirasawa, E., Watanabe, H., Takami, H., Hassell, J.R. and Yamada, Y. (1999) Perlecan is essential for cartilage and cephalic development. *Nat Genet*, **23**, 354-358.

Arteaga-Solis, E., Gayraud, B., Lee, S.Y., Shum, L., Sakai, L. and Ramirez, F. (2001) Regulation of limb patterning by extracellular microfibrils. *J Cell Biol*, **154**, 275-281.

Ashworth, J.L., Kielty, C.M. and McLeod, D. (2000) Fibrillin and the eye. *Br J Ophthalmol*, **84**, 1312-1317.

Aviezer, D., Hecht, D., Safran, M., Eisinger, M., David, G. and Yayon, A. (1994) Perlecan, basal lamina proteoglycan, promotes basic fibroblast growth factor-receptor binding, mitogenesis, and angiogenesis. *Cell*, **79**, 1005-1013.

Ayad, S., Evans, H., Weiss, J.B. and Holt, L. (1984) Type VI collagen but not type V collagen is present in cartilage. *Coll Relat Res*, **4**, 165-168.

Baldock, C., Koster, A.J., Ziese, U., Rock, M.J., Sherratt, M.J., Kadler, K.E., Shuttleworth, C.A. and Kielty, C.M. (2001) The supramolecular organization of fibrillin-rich microfibrils. *J Cell Biol*, **152**, 1045-1056.

Baldock, C., Siegler, V., Bax, D.V., Cain, S.A., Mellody, K.T., Marson, A., Haston, J.L., Berry, R., Wang, M.C., Grossmann, J.G., Roessle, M., Kielty, C.M. and Wess, T.J. (2006) Nanostructure of fibrillin-1 reveals compact conformation of EGF arrays and mechanism for extensibility. *Proc Natl Acad Sci U S A*, **103**, 11922-11927.

Batmunkh, E., Tatrai, P., Szabo, E., Lodi, C., Holczbauer, A., Paska, C., Kupcsulik, P., Kiss, A., Schaff, Z. and Kovalszky, I. (2007) Comparison of the expression of agrin, a basement membrane heparan sulfate proteoglycan, in cholangiocarcinoma and hepatocellular carcinoma. *Hum Pathol*, **38**, 1508-1515.

Battaglia, C., Mayer, U., Aumailley, M. and Timpl, R. (1992) Basement-membrane heparan sulfate proteoglycan binds to laminin by its heparan sulfate chains and to nidogen by sites in the protein core. *Eur J Biochem*, **208**, 359-366.

Bax, D.V., Bernard, S.E., Lomas, A., Morgan, A., Humphries, J., Shuttleworth, C.A., Humphries, M.J. and Kielty, C.M. (2003) Cell adhesion to fibrillin-1 molecules and microfibrils is mediated by alpha 5 beta 1 and alpha v beta 3 integrins. *J Biol Chem*, **278**, 34605-34616.

Bax, D.V., Mahalingam, Y., Cain, S., Mellody, K., Freeman, L., Younger, K., Shuttleworth, C.A., Humphries, M.J., Couchman, J.R. and Kielty, C.M. (2007) Cell adhesion to fibrillin-1: identification of an Arg-Gly-Asp-dependent synergy region and a heparin-binding site that regulates focal adhesion formation. *J Cell Sci*, **120**, 1383-1392.

Beauvais, D.M. and Rapraeger, A.C. (2004) Syndecans in tumor cell adhesion and signaling. *Reprod Biol Endocrinol*, **2**, 3.

Bellin, R., Capila, I., Lincecum, J., Park, P.W., Reizes, O. and Bernfield, M.R. (2002) Unlocking the secrets of syndecans: transgenic organisms as a potential key. *Glycoconj J*, **19**, 295-304.

Bernfield, M., Gotte, M., Park, P.W., Reizes, O., Fitzgerald, M.L., Lincecum, J. and Zako, M. (1999) Functions of cell surface heparan sulfate proteoglycans. *Annu Rev Biochem*, **68**, 729-777.

Bidanset, D.J., Guidry, C., Rosenberg, L.C., Choi, H.U., Timpl, R. and Hook, M. (1992) Binding of the proteoglycan decorin to collagen type VI. *J Biol Chem*, **267**, 5250-5256.

Billings, P.C., Herrick, D.J., Howard, P.S., Kucich, U., Engelsberg, B.N. and Rosenbloom, J. (2000) Expression of betaig-h3 by human bronchial smooth muscle cells: localization To the extracellular matrix and nucleus. *Am J Respir Cell Mol Biol*, **22**, 352-359.

Billings, P.C., Whitbeck, J.C., Adams, C.S., Abrams, W.R., Cohen, A.J., Engelsberg, B.N., Howard, P.S. and Rosenbloom, J. (2002) The transforming growth factor-beta-inducible matrix protein (beta)ig-h3 interacts with fibronectin. *J Biol Chem*, **277**, 28003-28009.

Bix, G., Fu, J., Gonzalez, E.M., Macro, L., Barker, A., Campbell, S., Zutter, M.M., Santoro, S.A., Kim, J.K., Hook, M., Reed, C.C. and Iozzo, R.V. (2004) Endorepellin causes endothelial cell disassembly of actin cytoskeleton and focal adhesions through alpha2beta1 integrin. *J Cell Biol*, **166**, 97-109.

Bix, G. and Iozzo, R.V. (2008) Novel interactions of perlecan: unraveling perlecan's role in angiogenesis. *Microsc Res Tech*, **71**, 339-348.

Blyth, M., Foulds, N., Turner, C. and Bunyan, D. (2008) Severe Marfan syndrome due to FBN1 exon deletions. *Am J Med Genet A*, **146A**, 1320-1324.

Boldt, A., Wetzel, U., Lauschke, J., Weigl, J., Gummert, J., Hindricks, G., Kottkamp, H. and Dhein, S. (2004) Fibrosis in left atrial tissue of patients with atrial fibrillation with and without underlying mitral valve disease. *Heart*, **90**, 400-405.

Bonaldo, P., Braghetta, P., Zanetti, M., Piccolo, S., Volpin, D. and Bressan, G.M. (1998) Collagen VI deficiency induces early onset myopathy in the mouse: an animal model for Bethlem myopathy. *Hum Mol Genet*, **7**, 2135-2140.

Boulon, S., Ahmad, Y., Trinkle-Mulcahy, L., Verheggen, C., Cobley, A., Gregor, P., Bertrand, E., Whitehorn, M. and Lamond, A.I. Establishment of a protein frequency library and its application in the reliable identification of specific protein interaction partners. *Mol Cell Proteomics*, **9**, 861-879.

Bradford, M.M. (1976) A rapid and sensitive method for the quantitation of microgram quantities of protein utilizing the principle of protein-dye binding. *Anal Biochem*, **72**, 248-254.

Breborowicz, A., Korybalska, K., Grzybowski, A., Wieczorowska-Tobis, K., Martis, L. and Oreopoulos, D.G. (1996) Synthesis of hyaluronic acid by human peritoneal mesothelial cells: effect of cytokines and dialysate. *Perit Dial Int*, **16**, 374-378.

Breborowicz, A., Wisniewska, J., Polubinska, A., Wieczorowska-Tobis, K., Martis, L. and Oreopoulos, D.G. (1998) Role of peritoneal mesothelial cells and fibroblasts in the synthesis of hyaluronan during peritoneal dialysis. *Perit Dial Int*, **18**, 382-386.

Bressan, G.M., Daga-Gordini, D., Colombatti, A., Castellani, I., Marigo, V. and Volpin, D. (1993) Emilin, a component of elastic fibers preferentially located at the elastin-microfibrils interface. *J Cell Biol*, **121**, 201-212.

Brockington, M., Brown, S.C., Lampe, A., Yuva, Y., Feng, L., Jimenez-Mallebrera, C., Sewry, C.A., Flanigan, K.M., Bushby, K. and Muntoni, F. (2004) Prenatal diagnosis of Ullrich congenital muscular dystrophy using haplotype analysis and collagen VI immunocytochemistry. *Prenat Diagn*, **24**, 440-444.

Broekelmann, T.J., Kozel, B.A., Ishibashi, H., Werneck, C.C., Keeley, F.W., Zhang, L. and Mecham, R.P. (2005) Tropoelastin interacts with cell-surface glycosaminoglycans via its COOH-terminal domain. *J Biol Chem*, **280**, 40939-40947.

Brown-Augsburger, P., Broekelmann, T., Mecham, L., Mercer, R., Gibson, M.A., Cleary, E.G., Abrams, W.R., Rosenbloom, J. and Mecham, R.P. (1994) Microfibril-associated glycoprotein binds to the carboxyl-terminal domain of tropoelastin and is a substrate for transglutaminase. *J Biol Chem*, **269**, 28443-28449.

Bruns, R.R., Press, W., Engvall, E., Timpl, R. and Gross, J. (1986) Type VI collagen in extracellular, 100-nm periodic filaments and fibrils: identification by immunoelectron microscopy. *J Cell Biol*, **103**, 393-404.

Bujan, J., Gimeno, M.J., Jimenez, J.A., Kielty, C.M., Mecham, R.P. and Bellon, J.M. (2003) Expression of elastic components in healthy and varicose veins. *World J Surg*, **27**, 901-905.

Burg, M.A., Tillet, E., Timpl, R. and Stallcup, W.B. (1996) Binding of the NG2 proteoglycan to type VI collagen and other extracellular matrix molecules. *J Biol Chem*, **271**, 26110-26116.

Cain, S.A., Baldock, C., Gallagher, J., Morgan, A., Bax, D.V., Weiss, A.S., Shuttleworth, C.A. and Kielty, C.M. (2005) Fibrillin-1 interactions with heparin. Implications for microfibril and elastic fiber assembly. *J Biol Chem*, **280**, 30526-30537.

Cain, S.A., Baldwin, A.K., Mahalingam, Y., Raynal, B., Jowitt, T.A., Shuttleworth, C.A., Couchman, J.R. and Kielty, C.M. (2008) Heparan sulfate regulates fibrillin-1 N- and C-terminal interactions. *J Biol Chem*, **283**, 27017-27027.

Cain, S.A., McGovern, A., Small, E., Ward, L.J., Baldock, C., Shuttleworth, A. and Kielty, C.M. (2009) Defining elastic fiber interactions by molecular fishing: an affinity purification and mass spectrometry approach. *Mol Cell Proteomics*, **8**, 2715-2732.

Camacho, C.J. and Vajda, S. (2001) Protein docking along smooth association pathways. *Proc Natl Acad Sci U S A*, **98**, 10636-10641.

Camacho Vanegas, O., Bertini, E., Zhang, R.Z., Petrini, S., Minosse, C., Sabatelli, P., Giusti, B., Chu, M.L. and Pepe, G. (2001) Ullrich scleroatonic muscular dystrophy is caused by recessive mutations in collagen type VI. *Proc Natl Acad Sci U S A*, **98**, 7516-7521.

Cardy, C.M. and Handford, P.A. (1998) Metal ion dependency of microfibrils supports a rod-like conformation for fibrillin-1 calcium-binding epidermal growth factor-like domains. *J Mol Biol*, **276**, 855-860.

Carson, D.D., DeSouza, M.M. and Regisford, E.G. (1998) Mucin and proteoglycan functions in embryo implantation. *Bioessays*, **20**, 577-583.

Carson, D.D., Tang, J.P. and Julian, J. (1993) Heparan sulfate proteoglycan (perlecan) expression by mouse embryos during acquisition of attachment competence. *Dev Biol*, **155**, 97-106.

Carta, L., Pereira, L., Arteaga-Solis, E., Lee-Arteaga, S.Y., Lenart, B., Starcher, B., Merkel, C.A., Sukoyan, M., Kerkis, A., Hazeki, N., Keene, D.R., Sakai, L.Y. and Ramirez, F. (2006) Fibrillins 1 and 2 perform partially overlapping functions during aortic development. *J Biol Chem*, **281**, 8016-8023.

Castelletti, F., Donadelli, R., Banterla, F., Hildebrandt, F., Zipfel, P.F., Bresin, E., Otto, E., Skerka, C., Renieri, A., Todeschini, M., Caprioli, J., Caruso, R.M., Artuso, R.,

Remuzzi, G. and Noris, M. (2008) Mutations in FN1 cause glomerulopathy with fibronectin deposits. *Proc Natl Acad Sci U S A*, **105**, 2538-2543.
Cha, J., Kwak, T., Butmarc, J., Kim, T.A., Yufit, T., Carson, P., Kim, S.J. and Falanga, V. (2008) Fibroblasts from non-healing human chronic wounds show decreased expression of beta ig-h3, a TGF-beta inducible protein. *J Dermatol Sci*, **50**, 15-23.
Chakravarti, R., Sapountzi, V. and Adams, J.C. (2005) Functional role of syndecan-1 cytoplasmic V region in lamellipodial spreading, actin bundling, and cell migration. *Mol Biol Cell*, **16**, 3678-3691.
Chang, J., Nakajima, H. and Poole, C.A. (1997) Structural colocalisation of type VI collagen and fibronectin in agarose cultured chondrocytes and isolated chondrons extracted from adult canine tibial cartilage. *J Anat*, **190 (Pt 4)**, 523-532.
Charbonneau, N.L., Dzamba, B.J., Ono, R.N., Keene, D.R., Corson, G.M., Reinhardt, D.P. and Sakai, L.Y. (2003) Fibrillins can co-assemble in fibrils, but fibrillin fibril composition displays cell-specific differences. *J Biol Chem*, **278**, 2740-2749.
Charbonneau, N.L., Ono, R.N., Corson, G.M., Keene, D.R. and Sakai, L.Y. (2004) Fine tuning of growth factor signals depends on fibrillin microfibril networks. *Birth Defects Res C Embryo Today*, **72**, 37-50.
Chaudhry, S.S., Gazzard, J., Baldock, C., Dixon, J., Rock, M.J., Skinner, G.C., Steel, K.P., Kielty, C.M. and Dixon, M.J. (2001) Mutation of the gene encoding fibrillin-2 results in syndactyly in mice. *Hum Mol Genet*, **10**, 835-843.
Chen, E., Hermanson, S. and Ekker, S.C. (2004) Syndecan-2 is essential for angiogenic sprouting during zebrafish development. *Blood*, **103**, 1710-1719.
Chen, Q., Sivakumar, P., Barley, C., Peters, D.M., Gomes, R.R., Farach-Carson, M.C. and Dallas, S.L. (2007) Potential role for heparan sulfate proteoglycans in regulation of transforming growth factor-beta (TGF-beta) by modulating assembly of latent TGF-beta-binding protein-1. *J Biol Chem*, **282**, 26418-26430.
Chernousov, M.A. and Carey, D.J. (1993) N-syndecan (syndecan 3) from neonatal rat brain binds basic fibroblast growth factor. *J Biol Chem*, **268**, 16810-16814.
Cheung, C.L., Sham, P.C., Chan, V., Paterson, A.D., Luk, K.D. and Kung, A.W. (2008) Identification of LTBP2 on chromosome 14q as a novel candidate gene for bone mineral density variation and fracture risk association. *J Clin Endocrinol Metab*, **93**, 4448-4455.
Choudhury, R., McGovern, A., Ridley, C., Cain, S.A., Baldwin, A., Wang, M.C., Guo, C., Mironov, A., Jr., Drymoussi, Z., Trump, D., Shuttleworth, A., Baldock, C. and Kielty, C.M. (2009) Differential regulation of elastic fiber formation by fibulin-4 and -5. *J Biol Chem*, **284**, 24553-24567.
Chung, K.Y., Taylor, J.S., Shum, D.K. and Chan, S.O. (2000) Axon routing at the optic chiasm after enzymatic removal of chondroitin sulfate in mouse embryos. *Development*, **127**, 2673-2683.
Cizmeci-Smith, G., Langan, E., Youkey, J., Showalter, L.J. and Carey, D.J. (1997) Syndecan-4 is a primary-response gene induced by basic fibroblast growth factor and arterial injury in vascular smooth muscle cells. *Arterioscler Thromb Vasc Biol*, **17**, 172-180.
Clarke, A.W., Arnspang, E.C., Mithieux, S.M., Korkmaz, E., Braet, F. and Weiss, A.S. (2006) Tropoelastin massively associates during coacervation to form quantized protein spheres. *Biochemistry*, **45**, 9989-9996.
Cleary, E.G. and Gibson, M.A. (1983) Elastin-associated microfibrils and microfibrillar proteins. *Int Rev Connect Tissue Res*, **10**, 97-209.
Cleary, E.G., Sandberg, L.B. and Jackson, D.S. (1967) The changes in chemical composition during development of the bovine nuchal ligament. *J Cell Biol*, **33**, 469-479.
Cleary, E.G.a.G., M. A. (1996) *Elastic tissue, elastin and elastin-associated microfibrils*. Amsterdam: Harwood Academic Publishers.

Cohen, I.R., Grassel, S., Murdoch, A.D. and Iozzo, R.V. (1993) Structural characterization of the complete human perlecan gene and its promoter. *Proc Natl Acad Sci U S A*, **90**, 10404-10408.

Colombatti, A., Bonaldo, P., Ainger, K., Bressan, G.M. and Volpin, D. (1987) Biosynthesis of chick type VI collagen. I. Intracellular assembly and molecular structure. *J Biol Chem*, **262**, 14454-14460.

Colombatti, A., Doliana, R., Bot, S., Canton, A., Mongiat, M., Mungiguerra, G., Paron-Cilli, S. and Spessotto, P. (2000) The EMILIN protein family. *Matrix Biol*, **19**, 289-301.

Corson, G.M., Chalberg, S.C., Dietz, H.C., Charbonneau, N.L. and Sakai, L.Y. (1993) Fibrillin binds calcium and is coded by cDNAs that reveal a multidomain structure and alternatively spliced exons at the 5' end. *Genomics*, **17**, 476-484.

Corson, G.M., Charbonneau, N.L., Keene, D.R. and Sakai, L.Y. (2004) Differential expression of fibrillin-3 adds to microfibril variety in human and avian, but not rodent, connective tissues. *Genomics*, **83**, 461-472.

Costell, M., Gustafsson, E., Aszodi, A., Morgelin, M., Bloch, W., Hunziker, E., Addicks, K., Timpl, R. and Fassler, R. (1999) Perlecan maintains the integrity of cartilage and some basement membranes. *J Cell Biol*, **147**, 1109-1122.

Couchman, J.R. (2003) Syndecans: proteoglycan regulators of cell-surface microdomains? *Nat Rev Mol Cell Biol*, **4**, 926-937.

Curran, M.E., Atkinson, D.L., Ewart, A.K., Morris, C.A., Leppert, M.F. and Keating, M.T. (1993) The elastin gene is disrupted by a translocation associated with supravalvular aortic stenosis. *Cell*, **73**, 159-168.

Dabovic, B., Chen, Y., Colarossi, C., Obata, H., Zambuto, L., Perle, M.A. and Rifkin, D.B. (2002a) Bone abnormalities in latent TGF-[beta] binding protein (Ltbp)-3-null mice indicate a role for Ltbp-3 in modulating TGF-[beta] bioavailability. *J Cell Biol*, **156**, 227-232.

Dabovic, B., Chen, Y., Colarossi, C., Zambuto, L., Obata, H. and Rifkin, D.B. (2002b) Bone defects in latent TGF-beta binding protein (Ltbp)-3 null mice; a role for Ltbp in TGF-beta presentation. *J Endocrinol*, **175**, 129-141.

Dahn, R.D. and Fallon, J.F. (2000) Interdigital regulation of digit identity and homeotic transformation by modulated BMP signaling. *Science*, **289**, 438-441.

Dallas, S.L., Keene, D.R., Bruder, S.P., Saharinen, J., Sakai, L.Y., Mundy, G.R. and Bonewald, L.F. (2000) Role of the latent transforming growth factor beta binding protein 1 in fibrillin-containing microfibrils in bone cells in vitro and in vivo. *J Bone Miner Res*, **15**, 68-81.

Dallas, S.L., Miyazono, K., Skerry, T.M., Mundy, G.R. and Bonewald, L.F. (1995) Dual role for the latent transforming growth factor-beta binding protein in storage of latent TGF-beta in the extracellular matrix and as a structural matrix protein. *J Cell Biol*, **131**, 539-549.

Dallas, S.L., Sivakumar, P., Jones, C.J., Chen, Q., Peters, D.M., Mosher, D.F., Humphries, M.J. and Kielty, C.M. (2005) Fibronectin regulates latent transforming growth factor-beta (TGF beta) by controlling matrix assembly of latent TGF beta-binding protein-1. *J Biol Chem*, **280**, 18871-18880.

Danielson, K.G., Baribault, H., Holmes, D.F., Graham, H., Kadler, K.E. and Iozzo, R.V. (1997) Targeted disruption of decorin leads to abnormal collagen fibril morphology and skin fragility. *J Cell Biol*, **136**, 729-743.

David, G. (1993) Integral membrane heparan sulfate proteoglycans. *Faseb J*, **7**, 1023-1030.

David, G., van der Schueren, B., Marynen, P., Cassiman, J.J. and van den Berghe, H. (1992) Molecular cloning of amphiglycan, a novel integral membrane heparan sulfate proteoglycan expressed by epithelial and fibroblastic cells. *J Cell Biol*, **118**, 961-969.

Demir, E., Sabatelli, P., Allamand, V., Ferreiro, A., Moghadaszadeh, B., Makrelouf, M., Topaloglu, H., Echenne, B., Merlini, L. and Guicheney, P. (2002) Mutations in COL6A3 cause severe and mild phenotypes of Ullrich congenital muscular dystrophy. *Am J Hum Genet*, **70**, 1446-1458.

Denzer, A.J., Gesemann, M., Schumacher, B. and Ruegg, M.A. (1995) An amino-terminal extension is required for the secretion of chick agrin and its binding to extracellular matrix. *J Cell Biol*, **131**, 1547-1560.
Dietz, H.C. and Mecham, R.P. (2000) Mouse models of genetic diseases resulting from mutations in elastic fiber proteins. *Matrix Biol*, **19**, 481-488.
Dietz, H.C. and Pyeritz, R.E. (1995) Mutations in the human gene for fibrillin-1 (FBN1) in the Marfan syndrome and related disorders. *Hum Mol Genet*, **4 Spec No**, 1799-1809.
Dobolyi, A. and Palkovits, M. (2008) Expression of latent transforming growth factor beta binding proteins in the rat brain. *J Comp Neurol*, **507**, 1393-1408.
Dodge, G.R., Kovalszky, I., Chu, M.L., Hassell, J.R., McBride, O.W., Yi, H.F. and Iozzo, R.V. (1991) Heparan sulfate proteoglycan of human colon: partial molecular cloning, cellular expression, and mapping of the gene (HSPG2) to the short arm of human chromosome 1. *Genomics*, **10**, 673-680.
Dong, S., Cole, G.J. and Halfter, W. (2003) Expression of collagen XVIII and localization of its glycosaminoglycan attachment sites. *J Biol Chem*, **278**, 1700-1707.
Downing, A.K., Knott, V., Werner, J.M., Cardy, C.M., Campbell, I.D. and Handford, P.A. (1996) Solution structure of a pair of calcium-binding epidermal growth factor-like domains: implications for the Marfan syndrome and other genetic disorders. *Cell*, **85**, 597-605.
Dridi, S.M., Foucault Bertaud, A., Igondjo Tchen, S., Senni, K., Ejeil, A.L., Pellat, B., Lyonnet, S., Bonnet, D., Charpiot, P. and Godeau, G. (2005) Vascular wall remodeling in patients with supravalvular aortic stenosis and Williams Beuren syndrome. *J Vasc Res*, **42**, 190-201.
Dziadek, M., Fujiwara, S., Paulsson, M. and Timpl, R. (1985) Immunological characterization of basement membrane types of heparan sulfate proteoglycan. *Embo J*, **4**, 905-912.
Eisenberg, R., Young, D., Jacobson, B. and Boito, A. (1964) Familial Supravalvular Aortic Stenosis. *Am J Dis Child*, **108**, 341-347.
Eldadah, Z.A., Brenn, T., Furthmayr, H. and Dietz, H.C. (1995) Expression of a mutant human fibrillin allele upon a normal human or murine genetic background recapitulates a Marfan cellular phenotype. *J Clin Invest*, **95**, 874-880.
El-Hallous, E., Sasaki, T., Hubmacher, D., Getie, M., Tiedemann, K., Brinckmann, J., Batge, B., Davis, E.C. and Reinhardt, D.P. (2007) Fibrillin-1 interactions with fibulins depend on the first hybrid domain and provide an adaptor function to tropoelastin. *J Biol Chem*, **282**, 8935-8946.
Engel, J., Furthmayr, H., Odermatt, E., von der Mark, H., Aumailley, M., Fleischmajer, R. and Timpl, R. (1985) Structure and macromolecular organization of type VI collagen. *Ann N Y Acad Sci*, **460**, 25-37.
Engvall, E., Hessle, H. and Klier, G. (1986) Molecular assembly, secretion, and matrix deposition of type VI collagen. *J Cell Biol*, **102**, 703-710.
Escribano, J., Hernando, N., Ghosh, S., Crabb, J. and Coca-Prados, M. (1994) cDNA from human ocular ciliary epithelium homologous to beta ig-h3 is preferentially expressed as an extracellular protein in the corneal epithelium. *J Cell Physiol*, **160**, 511-521.
Esteve-Romero, J.S., Bossi, A. and Righetti, P.G. (1996) Purification of thermamylase in multicompartment electrolyzers with isoelectric membranes: the problem of protein solubility. *Electrophoresis*, **17**, 1242-1247.
Eswarakumar, V.P., Lax, I. and Schlessinger, J. (2005) Cellular signaling by fibroblast growth factor receptors. *Cytokine Growth Factor Rev*, **16**, 139-149.
Ethell, I.M., Irie, F., Kalo, M.S., Couchman, J.R., Pasquale, E.B. and Yamaguchi, Y. (2001) EphB/syndecan-2 signaling in dendritic spine morphogenesis. *Neuron*, **31**, 1001-1013.
Ewart, A.K., Jin, W., Atkinson, D., Morris, C.A. and Keating, M.T. (1994) Supravalvular aortic stenosis associated with a deletion disrupting the elastin gene. *J Clin Invest*, **93**, 1071-1077.

Ewart, A.K., Morris, C.A., Atkinson, D., Jin, W., Sternes, K., Spallone, P., Stock, A.D., Leppert, M. and Keating, M.T. (1993) Hemizygosity at the elastin locus in a developmental disorder, Williams syndrome. *Nat Genet*, **5**, 11-16.

Eyre, D.R., Wu, J.J. and Apone, S. (1987) A growing family of collagens in articular cartilage: identification of 5 genetically distinct types. *J Rheumatol*, **14 Spec No**, 25-27.

Farach, M.C., Tang, J.P., Decker, G.L. and Carson, D.D. (1987) Heparin/heparan sulfate is involved in attachment and spreading of mouse embryos in vitro. *Dev Biol*, **123**, 401-410.

Farach-Carson, M.C. and Carson, D.D. (2007) Perlecan--a multifunctional extracellular proteoglycan scaffold. *Glycobiology*, **17**, 897-905.

Fears, C.Y., Gladson, C.L. and Woods, A. (2006) Syndecan-2 is expressed in the microvasculature of gliomas and regulates angiogenic processes in microvascular endothelial cells. *J Biol Chem*, **281**, 14533-14536.

Ferguson, J.W., Mikesh, M.F., Wheeler, E.F. and LeBaron, R.G. (2003) Developmental expression patterns of Beta-ig (betaIG-H3) and its function as a cell adhesion protein. *Mech Dev*, **120**, 851-864.

Finnis, M.L. and Gibson, M.A. (1997) Microfibril-associated glycoprotein-1 (MAGP-1) binds to the pepsin-resistant domain of the alpha3(VI) chain of type VI collagen. *J Biol Chem*, **272**, 22817-22823.

Fitzgerald, M.L., Wang, Z., Park, P.W., Murphy, G. and Bernfield, M. (2000) Shedding of syndecan-1 and -4 ectodomains is regulated by multiple signaling pathways and mediated by a TIMP-3-sensitive metalloproteinase. *J Cell Biol*, **148**, 811-824.

Forsberg, E., Pejler, G., Ringvall, M., Lunderius, C., Tomasini-Johansson, B., Kusche-Gullberg, M., Eriksson, I., Ledin, J., Hellman, L. and Kjellen, L. (1999) Abnormal mast cells in mice deficient in a heparin-synthesizing enzyme. *Nature*, **400**, 773-776.

Freeman, L.J., Lomas, A., Hodson, N., Sherratt, M.J., Mellody, K.T., Weiss, A.S., Shuttleworth, A. and Kielty, C.M. (2005) Fibulin-5 interacts with fibrillin-1 molecules and microfibrils. *Biochem J*, **388**, 1-5.

Friedrich, M.V., Gohring, W., Morgelin, M., Brancaccio, A., David, G. and Timpl, R. (1999) Structural basis of glycosaminoglycan modification and of heterotypic interactions of perlecan domain V. *J Mol Biol*, **294**, 259-270.

Fujiki, K., Hotta, Y., Nakayasu, K., Yokoyama, T., Takano, T., Yamaguchi, T. and Kanai, A. (1998) A new L527R mutation of the betaIGH3 gene in patients with lattice corneal dystrophy with deep stromal opacities. *Hum Genet*, **103**, 286-289.

Furthmayr, H., Wiedemann, H., Timpl, R., Odermatt, E. and Engel, J. (1983) Electron-microscopical approach to a structural model of intima collagen. *Biochem J*, **211**, 303-311.

Gallagher, J.T. (1989) The extended family of proteoglycans: social residents of the pericellular zone. *Curr Opin Cell Biol*, **1**, 1201-1218.

Gallo, R., Kim, C., Kokenyesi, R., Adzick, N.S. and Bernfield, M. (1996) Syndecans-1 and -4 are induced during wound repair of neonatal but not fetal skin. *J Invest Dermatol*, **107**, 676-683.

Galvani, M., Rovatti, L., Hamdan, M., Herbert, B. and Righetti, P.G. (2001) Protein alkylation in the presence/absence of thiourea in proteome analysis: a matrix assisted laser desorption/ionization-time of flight-mass spectrometry investigation. *Electrophoresis*, **22**, 2066-2074.

George, E.L., Georges-Labouesse, E.N., Patel-King, R.S., Rayburn, H. and Hynes, R.O. (1993) Defects in mesoderm, neural tube and vascular development in mouse embryos lacking fibronectin. *Development*, **119**, 1079-1091.

Giancotti, F.G. and Ruoslahti, E. (1999) Integrin signaling. *Science*, **285**, 1028-1032.

Gibson, M.A. and Cleary, E.G. (1987) The immunohistochemical localisation of microfibril-associated glycoprotein (MAGP) in elastic and non-elastic tissues. *Immunol Cell Biol*, **65 (Pt 4)**, 345-356.

Gibson, M.A., Finnis, M.L., Kumaratilake, J.S. and Cleary, E.G. (1998) Microfibril-associated glycoprotein-2 (MAGP-2) is specifically associated with fibrillin-containing microfibrils but exhibits more restricted patterns of tissue localization and developmental expression than its structural relative MAGP-1. *J Histochem Cytochem*, **46**, 871-886.

Gibson, M.A., Hatzinikolas, G., Davis, E.C., Baker, E., Sutherland, G.R. and Mecham, R.P. (1995) Bovine latent transforming growth factor beta 1-binding protein 2: molecular cloning, identification of tissue isoforms, and immunolocalization to elastin-associated microfibrils. *Mol Cell Biol*, **15**, 6932-6942.

Gibson, M.A., Hatzinikolas, G., Kumaratilake, J.S., Sandberg, L.B., Nicholl, J.K., Sutherland, G.R. and Cleary, E.G. (1996) Further characterization of proteins associated with elastic fiber microfibrils including the molecular cloning of MAGP-2 (MP25). *J Biol Chem*, **271**, 1096-1103.

Gibson, M.A., Kumaratilake, J.S. and Cleary, E.G. (1989) The protein components of the 12-nanometer microfibrils of elastic and nonelastic tissues. *J Biol Chem*, **264**, 4590-4598.

Gibson, M.A., Kumaratilake, J.S. and Cleary, E.G. (1997) Immunohistochemical and ultrastructural localization of MP78/70 (betaig-h3) in extracellular matrix of developing and mature bovine tissues. *J Histochem Cytochem*, **45**, 1683-1696.

Gibson, M.A., Sandberg, L.B., Grosso, L.E. and Cleary, E.G. (1991) Complementary DNA cloning establishes microfibril-associated glycoprotein (MAGP) to be a discrete component of the elastin-associated microfibrils. *J Biol Chem*, **266**, 7596-7601.

Giltay, R., Kostka, G. and Timpl, R. (1997) Sequence and expression of a novel member (LTBP-4) of the family of latent transforming growth factor-beta binding proteins. *FEBS Lett*, **411**, 164-168.

Giltay, R., Timpl, R. and Kostka, G. (1999) Sequence, recombinant expression and tissue localization of two novel extracellular matrix proteins, fibulin-3 and fibulin-4. *Matrix Biol*, **18**, 469-480.

Gleizes, P.E., Beavis, R.C., Mazzieri, R., Shen, B. and Rifkin, D.B. (1996) Identification and characterization of an eight-cysteine repeat of the latent transforming growth factor-beta binding protein-1 that mediates bonding to the latent transforming growth factor-beta1. *J Biol Chem*, **271**, 29891-29896.

Goessler, U.R., Bugert, P., Bieback, K., Deml, M., Sadick, H., Hormann, K. and Riedel, F. (2005) In-vitro analysis of the expression of TGFbeta -superfamily-members during chondrogenic differentiation of mesenchymal stem cells and chondrocytes during dedifferentiation in cell culture. *Cell Mol Biol Lett*, **10**, 345-362.

Gohring, W., Sasaki, T., Heldin, C.H. and Timpl, R. (1998) Mapping of the binding of platelet-derived growth factor to distinct domains of the basement membrane proteins BM-40 and perlecan and distinction from the BM-40 collagen-binding epitope. *Eur J Biochem*, **255**, 60-66.

Gorg, A., Postel, W. and Gunther, S. (1988) The current state of two-dimensional electrophoresis with immobilized pH gradients. *Electrophoresis*, **9**, 531-546.

Goutebroze, L., Carnaud, M., Denisenko, N., Boutterin, M.C. and Girault, J.A. (2003) Syndecan-3 and syndecan-4 are enriched in Schwann cell perinodal processes. *BMC Neurosci*, **4**, 29.

Govindraj, P., West, L., Smith, S. and Hassell, J.R. (2006) Modulation of FGF-2 binding to chondrocytes from the developing growth plate by perlecan. *Matrix Biol*, **25**, 232-239.

Greene, D.K., Tumova, S., Couchman, J.R. and Woods, A. (2003) Syndecan-4 associates with alpha-actinin. *J Biol Chem*, **278**, 7617-7623.

Gregory, K.E., Ono, R.N., Charbonneau, N.L., Kuo, C.L., Keene, D.R., Bachinger, H.P. and Sakai, L.Y. (2005) The prodomain of BMP-7 targets the BMP-7 complex to the extracellular matrix. *J Biol Chem*, **280**, 27970-27980.

Gromova, I., and Celis J. E. (2006) Protein Detection in Gels by silver Staining: A Procedure Compatible with Mass-Spectrometry. In Celis, J.E., Carter N., Hunter T., Simons K.,

Small J. V and Shotton D (ed.), *Cell Biology: A Laboratory Handbook.* Elsevier. Academic Press.

Guilak, F., Alexopoulos, L.G., Upton, M.L., Youn, I., Choi, J.B., Cao, L., Setton, L.A. and Haider, M.A. (2006) The pericellular matrix as a transducer of biomechanical and biochemical signals in articular cartilage. *Ann N Y Acad Sci*, **1068**, 498-512.

Gumbiner, B.M. (1996) Cell adhesion: the molecular basis of tissue architecture and morphogenesis. *Cell*, **84**, 345-357.

Gutman, A. and Kornblihtt, A.R. (1987) Identification of a third region of cell-specific alternative splicing in human fibronectin mRNA. *Proc Natl Acad Sci U S A*, **84**, 7179-7182.

Ha, N.T., Fujiki, K., Hotta, Y., Nakayasu, K. and Kanai, A. (2000) Q118X mutation of M1S1 gene caused gelatinous drop-like corneal dystrophy: the P501T of BIGH3 gene found in a family with gelatinous drop-like corneal dystrophy. *Am J Ophthalmol*, **130**, 119-120.

Habashi, J.P., Judge, D.P., Holm, T.M., Cohn, R.D., Loeys, B.L., Cooper, T.K., Myers, L., Klein, E.C., Liu, G., Calvi, C., Podowski, M., Neptune, E.R., Halushka, M.K., Bedja, D., Gabrielson, K., Rifkin, D.B., Carta, L., Ramirez, F., Huso, D.L. and Dietz, H.C. (2006) Losartan, an AT1 antagonist, prevents aortic aneurysm in a mouse model of Marfan syndrome. *Science*, **312**, 117-121.

Hacker, U., Nybakken, K. and Perrimon, N. (2005) Heparan sulphate proteoglycans: the sweet side of development. *Nat Rev Mol Cell Biol*, **6**, 530-541.

Hagiwara, H., Schroter-Kermani, C. and Merker, H.J. (1993) Localization of collagen type VI in articular cartilage of young and adult mice. *Cell Tissue Res*, **272**, 155-160.

Han, I., Park, H. and Oh, E.S. (2004) New insights into syndecan-2 expression and tumourigenic activity in colon carcinoma cells. *J Mol Histol*, **35**, 319-326.

Hanssen, E., Reinboth, B. and Gibson, M.A. (2003) Covalent and non-covalent interactions of betaig-h3 with collagen VI. Beta ig-h3 is covalently attached to the amino-terminal region of collagen VI in tissue microfibrils. *J Biol Chem*, **278**, 24334-24341.

Hashimoto, K., Noshiro, M., Ohno, S., Kawamoto, T., Satakeda, H., Akagawa, Y., Nakashima, K., Okimura, A., Ishida, H., Okamoto, T., Pan, H., Shen, M., Yan, W. and Kato, Y. (1997) Characterization of a cartilage-derived 66-kDa protein (RGD-CAP/beta ig-h3) that binds to collagen. *Biochim Biophys Acta*, **1355**, 303-314.

Haslinger, B., Mandl-Weber, S., Sellmayer, A. and Sitter, T. (2001) Hyaluronan fragments induce the synthesis of MCP-1 and IL-8 in cultured human peritoneal mesothelial cells. *Cell Tissue Res*, **305**, 79-86.

Hayashi, K., Madri, J.A. and Yurchenco, P.D. (1992) Endothelial cells interact with the core protein of basement membrane perlecan through beta 1 and beta 3 integrins: an adhesion modulated by glycosaminoglycan. *J Cell Biol*, **119**, 945-959.

Henderson, M., Polewski, R., Fanning, J.C. and Gibson, M.A. (1996) Microfibril-associated glycoprotein-1 (MAGP-1) is specifically located on the beads of the beaded-filament structure for fibrillin-containing microfibrils as visualized by the rotary shadowing technique. *J Histochem Cytochem*, **44**, 1389-1397.

Hennekam, R.C. (2005) Severe infantile Marfan syndrome versus neonatal Marfan syndrome. *Am J Med Genet A*, **139**, 1.

Herbert, B. (1999) Advances in protein solubilisation for two-dimensional electrophoresis. *Electrophoresis*, **20**, 660-663.

Herbert, B.R., Molloy, M.P., Gooley, A.A., Walsh, B.J., Bryson, W.G. and Williams, K.L. (1998) Improved protein solubility in two-dimensional electrophoresis using tributyl phosphine as reducing agent. *Electrophoresis*, **19**, 845-851.

Heremans, A., De Cock, B., Cassiman, J.J., Van den Berghe, H. and David, G. (1990) The core protein of the matrix-associated heparan sulfate proteoglycan binds to fibronectin. *J Biol Chem*, **265**, 8716-8724.

Hienola, A., Tumova, S., Kulesskiy, E. and Rauvala, H. (2006) N-syndecan deficiency impairs neural migration in brain. *J Cell Biol*, **174**, 569-580.

Higuchi, I., Suehara, M., Iwaki, H., Nakagawa, M., Arimura, K. and Osame, M. (2001) Collagen VI deficiency in Ullrich's disease. *Ann Neurol*, **49**, 544.

Hinek, A., Braun, K.R., Liu, K., Wang, Y. and Wight, T.N. (2004) Retrovirally mediated overexpression of versican v3 reverses impaired elastogenesis and heightened proliferation exhibited by fibroblasts from Costello syndrome and Hurler disease patients. *Am J Pathol*, **164**, 119-131.

Hinkes, M.T., Goldberger, O.A., Neumann, P.E., Kokenyesi, R. and Bernfield, M. (1993) Organization and promoter activity of the mouse syndecan-1 gene. *J Biol Chem*, **268**, 11440-11448.

Hirai, M., Horiguchi, M., Ohbayashi, T., Kita, T., Chien, K.R. and Nakamura, T. (2007) Latent TGF-beta-binding protein 2 binds to DANCE/fibulin-5 and regulates elastic fiber assembly. *Embo J*, **26**, 3283-3295.

Hirani, R., Hanssen, E. and Gibson, M.A. (2007) LTBP-2 specifically interacts with the amino-terminal region of fibrillin-1 and competes with LTBP-1 for binding to this microfibrillar protein. *Matrix Biol*, **26**, 213-223.

Hirano, K., Hotta, Y., Fujiki, K. and Kanai, A. (2000) Corneal amyloidosis caused by Leu518Pro mutation of betaig-h3 gene. *Br J Ophthalmol*, **84**, 583-585.

Ho, C.L. and Walton, D.S. (2004) Primary congenital glaucoma: 2004 update. *J Pediatr Ophthalmol Strabismus*, **41**, 271-288; quiz 300-271.

Hocking, A.M., Shinomura, T. and McQuillan, D.J. (1998) Leucine-rich repeat glycoproteins of the extracellular matrix. *Matrix Biol*, **17**, 1-19.

Hopf, M., Gohring, W., Kohfeldt, E., Yamada, Y. and Timpl, R. (1999) Recombinant domain IV of perlecan binds to nidogens, laminin-nidogen complex, fibronectin, fibulin-2 and heparin. *Eur J Biochem*, **259**, 917-925.

Hopf, M., Gohring, W., Mann, K. and Timpl, R. (2001) Mapping of binding sites for nidogens, fibulin-2, fibronectin and heparin to different IG modules of perlecan. *J Mol Biol*, **311**, 529-541.

Horowitz, A., Tkachenko, E. and Simons, M. (2002) Fibroblast growth factor-specific modulation of cellular response by syndecan-4. *J Cell Biol*, **157**, 715-725.

Howell, J.M., Winstone, T.L., Coorssen, J.R. and Turner, R.J. (2006) An evaluation of in vitro protein-protein interaction techniques: assessing contaminating background proteins. *Proteomics*, **6**, 2050-2069.

Hu, Q., Reymond, J.L., Pinel, N., Zabot, M.T. and Urban, Z. (2006) Inflammatory destruction of elastic fibers in acquired cutis laxa is associated with missense alleles in the elastin and fibulin-5 genes. *J Invest Dermatol*, **126**, 283-290.

Hubmacher, D., El-Hallous, E.I., Nelea, V., Kaartinen, M.T., Lee, E.R. and Reinhardt, D.P. (2008) Biogenesis of extracellular microfibrils: Multimerization of the fibrillin-1 C terminus into bead-like structures enables self-assembly. *Proc Natl Acad Sci U S A*, **105**, 6548-6553.

Hubmacher, D., Tiedemann, K. and Reinhardt, D.P. (2006) Fibrillins: from biogenesis of microfibrils to signaling functions. *Curr Top Dev Biol*, **75**, 93-123.

Humphries, D.E., Wong, G.W., Friend, D.S., Gurish, M.F., Qiu, W.T., Huang, C., Sharpe, A.H. and Stevens, R.L. (1999) Heparin is essential for the storage of specific granule proteases in mast cells. *Nature*, **400**, 769-772.

Hynes, R.O. (1992) Integrins: versatility, modulation, and signaling in cell adhesion. *Cell*, **69**, 11-25.

Hyytiainen, M. and Keski-Oja, J. (2003) Latent TGF-beta binding protein LTBP-2 decreases fibroblast adhesion to fibronectin. *J Cell Biol*, **163**, 1363-1374.

Hyytiainen, M., Penttinen, C. and Keski-Oja, J. (2004) Latent TGF-beta binding proteins: extracellular matrix association and roles in TGF-beta activation. *Crit Rev Clin Lab Sci*, **41**, 233-264.

Hyytiainen, M., Taipale, J., Heldin, C.H. and Keski-Oja, J. (1998) Recombinant latent transforming growth factor beta-binding protein 2 assembles to fibroblast

extracellular matrix and is susceptible to proteolytic processing and release. *J Biol Chem*, **273**, 20669-20676.
Iozzo, R.V. (1998) Matrix proteoglycans: from molecular design to cellular function. *Annu Rev Biochem*, **67**, 609-652.
Iozzo, R.V. (2005) Basement membrane proteoglycans: from cellar to ceiling. *Nat Rev Mol Cell Biol*, **6**, 646-656.
Iozzo, R.V., Cohen, I.R., Grassel, S. and Murdoch, A.D. (1994) The biology of perlecan: the multifaceted heparan sulphate proteoglycan of basement membranes and pericellular matrices. *Biochem J*, **302 (Pt 3)**, 625-639.
Iozzo, R.V. and San Antonio, J.D. (2001) Heparan sulfate proteoglycans: heavy hitters in the angiogenesis arena. *J Clin Invest*, **108**, 349-355.
Ishikawa, H., Sugie, K., Murayama, K., Awaya, A., Suzuki, Y., Noguchi, S., Hayashi, Y.K., Nonaka, I. and Nishino, I. (2004) Ullrich disease due to deficiency of collagen VI in the sarcolemma. *Neurology*, **62**, 620-623.
Isogai, Z., Aspberg, A., Keene, D.R., Ono, R.N., Reinhardt, D.P. and Sakai, L.Y. (2002) Versican interacts with fibrillin-1 and links extracellular microfibrils to other connective tissue networks. *J Biol Chem*, **277**, 4565-4572.
Isogai, Z., Ono, R.N., Ushiro, S., Keene, D.R., Chen, Y., Mazzieri, R., Charbonneau, N.L., Reinhardt, D.P., Rifkin, D.B. and Sakai, L.Y. (2003) Latent transforming growth factor beta-binding protein 1 interacts with fibrillin and is a microfibril-associated protein. *J Biol Chem*, **278**, 2750-2757.
Jaye, M., Schlessinger, J. and Dionne, C.A. (1992) Fibroblast growth factor receptor tyrosine kinases: molecular analysis and signal transduction. *Biochim Biophys Acta*, **1135**, 185-199.
Jensen, S.A., Reinhardt, D.P., Gibson, M.A. and Weiss, A.S. (2001) Protein interaction studies of MAGP-1 with tropoelastin and fibrillin-1. *J Biol Chem*, **276**, 39661-39666.
Jobsis, G.J., Boers, J.M., Barth, P.G. and de Visser, M. (1999) Bethlem myopathy: a slowly progressive congenital muscular dystrophy with contractures. *Brain*, **122 (Pt 4)**, 649-655.
Jobsis, G.J., Keizers, H., Vreijling, J.P., de Visser, M., Speer, M.C., Wolterman, R.A., Baas, F. and Bolhuis, P.A. (1996) Type VI collagen mutations in Bethlem myopathy, an autosomal dominant myopathy with contractures. *Nat Genet*, **14**, 113-115.
Jovanovic, J., Takagi, J., Choulier, L., Abrescia, N.G., Stuart, D.I., van der Merwe, P.A., Mardon, H.J. and Handford, P.A. (2007) alphaVbeta6 is a novel receptor for human fibrillin-1. Comparative studies of molecular determinants underlying integrin-rgd affinity and specificity. *J Biol Chem*, **282**, 6743-6751.
Kallunki, P. and Tryggvason, K. (1992) Human basement membrane heparan sulfate proteoglycan core protein: a 467-kD protein containing multiple domains resembling elements of the low density lipoprotein receptor, laminin, neural cell adhesion molecules, and epidermal growth factor. *J Cell Biol*, **116**, 559-571.
Kantola, A.K., Keski-Oja, J. and Koli, K. (2008) Fibronectin and heparin binding domains of latent TGF-beta binding protein (LTBP)-4 mediate matrix targeting and cell adhesion. *Exp Cell Res*, **314**, 2488-2500.
Kanzaki, T., Olofsson, A., Moren, A., Wernstedt, C., Hellman, U., Miyazono, K., Claesson-Welsh, L. and Heldin, C.H. (1990) TGF-beta 1 binding protein: a component of the large latent complex of TGF-beta 1 with multiple repeat sequences. *Cell*, **61**, 1051-1061.
Kato, M., Wang, H., Kainulainen, V., Fitzgerald, M.L., Ledbetter, S., Ornitz, D.M. and Bernfield, M. (1998) Physiological degradation converts the soluble syndecan-1 ectodomain from an inhibitor to a potent activator of FGF-2. *Nat Med*, **4**, 691-697.
Keene, D.R., Engvall, E. and Glanville, R.W. (1988) Ultrastructure of type VI collagen in human skin and cartilage suggests an anchoring function for this filamentous network. *J Cell Biol*, **107**, 1995-2006.

Keene, D.R., Sakai, L.Y. and Burgeson, R.E. (1991) Human bone contains type III collagen, type VI collagen, and fibrillin: type III collagen is present on specific fibers that may mediate attachment of tendons, ligaments, and periosteum to calcified bone cortex. *J Histochem Cytochem*, **39**, 59-69.

Kelleher, C.M., McLean, S.E. and Mecham, R.P. (2004) Vascular extracellular matrix and aortic development. *Curr Top Dev Biol*, **62**, 153-188.

Kielty, C., and Grant, EM. (2002) The Collagen Family: Structure, Assembly, and Organisation in the Extracellular Matrix. In Royce, P.M., and Steinmann, B (ed.), *Connective Tissues and its Heritable Disorders- Molecular, Genetics and medical aspects*. Wiley-Liss, New York.

Kielty, C.M. (2006) Elastic fibres in health and disease. *Expert Rev Mol Med*, **8**, 1-23.

Kielty, C.M., Hanssen, E. and Shuttleworth, C.A. (1998) Purification of fibrillin-containing microfibrils and collagen VI microfibrils by density gradient centrifugation. *Anal Biochem*, **255**, 108-112.

Kielty, C.M., Sherratt, M.J., Marson, A. and Baldock, C. (2005) Fibrillin microfibrils. *Adv Protein Chem*, **70**, 405-436.

Kielty, C.M., Sherratt, M.J. and Shuttleworth, C.A. (2002) Elastic fibres. *J Cell Sci*, **115**, 2817-2828.

Kielty, C.M. and Shuttleworth, C.A. (1993) The role of calcium in the organization of fibrillin microfibrils. *FEBS Lett*, **336**, 323-326.

Kielty, C.M. and Shuttleworth, C.A. (1995) Fibrillin-containing microfibrils: structure and function in health and disease. *Int J Biochem Cell Biol*, **27**, 747-760.

Kielty, C.M. and Shuttleworth, C.A. (1997) Microfibrillar elements of the dermal matrix. *Microsc Res Tech*, **38**, 413-427.

Kielty, C.M., Whittaker, S.P., Grant, M.E. and Shuttleworth, C.A. (1991) Type VI collagen forms a structural association with hyaluronan in vivo. *Biochem Soc Trans*, **19**, 384S.

Kielty, C.M., Whittaker, S.P. and Shuttleworth, C.A. (1996) Fibrillin: evidence that chondroitin sulphate proteoglycans are components of microfibrils and associate with newly synthesised monomers. *FEBS Lett*, **386**, 169-173.

Kim, J.E., Han, M.S., Bae, Y.C., Kim, H.K., Kim, T.I., Kim, E.K. and Kim, I.S. (2007) Anterior segment dysgenesis after overexpression of transforming growth factor-beta-induced gene, beta igh3, in the mouse eye. *Mol Vis*, **13**, 1942-1952.

Kim, J.E., Jeong, H.W., Nam, J.O., Lee, B.H., Choi, J.Y., Park, R.W., Park, J.Y. and Kim, I.S. (2002) Identification of motifs in the fasciclin domains of the transforming growth factor-beta-induced matrix protein betaig-h3 that interact with the alphavbeta5 integrin. *J Biol Chem*, **277**, 46159-46165.

Kim, J.E., Kim, S.J., Lee, B.H., Park, R.W., Kim, K.S. and Kim, I.S. (2000) Identification of motifs for cell adhesion within the repeated domains of transforming growth factor-beta-induced gene, betaig-h3. *J Biol Chem*, **275**, 30907-30915.

Kinsey, R., Williamson, M.R., Chaudhry, S., Mellody, K.T., McGovern, A., Takahashi, S., Shuttleworth, C.A. and Kielty, C.M. (2008) Fibrillin-1 microfibril deposition is dependent on fibronectin assembly. *J Cell Sci*, **121**, 2696-2704.

Kitahama, S., Gibson, M.A., Hatzinikolas, G., Hay, S., Kuliwaba, J.L., Evdokiou, A., Atkins, G.J. and Findlay, D.M. (2000) Expression of fibrillins and other microfibril-associated proteins in human bone and osteoblast-like cells. *Bone*, **27**, 61-67.

Kitahara, O., Furukawa, Y., Tanaka, T., Kihara, C., Ono, K., Yanagawa, R., Nita, M.E., Takagi, T., Nakamura, Y. and Tsunoda, T. (2001) Alterations of gene expression during colorectal carcinogenesis revealed by cDNA microarrays after laser-capture microdissection of tumor tissues and normal epithelia. *Cancer Res*, **61**, 3544-3549.

Klass, C.M., Couchman, J.R. and Woods, A. (2000) Control of extracellular matrix assembly by syndecan-2 proteoglycan. *J Cell Sci*, **113 (Pt 3)**, 493-506.

Klintworth, G.K. (2003) The molecular genetics of the corneal dystrophies--current status. *Front Biosci*, **8**, d687-713.

Kobayashi, N., Kostka, G., Garbe, J.H., Keene, D.R., Bachinger, H.P., Hanisch, F.G., Markova, D., Tsuda, T., Timpl, R., Chu, M.L. and Sasaki, T. (2007) A comparative analysis of the fibulin protein family. Biochemical characterization, binding interactions, and tissue localization. *J Biol Chem*, **282**, 11805-11816.

Kojima, T., Shworak, N.W. and Rosenberg, R.D. (1992) Molecular cloning and expression of two distinct cDNA-encoding heparan sulfate proteoglycan core proteins from a rat endothelial cell line. *J Biol Chem*, **267**, 4870-4877.

Koli, K., Saharinen, J., Hyytiainen, M., Penttinen, C. and Keski-Oja, J. (2001) Latency, activation, and binding proteins of TGF-beta. *Microsc Res Tech*, **52**, 354-362.

Kondo, T., Seike, M., Mori, Y., Fujii, K., Yamada, T. and Hirohashi, S. (2003) Application of sensitive fluorescent dyes in linkage of laser microdissection and two-dimensional gel electrophoresis as a cancer proteomic study tool. *Proteomics*, **3**, 1758-1766.

Kornblihtt, A.R., Vibe-Pedersen, K. and Baralle, F.E. (1984) Human fibronectin: molecular cloning evidence for two mRNA species differing by an internal segment coding for a structural domain. *Embo J*, **3**, 221-226.

Kozel, B.A., Ciliberto, C.H. and Mecham, R.P. (2004) Deposition of tropoelastin into the extracellular matrix requires a competent elastic fiber scaffold but not live cells. *Matrix Biol*, **23**, 23-34.

Kramer, K.L., Barnette, J.E. and Yost, H.J. (2002) PKCgamma regulates syndecan-2 inside-out signaling during xenopus left-right development. *Cell*, **111**, 981-990.

Kramer, K.L. and Yost, H.J. (2002) Ectodermal syndecan-2 mediates left-right axis formation in migrating mesoderm as a cell-nonautonomous Vg1 cofactor. *Dev Cell*, **2**, 115-124.

Kuo, H.J., Keene, D.R. and Glanville, R.W. (1989) Orientation of type VI collagen monomers in molecular aggregates. *Biochemistry*, **28**, 3757-3762.

Kuo, H.J., Maslen, C.L., Keene, D.R. and Glanville, R.W. (1997) Type VI collagen anchors endothelial basement membranes by interacting with type IV collagen. *J Biol Chem*, **272**, 26522-26529.

Kupfer, C. and Kaiser-Kupfer, M.I. (1979) Observations on the development of the anterior chamber angle with reference to the pathogenesis of congenital glaucomas. *Am J Ophthalmol*, **88**, 424-426.

Lack, J., O'Leary, J.M., Knott, V., Yuan, X., Rifkin, D.B., Handford, P.A. and Downing, A.K. (2003) Solution structure of the third TB domain from LTBP1 provides insight into assembly of the large latent complex that sequesters latent TGF-beta. *J Mol Biol*, **334**, 281-291.

Laemmli, U.K. (1970) Cleavage of structural proteins during the assembly of the head of bacteriophage T4. *Nature*, **227**, 680-685.

Lalwani, S., Tutu, E. and Vigh, G. (2005) Synthesis and characterization of quaternary ammonium dicarboxylic acid isoelectric buffers and their use in pH-biased isoelectric trapping separations. *Electrophoresis*, **26**, 2047-2055.

Lampe, A.K. and Bushby, K.M. (2005) Collagen VI related muscle disorders. *J Med Genet*, **42**, 673-685.

LeBaron, R.G., Bezverkov, K.I., Zimber, M.P., Pavelec, R., Skonier, J. and Purchio, A.F. (1995) Beta IG-H3, a novel secretory protein inducible by transforming growth factor-beta, is present in normal skin and promotes the adhesion and spreading of dermal fibroblasts in vitro. *J Invest Dermatol*, **104**, 844-849.

LeBleu, V.S., Macdonald, B. and Kalluri, R. (2007) Structure and function of basement membranes. *Exp Biol Med (Maywood)*, **232**, 1121-1129.

Lee, B., Godfrey, M., Vitale, E., Hori, H., Mattei, M.G., Sarfarazi, M., Tsipouras, P., Ramirez, F. and Hollister, D.W. (1991) Linkage of Marfan syndrome and a phenotypically related disorder to two different fibrillin genes. *Nature*, **352**, 330-334.

Lee, K., Pi, k., Lee, K. (2009) Buffer optimization for high resolution of human lung cancer tissue proteins by two-dimensional gel electrophoresis. *Biotechnol Lett*, **31**, 31-37.

Lee, S.S., Knott, V., Jovanovic, J., Harlos, K., Grimes, J.M., Choulier, L., Mardon, H.J., Stuart, D.I. and Handford, P.A. (2004) Structure of the integrin binding fragment from fibrillin-1 gives new insights into microfibril organization. *Structure*, **12**, 717-729.

Li, D.Y., Brooke, B., Davis, E.C., Mecham, R.P., Sorensen, L.K., Boak, B.B., Eichwald, E. and Keating, M.T. (1998a) Elastin is an essential determinant of arterial morphogenesis. *Nature*, **393**, 276-280.

Li, D.Y., Faury, G., Taylor, D.G., Davis, E.C., Boyle, W.A., Mecham, R.P., Stenzel, P., Boak, B. and Keating, M.T. (1998b) Novel arterial pathology in mice and humans hemizygous for elastin. *J Clin Invest*, **102**, 1783-1787.

Li, D.Y., Toland, A.E., Boak, B.B., Atkinson, D.L., Ensing, G.J., Morris, C.A. and Keating, M.T. (1997) Elastin point mutations cause an obstructive vascular disease, supravalvular aortic stenosis. *Hum Mol Genet*, **6**, 1021-1028.

Lim, S.T., Longley, R.L., Couchman, J.R. and Woods, A. (2003) Direct binding of syndecan-4 cytoplasmic domain to the catalytic domain of protein kinase C alpha (PKC alpha) increases focal adhesion localization of PKC alpha. *J Biol Chem*, **278**, 13795-13802.

Lin, X. (2004) Functions of heparan sulfate proteoglycans in cell signaling during development. *Development*, **131**, 6009-6021.

Loeser, R.F. (1997) Growth factor regulation of chondrocyte integrins. Differential effects of insulin-like growth factor 1 and transforming growth factor beta on alpha 1 beta 1 integrin expression and chondrocyte adhesion to type VI collagen. *Arthritis Rheum*, **40**, 270-276.

Lopes, C.C., Dietrich, C.P. and Nader, H.B. (2006) Specific structural features of syndecans and heparan sulfate chains are needed for cell signaling. *Braz J Med Biol Res*, **39**, 157-167.

Mangasser-Stephan, K. and Gressner, A.M. (1999) Molecular and functional aspects of latent transforming growth factor-beta binding protein: just a masking protein? *Cell Tissue Res*, **297**, 363-370.

Mark, K., Soroken, L.,. (2002) Adhesive Glycoproteins. In Royce, P.M., and Steinmann, B (ed.), *Connective Tissues and its Heritable Disorders-Molecular, Genetics and medical aspects*. Wiley-Liss, New York, pp. 159-221.

Marouga, R., David, S. and Hawkins, E. (2005) The development of the DIGE system: 2D fluorescence difference gel analysis technology. *Anal Bioanal Chem*, **382**, 669-678.

Marson, A., Rock, M.J., Cain, S.A., Freeman, L.J., Morgan, A., Mellody, K., Shuttleworth, C.A., Baldock, C. and Kielty, C.M. (2005) Homotypic fibrillin-1 interactions in microfibril assembly. *J Biol Chem*, **280**, 5013-5021.

Masse, M., Cserhalmi-Friedman, P.B., Falanga, V., Celebi, J.T., Martinez-Mir, A. and Christiano, A.M. (2005) Identification of novel type VII collagen gene mutations resulting in severe recessive dystrophic epidermolysis bullosa. *Clin Exp Dermatol*, **30**, 289-293.

McDevitt, C.A., Marcelino, J. and Tucker, L. (1991) Interaction of intact type VI collagen with hyaluronan. *FEBS Lett*, **294**, 167-170.

McGettrick, A.J., Knott, V., Willis, A. and Handford, P.A. (2000) Molecular effects of calcium binding mutations in Marfan syndrome depend on domain context. *Hum Mol Genet*, **9**, 1987-1994.

McKee, C.M., Penno, M.B., Cowman, M., Burdick, M.D., Strieter, R.M., Bao, C. and Noble, P.W. (1996) Hyaluronan (HA) fragments induce chemokine gene expression in alveolar macrophages. The role of HA size and CD44. *J Clin Invest*, **98**, 2403-2413.

McLaughlin, P.J., Chen, Q., Horiguchi, M., Starcher, B.C., Stanton, J.B., Broekelmann, T.J., Marmorstein, A.D., McKay, B., Mecham, R., Nakamura, T. and Marmorstein, L.Y. (2006) Targeted disruption of fibulin-4 abolishes elastogenesis and causes perinatal lethality in mice. *Mol Cell Biol*, **26**, 1700-1709.

Mecham, R.P., and Davis, E. (1994) In P.D Yurchenco, D.E.B., and R.P Mecham (ed.), *Elastic fiber structure and assembly: Extracellular Matrix Assembly and Structure*. Academic Press, New York, pp. 281-314.

Melrose, J., Hayes, A.J., Whitelock, J.M. and Little, C.B. (2008) Perlecan, the "jack of all trades" proteoglycan of cartilaginous weight-bearing connective tissues. *Bioessays*, **30**, 457-469.

Mercuri, E., Lampe, A., Allsop, J., Knight, R., Pane, M., Kinali, M., Bonnemann, C., Flanigan, K., Lapini, I., Bushby, K., Pepe, G. and Muntoni, F. (2005) Muscle MRI in Ullrich congenital muscular dystrophy and Bethlem myopathy. *Neuromuscul Disord*, **15**, 303-310.

Mertens, G., Cassiman, J.J., Van den Berghe, H., Vermylen, J. and David, G. (1992) Cell surface heparan sulfate proteoglycans from human vascular endothelial cells. Core protein characterization and antithrombin III binding properties. *J Biol Chem*, **267**, 20435-20443.

Metcalfe, K., Rucka, A.K., Smoot, L., Hofstadler, G., Tuzler, G., McKeown, P., Siu, V., Rauch, A., Dean, J., Dennis, N., Ellis, I., Reardon, W., Cytrynbaum, C., Osborne, L., Yates, J.R., Read, A.P., Donnai, D. and Tassabehji, M. (2000) Elastin: mutational spectrum in supravalvular aortic stenosis. *Eur J Hum Genet*, **8**, 955-963.

Miao, M., Bellingham, C.M., Stahl, R.J., Sitarz, E.E., Lane, C.J. and Keeley, F.W. (2003) Sequence and structure determinants for the self-aggregation of recombinant polypeptides modeled after human elastin. *J Biol Chem*, **278**, 48553-48562.

Miao, M., Cirulis, J.T., Lee, S. and Keeley, F.W. (2005) Structural determinants of cross-linking and hydrophobic domains for self-assembly of elastin-like polypeptides. *Biochemistry*, **44**, 14367-14375.

Michelacci, Y.M. (2003) Collagens and proteoglycans of the corneal extracellular matrix. *Braz J Med Biol Res*, **36**, 1037-1046.

Midwood, K.S. and Schwarzbauer, J.E. (2002) Elastic fibers: building bridges between cells and their matrix. *Curr Biol*, **12**, R279-281.

Milewicz, D.M., Urban, Z. and Boyd, C. (2000) Genetic disorders of the elastic fiber system. *Matrix Biol*, **19**, 471-480.

Miner, J.H., Li, C., Mudd, J.L., Go, G. and Sutherland, A.E. (2004) Compositional and structural requirements for laminin and basement membranes during mouse embryo implantation and gastrulation. *Development*, **131**, 2247-2256.

Miner, J.H. and Yurchenco, P.D. (2004) Laminin functions in tissue morphogenesis. *Annu Rev Cell Dev Biol*, **20**, 255-284.

Miosge, N., Hartmann, M., Maelicke, C. and Herken, R. (2004) Expression of collagen type I and type II in consecutive stages of human osteoarthritis. *Histochem Cell Biol*, **122**, 229-236.

Mithieux, S.M. and Weiss, A.S. (2005) Elastin. *Adv Protein Chem*, **70**, 437-461.

Miyazono, K., Olofsson, A., Colosetti, P. and Heldin, C.H. (1991) A role of the latent TGF-beta 1-binding protein in the assembly and secretion of TGF-beta 1. *Embo J*, **10**, 1091-1101.

Mohan, P.S. and Spiro, R.G. (1991) Characterization of heparan sulfate proteoglycan from calf lens capsule and proteoglycans synthesized by cultured lens epithelial cells. Comparison with other basement membrane proteoglycans. *J Biol Chem*, **266**, 8567-8575.

Mongiat, M., Taylor, K., Otto, J., Aho, S., Uitto, J., Whitelock, J.M. and Iozzo, R.V. (2000) The protein core of the proteoglycan perlecan binds specifically to fibroblast growth factor-7. *J Biol Chem*, **275**, 7095-7100.

Moren, A., Olofsson, A., Stenman, G., Sahlin, P., Kanzaki, T., Claesson-Welsh, L., ten Dijke, P., Miyazono, K. and Heldin, C.H. (1994) Identification and characterization of LTBP-2, a novel latent transforming growth factor-beta-binding protein. *J Biol Chem*, **269**, 32469-32478.

Mundhenke, C., Meyer, K., Drew, S. and Friedl, A. (2002) Heparan sulfate proteoglycans as regulators of fibroblast growth factor-2 receptor binding in breast carcinomas. *Am J Pathol*, **160**, 185-194.

Munier, F.L., Frueh, B.E., Othenin-Girard, P., Uffer, S., Cousin, P., Wang, M.X., Heon, E., Black, G.C., Blasi, M.A., Balestrazzi, E., Lorenz, B., Escoto, R., Barraquer, R., Hoeltzenbein, M., Gloor, B., Fossarello, M., Singh, A.D., Arsenijevic, Y., Zografos, L. and Schorderet, D.F. (2002) BIGH3 mutation spectrum in corneal dystrophies. *Invest Ophthalmol Vis Sci*, **43**, 949-954.

Munier, F.L., Korvatska, E., Djemai, A., Le Paslier, D., Zografos, L., Pescia, G. and Schorderet, D.F. (1997) Kerato-epithelin mutations in four 5q31-linked corneal dystrophies. *Nat Genet*, **15**, 247-251.

Murdoch, A.D., Liu, B., Schwarting, R., Tuan, R.S. and Iozzo, R.V. (1994) Widespread expression of perlecan proteoglycan in basement membranes and extracellular matrices of human tissues as detected by a novel monoclonal antibody against domain III and by in situ hybridization. *J Histochem Cytochem*, **42**, 239-249.

Nagase, T., Nakayama, M., Nakajima, D., Kikuno, R. and Ohara, O. (2001) Prediction of the coding sequences of unidentified human genes. XX. The complete sequences of 100 new cDNA clones from brain which code for large proteins in vitro. *DNA Res*, **8**, 85-95.

Nakamura, T., Lozano, P.R., Ikeda, Y., Iwanaga, Y., Hinek, A., Minamisawa, S., Cheng, C.F., Kobuke, K., Dalton, N., Takada, Y., Tashiro, K., Ross Jr, J., Honjo, T. and Chien, K.R. (2002) Fibulin-5/DANCE is essential for elastogenesis in vivo. *Nature*, **415**, 171-175.

Narayanan, A.S., Page, R.C., Kuzan, F. and Cooper, C.G. (1978) Elastin cross-linking in vitro. Studies on factors influencing the formation of desmosines by lysyl oxidase action on tropoelastin. *Biochem J*, **173**, 857-862.

Nareyeck, G., Seidler, D.G., Troyer, D., Rauterberg, J., Kresse, H. and Schonherr, E. (2004) Differential interactions of decorin and decorin mutants with type I and type VI collagens. *Eur J Biochem*, **271**, 3389-3398.

Neptune, E.R., Frischmeyer, P.A., Arking, D.E., Myers, L., Bunton, T.E., Gayraud, B., Ramirez, F., Sakai, L.Y. and Dietz, H.C. (2003) Dysregulation of TGF-beta activation contributes to pathogenesis in Marfan syndrome. *Nat Genet*, **33**, 407-411.

Ng, C.M., Cheng, A., Myers, L.A., Martinez-Murillo, F., Jie, C., Bedja, D., Gabrielson, K.L., Hausladen, J.M., Mecham, R.P., Judge, D.P. and Dietz, H.C. (2004) TGF-beta-dependent pathogenesis of mitral valve prolapse in a mouse model of Marfan syndrome. *J Clin Invest*, **114**, 1586-1592.

Nischt, R., Pottgiesser, J., Krieg, T., Mayer, U., Aumailley, M. and Timpl, R. (1991) Recombinant expression and properties of the human calcium-binding extracellular matrix protein BM-40. *Eur J Biochem*, **200**, 529-536.

Noguera, I., Obata, H., Gualandris, A., Cowin, P. and Rifkin, D.B. (2003) Molecular cloning of the mouse Ltbp-1 gene reveals tissue specific expression of alternatively spliced forms. *Gene*, **308**, 31-41.

Nunes, I., Gleizes, P.E., Metz, C.N. and Rifkin, D.B. (1997) Latent transforming growth factor-beta binding protein domains involved in activation and transglutaminase-dependent cross-linking of latent transforming growth factor-beta. *J Cell Biol*, **136**, 1151-1163.

Nzeusseu Toukap, A., Galant, C., Theate, I., Maudoux, A.L., Lories, R.J., Houssiau, F.A. and Lauwerys, B.R. (2007) Identification of distinct gene expression profiles in the synovium of patients with systemic lupus erythematosus. *Arthritis Rheum*, **56**, 1579-1588.

Odermatt, E., Risteli, J., van Delden, V. and Timpl, R. (1983) Structural diversity and domain composition of a unique collagenous fragment (intima collagen) obtained from human placenta. *Biochem J*, **211**, 295-302.

O'Farrell, P.H. (1975) High resolution two-dimensional electrophoresis of proteins. *J Biol Chem*, **250**, 4007-4021.
Oklu, R. and Hesketh, R. (2000) The latent transforming growth factor beta binding protein (LTBP) family. *Biochem J*, **352 Pt 3**, 601-610.
Oklu, R., Hesketh, T.R., Metcalfe, J.C. and Kemp, P.R. (1998) Expression of alternatively spliced human latent transforming growth factor beta binding protein-1. *FEBS Lett*, **435**, 143-148.
Olofsson, A., Ichijo, H., Moren, A., ten Dijke, P., Miyazono, K. and Heldin, C.H. (1995) Efficient association of an amino-terminally extended form of human latent transforming growth factor-beta binding protein with the extracellular matrix. *J Biol Chem*, **270**, 31294-31297.
Olsen, J.V., Ong, S.E. and Mann, M. (2004) Trypsin cleaves exclusively C-terminal to arginine and lysine residues. *Mol Cell Proteomics*, **3**, 608-614.
Olson, T.M., Michels, V.V., Lindor, N.M., Pastores, G.M., Weber, J.L., Schaid, D.J., Driscoll, D.J., Feldt, R.H. and Thibodeau, S.N. (1993) Autosomal dominant supravalvular aortic stenosis: localization to chromosome 7. *Hum Mol Genet*, **2**, 869-873.
Ong, S.E., Blagoev, B., Kratchmarova, I., Kristensen, D.B., Steen, H., Pandey, A. and Mann, M. (2002) Stable isotope labeling by amino acids in cell culture, SILAC, as a simple and accurate approach to expression proteomics. *Mol Cell Proteomics*, **1**, 376-386.
Ong, S.E. and Mann, M. (2006) A practical recipe for stable isotope labeling by amino acids in cell culture (SILAC). *Nat Protoc*, **1**, 2650-2660.
Ottani, V., Martini, D., Franchi, M., Ruggeri, A. and Raspanti, M. (2002) Hierarchical structures in fibrillar collagens. *Micron*, **33**, 587-596.
Park, S.W., Bae, J. S., et al. (2004) Beta ig-h3 promotes renal proximal tubular epithelial cell adhesion, migration and proliferation through the interaction with alpha3beta1 integrin. *Experimetal and Molecular medicine*, **36**, 211-219.
Parsi, M.K., Adams, J.R., Whitelock, J. and Gibson, M.A. LTBP-2 has multiple heparin/heparan sulfate binding sites. *Matrix Biol*.
Pearlstein, E., Gold, L.I. and Garcia-Pardo, A. (1980) Fibronectin: a review of its structure and biological activity. *Mol Cell Biochem*, **29**, 103-128.
Pei, Y.F. and Rhodin, J.A. (1970) The prenatal development of the mouse eye. *Anat Rec*, **168**, 105-125.
Peng, H.B., Xie, H., Rossi, S.G. and Rotundo, R.L. (1999) Acetylcholinesterase clustering at the neuromuscular junction involves perlecan and dystroglycan. *J Cell Biol*, **145**, 911-921.
Penner, A.S., Rock, M.J., Kielty, C.M. and Shipley, J.M. (2002) Microfibril-associated glycoprotein-2 interacts with fibrillin-1 and fibrillin-2 suggesting a role for MAGP-2 in elastic fiber assembly. *J Biol Chem*, **277**, 35044-35049.
Penttinen, C., Saharinen, J., Weikkolainen, K., Hyytiainen, M. and Keski-Oja, J. (2002) Secretion of human latent TGF-beta-binding protein-3 (LTBP-3) is dependent on co-expression of TGF-beta. *J Cell Sci*, **115**, 3457-3468.
Pereira, L., Andrikopoulos, K., Tian, J., Lee, S.Y., Keene, D.R., Ono, R., Reinhardt, D.P., Sakai, L.Y., Biery, N.J., Bunton, T., Dietz, H.C. and Ramirez, F. (1997) Targetting of the gene encoding fibrillin-1 recapitulates the vascular aspect of Marfan syndrome. *Nat Genet*, **17**, 218-222.
Perrimon, N. and Bernfield, M. (2001) Cellular functions of proteoglycans--an overview. *Semin Cell Dev Biol*, **12**, 65-67.
Pezet, M., Jacob, M.P., Escoubet, B., Gheduzzi, D., Tillet, E., Perret, P., Huber, P., Quaglino, D., Vranckx, R., Li, D.Y., Starcher, B., Boyle, W.A., Mecham, R.P. and Faury, G. (2008) Elastin haploinsufficiency induces alternative aging processes in the aorta. *Rejuvenation Res*, **11**, 97-112.
Pfaff, M., Aumailley, M., Specks, U., Knolle, J., Zerwes, H.G. and Timpl, R. (1993) Integrin and Arg-Gly-Asp dependence of cell adhesion to the native and unfolded triple helix of collagen type VI. *Exp Cell Res*, **206**, 167-176.

Pfaff, M., Reinhardt, D.P., Sakai, L.Y. and Timpl, R. (1996) Cell adhesion and integrin binding to recombinant human fibrillin-1. *FEBS Lett*, **384**, 247-250.

Pierce, A., Lyon, M., Hampson, I.N., Cowling, G.J. and Gallagher, J.T. (1992) Molecular cloning of the major cell surface heparan sulfate proteoglycan from rat liver. *J Biol Chem*, **267**, 3894-3900.

Poole, C.A. (1997) Articular cartilage chondrons: form, function and failure. *J Anat*, **191 (Pt 1)**, 1-13.

Poole, C.A., Ayad, S. and Schofield, J.R. (1988) Chondrons from articular cartilage: I. Immunolocalization of type VI collagen in the pericellular capsule of isolated canine tibial chondrons. *J Cell Sci*, **90 (Pt 4)**, 635-643.

Prosser, I.W., Gibson, M.A. and Cleary, E.G. (1984) Microfibrillar protein from elastic tissue: a critical evaluation. *Aust J Exp Biol Med Sci*, **62 (Pt 4)**, 485-505.

Putnam, E.A., Zhang, H., Ramirez, F. and Milewicz, D.M. (1995) Fibrillin-2 (FBN2) mutations result in the Marfan-like disorder, congenital contractural arachnodactyly. *Nat Genet*, **11**, 456-458.

Pyeritz, R.E. (2000) The Marfan syndrome. *Annu Rev Med*, **51**, 481-510.

Quondamatteo, F., Reinhardt, D.P., Charbonneau, N.L., Pophal, G., Sakai, L.Y. and Herken, R. (2002) Fibrillin-1 and fibrillin-2 in human embryonic and early fetal development. *Matrix Biol*, **21**, 637-646.

Rabilloud, T. (1996) Solubilization of proteins for electrophoretic analyses. *Electrophoresis*, **17**, 813-829.

Rabilloud, T., Adessi, C., Giraudel, A. and Lunardi, J. (1997) Improvement of the solubilization of proteins in two-dimensional electrophoresis with immobilized pH gradients. *Electrophoresis*, **18**, 307-316.

Raghunath, M., Putnam, E.A., Ritty, T., Hamstra, D., Park, E.S., Tschodrich-Rotter, M., Peters, R., Rehemtulla, A. and Milewicz, D.M. (1999) Carboxy-terminal conversion of profibrillin to fibrillin at a basic site by PACE/furin-like activity required for incorporation in the matrix. *J Cell Sci*, **112 (Pt 7)**, 1093-1100.

Ramirez, F. and Dietz, H.C. (2007) Fibrillin-rich microfibrils: Structural determinants of morphogenetic and homeostatic events. *J Cell Physiol*, **213**, 326-330.

Ramirez, F. and Sakai, L.Y. Biogenesis and function of fibrillin assemblies. *Cell Tissue Res*, **339**, 71-82.

Ramirez, F., Sakai, L.Y., Rifkin, D.B. and Dietz, H.C. (2007) Extracellular microfibrils in development and disease. *Cell Mol Life Sci*, **64**, 2437-2446.

Ramos Arroyo, M.A., Weaver, D.D. and Beals, R.K. (1985) Congenital contractural arachnodactyly. Report of four additional families and review of literature. *Clin Genet*, **27**, 570-581.

Rapraeger, A., Jalkanen, M., Endo, E., Koda, J. and Bernfield, M. (1985) The cell surface proteoglycan from mouse mammary epithelial cells bears chondroitin sulfate and heparan sulfate glycosaminoglycans. *J Biol Chem*, **260**, 11046-11052.

Rapraeger, A.C. (2000) Syndecan-regulated receptor signaling. *J Cell Biol*, **149**, 995-998.

Raulo, E., Chernousov, M.A., Carey, D.J., Nolo, R. and Rauvala, H. (1994) Isolation of a neuronal cell surface receptor of heparin binding growth-associated molecule (HB-GAM). Identification as N-syndecan (syndecan-3). *J Biol Chem*, **269**, 12999-13004.

Reale, E., Groos, S., Luciano, L., Eckardt, C. and Eckardt, U. (2001) In the mammalian eye type VI collagen tetramers form three morphologically different aggregates. *Matrix Biol*, **20**, 37-51.

Reinboth, B., Hanssen, E., Cleary, E.G. and Gibson, M.A. (2002) Molecular interactions of biglycan and decorin with elastic fiber components: biglycan forms a ternary complex with tropoelastin and microfibril-associated glycoprotein 1. *J Biol Chem*, **277**, 3950-3957.

Reinboth, B., Thomas, J., Hanssen, E. and Gibson, M.A. (2006) Beta ig-h3 interacts directly with biglycan and decorin, promotes collagen VI aggregation, and participates in ternary complexing with these macromolecules. *J Biol Chem*, **281**, 7816-7824.

Reinhardt, D.P., Keene, D.R., Corson, G.M., Poschl, E., Bachinger, H.P., Gambee, J.E. and Sakai, L.Y. (1996a) Fibrillin-1: organization in microfibrils and structural properties. *J Mol Biol*, **258**, 104-116.

Reinhardt, D.P., Mechling, D.E., Boswell, B.A., Keene, D.R., Sakai, L.Y. and Bachinger, H.P. (1997a) Calcium determines the shape of fibrillin. *J Biol Chem*, **272**, 7368-7373.

Reinhardt, D.P., Ono, R.N. and Sakai, L.Y. (1997b) Calcium stabilizes fibrillin-1 against proteolytic degradation. *J Biol Chem*, **272**, 1231-1236.

Reinhardt, D.P., Sasaki, T., Dzamba, B.J., Keene, D.R., Chu, M.L., Gohring, W., Timpl, R. and Sakai, L.Y. (1996b) Fibrillin-1 and fibulin-2 interact and are colocalized in some tissues. *J Biol Chem*, **271**, 19489-19496.

Rifkin, D.B. (2005) Latent transforming growth factor-beta (TGF-beta) binding proteins: orchestrators of TGF-beta availability. *J Biol Chem*, **280**, 7409-7412.

Ritty, T.M., Broekelmann, T., Tisdale, C., Milewicz, D.M. and Mecham, R.P. (1999) Processing of the fibrillin-1 carboxyl-terminal domain. *J Biol Chem*, **274**, 8933-8940.

Ritty, T.M., Broekelmann, T.J., Werneck, C.C. and Mecham, R.P. (2003a) Fibrillin-1 and -2 contain heparin-binding sites important for matrix deposition and that support cell attachment. *Biochem J*, **375**, 425-432.

Ritty, T.M., Ditsios, K. and Starcher, B.C. (2002) Distribution of the elastic fiber and associated proteins in flexor tendon reflects function. *Anat Rec*, **268**, 430-440.

Ritty, T.M., Roth, R. and Heuser, J.E. (2003b) Tendon cell array isolation reveals a previously unknown fibrillin-2-containing macromolecular assembly. *Structure*, **11**, 1179-1188.

Roark, E.F., Keene, D.R., Haudenschild, C.C., Godyna, S., Little, C.D. and Argraves, W.S. (1995) The association of human fibulin-1 with elastic fibers: an immunohistological, ultrastructural, and RNA study. *J Histochem Cytochem*, **43**, 401-411.

Robb, B.W., Wachi, H., Schaub, T., Mecham, R.P. and Davis, E.C. (1999) Characterization of an in vitro model of elastic fiber assembly. *Mol Biol Cell*, **10**, 3595-3605.

Roberts, G.C. and Critchley, D.R. (2009) Structural and biophysical properties of the integrin-associated cytoskeletal protein talin. *Biophys Rev*, **1**, 61-69.

Rock, M.J., Cain, S.A., Freeman, L.J., Morgan, A., Mellody, K., Marson, A., Shuttleworth, C.A., Weiss, A.S. and Kielty, C.M. (2004) Molecular basis of elastic fiber formation. Critical interactions and a tropoelastin-fibrillin-1 cross-link. *J Biol Chem*, **279**, 23748-23758.

Rose, M.J. and Page, C. (2004) Glycosaminoglycans and the regulation of allergic inflammation. *Curr Drug Targets Inflamm Allergy*, **3**, 221-225.

Rosenbloom, J., Abrams, W.R. and Mecham, R. (1993) Extracellular matrix 4: the elastic fiber. *Faseb J*, **7**, 1208-1218.

Ruoslahti, E. (1996) RGD and other recognition sequences for integrins. *Annu Rev Cell Dev Biol*, **12**, 697-715.

Sabatier, L., Chen, D., Fagotto-Kaufmann, C., Hubmacher, D., McKee, M.D., Annis, D.S., Mosher, D.F. and Reinhardt, D.P. (2009) Fibrillin assembly requires fibronectin. *Mol Biol Cell*, **20**, 846-858.

Saharinen, J., Hyytiainen, M., Taipale, J. and Keski-Oja, J. (1999) Latent transforming growth factor-beta binding proteins (LTBPs)--structural extracellular matrix proteins for targeting TGF-beta action. *Cytokine Growth Factor Rev*, **10**, 99-117.

Saharinen, J. and Keski-Oja, J. (2000) Specific sequence motif of 8-Cys repeats of TGF-beta binding proteins, LTBPs, creates a hydrophobic interaction surface for binding of small latent TGF-beta. *Mol Biol Cell*, **11**, 2691-2704.

Saharinen, J., Taipale, J. and Keski-Oja, J. (1996) Association of the small latent transforming growth factor-beta with an eight cysteine repeat of its binding protein LTBP-1. *Embo J*, **15**, 245-253.

Saharinen, J., Taipale, J., Monni, O. and Keski-Oja, J. (1998) Identification and characterization of a new latent transforming growth factor-beta-binding protein, LTBP-4. *J Biol Chem*, **273**, 18459-18469.

Sakai, L.Y., Keene, D.R. and Engvall, E. (1986) Fibrillin, a new 350-kD glycoprotein, is a component of extracellular microfibrils. *J Cell Biol*, **103**, 2499-2509.
Sampath, T.K., Coughlin, J.E., Whetstone, R.M., Banach, D., Corbett, C., Ridge, R.J., Ozkaynak, E., Oppermann, H. and Rueger, D.C. (1990) Bovine osteogenic protein is composed of dimers of OP-1 and BMP-2A, two members of the transforming growth factor-beta superfamily. *J Biol Chem*, **265**, 13198-13205.
San Martin, S., Soto-Suazo, M. and Zorn, T.M. (2004) Perlecan and syndecan-4 in uterine tissues during the early pregnancy in mice. *Am J Reprod Immunol*, **52**, 53-59.
Sasaki, H., Kobayashi, Y., Nakashima, Y., Moriyama, S., Yukiue, H., Kaji, M., Kiriyama, M., Fukai, I., Yamakawa, Y. and Fujii, Y. (2002) Beta IGH3, a TGF-beta inducible gene, is overexpressed in lung cancer. *Jpn J Clin Oncol*, **32**, 85-89.
Sasaki, T., Hohenester, E., Zhang, R.Z., Gotta, S., Speer, M.C., Tandan, R., Timpl, R. and Chu, M.L. (2000) A Bethlem myopathy Gly to Glu mutation in the von Willebrand factor A domain N2 of the collagen alpha3(VI) chain interferes with protein folding. *Faseb J*, **14**, 761-768.
Sasisekharan, R., Raman, R. and Prabhakar, V. (2006) Glycomics approach to structure-function relationships of glycosaminoglycans. *Annu Rev Biomed Eng*, **8**, 181-231.
Scacheri, P.C., Gillanders, E.M., Subramony, S.H., Vedanarayanan, V., Crowe, C.A., Thakore, N., Bingler, M. and Hoffman, E.P. (2002) Novel mutations in collagen VI genes: expansion of the Bethlem myopathy phenotype. *Neurology*, **58**, 593-602.
Schwarzbauer, J.E. (1991) Identification of the fibronectin sequences required for assembly of a fibrillar matrix. *J Cell Biol*, **113**, 1463-1473.
Schwarzbauer, J.E., Patel, R.S., Fonda, D. and Hynes, R.O. (1987) Multiple sites of alternative splicing of the rat fibronectin gene transcript. *Embo J*, **6**, 2573-2580.
Schwarzbauer, J.E., Tamkun, J.W., Lemischka, I.R. and Hynes, R.O. (1983) Three different fibronectin mRNAs arise by alternative splicing within the coding region. *Cell*, **35**, 421-431.
Seftalioglu, A. and Karakus, S. (2003) Syndecan-1/CD138 expression in normal myeloid, acute lymphoblastic and myeloblastic leukemia cells. *Acta Histochem*, **105**, 213-221.
Sengle, G., Charbonneau, N.L., Ono, R.N., Sasaki, T., Alvarez, J., Keene, D.R., Bachinger, H.P. and Sakai, L.Y. (2008) Targeting of bone morphogenetic protein growth factor complexes to fibrillin. *J Biol Chem*, **283**, 13874-13888.
Shaw, J., Rowlinson, R., Nickson, J., Stone, T., Sweet, A., Williams, K. and Tonge, R. (2003) Evaluation of saturation labelling two-dimensional difference gel electrophoresis fluorescent dyes. *Proteomics*, **3**, 1181-1195.
Shipley, J.M., Mecham, R.P., Maus, E., Bonadio, J., Rosenbloom, J., McCarthy, R.T., Baumann, M.L., Frankfater, C., Segade, F. and Shapiro, S.D. (2000) Developmental expression of latent transforming growth factor beta binding protein 2 and its requirement early in mouse development. *Mol Cell Biol*, **20**, 4879-4887.
Skonier, J., Bennett, K., Rothwell, V., Kosowski, S., Plowman, G., Wallace, P., Edelhoff, S., Disteche, C., Neubauer, M., Marquardt, H. and et al. (1994) beta ig-h3: a transforming growth factor-beta-responsive gene encoding a secreted protein that inhibits cell attachment in vitro and suppresses the growth of CHO cells in nude mice. *DNA Cell Biol*, **13**, 571-584.
Skonier, J., Neubauer, M., Madisen, L., Bennett, K., Plowman, G.D. and Purchio, A.F. (1992) cDNA cloning and sequence analysis of beta ig-h3, a novel gene induced in a human adenocarcinoma cell line after treatment with transforming growth factor-beta. *DNA Cell Biol*, **11**, 511-522.
Smith, L.T. (1994) Patterns of type VI collagen compared to types I, III and V collagen in human embryonic and fetal skin and in fetal skin-derived cell cultures. *Matrix Biol*, **14**, 159-170.
Smith, S.E., French, M.M., Julian, J., Paria, B.C., Dey, S.K. and Carson, D.D. (1997) Expression of heparan sulfate proteoglycan (perlecan) in the mouse blastocyst is regulated during normal and delayed implantation. *Dev Biol*, **184**, 38-47.

Smith, S.M., West, L.A., Govindraj, P., Zhang, X., Ornitz, D.M. and Hassell, J.R. (2007) Heparan and chondroitin sulfate on growth plate perlecan mediate binding and delivery of FGF-2 to FGF receptors. *Matrix Biol*, **26**, 175-184.

Smyth, N., Vatansever, H.S., Murray, P., Meyer, M., Frie, C., Paulsson, M. and Edgar, D. (1999) Absence of basement membranes after targeting the LAMC1 gene results in embryonic lethality due to failure of endoderm differentiation. *J Cell Biol*, **144**, 151-160.

Sottile, J. and Mosher, D.F. (1993) Assembly of fibronectin molecules with mutations or deletions of the carboxyl-terminal type I modules. *Biochemistry*, **32**, 1641-1647.

Specks, U., Mayer, U., Nischt, R., Spissinger, T., Mann, K., Timpl, R., Engel, J. and Chu, M.L. (1992) Structure of recombinant N-terminal globule of type VI collagen alpha 3 chain and its binding to heparin and hyaluronan. *Embo J*, **11**, 4281-4290.

Spissinger, T. and Engel, J. (1995) Type VI collagen beaded microfibrils from bovine cornea depolymerize at acidic pH, and depolymerization and polymerization are not influenced by hyaluronan. *Matrix Biol*, **14**, 499-505.

Staprans, I., Piel, C.F. and Felts, J.M. (1986) Analysis of selected plasma constituents in continuous ambulatory peritoneal dialysis effluent. *Am J Kidney Dis*, **7**, 490-494.

Steinberg, T.H., Chernokalskaya, E., Berggren, K., Lopez, M.F., Diwu, Z., Haugland, R.P. and Patton, W.F. (2000) Ultrasensitive fluorescence protein detection in isoelectric focusing gels using a ruthenium metal chelate stain. *Electrophoresis*, **21**, 486-496.

Sterner-Kock, A., Thorey, I.S., Koli, K., Wempe, F., Otte, J., Bangsow, T., Kuhlmeier, K., Kirchner, T., Jin, S., Keski-Oja, J. and von Melchner, H. (2002) Disruption of the gene encoding the latent transforming growth factor-beta binding protein 4 (LTBP-4) causes abnormal lung development, cardiomyopathy, and colorectal cancer. *Genes Dev*, **16**, 2264-2273.

Sterzel, R.B., Hartner, A., Schlotzer-Schrehardt, U., Voit, S., Hausknecht, B., Doliana, R., Colombatti, A., Gibson, M.A., Braghetta, P. and Bressan, G.M. (2000) Elastic fiber proteins in the glomerular mesangium in vivo and in cell culture. *Kidney Int*, **58**, 1588-1602.

Switzer, R.C., 3rd, Merril, C.R. and Shifrin, S. (1979) A highly sensitive silver stain for detecting proteins and peptides in polyacrylamide gels. *Anal Biochem*, **98**, 231-237.

Taipale, J., Lohi, J., Saarinen, J., Kovanen, P.T. and Keski-Oja, J. (1995) Human mast cell chymase and leukocyte elastase release latent transforming growth factor-beta 1 from the extracellular matrix of cultured human epithelial and endothelial cells. *J Biol Chem*, **270**, 4689-4696.

Takeshita, S., Kikuno, R., Tezuka, K. and Amann, E. (1993) Osteoblast-specific factor 2: cloning of a putative bone adhesion protein with homology with the insect protein fasciclin I. *Biochem J*, **294 (Pt 1)**, 271-278.

Tannu, N.S. and Hemby, S.E. (2006) Two-dimensional fluorescence difference gel electrophoresis for comparative proteomics profiling. *Nat Protoc*, **1**, 1732-1742.

Taylor, K.R. and Gallo, R.L. (2006) Glycosaminoglycans and their proteoglycans: host-associated molecular patterns for initiation and modulation of inflammation. *Faseb J*, **20**, 9-22.

Teder, P., Vandivier, R.W., Jiang, D., Liang, J., Cohn, L., Pure, E., Henson, P.M. and Noble, P.W. (2002) Resolution of lung inflammation by CD44. *Science*, **296**, 155-158.

Thiede, B., Treumann, A., Kretschmer, A., Sohlke, J. and Rudel, T. (2005) Shotgun proteome analysis of protein cleavage in apoptotic cells. *Proteomics*, **5**, 2123-2130.

Tiedemann, K., Batge, B., Muller, P.K. and Reinhardt, D.P. (2001) Interactions of fibrillin-1 with heparin/heparan sulfate, implications for microfibrillar assembly. *J Biol Chem*, **276**, 36035-36042.

Tiedemann, K., Sasaki, T., Gustafsson, E., Gohring, W., Batge, B., Notbohm, H., Timpl, R., Wedel, T., Schlotzer-Schrehardt, U. and Reinhardt, D.P. (2005) Microfibrils at basement membrane zones interact with perlecan via fibrillin-1. *J Biol Chem*, **280**, 11404-11412.

Timpl, R., and Chu, M. L.,. (1994) In Yurchenco, P.D., Birk, D., and Micham, R. P., (ed.), *In Extracellular Matrix Assembly and Structure*. Academic Press, Inc, New York, pp. 207-242.

Timpl, R. and Brown, J.C. (1996) Supramolecular assembly of basement membranes. *Bioessays*, **18**, 123-132.

Tkachenko, E., Rhodes, J.M. and Simons, M. (2005) Syndecans: new kids on the signaling block. *Circ Res*, **96**, 488-500.

Todorovic, V., Frendewey, D., Gutstein, D.E., Chen, Y., Freyer, L., Finnegan, E., Liu, F., Murphy, A., Valenzuela, D., Yancopoulos, G. and Rifkin, D.B. (2007) Long form of latent TGF-beta binding protein 1 (Ltbp1L) is essential for cardiac outflow tract septation and remodeling. *Development*, **134**, 3723-3732.

Trask, B.C., Trask, T.M., Broekelmann, T. and Mecham, R.P. (2000a) The microfibrillar proteins MAGP-1 and fibrillin-1 form a ternary complex with the chondroitin sulfate proteoglycan decorin. *Mol Biol Cell*, **11**, 1499-1507.

Trask, T.M., Ritty, T.M., Broekelmann, T., Tisdale, C. and Mecham, R.P. (1999) N-terminal domains of fibrillin 1 and fibrillin 2 direct the formation of homodimers: a possible first step in microfibril assembly. *Biochem J*, **340 (Pt 3)**, 693-701.

Trask, T.M., Trask, B.C., Ritty, T.M., Abrams, W.R., Rosenbloom, J. and Mecham, R.P. (2000b) Interaction of tropoelastin with the amino-terminal domains of fibrillin-1 and fibrillin-2 suggests a role for the fibrillins in elastic fiber assembly. *J Biol Chem*, **275**, 24400-24406.

Trinkle-Mulcahy, L., Boulon, S., Lam, Y.W., Urcia, R., Boisvert, F.M., Vandermoere, F., Morrice, N.A., Swift, S., Rothbauer, U., Leonhardt, H. and Lamond, A. (2008) Identifying specific protein interaction partners using quantitative mass spectrometry and bead proteomes. *J Cell Biol*, **183**, 223-239.

Tsen, G., Halfter, W., Kroger, S. and Cole, G.J. (1995) Agrin is a heparan sulfate proteoglycan. *J Biol Chem*, **270**, 3392-3399.

Tsuji, T., Okada, F., Yamaguchi, K. and Nakamura, T. (1990) Molecular cloning of the large subunit of transforming growth factor type beta masking protein and expression of the mRNA in various rat tissues. *Proc Natl Acad Sci U S A*, **87**, 8835-8839.

Unlu, M., Morgan, M.E. and Minden, J.S. (1997) Difference gel electrophoresis: a single gel method for detecting changes in protein extracts. *Electrophoresis*, **18**, 2071-2077.

Unsold, C., Hyytiainen, M., Bruckner-Tuderman, L. and Keski-Oja, J. (2001) Latent TGF-beta binding protein LTBP-1 contains three potential extracellular matrix interacting domains. *J Cell Sci*, **114**, 187-197.

Urban, Z., Gao, J., Pope, F.M. and Davis, E.C. (2005) Autosomal dominant cutis laxa with severe lung disease: synthesis and matrix deposition of mutant tropoelastin. *J Invest Dermatol*, **124**, 1193-1199.

Urban, Z., Michels, V.V., Thibodeau, S.N., Davis, E.C., Bonnefont, J.P., Munnich, A., Eyskens, B., Gewillig, M., Devriendt, K. and Boyd, C.D. (2000) Isolated supravalvular aortic stenosis: functional haploinsufficiency of the elastin gene as a result of nonsense-mediated decay. *Hum Genet*, **106**, 577-588.

Urban, Z., Zhang, J., Davis, E.C., Maeda, G.K., Kumar, A., Stalker, H., Belmont, J.W., Boyd, C.D. and Wallace, M.R. (2001) Supravalvular aortic stenosis: genetic and molecular dissection of a complex mutation in the elastin gene. *Hum Genet*, **109**, 512-520.

Van den Bergh, G., Clerens, S., Vandesande, F. and Arckens, L. (2003) Reversed-phase high-performance liquid chromatography prefractionation prior to two-dimensional difference gel electrophoresis and mass spectrometry identifies new differentially expressed proteins between striate cortex of kitten and adult cat. *Electrophoresis*, **24**, 1471-1481.

Vehvilainen, P., Hyytiainen, M. and Keski-Oja, J. (2003) Latent transforming growth factor-beta-binding protein 2 is an adhesion protein for melanoma cells. *J Biol Chem*, **278**, 24705-24713.

Vehvilainen, P., Hyytiainen, M. and Keski-Oja, J. (2009) Matrix association of latent TGF-beta binding protein-2 (LTBP-2) is dependent on fibrillin-1. *J Cell Physiol*, **221**, 586-593.
Vermeulen, M., Hubner, N.C. and Mann, M. (2008) High confidence determination of specific protein-protein interactions using quantitative mass spectrometry. *Curr Opin Biotechnol*, **19**, 331-337.
Vincourt, J.B., Lionneton, F., Kratassiouk, G., Guillemin, F., Netter, P., Mainard, D. and Magdalou, J. (2006) Establishment of a reliable method for direct proteome characterization of human articular cartilage. *Mol Cell Proteomics*, **5**, 1984-1995.
Vrhovski, B., Jensen, S. and Weiss, A.S. (1997) Coacervation characteristics of recombinant human tropoelastin. *Eur J Biochem*, **250**, 92-98.
Wagenseil, J.E. and Mecham, R.P. (2007) New insights into elastic fiber assembly. *Birth Defects Res C Embryo Today*, **81**, 229-240.
Wess, T.J. (2005) Collagen fibril form and function. *Adv Protein Chem*, **70**, 341-374.
Whitelock, J. (2001) Purification of perlecan from endothelial cells. *Methods Mol Biol*, **171**, 27-34.
Whitelock, J.M., Melrose, J. and Iozzo, R.V. (2008) Diverse cell signaling events modulated by perlecan. *Biochemistry*, **47**, 11174-11183.
Whiteman, P. and Handford, P.A. (2003) Defective secretion of recombinant fragments of fibrillin-1: implications of protein misfolding for the pathogenesis of Marfan syndrome and related disorders. *Hum Mol Genet*, **12**, 727-737.
Wiberg, C., Hedbom, E., Khairullina, A., Lamande, S.R., Oldberg, A., Timpl, R., Morgelin, M. and Heinegard, D. (2001) Biglycan and decorin bind close to the n-terminal region of the collagen VI triple helix. *J Biol Chem*, **276**, 18947-18952.
Wiberg, C., Heinegard, D., Wenglen, C., Timpl, R. and Morgelin, M. (2002) Biglycan organizes collagen VI into hexagonal-like networks resembling tissue structures. *J Biol Chem*, **277**, 49120-49126.
Wiberg, C., Klatt, A.R., Wagener, R., Paulsson, M., Bateman, J.F., Heinegard, D. and Morgelin, M. (2003) Complexes of matrilin-1 and biglycan or decorin connect collagen VI microfibrils to both collagen II and aggrecan. *J Biol Chem*, **278**, 37698-37704.
Wilcox-Adelman, S.A., Denhez, F., Iwabuchi, T., Saoncella, S., Calautti, E. and Goetinck, P.F. (2002) Syndecan-4: dispensable or indispensable? *Glycoconj J*, **19**, 305-313.
Wu, J.J., Eyre, D.R. and Slayter, H.S. (1987) Type VI collagen of the intervertebral disc. Biochemical and electron-microscopic characterization of the native protein. *Biochem J*, **248**, 373-381.
Wu, X.X., Gordon, R.E., Glanville, R.W., Kuo, H.J., Uson, R.R. and Rand, J.H. (1996) Morphological relationships of von Willebrand factor, type VI collagen, and fibrillin in human vascular subendothelium. *Am J Pathol*, **149**, 283-291.
Yamamoto, S., Okada, M., Tsujikawa, M., Shimomura, Y., Nishida, K., Inoue, Y., Watanabe, H., Maeda, N., Kurahashi, H., Kinoshita, S., Nakamura, Y. and Tano, Y. (1998) A kerato-epithelin (betaig-h3) mutation in lattice corneal dystrophy type IIIA. *Am J Hum Genet*, **62**, 719-722.
Yamanaka, M., Kimura, F., Kagata, Y., Kondoh, N., Asano, T., Yamamoto, M. and Hayakawa, M. (2008) BIGH3 is overexpressed in clear cell renal cell carcinoma. *Oncol Rep*, **19**, 865-874.
Yanagisawa, H., Davis, E.C., Starcher, B.C., Ouchi, T., Yanagisawa, M., Richardson, J.A. and Olson, E.N. (2002) Fibulin-5 is an elastin-binding protein essential for elastic fibre development in vivo. *Nature*, **415**, 168-171.
Yin, W., Smiley, E. and Bonadio, J. (1998) Alternative splicing of LTBP-3. *Biochem Biophys Res Commun*, **245**, 454-458.
Yoneda, A. and Couchman, J.R. (2003) Regulation of cytoskeletal organization by syndecan transmembrane proteoglycans. *Matrix Biol*, **22**, 25-33.

Yurchenco, P.D., Cheng, Y.S., Campbell, K. and Li, S. (2004) Loss of basement membrane, receptor and cytoskeletal lattices in a laminin-deficient muscular dystrophy. *J Cell Sci*, **117**, 735-742.

Zajchowski, D.A., Bartholdi, M.F., Gong, Y., Webster, L., Liu, H.L., Munishkin, A., Beauheim, C., Harvey, S., Ethier, S.P. and Johnson, P.H. (2001) Identification of gene expression profiles that predict the aggressive behavior of breast cancer cells. *Cancer Res*, **61**, 5168-5178.

Zhang, H., Apfelroth, S.D., Hu, W., Davis, E.C., Sanguineti, C., Bonadio, J., Mecham, R.P. and Ramirez, F. (1994) Structure and expression of fibrillin-2, a novel microfibrillar component preferentially located in elastic matrices. *J Cell Biol*, **124**, 855-863.

Zhang, H., Hu, W. and Ramirez, F. (1995) Developmental expression of fibrillin genes suggests heterogeneity of extracellular microfibrils. *J Cell Biol*, **129**, 1165-1176.

Zhang, M.C., He, L., Giro, M., Yong, S.L., Tiller, G.E. and Davidson, J.M. (1999) Cutis laxa arising from frameshift mutations in exon 30 of the elastin gene (ELN). *J Biol Chem*, **274**, 981-986.

Zhang, Y., Conrad, A.H., Tasheva, E.S., An, K., Corpuz, L.M., Kariya, Y., Suzuki, K. and Conrad, G.W. (2005) Detection and quantification of sulfated disaccharides from keratan sulfate and chondroitin/dermatan sulfate during chick corneal development by ESI-MS/MS. *Invest Ophthalmol Vis Sci*, **46**, 1604-1614.

Zhao, L., Liang, T., Xu, J., Lin, H., Li, D. and Qi, Y. (2009) Two novel FBN1 mutations associated with ectopia lentis and marfanoid habitus in two Chinese families. *Mol Vis*, **15**, 826-832.

Zheng, Q., Davis, E.C., Richardson, J.A., Starcher, B.C., Li, T., Gerard, R.D. and Yanagisawa, H. (2007) Molecular analysis of fibulin-5 function during de novo synthesis of elastic fibers. *Mol Cell Biol*, **27**, 1083-1095.

Zimmermann, D.R., Trueb, B., Winterhalter, K.H., Witmer, R. and Fischer, R.W. (1986) Type VI collagen is a major component of the human cornea. *FEBS Lett*, **197**, 55-58.

Zinn, K., McAllister, L. and Goodman, C.S. (1988) Sequence analysis and neuronal expression of fasciclin I in grasshopper and Drosophila. *Cell*, **53**, 577-587.